UNIVERSIDADE FEDERAL DE MINAS GERAIS
INSTITUTO DE CIÊNCIAS EXATAS
DEPARTAMENTO DE ESTATÍSTICA
PROGRAMA DE PÓS-GRADUAÇÃO EM ESTATÍSTICA

GUILHERME AUGUSTO VELOSO

DYNAMIC GENERAL PATH MODELS FOR DEGRADATION DATA

Belo Horizonte
2022

GUILHERME AUGUSTO VELOSO

DYNAMIC GENERAL PATH MODELS FOR DEGRADATION DATA

Texto desenvolvido para avaliação da tese de doutorado apresentada ao Programa de Pós-Graduação do Departamento de Estatística da Universidade Federal de Minas Gerais como parte dos requisitos para a obtenção do grau de Doutor em Estatística.

Orientadores: Profa. Dra. Rosangela Helena Loschi e Prof. Dr. Thiago Rezende dos Santos

Belo Horizonte
2022

© 2022, Guilherme Augusto Veloso.
Todos os direitos reservados

Veloso, Guilherme Augusto.

V443d Dynamic general path models for degradation data [manuscrito] / Guilherme Augusto Veloso. – 2022.
123 f. il.

Orientadora: Rosangela Helena Loschi.
Coorientador: Thiago Rezende dos Santos.
Tese (doutorado) - Universidade Federal de Minas Gerais, Instituto de Ciências Exatas, Departamento de Estatística.
Referências: f.120

1. Estatística – Teses. 2. Degradação- Modelos – Teses. 3. Sistemas dinâmicos – Teses. 4. Análise do tempo de falha – Teses. I. Loschi, Rosangela Helena. II Santos, Thiago Rezende dos. III. Universidade Federal de Minas Gerais, Instituto de Ciências Exatas, Departamento de Estatísitca. IV.Título.

CDU 519.2(043)

Ficha catalográfica elaborada pela bibliotecária Belkiz Inez Rezende Costa
CRB 6/1510 Universidade Federal de Minas Gerais - ICEx

UNIVERSIDADE FEDERAL DE MINAS GERAIS

PROGRAMA DE PÓS-GRADUAÇÃO EM ESTATÍSTICA

UFMG

ATA DA DEFESA DE TESE DE DOUTORADO DE GUILHERME AUGUSTO VELOSO, MATRICULADO, SOB O Nº 2018.665.108, NO PROGRAMA DE PÓS-GRADUAÇÃO EM ESTATÍSTICA, DO INSTITUTO DE CIÊNCIAS EXATAS, DA UNIVERSIDADE FEDERAL DE MINAS GERAIS, REALIZADA NO DIA 11 DE FEVEREIRO DE 2022.

Aos 11 dias do mês de Fevereiro de 2022, às 13h30, em reunião pública virtual No. 71 (conforme orientações para a atividade de defesa de tese durante a vigência da Portaria PRPG nº 1819), reuniu-se a Comissão Examinadora homologada pelo Colegiado do Programa de Pós-Graduação em Estatística, formada pelos os professores abaixo relacionados, para julgar a defesa de tese do aluno Guilherme Augusto Veloso, nº matrícula 2018.665.108, intitulada "*DYNAMIC GENERAL PATH MODELS FOR DEGRADATION DATA*", requisito final para obtenção do Grau de Doutor em Estatística. Abrindo a sessão, a Senhora Presidente da Comissão, Profa. Rosangela Helena Loschi, passou a palavra ao aluno para apresentação de seu trabalho. Seguiu-se a arguição pelos examinadores com a respectiva defesa do aluno. Após a defesa, os membros da banca examinadora reuniram-se reservadamente sem a presença do aluno e do público, para julgamento e expedição do resultado final. Foi atribuída a seguinte indicação:

(x) Aprovada.
( ) Reprovada com resubmissão do texto em ____ dias.
( ) Reprovada com resubmissão do texto e nova defesa em ____ dias.
( ) Reprovada.

O resultado final foi comunicado publicamente ao(à) aluno(a) pelo(a) Senhor(a) Presidente da Comissão. Nada mais havendo a tratar, o(a) Presidente encerrou a reunião e lavrou a presente Ata, que será assinada por todos os membros participantes da banca examinadora. Belo Horizonte, 11 de fevereiro de 2022.

Profa. Rosangela Helena Loschi
(Orientadora EST/UFMG)

Prof. Thiago Rezende dos Santos
Co-orientador - (EST/UFMG)

Prof. Fabio Nogueira Demarqui)
(EST/UFMG)

Prof. Gustavo Leonel Gilardoni Avalle
(EST/UnB)

Prof(a). Hedibert Freitas Lopes
(INSPER)

Prof(a). Magda Carvalho Pires
(EST/UFMG)

Observações:
1. No caso de aprovação da tese, a banca pode solicitar modificações a serem feitas na versão final do texto. Neste caso, o texto final deve ser aprovado pelo orientador da tese. O pedido de expedição do diploma do candidato fica condicionado à submissão e aprovação, pelo orientador, da versão final do texto.
2. No caso de reprovação da tese com resubmissão do texto, o candidato deve submeter o novo texto dentro do prazo estipulado pela banca, que deve ser de no máximo 6 (seis) meses. O novo texto deve ser avaliado por todos os membros da banca que então decidirão pela aprovação ou reprovação da tese.
3. No caso de reprovação da tese com resubmissão do texto e nova defesa, o candidato deve submeter o novo texto com a antecedência à nova defesa que o orientador julgar adequada. A nova defesa, mediante todos os membros da banca, deve ser realizada dentro do prazo estipulado pela banca, que deve ser de no máximo 6 (seis) meses. O novo texto deve ser avaliado por todos os membros da banca. Baseada no novo texto e na nova defesa, a banca decidirá pela aprovação ou reprovação da tese.

Dedico este trabalho a todos que acreditam na ciência

Resumo

Os modelos gerais para perfis de degradação assumem que existe uma forma funcional regular comum a todas as unidades experimentais relacionando o tempo e a degradação. Os efeitos aleatórios do ambiente podem afetar as trajetórias de degradação dessas unidades e, consequentemente, a forma funcional assumida se torna uma aproximação muito abrupta da realidade e estimativas viciadas para os tempos de falha são obtidas. Considerando a natureza temporal dos dados de degradação, os modelos dinâmicos surgem como uma alternativa para modelar tais dados, uma vez que fazem uma aproximação por partes para a forma verdadeira do caminho de degradação. A presente tese de doutorado inicia apresentando os conjuntos de dados que motivam nosso trabalho juntamente com uma breve revisão dos modelos de degradação recorrentes na literatura. A introdução também traz uma descrição detalhada das contribuições dos três modelos propostos neste texto. O primeiro deles introduz um modelo de degradação linear dinâmico para abordar situações onde os caminhos de degradação não evoluem regularmente ao longo do tempo. Esse modelo é uma extensão do que foi desenvolvido no meu mestrado, por assumir a presença de um intercepto que evolui dinamicamente ao longo do tempo. O segundo modelo está voltado para descrever o comportamento de dados de degradação positivos. As medidas de degradação são modeladas de acordo com uma distribuição gama e a taxa de degradação é dependente de duas componentes. A primeira quantifica as características físicas de cada unidade e a outra é dinâmica e representa os efeitos aleatórios do ambiente comum. Assim como no primeiro modelo, o último modelo proposto assume que as medidas de degradação são normalmente distribuidas. Estendendo a primeira proposta, este modelo assume que a taxa de degradação se decompõe nos mesmos dois fatores conisderados no segundo modelo. No entanto, assume que o efeito que quantifica as caracteristicas fisicas do dispositivo é função de covariáveis. Esta abordagem introduz mais flexibilidade à análise uma vez que, em alguns testes de degradação, múltiplas caracterísitcas são observadas para entender os diferentes aspectos da confiabilidade do sistema. O texto termina trazendo um resumo compacto dos métodos e resultados obtidos nos estudos desenvolvidos ao longo da tese, juntamente com tópicos relevantes para pesquisas futuras.

Palavras-chave: Modelos de Degradação, Modelos Dinâmicos, Distribuição do Tempo até a Falha.

Abstract

The general degradation path models assume that there is a regular functional form common to all experimental units relating time and degradation. The random effects of the environment can affect the degradation trajectories of these units and, consequently, the assumed functional form becomes a very abrupt approximation of reality and biased estimates for failure times are obtained. Considering the temporal nature of degradation data, dynamic models emerge as an alternative to model such data, as they make an approximation by parts for the true form of the degradation path. The present doctoral thesis begins by presenting the datasets that motivate our work, together with a brief review of the degradation models that recur in the literature. The introduction also provides a detailed description of the contributions of the three models proposed in this text. The first one introduces a dynamic linear degradation model to address situations where degradation paths do not evolve regularly over time. This model is an extension of what was developed in my master's, as it assumes the presence of an intercept that dynamically evolves over time. The second model is aimed at describing the behavior of positive degradation data. Degradation measures are modeled according to a gamma distribution and the degradation rate is dependent on two components. The first quantifies the physical characteristics of each unit and the other is dynamic and represents the random effects of the common environment. As in the first model, the last proposed model assumes that degradation measures are normally distributed. Extending the first proposal, this model assumes that the degradation rate breaks down into the same two factors considered in the second model. However, it assumes that the effect that quantifies the physical characteristics of the device is a function of covariates. This approach introduces more flexibility to the analysis since, in some degradation tests, multiple characteristics are observed to understand different aspects of system reliability. The text ends with a compact summary of the methods and results obtained in the studies carried out throughout the thesis, together with relevant topics for future research.

Keywords: Degradation Models, Dynamic Models, Failure Time Distribution.

Contents

1 Introduction **9**

1.1 Motivating Practical Situations . . . 9

1.1.1 Train Wheels Degradation Data . . . 10

1.1.2 Laser Emitters Degradation Data . . . 11

1.1.3 IRLEDs Degradation Data . . . 12

1.1.4 Fatigue Crack-Size Data . . . 13

1.1.5 Stress Relaxation Data . . . 14

1.1.6 Scar Width Degradation Data . . . 15

1.2 Degradation Models . . . 16

1.2.1 Stochastic Processes Models . . . 16

1.2.2 General Degradation Path Models . . . 17

1.3 Linear Degradation Model . . . 18

1.4 Contributions to Degradation Models . . . 20

References . . . 21

2 Dynamic Linear Degradation Model: Dealing with Heterogeneity in Degradation Paths **24**

2.1 Introduction . . . 25

2.2 Dynamic linear degradation model . . . 28

2.2.1 Posterior inference . . . 30

2.3 Inference for failure time . . . 32

2.4 Simulation studies . . . 34

2.4.1 Simulation I: Analyzing Weibull data . . . 35

2.4.2 Simulation II: Normal data under dynamic structure . . . 36

2.4.3 Simulation III: Heterogeneous degradation paths . . . 38

2.5 Case Studies . . . 39

2.5.1 Case study 1: Laser emitters data . . . 40

2.5.2 Case Study 2: IRLEDs data . . . 43

2.6 Conclusions . . . 45

References . . . 46

Appendix . . . 49

A1 Case Study 3: Train Wheels Degradation Data 49

3 Dynamic Multivariate Gamma Model: a General Path Approach for Positive Degradation Measurements 53

3.1 Introduction 54
3.2 Dynamic Multivariate Gamma Model 58
3.2.1 The Model Identifiability 61
3.2.2 Posterior inference 64
3.3 Inference for Failure Time 69
3.3.1 Inference for Units Under Test 69
3.3.2 Future Unit 70
3.4 Simulation Studies: The effect of the prior distributions for θ_0 and γ 71
3.5 Case Studies 76
3.5.1 Case Study 1: Fatigue Crack Size Data 76
3.5.2 Case Study 2: Stress Relaxation Data 80
3.6 Concluding Remarks 83
References 84
Supplementary Materials 89
S1 Proofs and Technical Details 89
S2 Additional Simulation Studies 90
S2.1 The effect of the prior distributions for γ 90
S2.2 The effect of the prior distributions for $\lambda_i,\ i = 1, 2, \ldots, n$ 93
S2.3 Degradation forecasts K-steps ahead, K large 93
S3 A Closer Look at our Case Studies 96
S3.1 Fatigue Crack Size Data 96
S3.2 Stress Relaxation Data 98

4 General Path Dynamic Model for Degradation Data with Fixed Covariates 101

4.1 Introduction 102
4.2 Dynamic Degradation Model with Fixed Covariates 103
4.2.1 Posterior Inference 104
4.3 Failure Time Distribution 107
4.4 Simulation Study 108
4.5 Case Study: Scar Width Degradation Data 117
4.6 Future Research 124
4.6.1 New Motivating Practical Situations 124
References 128

5 Final Discussion and Future Work Directions 129

Chapter 1

Introduction

Much of the reliability literature deals with data in which the observed measure is the failure time (or lifetime) of the devices and the main objective is to characterize how reliable the products are. However, for those highly reliable systems, it is common to be faced with situations in which few or even no failures are observed at the end of the study, resulting in a high rate of censoring. In these cases, the costs of carrying out the experiments are high and they end up without enough information about the lifetimes for an adequate statistical inference.

An alternative way to assess the reliability of highly reliable systems is to consider accelerated life tests [Meeker and Escobar, 1998]. The units are stimulated through accelerating variables such as temperature, pressure or voltage. These external factors aims at a fast gathering of information, because it induces the failure of the units under test to occur more quickly. Meanwhile, even using this methodology, it is possible to face with situations in which few or no failures occur.

Another way to approach this problem is to obtain information about the system's reliability through some indirect mechanism such as degradation. Given a critical degradation threshold, it is possible to make inference for the failure time of the units under test and a future one. In this chapter, we provide the motivating practical situations that were analyzed in this work together with an overview of existing degradation models in the literature. In addition, we review the properties of the linear degradation model, which serves as a comparison to our proposed methodology. This chapter ends with a detailing of the contribution associated to each model proposed throughout the text.

1.1 Motivating Practical Situations

A specific literature has been disseminated nowadays and makes use of degradation data to circumvent the problem of excessive censoring as an alternative to failure time data in reliability studies. Some pioneering and relevant works about degradation models are those of Hamada [2005], Robinson and Crowder [2000], Lu and Meeker [1993], Lu *et al.* [1997] and Chiao and Hamada [1996]. In the degradation tests, although the variable of interest is the failure time

or lifetime of the units under test, this is not observed. The degradation measures of some characteristic taken over time compose the answer and bring information about the failure time of the units. To conduct a test like this, it is necessary to first define a critical degradation threshold D_f when the failure occurs and, subsequently, collect the measurements of some degradation mechanism in the units under test at different and not necessarily equidistant inspection times.

The justification for using this approach is that many failures in practice are result of degradation mechanisms inherent to those failures. In engineering, these mechanisms are, for example, equipment fatigue, cracking, corrosion and oxidation. One of the advantages of this methodology compared to using failure time data is its ability to produce satisfactory inferences even when no unit under test fails. In this section, we highlight the datasets that motivate our work. More details of all datasets can be obtained by considering the cited references.

1.1.1 Train Wheels Degradation Data

This study was conducted by a railway company in Belo Horizonte to assess the reliability of train wheels [Freitas *et al.*, 2009]. To this end, 14 trains were selected at random from 25 that were in operation. For the chosen trains, only the motor wagons were considered, since their characteristics with respect to the mode of operation accelerate the wear of the wheels. These are made of forged and rolled steel and have an initial diameter of 966 mm. In each train, 13 diameter measurements were collected for each of the 8 wheel positions of the motor wagon. The measurements were made at equally spaced inspection times given in kilometers (km): $t_1 = 0$ km, $t_2 = 50000$ km, $\ldots, t_{13} = 600000$ km . Figure 1.1 shows the accumulated degradation paths obtained for the 14 wheels allocated to the MA11 position together with the increments (how much the unit under test degraded at a given moment) for some trains.

Each path shows the evolution of the degradation of a wheel over time. The engineering team determined that the critical reduction in diameter occurs when it reaches 889mm. Thus, the critical degradation threshold D_f assumes a value of 77mm (996mm - 889mm). This quantity has an important role in the modeling of degradation data because the failure is defined considering this value. In the present dataset, a wheel is considered to have failed when its wear over the inspection times exceeds this critical threshold. Particularly in the MA11 position, the wheels that have failed are no longer observed.

When looking at the graph of the accumulated degradation measurements in the Figure 1.1, the paths are approximately linear. However, observing the degradation increments, some paths present an abrupt change at the beginning of the study. If this early change in the increments is not taken into account, some biased conclusions can be drawn. This means that, to analyze these data correctly, the proposed methodology needs to be adaptable to fluctuations that the degradation trajectories may have.

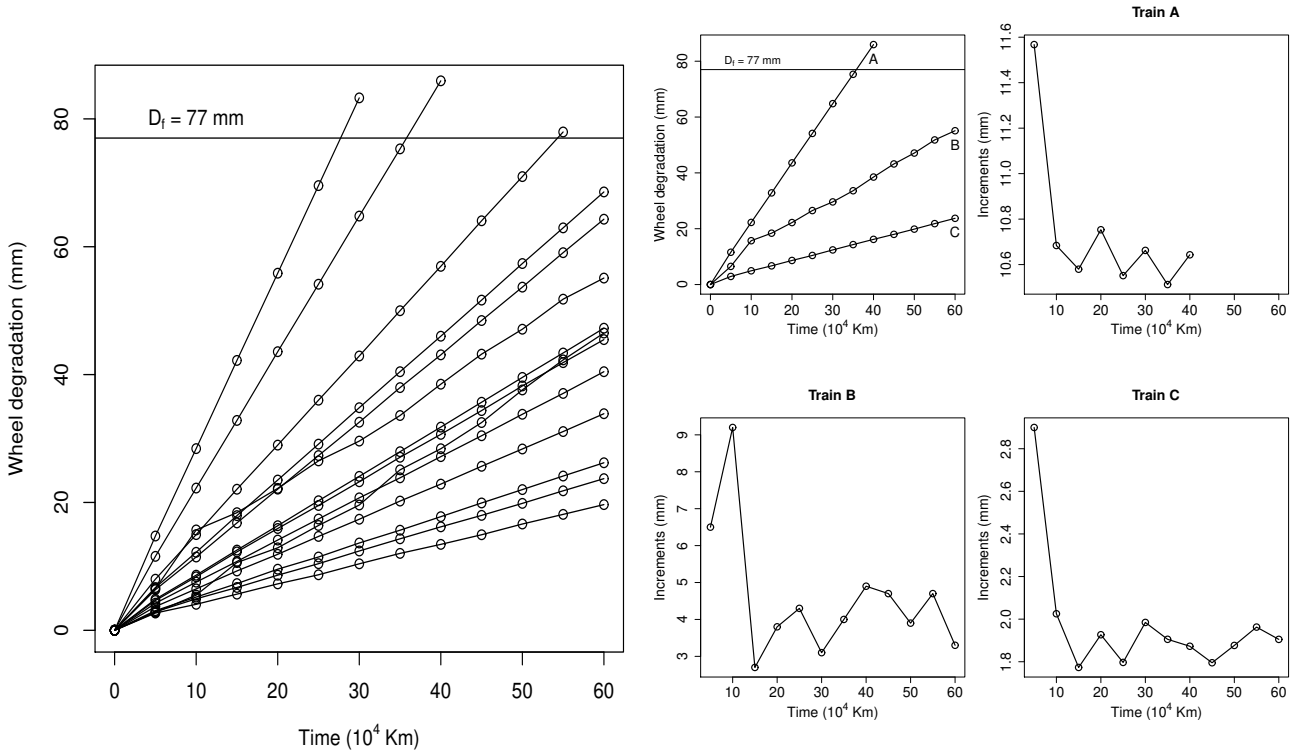

Figure 1.1: Degradation paths of train wheels degradation data of position MA11 and increments for some units under test

1.1.2 Laser Emitters Degradation Data

The data referring to the operating current in laser emitters, presented in Meeker and Escobar [1998], compose another recurrent dataset in the literature on degradation models. The light intensity of laser emitters degrades over time if the standard operating current is kept constant. For the same light intensity to be generated, the current needs to be calibrated over time. A sample of 15 laser emitters was monitored for 4000 hours of operation and in each of them, the percentage of increase in the standard operating current calculated in relation to the nominal current at the beginning of the test was recorded, with an interval of 250 hours. So, there are a total of 17 measurements of this percentage in each laser emitter and it was established that the failure occurs if it exceeds $D_f = 10\%$. Figure 1.2 shows the graph of the degradation paths for the 15 laser emitting units considered in the study in addition to the increments for some units under test.

In degradation models, an important step is to estimate the failure time distribution and the quantities of interest in reliability such as the remaining useful life. At this point in the analysis, it becomes necessary to consider what type of information from the model fit is being carried out so that inferential methods are constructed to estimate this distribution. The degradation path C in Figure 1.2, which is close to failing, is an example in which there is a structural

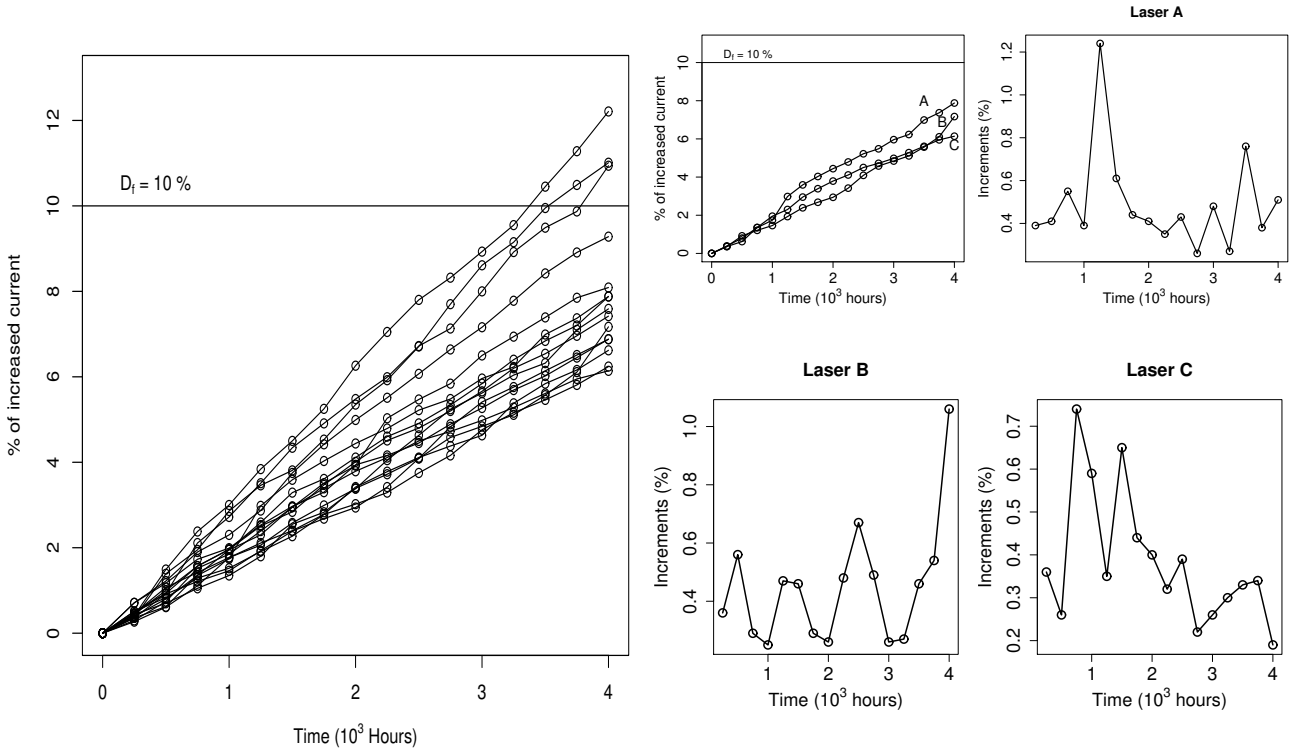

Figure 1.2: Degradation paths of laser emitters degradation data and increments for some units under test

break in the degradation rate throughout the study. It is noted in this laser emitter that, after 1750 hours, the degradation increments decrease until reaching its lowest value at the end of the test. When allowing dynamic degradation rates, this allows the possibility of evaluating the final behavior of the degradation path of this unit and making it responsible for taking the information to estimate its failure time distribution. This is useful not only to better estimate the reliability of the system, but also to individually predict the failure time of a specific unit under test in a context of preventive maintenance.

1.1.3 IRLEDs Degradation Data

Infrared light-emitting diodes (IRLEDs) are an example of high-reliable devices widely used in communication systems [Yang, 2007]. These optoeletronic devices have a wavelength of which is 880 nm and the design operating current, 50 mA. The degradation mechanism associated with these devices is measured mainly by the variation ratio of luminous power and a failure occurs when this ratio is greater than 30%. In a context of accelerated degradation tests, 40 units were sampled and divided into two groups to estimate the reliability at the operating current of 50 mA. A group of 25 units was tested at 170 mA and another one of 15 units was tested at 320 mA.

The first group is represented in Figure 1.3. These units were inspected for luminous power before and during testing at not equally spaced times: 0, 24, 48, 96, 155, 368, 768, 1130, 1536,

1905, 2263, and 2550 hours. To reinforce the distinction in the behavior of these 25 degradation paths, three of them (IRLEDs A, B and C) are highlighted on the right side of the figure together with how much they degraded in each inspection time (increments). As in Wang *et al.* [2017], a reduced threshold ($D_f = 20\%$) is used here to describe these data. Only four of the 25 units under test have failed wchich represents just 16% of the total devices. If this dataset was analyzed from the failure time data approach, the inference would certainly be compromised.

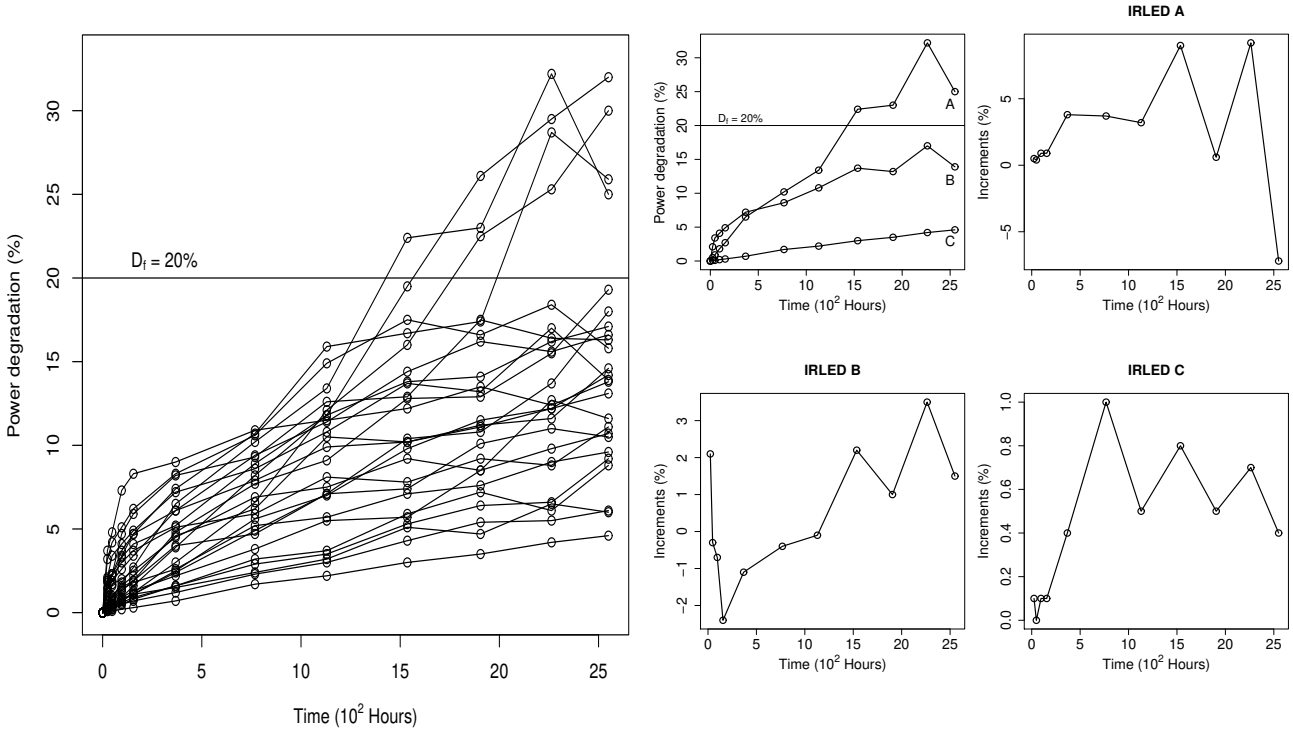

Figure 1.3: Degradation paths of IRLEDs data and increments for some units under test

The degradation path of IRLED C in Figure 1.3 is aproximately linear. However, the degradation paths of IRLEDs A and B , for instance, may be better approximated by piecewise linear or polynomial structures. Such variations in the degradation rates along time may be produced by factors that sometimes are beyond our control, such as external factors, measurement errors or system imperfections. If it is possible to obtain information about environmental factors, they can be included into the model as time-dependent covariates and the randomness of the degradation paths would be reduced [Hong *et al.*, 2005].

1.1.4 Fatigue Crack-Size Data

A recurrent dataset in the literature of degradation models with non-linear trajectories is the fatigue crack-size data, presented in Meeker and Escobar [1998]. Figure 1.4 shows the size of fatigue cracks in inches as a function of ten thousand cycles of applied stress for 10 test specimens, together with the behaviour of their degradation increments over time. The critical

degradation threshold stablished is 0.7 inches and only one unit under test failed during the study.

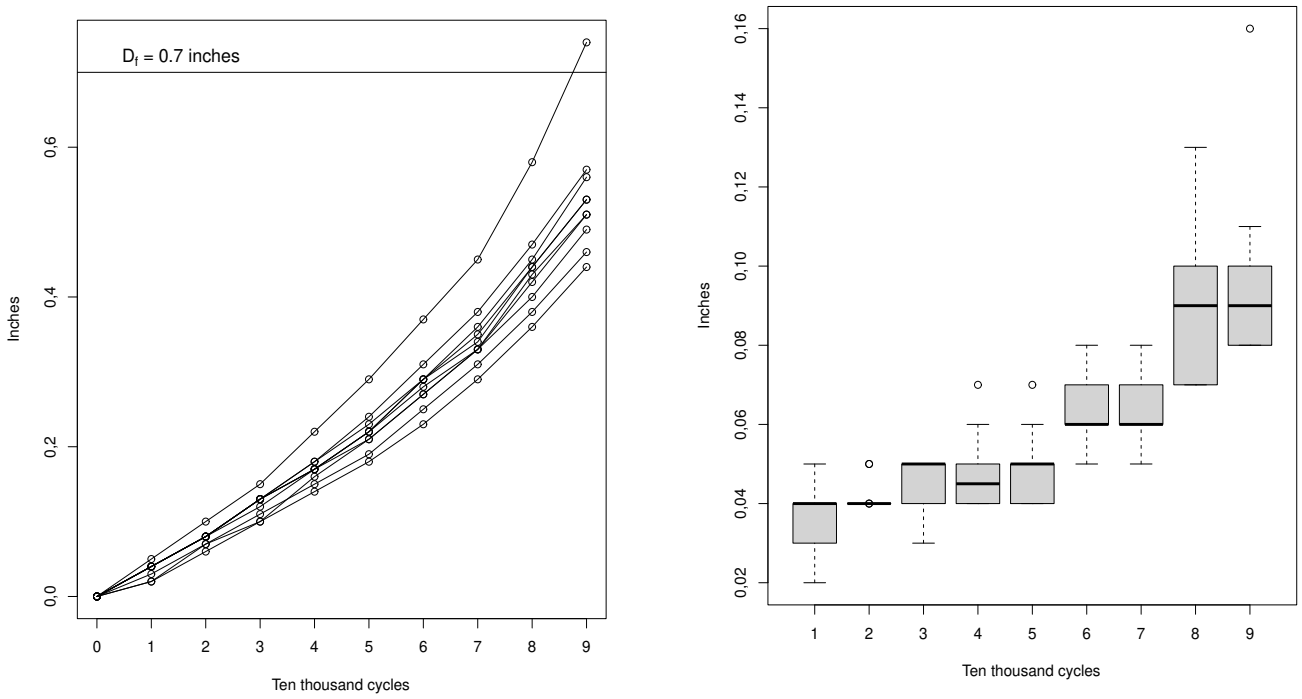

Figure 1.4: Degradation paths of fatigue crack-size data and the boxplot of the degradation increments over time

Note that the degradation increments of the units under test tend to increase over time. Thus, it is necessary that the structure of the proposed methodology to analyze these data incorporates the non-linear behavior so that the inference about the failure time of the units under test is not compromised.

1.1.5 Stress Relaxation Data

Stress relaxation is the loss of stress in a component subjected to a constant strain over time. The contacts of electrical connectors often fail due to excessive stress relaxation [Yang, 2007]. To estimate the reliability of a type of connectors, a sample of 18 units was randomly selected and divided into three equal groups, which were tested at 65, 85, and 100^{o}C. The stress relaxation data tested at 100^{o}C was evaluated at non equidistant inspection times given by 46, 108, 212, 344, 446, 626, 729, 927, 1005 and 1218 hours. The degradation paths are plotted in Figure 1.5.

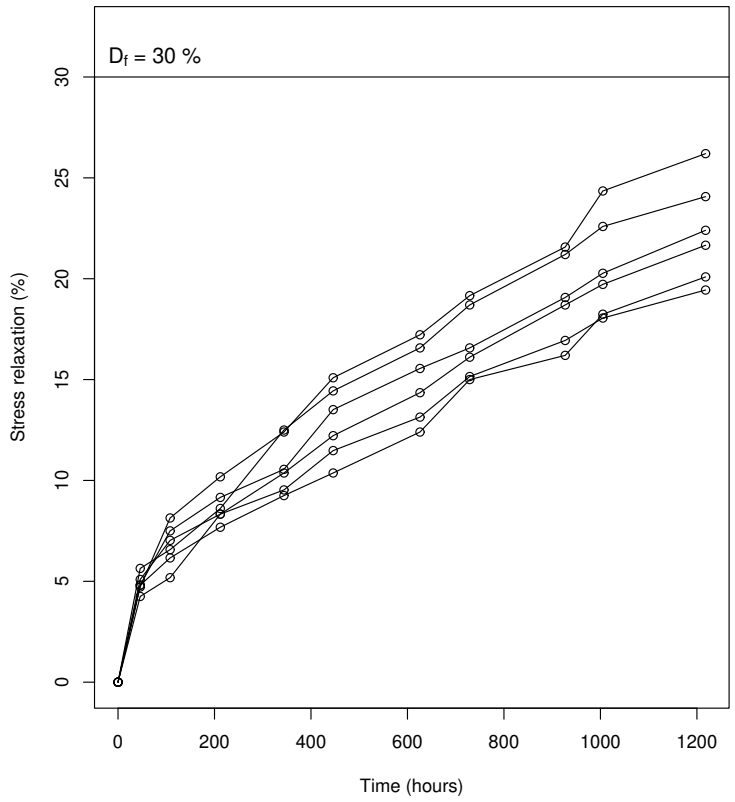

Figure 1.5: Stress relaxation data tested at 100^{o}C

The electrical connector is said to have failed if the stress relaxation exceeds 30%. Note that no unit under test has failed. This is not a problem for degradation models. It is enough that the critical threshold D_f is established for the inference to be well conducted for the failure time of the units under test and for a future one. This dataset is also non-linear, but unlike the previous dataset, the units in the stress relaxation data tend to fail less and less over time. The remaining useful life of some units under test may be longer than the study time (1218 hours). This reinforces the need to use degradation models to analyze the data together with a non-linear structure.

1.1.6 Scar Width Degradation Data

An experiment was conducted to test the wear resistance of a particular metal alloy [Meeker and Escobar, 1998]. The sliding test was conducted over a range of different applied weights in order to study the effect of weight and to gain a better understanding of the wear mechanism. Thus, 12 units were tested and divided according to different applied weights of 0.10kg, 0.05kg and 0.01kg. These units were monitored over 9 non-equidistant inspection times and it was established that the critical threshold of the scar width is D_f =50 microns. Figure 1.6 shows the resulting degradation paths.

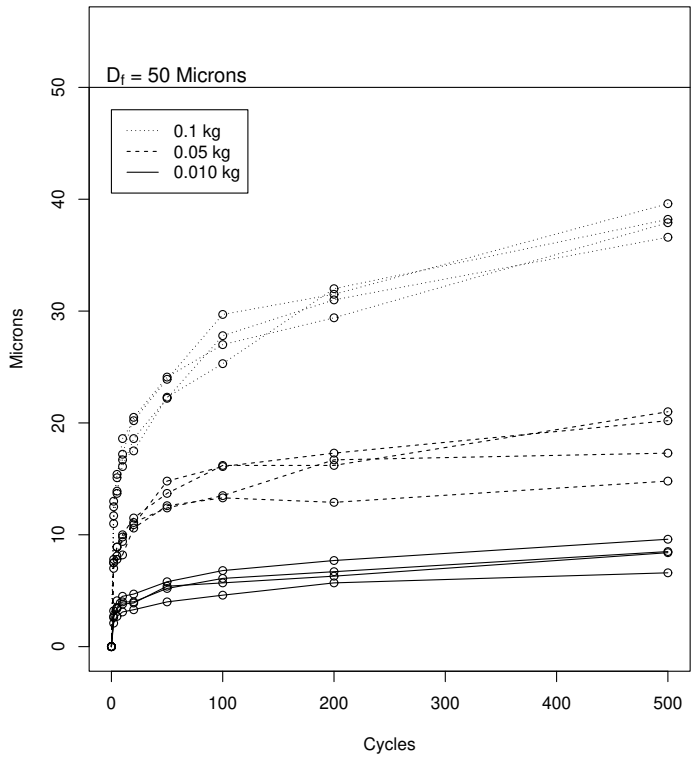

Figure 1.6: Scar width resulting from a metal-to-metal sliding test for different applied weights

From Figure 1.6, the effect of weight on the degradation trajectories is evident. In addition, all units have their trajectories degrading more at the beginning and showing less wear throughout the study. It would be of interest to quantify the effect of moving from one class to another with regard to failure time. Furthermore, as the trajectories are very similar, quantifying the effect of the common environment on degradation rates would be of practical importance. To analyze these data, therefore, we need a degradation model that incorporates fixed covariates in its structure.

1.2 Degradation Models

In the literature on degradation models, it is important to highlight the basic approaches that have become recurrent in the most recent works. In Ye and Xie [2015], the authors classify the degradation models in three approaches: stochastic processes models, general degradation path models and models that permeate these two classes.

1.2.1 Stochastic Processes Models

In the first class, it is assumed that degradation is a random process over time and the Wiener process has been intensively applied to model degradation data. Doksum and Hoyland [1993] assume that the degradation of a cable insulation follows a Wiener process and that the failure

data can be analyzed using the Inverse Normal distribution. In Park and Padgett [2005] and Wang *et al.* [2017], the same process is used to analyze fatigue data in metals and infrared light-emitting diodes degradation data, respectively. Si *et al.* [2013] developed a degradation model based on the Wiener process with a recursive filtering algorithm to estimate the remaining useful life of products with high reliability. The first Wiener process model considering random effects to analyze degradation data was developed in Peng and Tseng [2009] and extensions were considered in Peng and Tseng [2013] and Wang *et al.* [2010].

When degradation paths are monotonic, the gamma process becomes an alternative. The works of Bagdonavicius *et al.* [2010] and Lawless and Crowder [2004] use the gamma process considering the insertion of covariates and random effects. Another common process to analyze degradation data is the inverse Gaussian one, which appears as an alternative to the two previous processes (Wiener and gamma) when these become inadequate for data analysis in practice. In Wang and Xu [2010], a semi-parametric estimation procedure based on the EM algorithm was proposed for the Inverse Gaussian process. On the other hand, in Peng *et al.* [2014], Bayesian methods for the same process were developed in the context of degradation data.

As pointed out in Ye and Xie [2015], the stochastic processes are a natural choice for modelling the randomness in degradation processes caused by environmental factors. However, most stochastic process models are often so complex that it is not handy to use for engineers. Thus, not good properties can be obtained from these complex processes.

1.2.2 General Degradation Path Models

The general degradation path models are presented in Lu and Meeker [1993]. The analysis of the degradation tests using this approach is divided in two stages. Since these data have characteristics of longitudinal studies, in the first stage, a mixed linear or non linear model for a continuous response variable is fitted. The adopted functional form for the degradation paths is assumed to be the same for all population. For each specific unit, the true degradation path is a function of time conditional on the random-effects parameters representing the units feature. Finishing the first step, the unknown parameters of the model are estimated. The second step of this approach is to estimate the failure time distribution. This estimation depends on the model structure and can be obtained analytically, through Monte Carlo simulations or some other computational procedure.

When there is a linear relationship between the degradation measurements and time, the linear degradation model is established (Section 1.3). This model is used in Freitas *et al.* [2009] and Freitas *et al.* [2010] to analyze the train wheels degradation data from both the classical and Bayesian perspectives. Based on different practical problems, there are other ways to specify the functional form to which degradation paths are subject. Bae and Kvam [2004] extend the linear model by assuming that there are two phases in the degradation process. Shiau and Lin [1999] propose non-parametric regression methods to estimate the functional

form and in Zhou and Gebraeel [2014], the authors estimate the functional form using a cubic spline. Under a Bayesian perspective, Robinson and Crowder [2000] and Hamada [2005] discuss estimation using the general degradation path models. Pan and Crispin [2011] use a Bayesian hierarchical model to analyze an experiment with LEDs. Santos and Loschi [2020] and Yuan and Ji [2014] consider linear degradation models to approach heterogeneous populations. They assume a linear structure for the degradation paths and, to account for heterogeneity, mixture of distributions are assumed to make the behaviour of the random effects (degradation rates).

According to Ye and Xie [2015], the general degradation path models are more flexible in incorporating random effects than models by stochastic processes. However, the authors argue that in some applications the underlying degradation path is a great simplification of the reality and the measurement errors can be negligible.

1.3 Linear Degradation Model

In this section, we review the linear degradation model. This review is necessary, as this model is the basis of the general degradation path models. Furthermore, the entire methodology proposed in this doctoral dissertation was designed based on the limitations observed in this model. Specifically, the linear degradation model is defined as follows:

$$Y_{ij} = D(t_{ij}, \beta_i) + \epsilon_{ij} = \frac{1}{\beta_i} t_{ij} + \epsilon_{ij},\ i = 1, 2, \cdots, n \text{ and } j = 1, 2, \cdots, m_i, \tag{1.1}$$

where Y_{ij} is the jth degradation measurement for unit i, $D(t_{ij}, \beta_i)$ is the true degradation path for the i-th unit, β_i is a scalar component of random effects, t_{ij} is the jth inspection time for unit i and ϵ_{ij} is the observational error having the usual assumption that $\epsilon_{ij}|\sigma_\epsilon^2 \overset{iid}{\sim} \mathrm{N}(0, \sigma_\epsilon^2)$, with unknown σ_ϵ^2. The scalar β_i is responsible for including the particularities of unit i in the model and indicate the slope of the line associated with its degradation path, being interpreted as the unit's degradation rate. After establishing the distribution for the random effects of the model, the Bayesian inference together with MCMC schemes can be used to estimate the unknown parameters of interest. The true degradation path in (1.1) can also be written as $D(t_{ij}, \beta_i) = \beta_i t_{ij}$.

With the model parameters properly estimated, the next step is to make an inference about the failure time distribution of the units under test and for a future one. As the failure occurs when the degradation path reaches the critical threshold D_f, we obtain from the equation of the model (1.1) that $D_f = \frac{1}{\beta_i} T_i \ \Rightarrow\ T_i = \beta_i D_f$. Under a Bayesian perspective, the posterior predictive failure time distribution $F_{T_i|\boldsymbol{Y}}(t|\boldsymbol{y})$ can be derived as $F_{T_i|\boldsymbol{Y}}(t|\boldsymbol{y}) = F_{\beta_i|\boldsymbol{Y}}\left(\frac{t}{D_f}\right)$, where $\boldsymbol{Y} = (\boldsymbol{Y_1}, \boldsymbol{Y_2}, \cdots, \boldsymbol{Y_n})^t$, in which $\boldsymbol{Y_i} = (Y_{i1}, Y_{i2}, \cdots, Y_{im_i})^t$.

For the inference about the failure time of a unit under test, the estimate of $F_{T_i|\boldsymbol{Y}}(t|\boldsymbol{y})$ is obtained considering the sample of the marginal posterior distribution of β_i, associated with

i-th unit, according to the following scheme:

$$\left(\beta_i^{(1)}, \beta_i^{(2)}, \ \ldots \ , \beta_i^{(u)}\right) \Rightarrow \text{evaluate } \beta_i|\boldsymbol{y} \text{ in } T_i = D_f\beta_i \Rightarrow \left([T_i|\beta_i]^{(1)}, [T_i|\beta_i]^{(2)}, \ \ldots \ , [T_i|\beta_i]^{(u)}\right),$$

where u is the posterior sample size. Then, we have that:

$$\hat{F}_{T_i|\boldsymbol{Y}}(t|\boldsymbol{y}) = \frac{\sum_{j=1}^{u} \mathbb{1}\left\{[T_i|\beta_i]^{(j)} \leq t\right\}}{u}. \tag{1.2}$$

To make inference about the failure time of a future unit, we assume the sample of the posterior distribution of $\boldsymbol{\beta}|\boldsymbol{y}$ as the sample of the posterior distribution of $\beta_{n+1}|\boldsymbol{y}$, as described in Robinson and Crowder [2000]. Thus, the estimate of $F_{T_{n+1}|\boldsymbol{Y}}(t|\boldsymbol{y})$ is obtained according to the following scheme:

$$\begin{pmatrix} \beta_1^{(1)}, & \beta_1^{(2)}, & \ldots, & \beta_1^{(u)} \\ \beta_2^{(1)}, & \beta_2^{(2)}, & \ldots, & \beta_2^{(u)} \\ \vdots & \vdots & \ddots & \vdots \\ \beta_n^{(1)}, & \beta_n^{(2)}, & \ldots, & \beta_n^{(u)} \end{pmatrix} \Rightarrow \text{ evaluate } \beta_i|\boldsymbol{y} \text{ in } T_i = D_f\beta_i$$

$$\Rightarrow \begin{pmatrix} [T_1|\beta_1]^{(1)}, & [T_1|\beta_1]^{(2)}, & \ldots, & [T_1|\beta_1]^{(u)} \\ [T_2|\beta_2]^{(1)}, & [T_2|\beta_2]^{(2)}, & \ldots, & [T_2|\beta_2]^{(u)} \\ \vdots & \vdots & \ddots & \vdots \\ [T_n|\beta_n]^{(1)}, & [T_n|\beta_n]^{(2)}, & \ldots, & [T_n|\beta_n]^{(u)} \end{pmatrix}.$$

Then, we have that:

$$\hat{F}_{T_{n+1}|\boldsymbol{Y}}(t|\boldsymbol{y}) = \frac{\sum_{i}^{n}\sum_{j=1}^{u} \mathbb{1}\left\{[T_i|\beta_i]^{(j)} \leq t\right\}}{nu}. \tag{1.3}$$

In the work of Freitas *et al.* [2009], the train wheel degradation data (Figure 1.1) were analyzed from a classical perspective using the linear degradation model with the analytical, numerical and approximate approaches. Hamada [2005] used the model (1.1) to analyze operating current data on laser emitters (Figure 1.2) considering the Weibull distribution for the random effects. The use of more flexible distributions such as asymmetric and heavy tailed distributions is proposed in Oliveira *et al.* [2017].

The functional form used in the linear degradation model does not allow for structural breaks over time, that is, adaptations to the changes observed in the degradation trajectories are not allowed. Another limitation of this model is the use of the normal distribution for measures of the degradation mechanism. Finally, the linear degradation model given in 1.1 needs to be extended to be applied to datasets that have covariates.

1.4 Contributions to Degradation Models

In this section, we present the contributions of this doctoral dissertation to degradation models, together with the organization of the text. In Chapter 2, we revise the dynamic linear degradation model introduced by Veloso [2018]. This model assumes that the degradation rates vary along time providing a local linear approximation for the true degradation path. To account for limitations in this normal degradation model and motivated by the features presented by the IRLEDs degradation data (Figure 1.3), we extend the model by assuming also an intercept that evolves over time. The introduction of this component in the model brought new properties and resulted in new simulation studies. Chapter 2 is the paper that was published in Reliability Engineering & Systems Safety [Veloso and Loschi, 2021] and contains the details of the extensions mentioned before, together with the analysis of train wheels degradation data (Figure 1.1), laser emitters degradation data (Figure 1.2) and IRLEDs degradation data (Figure 1.3).

In Chapter 3, we introduce a dynamic multivariate gamma model (DMGM) for degradation data. This general degradation path model has a sequential update structure and the use of the gamma distribution for the degradation measurements. The proposed model allows the degradation rate to be decomposed into two components: a static component that measures the effect of unit specific features on the degradation and a dynamic one that quantifies the random effects of the common environment. This strategy produces a reduction in the dimension of the parametric space if compared to other dynamic models. Furthermore, we assume that the degradation measure relates to different functions of time, generating a more flexible model, allowing for the analysis of datasets following different degradation paths structure. The model identifiability is discussed and conditions are stablished for its validity. The relation between the failure time and the model parameters is stablished and we developed a MCMC procedure to estimate the failure time distribution for units under test and a future one. After conducting several simulation studies to evaluate the performance of the proposed model, the DMGM is applied to fatigue crack size data (Figure 1.4) and stress relaxation data (Figure 1.5). This chapter is the paper submitted to an international journal and is currently under revision.

The last contribution to degradation modelling is detailed in Chapter 4. The model developed in the chapter is also a normal dynamic degradation model as assumed in the first model. Extending this first approach, we now assume that the degradation rate is decomposed in the same two components considered in the DMGM but now with an addictive structure. We also assume that the effect that quantifies the specific physical features of the devices is a function of fixed covariates. This approach introduces more flexibility to the analysis since, in some degradation tests, multiple characteristics are observed to understand different aspects of system reliability. Therefore, this chapter details the entire inferential procedure for the proposed model parameters and failure times developed so far. The methodology is still under construction, but we obtained promising results in a brief simulation study and in the application of the scar width degradation data (Figure 1.6).

Finally, Chapter 5 closes this doctoral dissertation with a brief summary of the results

obtained in the previous chapters. In addition, we discuss interesting topics that might motivate our future research.

References

Bae, S. J., & Kvam, P. H. 2004. *A nonlinear random-coefficients model for degradation testing.* Technometrics, 46(4),460-469.

Bagdonavicius, V., Masiulaityte, I & Nikulin, MS. 2010 *Reliability estimation from failure-degradation data with covariates.* Advances in Degradation Modeling, Springer, 275-291, Springer.

Chiao, C.H. & Hamada, M. 1996 *Using degradation data from an experiment to achieve robust reliability for light emitting diodes.* Quality and Reliability Engineering International, 12(2), 89-94.

Doksum, K. A. & Hoyland, A. *Models for variable-stress accelerated life testing experiments based on wiener processes and the inverse gaussian distribution.* Theory of Probability & Its Applications, 37(1), 137-139.

Freitas, M. , Toledo, M. , Colosimo E. & Pires M. 2009 *Using degradation data do assess reliability: A case study on train wheel degradation..* Quality and Reliability Engineering International, 25, 607-629.

Freitas, M. A., Colosimo, E. A., Santos, T. R. & Pires, M. C. 2010 *Reliability assessment using degradation models: Bayesian and classical approaches.* Pesquisa Operacional, 30(1), 194-219.

Hamada, M. 2005 *Using degradation data to assess reliability.* Quality Engineering, 17, 615-620.

Hong, Y., Duan, Y., Meeker, W. Q. and Stanley, D. L. & Gu, X. 2015 *Statistical methods for degradation data with dynamic covariates information and an application to outdoor weathering data.* Technometrics, 57(2), 180-193.

Lawless, J. & Crowder, M. 2004 *Covariates and random effects in a gamma process model with application to degradation and failure.* Technometrics, 10(3), 213-227.

Lu, C. J. & Meeker, W. O. 1993 *Using degradation measures to estimate a time-to-failure distribution.* Technometrics, 35(2), 161-174.

Lu, J. C., Park, J. & Yang, Q. 1997 *Statistical inference of a time-to-failure distribution derived from linear degradation data..* Technometrics, 39(4), 391-400.

Meeker, W. Q. & Escobar, L. A. 1998 *Statistical Methods for Reliability Data*. Wiley Series in Probability and Statistics, First Edition.

Oliveira, R.P. B., Loschi, R. H. & Freitas, M. A. 2017 *Skew-heavy-tailed degradation models: An application to train wheel degradation*. IEEE Transactions on Reliability, 67(1), 129-141.

Pan, R. & Crispin, T. 2011 *A hierarchical modeling approach to accelerated degradation testing data analysis: A case study*. Quality and reliability engineering international, 27(2), 229-237.

Park, C. & Padgett, W. J. 2005 *New cumulative damage models for failure using stochastic processes as initial damage*. IEEE Transactions on Reliability, 54(3), 530-540.

Peng, C. & Tseng, S. *Mis-specification analysis of linear degradation models*. IEEE Transactions on Reliability, 58(3), 444-455.

Peng, C. & Tseng, S. 2013 *Statistical lifetime inference with skew-Wiener linear degradation models*. IEEE Transactions on Reliability, 62(2), 338-350.

Peng, W., Li, Y., Yang, Y., Huang, H. & Zuo, M. J 2014 *Inverse Gaussian process models for degradation analysis: A Bayesian perspective*. Reliability Engineering & System Safety, 130(2), 175-189.

Petris, G., Petrone, S. & Campagnoli, P. 2009 *Dynamic Linear Models with R*. Use R!,Springer New York.

Robinson, M. & Crowder, M. 2000 *Bayesian methods for a growth-curve degradation model with repeated measures*. Lifetime Data Anaysis, 6, 357-374.

Santos, C.C. & Loschi, R.H. 2020 *Semi-parametric Bayesian models for heterogeneous degradation data: An application to Laser data*. Reliability Engineering and System Safety *DOI: 10.1016/j.ress.2020.107038*.

Shiau, H. & Lin, H. 1999 *Analyzing accelerated degradation data by nonparametric regression*. IEEE Transactions on reliability, 48(2), 149-158.

Si, X., Wang, W., Hu, C., Chen, M. & Zhou, D. 2013 *A Wiener-process-based degradation model with a recursive filter algorithm for remaining useful life estimation*. Mechanical Systems and Signal Processing, 35(1), 219-237.

Team, R Core 2017 *R: A language and environment for statistical computing*. Vienna, Austria.

Veloso, G.A. 2018. *Uma abordagem dinâmica para o modelo linear de degradação sob a perspectiva Bayesiana* Dissertação de mestrado, Departamento de Estatística, Universidade Federal de Minas Gerais, Belo Horizonte.

Veloso, G. A., & Loschi, R. H. 2021. *Dynamic linear degradation model: Dealing with heterogeneity in degradation paths*. Reliability Engineering & System Safety, 210, 107446.

Wang, X. 2010 *Wiener processes with random effects for degradation data*. Journal of Multivariate Analysis, 101(2), 340-351.

Wang, Z., Cao, J., Ma, X., Qiu, H., Zhang, Y., Fu, H. & Krishnaswamy, S. 2017 *An improved independent increment process degradation model with bilinear properties*. Arabian Journal for Science and Engineering, 42(7), 2927-2936.

Wang, X. & Xu, D. 2010 *An inverse Gaussian process model for degradation data*. Technometrics, 52(2), 188-197.

West, M. & Harrison, J. 1997 *Bayesian forecasting and dynamic models*. Springer series in statistics, Springer, Second Edition.

Yang, G. 2007 *Life cycle reliability engineering*. John Wiley & Sons.

Ye, Zhi-Sheng & Xie, M. 2015 *Stochastic modelling and analysis of degradation for highly reliable products*. Applied Stochastic Models in Business and Industry, 31(1), 16-32.

Yuan, T & Ji, Y. 2014 *A hierarchical Bayesian degradation model for heterogeneous data*. IEEE Transactions on Reliability, 64(1), 63-70.

Zhou, R., Serban, N. & Gebraeel, N. 2014 *Degradation-based residual life prediction under different environments*. The Annals of Applied Statistics, 8(3), 1671-1689.

Chapter 2

Dynamic Linear Degradation Model: Dealing with Heterogeneity in Degradation Paths

Abstract

General path models are usually considered to model degradation data. Their popularity is mainly due to the simplicity with which these models allow to represent different degradation mechanisms. Such models assume that the functional form of the degradation path is common to all population and, in linear degradation models, it also assumes a time-invariant degradation rates for the units under test. This latter assumption is only reasonable if the devices constantly degrade over time. We introduce a dynamic linear degradation model to approach situations where the degradation paths do not regularly evolve through time. The proposed model assumes that degradation baselines and rates vary along time. This dynamic structure provides a local linear approximation for the true degradation path, which may assume different shapes. Inference for the failure times considers this sequential behavior and is discussed for future and under test units. We run a simulation study to evaluate the proposed model and to compare it to the Weibull linear degradation model. The train wheels, laser emitters and infrared light-emitting diodes datasets are analyzed considering this new methodology. Results show that the proposed model is competitive and an useful approach to model degradation data that assume different shapes for the degradation paths.

Keywords: FFBS, general path models, lifetime, random effects, reliability.

2.1 Introduction

With technological advances, reliability assessments for highly reliable systems based on lifetime data are cumbersome. This is a consequence of the small number of failures that occur during the experiment. System reliability can thus be indirectly assessed through some underlying mechanism that acts producing the failure as, for instance, the system degradation mechanism.

Degradation trials are longitudinal studies where degradation is measured over time in each unit. To take this dependence structure into account, two classes of degradation models have been considered [see Ye and Xie, 2015, for a more detailed discussion]. Stochastic process models assume that the degradation paths are a realization in time of a random process [Park and Padgett, 2005; Park, 2017; Peng and Tseng, 2013; Si et al., 2013; Wang et al., 2017]. Recently, Liu et al. [2020] introduced a gamma process model for systems subject to multiple dependent degradation processes and environmental influence. Copulas are used to model the dependence among the degradation measurements. Gao et al. [2020] propose a Weiner process to model degradation paths that abruptly change along the time. Peng and Cheng [2020] introduced a robust degradation model defining a Student-t degradation process. Stochastic processes models are the natural way to model the degradation caused by environmental factors that change over time. However, as pointed out by Ye and Xie [2015], this class of models usually does not have a clear physical justification being sometimes too complicated to be handled. Therefore, good properties may not be obtained.

Introduced to analyze degradation data by Lu and Meeker [1993a], the general path models account for such dependence by including random effects in the model structure [Hamada, 2005; Lu et al., 1996, 1997]. The random effects represent the features of the individual device and are associated with the degradation rate. In this class of models, the inference is performed in two stages involving a longitudinal data analysis to estimate the degradation model followed by the construction of the relationship between degradation and failure time to estimate the system reliability and any other statistic related to the failure time [Meeker and Escobar, 1998]. Some advantage of the general degradation path models includes the ease interpretation of the parameters in terms of degradation rate, the simplicity in its implementation and, more importantly, it permits flexible structures to incorporate random effects representing the individual devices or unit characteristics. Ye and Xie [2015] point out that the general path degradation models are an abrupt approximation of reality as assume a same regular functional form for the degradation paths of all units.

Formally, the general path model assumes that the accumulated degradation Y_{ij} for the ith unit until the inspection time t_{ij} is given by

$$Y_{ij} = D(t_{ij}; \boldsymbol{\alpha}, \boldsymbol{\beta}_i) + \epsilon_{ij}, \quad i = 1, \ldots, n, j = 1, \ldots, m_i, \tag{2.1}$$

in which $D(\cdot; \boldsymbol{\alpha}, \boldsymbol{\beta})$ denotes the true degradation path, $\boldsymbol{\alpha} = (\alpha_1, \ldots, \alpha_p)^t$ is a $p \times 1$ vector of parameters common to all units and $\boldsymbol{\beta}_i = (\beta_{i1}, \ldots, \beta_{ik})^t$ is the $k \times 1$ vector of random

effects related to unit i. The measurement error ϵ_{ij} at time t_{ij} is assumed to be independent and identically distributed (iid) with mean $E(\epsilon_{ij}) = 0$ and variance $V(\epsilon_{ij}) = \sigma_\epsilon^2$. As commonly assumed, we consider a centered normal distribution with variance σ_ϵ^2 denoted by $\varepsilon_{ij} \sim N(0, \sigma_\epsilon^2)$.

The relationship between time and degradation given by $D(\cdot; \boldsymbol{\alpha}, \boldsymbol{\beta})$ is, in general, inspired by the application problem to be solved and are defined taking into account the empirical analysis of the degradation paths. Most developments in general path models, that is the focus in this paper, assume that $D(t; \boldsymbol{\alpha}, \boldsymbol{\beta})$ is a straight line (see, for instance, the works by Lu and Meeker [1993a], Lu et al. [1996], Hamada [2005], Freitas et al. [2009], Kim [2017] and Oliveira et al. [2018] among many others). Non-linear degradation models are presented in Robinson and Crowder [2000a] and, more recently, in Guida et al. [2015] in which the authors proposed a polynomial type of degradation model with an autoregressive error to accommodate degradation paths of different shapes. Other classes of degradation models include delay time [Wang, 2012], shock [Cha et al, 2017; Ye et al., 2011] and data driven [Peng et al., 2013; Saha et al., 2009; Sotiris et al., 2010] models.

Different data features are introduced into the linear degradation models through the specification of the random effect distributions. Homogeneous populations are usually represented by normal, log-normal and Weibull distributions for the random effects. Under normal and log-normal degradations models [Freitas et al., 2010, 2009], likelihood estimators are easier to be implemented as analytical integration of the likelihood is possible. The Weibull degradation model is discussed by Hamada [2005] from the Bayesian point-of-view. Such a model is appealing as it accommodates different behaviors of the degradation rate. An interesting feature of the Weibull degradation model is the invariance property which assures that the lifetime is also Weibull distributed. This invariance property is also experienced by some models introduced by Oliveira et al. [2018] that assume skew-elliptical and the log-skew-elliptical distributions for the random effects. Such degradation models simultaneously accommodate skewness and heavy-tailed degradation behaviors providing a useful tool to analyze degradation data. Besides fitting skewness and heavy-tailed behavior, the finite mixture [Yuan and Ji, 2015] and the semi-parametric [Santos and Loschi, 2020] degradation models are also appropriate to model heterogeneous population data, that is characterized if the devices work in different conditions over time. In these scenarios, multi-modal behavior can be observed in the degradation or lifetime distributions. Heterogeneous populations are also focused by Xiang et al. [2013] and Lim et al. [2017].

The basic assumption of models that considers a linear structure for $D(\cdot; \boldsymbol{\alpha}, \boldsymbol{\beta})$ is that the degradation of the devices is constant along the time. This implies that the degradation increment $\Delta_{ij} = Y_{ij} - Y_{ij+1},\ j = 1, \ldots, m_i$ for each unit i under test does not vary over time. Such models take this behavior into account by considering that the degradation rate is a function of time-invariant random effects that reflect the unit characteristics. Although some random variation in the observed increments is expected due to the measurement error, tendencies or big variations in Δ_{ij} bring evidence against the linearity assumed for the true degradation path. In the laser emitters dataset previously analyzed by Meeker and Escobar

[1998] and Hamada [2005] (see Figure 2.1), it can be noticed that the degradation increment for some lasers emitters substantially varies along time. That is particularly observed for laser emitter C which degradation increments are big in the initial times and small in the final times and this unit is close to fail.

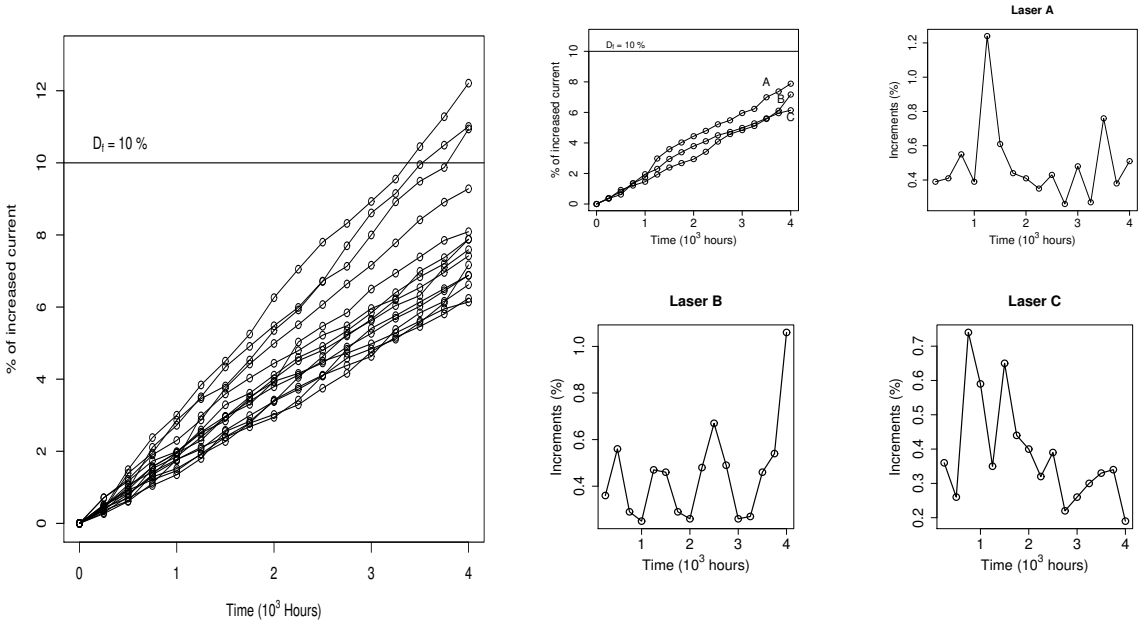

Figure 2.1: Degradation paths of laser emitters data and increments for some units

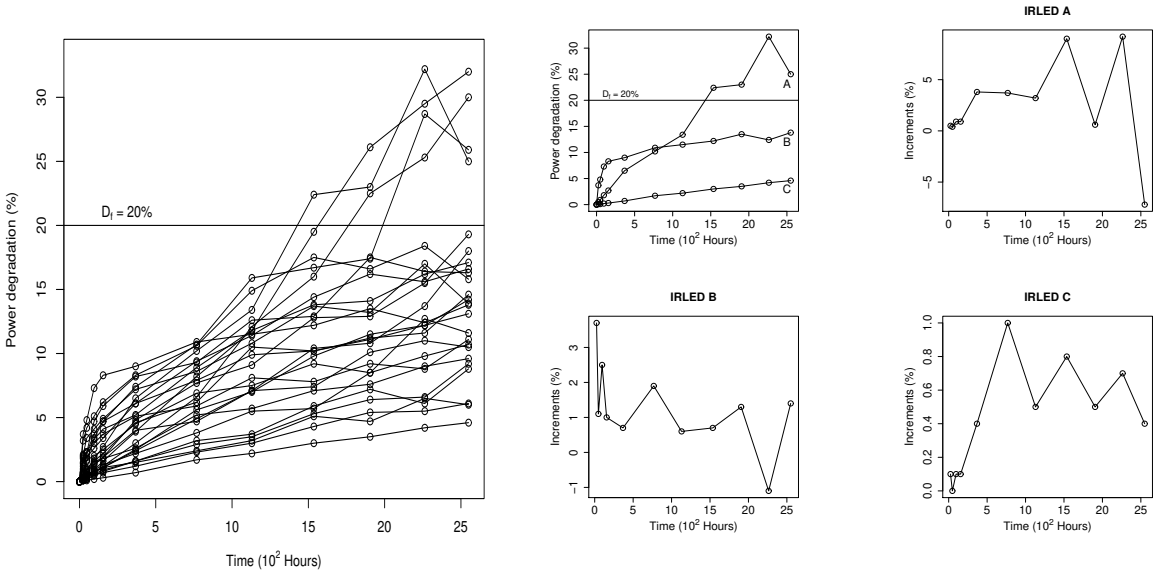

Figure 2.2: Degradation paths of IRLEDs data and increments for some units

Infrared light-emitting diodes (IRLEDs) dataset [Yang, 2007] exhibited in Figure 2.2 is another example where the assumption of the time-invariant degradation rate is not appropriate. Even for the degradation paths presenting linear behavior (e.g, IRLED C, Figure 2.2), the degradation increments vary along time. These data also present another interesting feature

that is not well fitted by a linear degradation model. The degradation paths of some units, IRLED A and IRLED B in Figure 2.2, for instance, may be better approximated by piecewise linear or polynomial structures. A possible approach to account for these data features is the Wiener process model assumed by Wang et al. [2017]. Such variations in the degradation rate along time may be produced by factors that sometimes are beyond our control, such as external factors, measurement errors or system imperfections. If it is possible to obtain information about environmental factors, they can be included into the model as time-dependent covariates and the randomness of the degradation paths would be reduced [Hong et al., 2015]. However, in many cases, information about factors affecting the system degradation is not available as it is the case in laser emitters and IRLEDs datasets.

Another limitation of the general path degradation models is that the functional form of the degradation paths $D(\cdot; \boldsymbol{\alpha}, \boldsymbol{\beta})$ is assumed to be common to all units of the population. This may be a strong assumption in many practical situations. As illustrated in Figure 2.2, the degradation paths for some IRLEDs may be well fitted by a linear structure. However, for some others, the degradation paths are better represented by a logarithmic or a root structures. In studies similar to this one, to assume a fix structure $D(\cdot; \boldsymbol{\alpha}, \boldsymbol{\beta})$ for all population may lead to inappropriate conclusions about the lifetime distribution. One way to overcome this problem is to consider a model with a flexible structure that is able to accommodate different shapes for the degradation paths.

To approach situations where the devices degrade in a heterogeneous way through time, we consider Bayesian models with dynamic structures [Petris et al., 2009; West and Harrison, 1997]. In Section 2, we introduce a dynamic linear degradation model in which the intercept and the slope are time-variant. The assumptions under the proposed model are that both the baseline degradations and the degradation rates are different in each measurement time. It also assumes a Markovian dependence among the degradation rates which relate them in the time. A similar assumption is done for the basal degradations. This time-variant linear structure provides the local piecewise linear approximation of the true degradation path $D(\cdot; \boldsymbol{\alpha}, \boldsymbol{\beta})$ in (2.1), which may assumes different shapes. We assume that units under test are subject to the same dynamic structure which is inherited by the failure time as discussed in Section 3.3. The inference is done under the Bayesian paradigm following West and Harrison [1997] and Petris et al. [2009]. The proposed model is compared to the Weibull linear degradation model through simulation studies (Section 2.4). These models are also fitted to analyze laser emitters and IRLEDs datasets (Section 2.5). The Appendix finish this work bringing an application of the proposed methodology to the train wheels degradation data [Freitas et al., 2009].

2.2 Dynamic linear degradation model

To build a dynamic general path model, we assume that characteristics related to individual units will vary along the time, that is, we consider in (2.1) that the vector of random effects

related to unit i will evolve through time.

Suppose that a sample of n independent units are under test. Let Y_{ij} be the degradation at unit i, $i = 1, 2, \ldots, n$, accumulated until the time j, $j = 1, 2, \ldots, m_i$ and m_i is the number of time intervals in which degradation is measured on unit i. Assume that all units under test are subject to the same dynamic structure which, in a general context, is given by

$$\begin{cases} Y_{ij} = D(t_{ij}; \boldsymbol{\alpha}, \boldsymbol{\theta}_{ij}) + \epsilon_{ij} \\ \boldsymbol{\theta}_{ij} = \boldsymbol{\theta}_{i(j-1)} + \boldsymbol{\epsilon}^*_{ij}, \end{cases} \tag{2.2}$$

where the true degradation path for each unit i is locally piecewise being equal to $D(t_{ij}; \boldsymbol{\alpha}, \boldsymbol{\theta}_{ij})$ in the time interval $(j-1, j)$, $\boldsymbol{\theta}_{ij}$, ϵ_{ij} and $\boldsymbol{\epsilon}^*_{ij}$, respectively, denote the vector of random effects or state vector, the model errors and the vector of evolution errors related to unit i at time j. The model in (2.2) imposes a Markovian relationship among the state vectors related to contiguous time intervals and $\boldsymbol{\theta}_{i0}$ is the state vector for unit i in the initial instant $j = 0$. We assume that the errors ϵ_{ij} and $\boldsymbol{\epsilon}^*_{ij}$, $j = 1, \ldots, m_i$, have both distributions centered at zero with time-invariant covariance matrix.

The function $D(t_{ij}; \boldsymbol{\alpha}, \boldsymbol{\theta}_{ij})$ may assume different shapes. In the following, we focus on situations where $D(t_{ij}; \boldsymbol{\alpha}, \boldsymbol{\theta}_{ij})$ is linear with slope β_{ij} and intercept λ_{ij} and, there are no covariates associated with the degradation mechanism. Hereafter, we omit the vector $\boldsymbol{\alpha}$ to simplify the notation and let $\boldsymbol{\theta}_{ij} = (\lambda_{ij}, \beta_{ij})$. The dynamic linear degradation model is hierarchically represented as

$$\begin{cases} Y_{ij} = \lambda_{ij} + \beta_{ij} t_{ij} + \epsilon_{ij}, \\ \lambda_{ij} = \lambda_{i(j-1)} + \nu_{ij}, \\ \beta_{ij} = \beta_{i(j-1)} + \omega_{ij}, \end{cases} \tag{2.3}$$

where λ_{ij} and β_{ij} denote, respectively, the baseline degradation and the degradation rate for unit i at measurement instant j, ϵ_{ij} is the model error and ν_{ij} and ω_{ij} are the evolution errors. The vector $\boldsymbol{\theta}_{i0} = (\lambda_{i0}, \beta_{i0})^T$ is the state vector for unit i in the initial instant $j = 0$. We assume that, for unit i, the errors ϵ_{ij}, $j = 1, \ldots, m_i$, are independent and identically distributed (iid) with a distribution centered at zero with time-invariant variance. Similar assumptions are considered for the evolution errors ν_{ij} and ω_{ij}. Additionally, we consider that the errors ϵ_{ij}, ν_{ij} and ω_{ij} are independent of each other. Specifically, in the following, we assume that $\epsilon_{ij} \overset{iid}{\sim} N(0, \sigma^2_\epsilon)$, $\nu_{ij} \overset{iid}{\sim} N(0, \sigma^2_\nu)$ and $\omega_{ij} \overset{iid}{\sim} N(0, \sigma^2_\omega)$.

Differently of the usual linear degradation models [Hamada, 2005; Lu and Meeker, 1993a], the model in expression (2.3) assumes that both the degradation baseline and rate for unit i are broken down into state components that evolve along the time. This structure allows to accommodate changes in the degradation increments not arising from the measurement error. Another advantage of assuming that degradation rate β_{ij} and the baseline degradation λ_{ij} randomly evolute through time is that it allows the model to accommodate fluctuations of such

parameters in different directions along the time. Thus, a more flexible model is obtained as it provides a piecewise linear approximations to the the true degradation path in (2.1), accommodating different forms of $D(\cdot;\boldsymbol{\alpha},\boldsymbol{\beta})$. This model also provide good inferences for situations where such parameters do not experience changes along the time as it occurs whenever the degradation paths are all linear. In fact, we recover the usual linear degradation model discussed, for instance, by Lu and Meeker [1993a] and Freitas et al. [2009], if for the jth state vector $\boldsymbol{\theta}_{ij} = (\lambda_{ij}, \beta_{ij})^T$ of unit i, $\lambda_{ij} = 0$ for all i and j and $\beta_{ij} = \beta_i$ for all j.

To facilitate the inference, following West and Harrison [1997], we consider the matrix representation of the proposed model in (2.3). For all $j \geq 1$, assume that

$$\begin{cases} \boldsymbol{Y_j} = \boldsymbol{F_j}\boldsymbol{\theta_j} + \boldsymbol{\epsilon_j} & \boldsymbol{\epsilon_j} \sim N_n(0, \sigma_\epsilon^2 \mathbb{I}_{n\times n}) \\ \boldsymbol{\theta_j} = \boldsymbol{\theta_{j-1}} + \boldsymbol{\gamma_j} & \boldsymbol{\gamma_j} \sim N_{2n}(0, \boldsymbol{\Gamma_j}), \end{cases}$$

where $\boldsymbol{Y_j} = (Y_{1j}, \ldots, Y_{nj})^T \in R^n$ is the n-dimensional column vector composed by the degradation measurement for all units at time j, $\boldsymbol{\theta_j} = (\lambda_{1j}, \ldots, \lambda_{nj}, \beta_{1j}, \ldots, \beta_{nj})^T$, $\boldsymbol{\epsilon_j} = (\epsilon_{1j}, \ldots, \epsilon_{nj})^T$, $\boldsymbol{\gamma_j} = (\nu_{1j}, \ldots, \nu_{nj}, \omega_{1j}, \ldots, \omega_{nj})^T$, $\boldsymbol{\Gamma_j} = \text{diag}\{\sigma_\nu^2, \sigma_\omega^2\} \otimes \mathbb{I}_{n\times n}$ is the $2n \times 2n$ covariance matrix, $\mathbb{I}_{p\times p}$ is the identity matrix of order p and the $n \times 2n$ regression matrix is

$$\boldsymbol{F_j} = \begin{pmatrix} 1 & 0 & \cdots & 0 & t_{1j} & 0 & \cdots & 0 \\ 0 & 1 & \cdots & 0 & 0 & t_{2j} & \cdots & 0 \\ \vdots & \vdots & \ddots & \vdots & \vdots & \vdots & \ddots & \vdots \\ 0 & 0 & \cdots & 1 & 0 & 0 & \cdots & t_{nj} \end{pmatrix}.$$

To complete the model specification, following West et al. [1985], for the state vector of parameters $\boldsymbol{\theta}_j$ at the initial time $j = 0$, we consider $\boldsymbol{\theta}_0 \sim N_{2n}(\boldsymbol{m}_0, \boldsymbol{C}_0)$, where $\boldsymbol{m}_0 \in \mathbb{R}^{2n}$ and $\boldsymbol{C}_0 \in \mathbb{R}^{2n} \times \mathbb{R}^{2n}$ are, respectively, the mean vector and the covariance matrix specified based on the available prior information. The prior distribution for θ_0 should reveal the initial knowledge about the degradation process in the population under test. Specifically, it should represent both the initial expectation about baseline degradation and the degradation rate for units in this population. Assuming the normal prior distribution for θ_0, there is a gain in inferential procedure since we obtain a exact inference. However, other prior specifications may be assumed if they better represent the prior knowledge about θ_0. For the variances, we assume $\psi_\epsilon = \sigma_\epsilon^{-2} \sim \text{Gamma}(a_1, b_1)$, $\psi_\nu = \sigma_\nu^{-2} \sim \text{Gamma}(a_2, b_2)$ and $\psi_\omega = \sigma_\omega^{-2} \sim \text{Gamma}(a_3, b_3)$, where $a_l > 0$ and $b_l > 0$, $l = 1, \ldots, 3$.

2.2.1 Posterior inference

To perform inference in dynamic models we must combine two operations: the evolution to build the prior distribution for $\boldsymbol{\theta}_j$ given the available degradation data until time $t-1$ and the updating to incorporate the degradation measured at time j to obtain the posterior distribution of $\boldsymbol{\theta}_j$.

Let $\boldsymbol{y_j} = (y_{1j}, \ldots, y_{nj})^T \in R^n$. Denote by $\boldsymbol{y_{1:J}} = (\boldsymbol{y_1}, \boldsymbol{y_2}, \ldots \boldsymbol{y_J})$ and $\boldsymbol{\theta_{0:J}} = (\boldsymbol{\theta}_0, \boldsymbol{\theta}_1, \ldots, \boldsymbol{\theta}_J)$, respectively, the degradation measurements and the states matrices for the n units under test and all time intervals, where $J = \max\{m_i,\ i = 1, \cdots, n\}$. If the data are unbalanced, some imputation methods must be used to replace the unobserved values. For the proposed model given in (2.3), we input the missing data using the approach proposed by Petris et al. [2009].

As we assume that $\epsilon_{ij} \overset{iid}{\sim} N(0, \sigma_\epsilon^2)$, given $\boldsymbol{\theta_{0:J}}$, ψ_ϵ, ψ_ν and ψ_ω, it follows that Y_{ij} are independent having a normal distribution with mean $\lambda_{ij} + \beta_{ij} t_{ij}$ and variance σ_ϵ^2. Consequently, the likelihood function is given by

$$\begin{aligned} \pi(\boldsymbol{y_{1:J}}|\boldsymbol{\theta_{0:J}}, \psi_\epsilon, \psi_\nu, \psi_\omega) &= \prod_{j=1}^{J}\prod_{i=1}^{n} \pi(y_{ij}|\lambda_{ij}, \beta_{ij}, \psi_\epsilon) \\ &= \left(\sqrt{\frac{\psi_\epsilon}{2\pi}}\right)^{Jn} \exp\left\{-\frac{\psi_\epsilon}{2}\sum_{j=1}^{J}\sum_{i=1}^{n}(y_{ij} - (\lambda_{ij} + \beta_{ij} t_{ij}))^2\right\}. \quad (2.4) \end{aligned}$$

To sample from the posterior distributions of $\boldsymbol{\theta_{0:J}}$, ψ_ϵ, ψ_ν and ψ_ω, we mix the likelihood function in (2.4) with the prior distributions for the parameters θ_0, ψ_ϵ, ψ_ν and ψ_ω that was previously mentioned and we use the following Markov chain Monte Carlo (MCMC) scheme. Samples of state parameter $\boldsymbol{\theta_{0:J}}$ are generated from the posterior full conditional distribution

$$\pi\left(\boldsymbol{\theta_{0:J}}|\psi_\epsilon, \psi_\nu, \psi_\omega, \boldsymbol{y_{1:J}}\right) = \pi(\boldsymbol{\theta_J}|\psi_\epsilon, \psi_\nu, \psi_\omega, \boldsymbol{y_{1:J}}) \prod_{j=0}^{J-1} \pi(\boldsymbol{\theta}_j|\boldsymbol{\theta}_{j+1:J}, \psi_\epsilon, \psi_\nu, \psi_\omega, \boldsymbol{y_{1:J}}), \quad (2.5)$$

where $\pi(\boldsymbol{\theta_J}|\psi_\epsilon, \psi_\nu, \psi_\omega, \boldsymbol{y_{1:J}})$ is the filtering distribution of the state vector of parameters $\boldsymbol{\theta_J}$ related to the last time interval J given in expression (2.6) and $\pi(\boldsymbol{\theta}_j|\boldsymbol{\theta}_{j+1:J}, \psi_\epsilon, \psi_\nu, \psi_\omega, \boldsymbol{y_{1:J}})$ is given in equation (2.7).

The filtering distribution is the inference for the state vector $\boldsymbol{\theta_J}$, based on the observations up to time interval J. For all $j = 1, \ldots, J$, it follows that

$$\pi(\boldsymbol{\theta_j}|\psi_\epsilon, \psi_\nu, \psi_\omega, \boldsymbol{y_{1:j}}) \sim N_{2n}(\boldsymbol{m_j}, \boldsymbol{C_j}), \quad (2.6)$$

where $\boldsymbol{m_j} = \boldsymbol{m_{j-1}} + \boldsymbol{R_j F_j^T Q_j^{-1}}(\boldsymbol{Y_j} - \boldsymbol{F_j m_j})$, $\boldsymbol{C_j} = \boldsymbol{R_j} - \boldsymbol{R_j F_j^T}[\boldsymbol{F_j R_j F_j'} + \boldsymbol{V_j}]^{-1}\boldsymbol{F_j R_j}$ and $\boldsymbol{R_j} = \boldsymbol{C_{j-1}} + \boldsymbol{\Gamma_j}$.

We sample from the posterior of the dynamic parameters considering the forward filtering backward sampling (FFBS) discussed by Carter and Kohn [1994] [see also Frühwirth-Schnatter, 1994; Shephard, 1994]. When using the normal distribution for the measures of the degradation mechanism and for the state components, the FFBS is the widely used approach for filtering. This method provides exact inference and is essentially the simulation of the smoothing recursions. Firstly, we generate $\boldsymbol{\theta_J}$ from its filtering distribution $\pi(\boldsymbol{\theta_J}|\psi_\epsilon, \psi_\nu, \psi_\omega, \boldsymbol{y_{1:J}}) \sim N_{2n}(m_J, C_J)$ and then, recursively, we draw samples of $\boldsymbol{\theta_j}$ from

$$\pi(\boldsymbol{\theta}_j|\boldsymbol{\theta}_{j+1:J}, \psi_\epsilon, \psi_\nu, \psi_\omega, \boldsymbol{y_{1:J}}) \sim N_{2n}(\boldsymbol{m_j} + \boldsymbol{C_j R_{j+1}^{-1}}(\boldsymbol{\theta_{j+1}} - \boldsymbol{m_{j+1}}), \boldsymbol{C_j} - \boldsymbol{C_j R_{j+1}^{-1} C_j}), \quad (2.7)$$

for $j = \mathbf{J}-1, \mathbf{J}-2, \ldots, 0$. Samples of ψ_ϵ, ψ_ν and ψ_ω are generated via Gibbs sampler assuming the distributions in the following.

(i) The posterior full conditional distribution of ψ_ϵ is

$$\begin{aligned}\pi(\psi_\epsilon|\psi_\nu,\psi_\omega,\boldsymbol{\theta_{0:J}},\boldsymbol{y_{1:J}}) &\propto \pi(\boldsymbol{y_{1:J}}|\boldsymbol{\theta_{0:J}},\psi_\epsilon,\psi_\nu,\psi_\omega)\pi(\psi_\epsilon)\\ &\propto \psi_\epsilon^{\frac{Jn}{2}}\exp\left\{-\frac{\psi_\epsilon}{2}\sum_{j=1}^{J}\sum_{i=1}^{n}(y_{ij}-(\lambda_{ij}+\beta_{ij}t_{ij}))^2\right\}\psi_\epsilon^{a_1-1}exp\left\{-b_1\psi_\epsilon\right\},\end{aligned}$$

that is, $\psi_\epsilon|\psi_\nu,\psi_\omega,\boldsymbol{\theta_{0:J}},\boldsymbol{y_{1:J}} \sim \text{Gamma}(a_1+Jn/2, b_1+1/2\sum_{i=1}^{n}\sum_{j=1}^{J}(y_{ij}-\lambda_{ij}-\beta_{ij}t_{ij})^2)$.

(ii) The posterior full conditional distribution of ψ_ν is given by

$$\begin{aligned}\pi(\psi_\nu|\psi_\epsilon,\psi_\omega,\boldsymbol{\theta_{0:J}},\boldsymbol{y_{1:J}}) &\propto \prod_{j=1}^{J}\prod_{i=1}^{n}\pi(\lambda_{ij}|\lambda_{i(j-1)},\psi_\nu)\pi(\psi_\nu)\\ &\propto \psi_\nu^{\frac{Jn}{2}}\exp\left\{-\frac{\psi_\nu}{2}\sum_{j=1}^{J}\sum_{i=1}^{n}(\lambda_{ij}-\lambda_{i(j-1)})^2\right\}\psi_\nu^{a_2-1}exp\left\{-b_2\psi_\nu\right\}.\end{aligned}$$

Consequently, $\psi_\nu|\psi_\epsilon,\psi_\omega,\boldsymbol{\theta_{0:J}},\boldsymbol{y_{1:J}} \sim \text{Gamma}(a_2+Jn/2, b_2+1/2\sum_{i=1}^{n}\sum_{j=1}^{J}\left(\lambda_{ij}-\lambda_{i(j-1)}\right)^2)$.

(iii) The posterior full conditional distribution of ψ_ν is given by

$$\begin{aligned}\pi(\psi_\omega|\psi_\epsilon,\psi_\nu,\boldsymbol{\theta_{0:J}},\boldsymbol{y_{1:J}}) &\propto \prod_{j=1}^{J}\prod_{i=1}^{n}\pi(\beta_{ij}|\beta_{i(j-1)},\psi_\omega)\pi(\psi_\omega)\\ &\propto \psi_\omega^{\frac{Jn}{2}}\exp\left\{-\frac{\psi_\omega}{2}\sum_{j=1}^{J}\sum_{i=1}^{n}(\beta_{ij}-\beta_{i(j-1)})^2\right\}\psi_\omega^{a_3-1}exp\left\{-b_3\psi_\omega\right\},\end{aligned}$$

thus, it follows that $\psi_\omega|\psi_\epsilon,\psi_\nu,\boldsymbol{\theta_{0:J}},\boldsymbol{y_{1:J}} \sim \text{Gamma}(a_3+Jn/2, b_3+1/2\sum_{i=1}^{n}\sum_{j=1}^{J}\left(\beta_{ij}-\beta_{i(j-1)}\right)^2)$.

The proposed model is implemented using the software *R* [R Development Core Team, 2018]. The FFBS step is performed using the *dlm* package [Petris et al., 2009].The R code is available upon request via email from the authors.

2.3 Inference for failure time

In degradation experiments, as the system reliability is indirectly accessed, a satisfactory analysis of it is attained even if the devices under test do no fail during the experiment. To determine the system reliability it is assumed that a failure occurs if the degradation path exceeds a certain predefined threshold D_f. The relationship between degradation and time, defined by the specified model, is thus taken into account to obtain the failure time distribution. The degradation threshold D_f is usually specified using the prior knowledge of the experts.

A sequential analysis of the degradation paths is performed if the dynamic linear degradation model in equation (2.3) is assumed. This sequential feature must also be considered whenever inferring the failure time of the units. We suppose that some units under test fail during the experiment and others fail after the maximum measurement instant J. Assume that a unit i fails at the time interval which lower bound is γ_i. If unit i do not fail during the experiment the bound $\gamma_i = J$, otherwise, $\gamma_i < J$. From the relationship between time and degradation given by the model in expression (2.3), the time to failure for the ith unit is given by $T_i = (D_f - \lambda_{i\gamma_i})\beta_{i\gamma_i}^{-1}$, where $\lambda_{i\gamma_i}$ and $\beta_{i\gamma_i}$ are the state components prior to failure for unit i. For units that do not fail during the experiment, inference for the failure time will consider the state vector related to the last time interval we measured the degradation [Petris et al., 2009]. Comparing the proposed model with the linear degradation model, both predict the non-observed degradation measurements, after time interval J, from a straight line. However, there is a subtle difference between the models. While under the linear degradation model this prediction is based on a non-local straight line, under the proposed model, it is based on the local linear approximation related to the last time interval. Consequently, under the proposed model, the posterior predictive cumulative distribution function (cdf) of the failure time of unit i is

$$F_{T_i|\boldsymbol{Y_{i:J}}}\left(t|\boldsymbol{y_{i:J}}\right) = 1 - \int_{-\infty}^{\infty} F_{\beta_{i\gamma_i}|\boldsymbol{y_{1:J}}}\left((D_f - u)t^{-1}|\boldsymbol{y_{1:J}}\right) f_{\lambda_{i\gamma_i}|\boldsymbol{y_{1:J}}}\left(u|\boldsymbol{y_{1:J}}\right) du, \tag{2.8}$$

where $F_{\beta_{i\gamma_i}|\boldsymbol{y_{1:J}}}(\cdot)$ and $f_{\lambda_{i\gamma_i}|\boldsymbol{y_{1:J}}}(\cdot)$ respectively denote the cdf of $\beta_{i\gamma_i}$ and the probability density function (pdf) of $\lambda_{i\gamma_i}$, given the observations $\boldsymbol{y_{1:J}}$.

We obtain a posterior sampling for the failure time of unit i as follows. Having available the posterior sample $\boldsymbol{\theta}_{i\gamma_i}^{(l)} = (\lambda_{i\gamma_i}^{(l)}, \beta_{i\gamma_i}^{(l)})^T$ of the degradation model parameters $\boldsymbol{\theta}_{i\gamma_i} = (\lambda_{i\gamma_i}, \beta_{i\gamma_i})^T$, we calculate $T_i^{(l)} = (D_f - \lambda_{i\gamma_i}^{(l)})(\beta_{i\gamma_i}^{(l)})^{-1}$, for $l = 1, \ldots L$. This is made by considering the following scheme

$$\begin{pmatrix} \lambda_{i\gamma_i}^{(1)}, & \lambda_{i\gamma_i}^{(2)}, & \ldots, & \lambda_{i\gamma_i}^{(L)} \\ \beta_{i\gamma_i}^{(1)}, & \beta_{i\gamma_i}^{(2)}, & \ldots, & \beta_{i\gamma_i}^{(L)} \end{pmatrix} \Rightarrow \text{ evaluate } \boldsymbol{\theta}_{i\gamma_i}|\boldsymbol{y} \text{ in } T_i = \frac{D_f - \lambda_{i\gamma_i}}{\beta_{i\gamma_i}} \Rightarrow \left(T_i|\boldsymbol{\theta}_{i\gamma_i}^{(1)}, T_i|\boldsymbol{\theta}_{i\gamma_i}^{(2)}, \ \ldots \ , T_i|\boldsymbol{\theta}_{i\gamma_i}^{(L)}\right)$$

The posterior predictive cdf of T_i evaluated at time t is approximated by

$$\hat{F}_{T_i|\boldsymbol{Y_{1:J}}}(t|\boldsymbol{y_{1:J}}) = \sum_{l=1}^{L} \mathbb{1}\{T_i^{(l)} \leq t\}/L.$$

.

In many practical situations, the remaining useful life (RUL) for units under test is of most interest. The RUL for a unit i under test that has been monitored until inspection time t_{im_i} is given by $RUL_i = E(T_i - t_{im_i}|T_i > t_{im_i})$. Under the Bayesian paradigm, the estimate for the RUL of a unit under i test, that has not failed, is given by

$$\overline{RUL_i} = \sum_{l=1}^{L} \frac{T_i^{(l)} - t_{im_i}}{L}$$

To calculate the posterior predictive cdf for the failure time T_{n+1} of a new device, we assume that T_{n+1} has the same distribution as the failure times T_i of the units under test. Following Robinson and Crowder [2000a], we assume that a posterior sample of $\boldsymbol{\theta}_{(n+1)j}$ is obtained sampling from the posterior distributions of the parameters $\boldsymbol{\theta}_{i\gamma_i}$, $i = 1, \ldots, n$, associated with the time intervals when unit i experienced the failure. Thus, to estimate $F_{T_{n+1}|\boldsymbol{Y_{1:J}}}(t|\boldsymbol{y_{1:J}})$ at time t we consider the total posterior sample of $\boldsymbol{\theta_{0:J}}$ and, for each sample $\boldsymbol{\theta}_{ij}^{(l)} = (\lambda_{i\gamma_i}^{(l)}, \beta_{i\gamma_i}^{(l)})^T$, we calculate $T_{n+1}^{(l)} = (D_f - \lambda_{i\gamma_i}^{(l)})(\beta_{i\gamma_i}^{(l)})^{-1}$, $i = 1, \ldots, n$, $l = 1, \ldots, L$, as follows

$$\begin{pmatrix} \lambda_{1\gamma_1}^{(1)} & \lambda_{1\gamma_1}^{(2)} & \ldots & \lambda_{1\gamma_1}^{(L)} \\ \beta_{1\gamma_1}^{(1)} & \beta_{1\gamma_1}^{(2)} & \ldots & \beta_{1\gamma_1}^{(L)} \\ \vdots & \vdots & \ddots & \vdots \\ \lambda_{n\gamma_n}^{(1)} & \lambda_{n\gamma_n}^{(2)} & \ldots & \lambda_{n\gamma_n}^{(L)} \\ \beta_{n\gamma_n}^{(1)} & \beta_{n\gamma_n}^{(2)} & \ldots & \beta_{n\gamma_n}^{(L)} \end{pmatrix} \Rightarrow \text{ evaluate } \boldsymbol{\theta}_{i\gamma_i}|\boldsymbol{y} \text{ in } T_{n+1} = \frac{D_f - \lambda_{i\gamma_i}}{\beta_{i\gamma_i}}$$

$$\Rightarrow \begin{pmatrix} T_i|\boldsymbol{\theta}_{1\gamma_1}^{(1)}, & T_i|\boldsymbol{\theta}_{1\gamma_1}^{(2)}, & \ldots, & T_i|\boldsymbol{\theta}_{1\gamma_1}^{(L)} \\ T_i|\boldsymbol{\theta}_{2\gamma_2}^{(1)}, & T_i|\boldsymbol{\theta}_{2\gamma_2}^{(2)}, & \ldots, & T_i|\boldsymbol{\theta}_{2\gamma_2}^{(L)} \\ \vdots & \vdots & \ddots & \vdots \\ T_i|\boldsymbol{\theta}_{n\gamma_n}^{(1)}, & T_i|\boldsymbol{\theta}_{n\gamma_n}^{(2)}, & \ldots, & T_i|\boldsymbol{\theta}_{n\gamma_n}^{(L)} \end{pmatrix}$$

The posterior estimate for the predictive cdf of T_{n+1} evaluated at time t is given by

$$\hat{F}_{T_{n+1}|\boldsymbol{Y_{1:J}}}(t|\boldsymbol{y_{1:J}}) = \sum_{l=1}^{L} \sum_{i=1}^{n} \mathbb{1}\left\{T_{n+1}^{(l)} \leq t\right\}/nL.$$

2.4 Simulation studies

We run a Monte Carlo study to evaluate the performance in predicting failures of the proposed dynamic linear degradation (DLD) model as well as to compare it to the well-known Weibull linear degradation (WLD) model [Hamada, 2005]. To mimic the real datasets to be analyzed in Section 2.5, we assume a balanced experiment in which the degradation is simultaneously measured in all n devices under test in m ($m = 10$ or 20) equally spaced times. To define the failure times, we set up a threshold of $D_f = 10$. Data are generated from linear models without intercept and assuming different distributions for the degradation rate β_i. In the first scenario, we assume a time-invariant and Weibull distributed degradation rate (WLD model). In the second simulation study, datasets are generated from the proposed model (DLD model). In both scenarios, the errors ϵ_{ij} are iid with normal distribution and time invariant-variance σ_ϵ^2. In the third scenario, our goal is to show the flexibility of our proposed model to analyze degradation data whenever the degradation paths have different shapes. Part of the degradation paths are generated from a linear model and the other part is generated from a non-linear degradation model. In this case, the assumptions on which the general path models are based are violated. A total of $R = 100$ replications is generated in each scenario.

To analyze the data, in Simulations I and II, DLD and WLD models without intercept are fitted. In Simulation III, data are also analyzed by fitting the DLD model with intercept. In all cases, we assume a flat prior distribution for the error precision by eliciting $\psi_\epsilon = \sigma_\epsilon^{-2} \sim \text{Gamma}(0.01, 0.01)$. In WLD model, *a priori*, we assume that $\kappa \sim \text{Gamma}(0.01, 0.01)$ and $\phi \sim \text{Gamma}(0.01, 0.01)$, where κ and ϕ are the parameters of the Weibull distribution.. To fit the proposed model, we assign $\boldsymbol{m}_0 = \mathbf{0} \in \mathbb{R}^d$ and $\boldsymbol{C}_0 = 1000 I_d$, where I_d denotes the identity matrix of order d. For DLD models with and without random degradation intercepts, d is given by $2n$ and n, respectively. We assume a flat prior distribution for the precisions parameters of the evolution errors ω_{ij} and ν_{ij} by eliciting $\psi_\omega \sim \text{Gamma}(0.01, 0.01)$ and $\psi_\nu \sim \text{Gamma}(0.01, 0.01)$..

The models are fitted collecting 1000 MCMC iterates after discarding the first 500 as the burn-in period and thinning by 10. For the DLD model with random degradation baseline, the thinning used is 30. Such MCMC parameters are also assumed in the case studies discussed in Section 2.5. The failure time for the ith unit under test, related to the rth replication, T_{ir}, is estimated through the posterior mean $\hat{T_{ir}}$ of the predictive distribution. To evaluate the model fitting quality, we consider the bias and the mean squared error (MSE) given, respectively, by $\text{Bias} = \frac{1}{nR}\sum_{i=1}^{n}\sum_{r=1}^{R}\left(T_{ir} - \hat{T_{ir}}\right)$ and $\text{MSE} = \frac{1}{nR}\sum_{i=1}^{n}\sum_{r=1}^{R}\left(T_{ir} - \hat{T_{ir}}\right)^2$.

2.4.1 Simulation I: Analyzing Weibull data

In this scenario, data are generated from the model $Y_{ij} = \beta_i t_{ij} + \epsilon_{ij}$ assuming $\epsilon_{ij} \overset{iid}{\sim} N(0, \sigma_\epsilon^2 = 0.2^2)$ and $\beta_i \overset{iid}{\sim} \text{Weibull}(\kappa = 4.5, \lambda = 2.2)$, $i = 1, \ldots, n$ and $j = 1, \ldots, m$. To evaluate the effect of the number of degradation paths in the posterior estimates, we generate the data assuming $n = 15$ and $n = 30$. The true failure time for the ith unit T_i is given by $D_f \beta_i^{-1}$, which is known from the beginning in non-dynamic models. Figure 2.3 shows the degradation paths for one of the generated data sets in which we assume $n = 15$. It also shows how samples with $m = 10$ and $m = 20$ measurements are obtained. In this scenario, the observed degradation paths present a random fluctuation around a straight line which is expected whenever the true degradation path is linear.

Table 2.1 shows the bias and MSE for the posterior mean estimates of the failure times. It also shows the covering percentage of the 95% highest posterior density (HPD) intervals of the failure times for the units under test provided by WLD and DLD models. On average, both models overestimate the true failure times of the units under test. The exception occurs if we fit the Weibull model to a scenario where there are $n = 30$ units under test and the degradation was measured in $m = 20$ different time intervals. Biases and MSE are smaller if the Weibull model is fitted. However, the coverage percentage of HPD intervals is below 95% under the Weibull model. Doubling the number of degradation measurements by letting $m = 20$, there is an improvement in both models' performance with a great reduction in the bias and the MSE. In these cases, the proposed and Weibull degradation models produce comparable point estimates for the failure time. The impact in the accuracy of failure time estimates is less evident if we increase the number n of sample units under test. Although there is a bias reduction, the

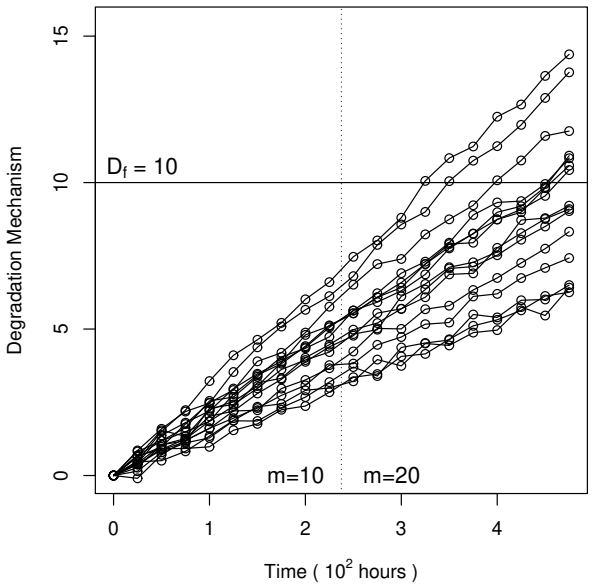

Figure 2.3: Example of the generated data with n = 15 units and how samples with m = 10 and m = 20 measurements are obtained, Weibull scenario.

MSE increases in almost all cases. These findings suggest that the increase in the number of degradation measurements should be preferred instead of increasing the number of sample units under test to obtain better estimates in degradation tests.

Table 2.1: Bias and MSE for the posterior means and the coverage percentage (CP) of the 95% HPD intervals for the failure time for units under test by fitting WLD and DLD models, Simulation I.

		n=15			n=30		
m	Model	Bias	MSE	CP	Bias	MSE	CP
10	WLD	-0.004	0.042	93.013	-0.001	0.043	93.527
	DLD	-0.021	0.066	96.707	-0.016	0.087	97.087
20	WLD	-0.002	0.004	93.400	0.001	0.006	94.280
	DLD	-0.004	0.014	97.333	-0.003	0.014	98.053

2.4.2 Simulation II: Normal data under dynamic structure

In the second scenario, data are generated from the dynamic model in (2.3) assuming $\lambda_{ij} = 0$ for all i and j. We assume $\sigma_\epsilon^2 = 0.12^2$ and $\beta_{0i} \overset{iid}{\sim} \mathrm{N}(2.2, \sigma_\epsilon^2 = 0.45^2)$. To evaluate the effect of the evolution variability in the posterior estimates, we consider $\sigma_\omega^2 = 0.01^2$, 0.02^2, 0.03^2, 0.04^2 and 0.05^2. The degradation paths are sequentially generated assuming $n = 15$ until they reach the degradation threshold. As the degradation measurements for a given unit are subject to both the observational ϵ_{ij} and the evolution ω_{ij} errors, more unstable degradation paths are expected. Besides, differently from what is obtained for Weibull data, the initial degradation rates do not bring direct information about the true failure time. To define the true failure time T_i for unit i, we consider the degradation rate β_{ik_i} in the time interval

immediately before path i reaches the threshold D_f. Thus, the true failure time T_i for unit i is defined as $T_i = D_f \beta_{ik_i}^{-1}$.

Figure 2.4 presents the degradation paths for a simulated data set considering $\sigma_\omega^2 = 0.05^2$. As expected, in this scenario, at least for part of the units, the behavior of the degradation paths changes along the time pointing out that the degradation rates for such units can not be constant as assumed in linear models. In this scenario, it will be more difficult to correctly estimate the real failure of these units.

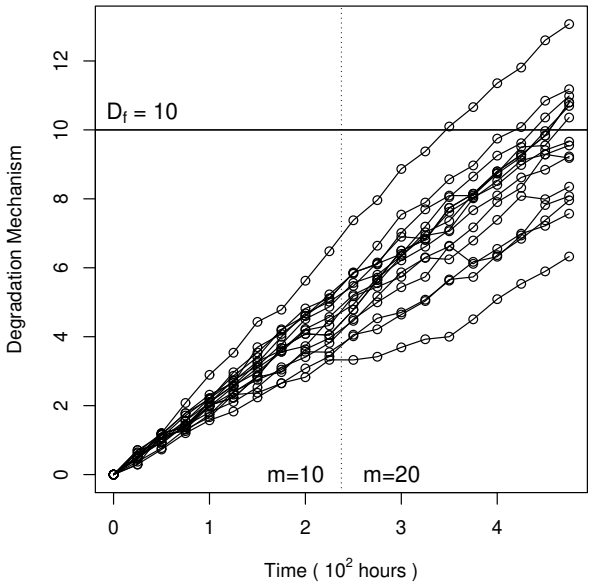

Figure 2.4: Example of the generated data with $\sigma_\omega^2 = 0.05^2$ and how samples with $m = 10$ and $m = 20$ measurements are obtained, dynamic normal data.

Table 2.2 shows some summaries we obtain by fitting WLD and DLD models to analyze these data. On average, the true failure times for the units under test are underestimated by both models. In general, the DLD model performs better producing less biased estimates with smaller MSE. As in the previous scenario, the posterior estimates are improved if we consider a high number o degradation measurements ($m = 20$) for each device. By assuming a high number of degradation measurements by units, estimates experience a reduction in both, the bias and the variability, and become more precise.

The evolution variance σ_w^2 impacts the quality of the posterior estimates. The greater the evolution variability, the worse the posterior estimates for the failure time are. It is worth mention, the poor performance of WLD for large values of σ_ω^2. For instance, for samples with $m = 20$ and $\sigma_\omega^2 \geq 0.03$, the coverage percentage of the HPD interval with probability 0.95 is higher than 74% if we fit the DLD model, and is smaller than 50% if data are analyzed using the WLD model. In conclusion, by fitting the WLD model, which assumes that the degradation rates do not evolute through time, we poorly estimate the failure time for the majority of the generated samples possibly leading to wrong decisions about the system reliability.

Table 2.2: Bias and MSE for the posterior means and the coverage percentage (CP) of the 95% HPD intervals for the failure time for units under test by fitting WLD and DLD models, Simulation II.

Scenario	m	Model	Bias	MSE	CP
$\sigma_w^2 = 0.01^2$	10	WLD	0.004	0.016	78.133
		DLD	0.001	0.019	89.467
	20	WLD	0.003	0.007	72.667
		DLD	-0.001	0.007	92.200
$\sigma_w^2 = 0.02^2$	10	WLD	0.023	0.104	54.680
		DLD	0.020	0.106	69.764
	20	WLD	0.021	0.067	53.401
		DLD	0.011	0.062	84.714
$\sigma_w^2 = 0.03^2$	10	WLD	0.043	0.160	43.333
		DLD	0.036	0.165	58.733
	20	WLD	0.036	0.094	46.067
		DLD	0.018	0.077	81.467
$\sigma_w^2 = 0.04^2$	10	WLD	0.063	0.323	35.102
		DLD	0.050	0.317	48.707
	20	WLD	0.056	0.191	41.293
		DLD	0.037	0.152	78.095
$\sigma_w^2 = 0.05^2$	10	WLD	0.145	0.867	31.271
		DLD	0.130	0.840	41.10
	20	WLD	0.120	0.582	39.381
		DLD	0.080	0.467	74.502

2.4.3 Simulation III: Heterogeneous degradation paths

This scenario was inspired by the IRLEDs degradation data presented in Figure 2.2, in which the units degradation paths do not assume the same functional form. The goal is to show the flexibility of the proposed model to analyze heterogeneous population where the degradation paths assume different shapes which can be linear non-linear.

The linear paths are generated from the model $Y_{ij} = \beta_i t_{ij} + \epsilon_{ij}$ where $\beta_i \overset{iid}{\sim}$ Weibull($\kappa = 5, \lambda = 2$), $i = 1, \ldots, n$ and $j = 1, \ldots, m$. For the degradation paths that do not have linear trajectories, the degradation paths are generated from the model $Y_{ij} = \beta_i \sqrt{t_{ij}} + \epsilon_{ij}$ where $\beta_i \overset{iid}{\sim}$ Weibull($\kappa = 10, \lambda = 5$), $i = 1, \ldots, n$ and $j = 1, \ldots, m$. In both cases, the observational errors ϵ_{ij} have a centered normal distribution and two values are assumed for the variance, $\sigma_\epsilon^2 = 0.2^2$ and 0.5^2. The true failure time for the ith unit T_i is given by $D_f \beta_i^{-1}$ and $(D_f \beta_i^{-1})^2$ for linear and non-linear degradation paths, respectively. The number of linear degradation paths n_l and non-linear degradation paths n_s are chosen such that $n_l + n_s = n = 15$. We consider $m = 20$ degradation measurements. Figure 2.5 presents the degradation paths for a simulated data set considering $\sigma_\epsilon^2 = 0.2^2$, $n_l = 10$ and $n_s = 5$.

To analyze the data, we fit the linear Weibull degradation model (W) and the dynamic linear degradation models with (DI) and without (D) dynamic baseline degradation. Table 2.3 shows that, in general, all models produce better estimates for the failure time in scenarios with few units presenting non-linear behavior. Both dynamic degradation models presented good performance and outperform the Weibull model in all scenarios showing their flexibility to model degradation data coming from heterogeneous populations. The DI model provide less biased estimates for the failure time in all scenarios and the higher CP for the HPD with

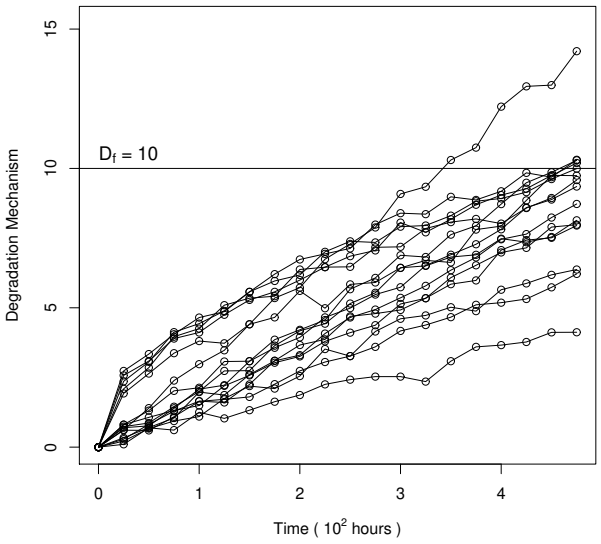

Figure 2.5: Example of a generated data with $\sigma_\epsilon^2 = 0.2^2$, $n_l = 10$ and $n_s = 5$.

probability 0.95 whenever there is more variability in the model error ($\sigma_\epsilon^2 = 0.5^2$). Although part of the data set favors the Weibull linear degradation model, Table 2.3 shows that it has the poorer performance providing more biased estimates, the highest MSE and the worse CP for the HPD with probability 0.95 in all scenarios. Its performance is even worse in scenarios with few units presenting linear behavior.

Table 2.3: Bias and MSE for the posterior means and the coverage percentage (CP) of the 95% HPD intervals for the failure time for units under test by fitting the linear Weibull degradation model (W) and dynamic linear degradation models with (DI) and without (D) dynamic degradation baseline Simulation III.

		$\sigma_\epsilon^2 = 0.2^2$			$\sigma_\epsilon^2 = 0.5^2$		
	Model	Bias	MSE	CP	Bias	MSE	CP
$n_l = 10$ and $n_s = 5$	W	0.249	0.421	73.467	0.262	0.523	75.800
	D	0.082	0.183	91.000	0.082	0.343	89.733
	DI	0.054	0.152	84.533	0.057	0.222	92.667
$n_l = 5$ and $n_s = 10$	W	0.515	0.918	54.133	0.472	0.795	56.200
	D	0.184	0.348	86.400	0.137	0.385	85.533
	DI	0.101	0.358	71.667	0.125	0.428	88.733

2.5 Case Studies

In this section, we analyze the two data sets presented in the introduction: laser emitters [Hamada, 2005; Meeker and Escobar, 1998] and IRLEDs [Yang, 2007] datasets. To analyze both datasets, Weibull and dynamic degradation linear models without intercept are fitted assuming the same prior specifications considered in the simulation studies. Given the non-linear feature of IRLEDs data, this dataset is also analyzed using the dynamic model with intercept varying along the time presented in expression (2.3). In this case, we additionally assume that, *a priori*,

$\psi_\nu = \sigma_\nu^{-2} \sim Gamma(0.01, 0.01)$. To evaluate the computational times, both applications were fitted on an Intel (R) Core (TM) i7-8550U 1.80GHz CPU with 8GB RAM

One of the main goals in reliability studies is the time-to-failure forecasting. In degradation trials, such a prediction is directly influenced by the model's capacity of predicting new degradation measures. In the following, we start evaluating the performance of DLD and WLD models to forecast new degradation measures in the unit under test considering both dataset. The Appendix brings a third study case that is an application of the proposed methodology to the train wheels degradation data [Freitas et al., 2009].

2.5.1 Case study 1: Laser emitters data

As described in Hamada [2005], the light output of laser emitters degrades over time if working at a fixed operating current. To have a constant light output, we need to increase the operating current over time. The system degradation is obtained measuring the percent increase in the operating current relative to the original operating current. The laser dataset in Figure 2.1, previously analyzed by Meeker and Escobar [1998] and Hamada [2005], corresponds to the laser degradation observed in a sample of $n = 15$ laser emitters every 250 hours from 0 to 4,000 hours. A total of $m = 17$ degradation measures is obtained for each laser emitter. A laser fails when its operating current (degradation path) reaches the threshold D_f of 10%.

The mean squared error (MSE), the mean absolute percentage error (MAPE), and the mean absolute deviance (MAD) for the forecasts (posterior means) for the degradation measurement are given in Table 2.4. According to all these criteria, the DLD model provides better predictions for the omitted observations independently of the number of observations we removed from the dataset. As expected, forecasts many steps ahead lose in quality. Removing around 41% of the data by selecting $l = 7$, the predicted value for the degradation experiences great bias and variability. These results show the existence of a more strong dependence between the future degradation measures and the last observed measurements in the degradation paths.

Figure 2.6 shows the forecasts and 95% HPD intervals for the omitted degradations obtained by fitting DLD and WLD models when $l = 5$, for the three selected laser emitters (Lasers A, B, and C) shown in Figure 2.1. Corroborating the findings in Table 2.4, the DLD model provides better forecasts for the omitted degradations. Results for Lasers A and B are much better as the true values belong to the 95% HPD intervals. Although both models poorly predict the omitted degradation for Laser C in which the degradation increments are less compatible with time-invariant assumption required in the usual linear models, the biases are smaller under the DLD model. The WLD model fails in forecasting the omitted values for Lasers A and C. In these cases, posterior distributions concentrate most of their probability mass far from the true values. As it can be noticed, the true values do not belong to the 95% HPD intervals.

Table 2.4: Forecasting accuracy measurements for WLD and DLD models, laser emitters data.

l	1		2		3		4		5		6		7	
Model	WLD	DLD	WLD	DLD	WLD	DLD	WLD	DLD	WLD	DLD	WLD	DLD	WLD	DLD
MSE	0.11	0.06												
MAPE	3.26	2.14												
MAD	0.25	0.18												
MSE	0.05	0.02	0.13	0.09										
MAPE	2.74	1.56	3.65	2.73										
MAD	0.19	0.12	0.27	0.22										
MSE	0.05	0.01	0.07	0.03	0.15	0.11								
MAPE	2.48	1.49	3.20	2.03	4.05	3.19								
MAD	0.17	0.10	0.23	0.15	0.30	0.25								
MSE	0.08	0.02	0.08	0.03	0.10	0.03	0.19	0.12						
MAPE	3.57	1.96	3.09	1.94	3.74	2.08	4.60	3.70						
MAD	0.23	0.13	0.21	0.12	0.27	0.15	0.34	0.29						
MSE	0.10	0.03	0.12	0.05	0.12	0.05	0.16	0.04	0.24	0.12				
MAPE	4.65	2.36	4.38	2.89	3.95	2.77	4.54	2.22	5.33	3.54				
MAD	0.28	0.14	0.28	0.19	0.27	0.19	0.33	0.15	0.39	0.27				
MSE	0.09	0.05	0.15	0.09	0.17	0.11	0.18	0.11	0.24	0.14	0.33	0.22		
MAPE	5.15	3.41	5.79	4.15	5.21	4.06	4.93	3.90	5.68	4.35	6.16	5.16		
MAD	0.28	0.19	0.34	0.25	0.33	0.27	0.34	0.27	0.41	0.32	0.46	0.39		
MSE	0.05	0.02	0.13	0.09	0.19	0.15	0.21	0.17	0.23	0.19	0.31	0.24	0.42	0.37
MAPE	4.13	2.67	6.14	5.23	6.62	5.98	6.02	5.61	5.93	5.31	6.71	6.20	6.83	6.96
MAD	0.20	0.13	0.33	0.28	0.39	0.35	0.38	0.36	0.40	0.36	0.48	0.45	0.50	0.52

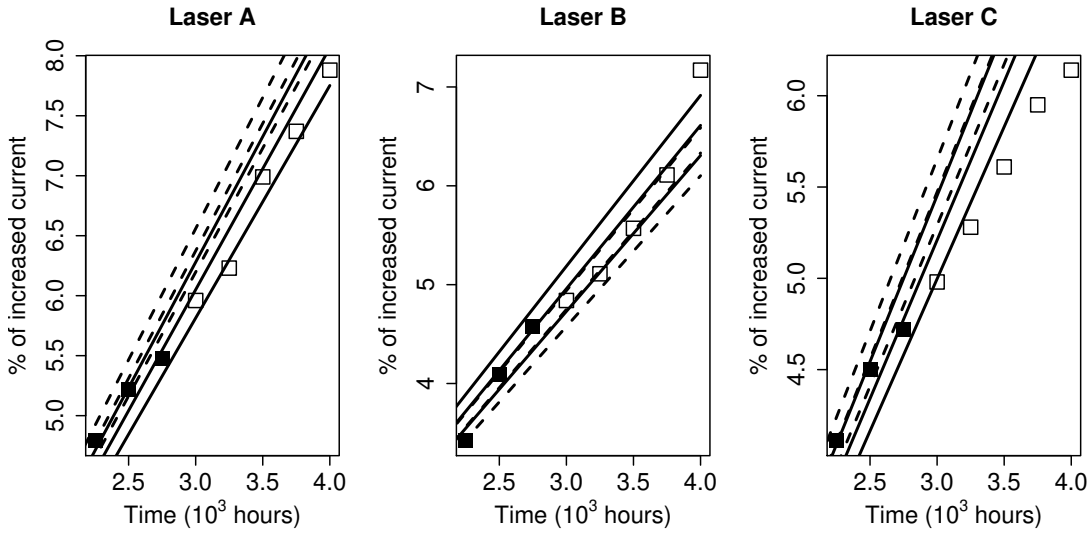

Figure 2.6: Forecast for $l = 5$ omitted observations (white squares) considering linear Weibull (dashed line) and dynamic (continuous line) degradation models for laser emitters A, B and C.

Table 2.5 displays the posterior estimates for the standard deviation components of both models. Posterior means and medians provided similar estimates under both models. The model variability is small under DLD model. By including an evolution component in the model, the variability associated with the measurement error has an average fall of 41.5%, going from 0.2 in the linear Weibull degradation model to 0.117 in the linear dynamic degradation model.

Table 2.5: Posterior Estimates for the standard deviation components of the fitted models, laser emitters data.

Model	Parameter	Mean	Median	St.Dev.	HPD 95%
WLD	σ_ϵ	0.200	0.199	0.009	[0.183 ; 0.218]
DLD	σ_ϵ	0.117	0.117	0.009	[0.101 ; 0.134]
	σ_ω	0.054	0.054	0.005	[0.044 ; 0.065]

Figure 2.7 presents the posterior means and 95% HPD intervals for the degradation rates of laser emitters A, B, and C provided by the DLM (continuous line) and WLD (dashed line) models.The WLD model assumes that the degradation rate for each unit is time-invariant and their estimates for Lasers A, B, and C, respectively, are 2.02, 1.62 and 1.67. The DLD model points out that the degradation rate for Lasers A and B in the first time interval is smaller than the one provided by the WDL model. Differently of what is obtained fitting the WDL model, the DLD model indicates that Lasers A and C experience a more intense degradation in the first six time intervals after which the degradation rate starts to decreases continuously along the time. In the case of Laser A this rate stabilizes around 1.97 in the last three-time intervals. The degradation rate for Laser B presents a different behavior, smoothly decreasing until the eighth time-interval and increasing after that. Assuming the DLD model, there is more posterior uncertainty about the degradation rates at the beginning of the study. The amplitude of the 95% HPD intervals are much higher in the first time-intervals than the ones obtained in the last intervals. This is explained by the small number of degradation measurements that are available at the beginning of the trial. As new observations are obtained, the amplitudes of the degradation rate intervals tend to decrease.

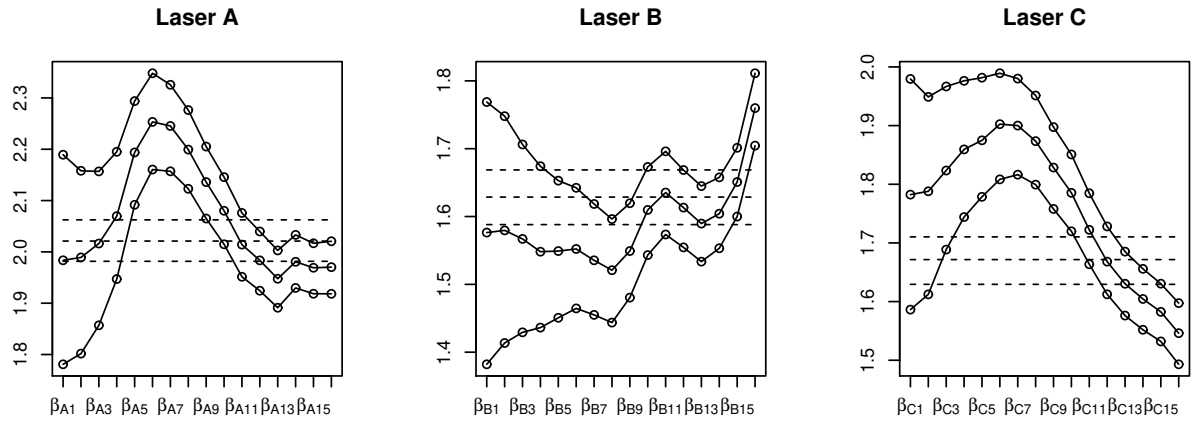

Figure 2.7: Posterior means and 95% credibility HPD intervals for the degradation rates adjusted by WLD (dashed line) and DLD (continuous line) models for laser emitters A to C

At the end of the study, the degradation rates provided by DLD and WLD models are different (see Figure 2.7). This difference influences the estimates for quantities of interest related to the failure time. Table 2.6 shows, for instance, that the mean time to failure, $\overline{RUL}$ and the percentiles of order 2.5%, 10.0%, 50.0% and 97.5%, for Lasers B provided by the DLD model are smaller that obtained by WDL model. The opposite is observed for Lasers A and C.

Table 2.6: Reliability (R), mean time to failure (MTTF), $\overline{RUL}$ and percentiles ($t_{p|\boldsymbol{Y}}(\alpha|\boldsymbol{y})$) of order α for the failure time (in 10^3 hours) posterior predictive distribution for laser emitters A, B and C and a new unit assuming WLD and DLD models.

Laser	Model	$R_{T\|\boldsymbol{Y}}(5000\|\boldsymbol{y})$	$\overline{RUL}\|\boldsymbol{y}$	$MTTF\|\boldsymbol{y}$	$t_{p\|\boldsymbol{Y}}(0.025\|\boldsymbol{y})$	$t_{p\|\boldsymbol{Y}}(0.1\|\boldsymbol{y})$	$t_{p\|\boldsymbol{Y}}(0.5\|\boldsymbol{y})$	$t_{p\|\boldsymbol{Y}}(0.975\|\boldsymbol{y})$
A	WLD	——	0.949	4.949	4.850	4.885	4.948	5.047
	DLD	——	1.078	5.078	4.945	4.989	5.078	5.214
B	WLD	——	2.141	6.141	5.992	6.042	6.139	6.296
	DLD	——	1.683	5.683	5.518	5.573	5.681	5.862
C	WLD	——	1.982	5.982	5.838	5.886	5.981	6.129
	DLD	——	2.472	6.472	6.255	6.328	6.470	6.699
New	WLD	0.604	——	5.093	3.302	3.614	5.267	6.440
	DLD	0.658	——	5.131	3.367	3.535	5.273	6.546

For a new laser emitter, Table 2.6 shows that both models produce similar posterior summaries for the posterior predictive distribution for the failure time being all those summaries a little higher if the DLD model is fitted. Based on the DLD model, for instance, we conclude that 10% of the laser emitters operating on the same conditions as those in the study will degrade beyond the threshold of 10% before 3.535 hours. Besides the estimated probability of a new laser not presenting the fault until the time of 5000 hours is 0.604 in the model Weibull and 0.658 in the dynamic model. To fit the WLD and DLD models, the computational times were 4.24 and 44.85 seconds, respectively.

2.5.2 Case Study 2: IRLEDs data

We analyze the infrared light-emitting diodes (IRLEDs) previously considered by Yang [2007] and Wang et al. [2017]. IRLEDs are high-reliability optoelectronic devices frequently used in communication systems. Yang [2007] considers the GaAs/GaAs IRLEDs in which the wavelength is 880 nm and operates under a design current of 50 mA. The variation ratio of luminous power is used to measure the devices performances. In an accelerated design, we will consider the sample of 25 units tested at 170 mA and an operating current of 50 mA. The test units were inspected for luminous power at 0, 24, 48, 96, 155, 368, 768, 1130, 1536, 1905, 2263, and 2550 hours. Figure 2.2 shows the values of the variation ratio at each inspection time. A failure occurs if the ratio is greater than 20%.

Some degradation paths are not linear as, for instance, for IRLEDs A and B. In this case, the usual structure of the linear degradation models is not appropriated. To analyze the data we fit the WLD model (W) and two approaches for the DLD model defined in (2.3), one assuming a simpler DLD model (D) where $\lambda_{ij} = 0$ for all i and j and the other allowing for the dynamic

degradation baseline λ_{ij} (DI). Table 2.7 shows the MSE, the MAPE and the MAD for the forecasts (posterior means) for the l omitted degradation measurements, $l = 1, \ldots, 5$, if these three models are assumed. As observed in the previous study, forecasts for many steps ahead are more biased under all models. However, both DLD models have better performance than the WLD model. By assuming the model DI, we obtained an upper performance mainly to predict the degradation many steps ahead.

The posterior estimates for σ_ϵ, σ_ν and σ_ω are given in Table 2.8. By assuming that all variability is only due to the dispersion of degradation measurement around the straight line $\beta_i t_{ij}$, the variance associated with the WLD model is very high and may explain the poor performance of this model for forecasting. By considering the piecewise linear structure assumed by the DI model, part of the variability associated with the degradation measures is explained by the variability inherent to the baseline degradation that is reasonable to expect when facing the polynomial structure observed in some degradation paths.

Table 2.7: Forecasting accuracy measurements for linear Weibull degradation model (W) and dynamic linear degradation models with (DI) and without (D) dynamic degradation baseline, IRLEDs data.

l	1			2			3			4			5		
Model	W	D	DI	W	D	DI	W	D	DI	W	D	DI	W	D	DI
MSE	15.86	9.96	9.80												
MAPE	20.73	13.75	13.17												
MAD	3.00	2.14	2.06												
MSE	11.77	6.74	6.43	24.94	9.56	6.58									
MAPE	21.89	13.47	12.28	27.64	15.09	11.96									
MAD	2.76	1.88	1.75	3.84	2.30	1.89									
MSE	13.84	5.43	4.18	24.44	9.33	5.44	48.30	25.48	15.21						
MAPE	26.01	14.95	12.89	32.37	19.11	14.40	39.78	25.14	17.93						
MAD	3.12	1.89	1.63	4.01	2.47	1.85	5.59	3.67	2.63						
MSE	11.73	5.92	3.78	32.19	17.96	9.39	53.71	30.56	13.69	89.64	54.58	22.96			
MAPE	27.22	17.22	13.42	39.94	25.76	17.83	48.04	30.71	19.92	55.96	39.22	25.53			
MAD	2.83	1.91	1.46	4.72	3.29	2.27	6.08	4.28	2.78	7.77	5.79	3.83			
MSE	7.83	2.68	1.42	29.45	13.38	5.00	67.80	37.15	15.71	108.08	60.54	23.23	168.88	100.69	40.25
MAPE	30.82	15.19	11.86	44.48	26.84	17.55	60.10	39.78	25.94	69.15	47.36	31.19	78.86	55.99	36.75
MAD	2.30	1.26	0.95	4.48	2.96	1.86	6.95	4.96	3.22	8.53	6.21	4.01	10.72	8.11	5.41

Table 2.8: Posterior Estimates for the standard deviation components of the fitted models, IRLED's data.

Model	Parameter	Mean	Median	St.Dev.	HPD 95%
W	σ_ϵ	2.102	2.098	0.090	[1.933 ; 2.284]
D	σ_ϵ	0.143	0.142	0.017	[0.111 ; 0.179]
	σ_ω	1.399	1.395	0.097	[1.215 ; 1.590]
DI	σ_ϵ	0.102	0.096	0.033	[0.047 ; 0.168]
	σ_ν	0.528	0.526	0.048	[0.438 ; 0.622]
	σ_ω	0.114	0.113	0.001	[0.098 ; 0.131]

Table 2.9 shows that the mean times to failure of IRLEDS A, B and C and of a new IRLED provided by the model DI is higher than that obtained by fitting models D and W. For a new IRLED operating on the same conditions as the units under test, model DI provides that the estimated probability of not failing until the time of 5000 hours is 0.328 and is higher than that

provided by the other two models. Except for IRLED A, in all other cases, estimates for the percentiles of order 2.5%, 10.0%, 50.0% and 97.5% tend to be higher under dynamic models.

Table 2.9: Reliability (R),$\overline{RUL}$, mean time to failure (MTTF) and percentiles ($t_{p|\boldsymbol{Y}}(0.025|\boldsymbol{y})$) of order α for the failure time (10^2 hours) posterior predictive distribution for IRLEDs A, B and C and a new unit assuming the Weibull and the dynamic models.

IRLED	Model	$R_{T\|\boldsymbol{Y}}(5000\|\boldsymbol{y})$	$\overline{RUL}\|\boldsymbol{y}$	$MTTF\|\boldsymbol{y}$	$t_{p\|\boldsymbol{Y}}(0.025\|\boldsymbol{y})$	$t_{p\|\boldsymbol{Y}}(0.1\|\boldsymbol{y})$	$t_{p\|\boldsymbol{Y}}(0.5\|\boldsymbol{y})$	$t_{p\|\boldsymbol{Y}}(0.975\|\boldsymbol{y})$
	W	——	——	16.393	15.206	15.605	16.361	17.716
A	D	——	——	15.584	13.609	14.232	15.507	17.990
	DI	——	——	17.216	16.299	16.584	17.178	18.351
	W	——	4.304	29.304	25.725	26.796	29.168	33.699
B	D	——	12.005	37.005	30.897	32.677	36.641	45.138
	DI	——	23.935	48.935	41.131	42.840	47.664	64.476
	W	——	81.967	106.967	68.978	77.154	100.438	183.609
C	D	——	99.392	124.392	71.026	80.698	109.925	254.324
	DI	——	102.240	127.240	76.886	85.017	109.500	254.481
	W	0.215	——	39.069	15.768	17.442	32.067	100.285
New	D	0.256	——	43.658	15.270	18.511	36.272	115.543
	DI	0.328	——	46.435	15.778	19.077	40.030	118.361

Regarding the computational times to run this application, it was needed 6.25 seconds and 1.26 minutes, respectively, for the models WLD and DLD without random intercept. To ensure low autocorrelation in the posterior samples, the DLD model with random intercept required a longer chain taking 19.15 minutes to run.

2.6 Conclusions

Extending previous works, we introduced a dynamic general path model to handle data which degradation rate and the baseline degradation are time-variant. The dynamic structure of the proposed model allows accommodating different behaviors of the degradation paths including linear and non-linear ones. Thus, the proposed model provides a solution for the "disadvantage" of the general path models pointed out by Ye and Xie [2015], proposing a functional form that is not regular along the time also allowing for structural breaks.

The proposed model was fitted to analyze simulated and real datasets. It was compared to the Weibull linear degradation model introduced by Hamada [2005], a model that is frequently used to analyze degradation data. We conclude, from the simulations, that the proposed model has better performance than the Weibull model to analyze data which degradation rate dynamically changes over time. It also shows to be a competitive model to analyze data coming from a population where the degradation rate for each unit does not change along the time. The analysis of real datasets showed that, by assuming a dynamic structure, the forecasts for the degradation measurements are less biased. If we consider forecasts are done many steps ahead, the proposed model performed much better than the Weibull model.

On the whole, our results show that to introduce "dynamic" in the linear degradation model, allowing the degradation rate and baseline degradation to evolute along time, produced a competitive model that shows to be a useful approach to model degradation data coming from

populations with different shapes for the degradation path. Despite its good performance, in our analysis, we only explore a dynamic model with a normal degradation rate. Possible extensions of this model may consider different distributions for this rate making the model even more flexible. Another limitation of the proposed model is the lack of parsimony. Although in the situations approached in the paper we did not experienced problems regarding the computational cost, the lack of parsimony may lead to a high computational cost if data to be analyzed are captured in a massive way and with high temporal resolution. To be effectively used in practical situations like these, we must look for strategies to reduce computational time without losing the quality in the inferences. A possible way to overcome problems related to the computational cost is to consider a reparametrization of the model [Aktekin et al, 2018], for instance, assuming that the degradation rate is decomposed in two components, one representing the influence of the environment and other representing the time effect on the degradation. However, there is no guarantee that this structure will provide better inference for the failure time. This is a new approach for the same problem that demands a deep study involving theoretical and computational aspects. These are interesting topics for future research.

References

Aktekin, T., Polson, N. and Soyer, R. [2018]. Sequential Bayesian analysis of multivariate count data, *Bayesian Analysis* **13**(2): 385-409.

Carter, C. K. and Kohn, R. [1994]. On Gibbs sampling for state space models, *Biometrika* **81**(3): 541–553.

Cha, Ji. Hwan and Finkelstein, M. [2017]. On Some Shock Models with Poisson and Generalized Poisson Shock Processes, *Statistical Modeling for Degradation Data*, Springer, pp. 67-79.

Freitas, M., dos Santos, T. R., Pires, M. C. and Colosimo, E. [2010]. A closer look at degradation models: Classical and Bayesian approaches, *in* M. S. Nikulin, N. Limnios, N. Balakrishman, W. Kahle and C. Huber-Carol (eds), *Advances in Degradation Modelling: Applications in reliability, Survival Analysis and Finance*, Birkhauser, New York, chapter 11, pp. 157–180.

Freitas, M., Toledo, M., Colosimo, E. and Pires, M. [2009]. Using degradation data do assess reliability: A case study on train wheel degradation., *Quality and Reliability Engineering International* **25**: 607–629.

Frühwirth-Schnatter, S. [1994]. Data augmentation and dynamic linear models, *Journal of Time Series Analysis* **15**(2): 183–202.

Gao, H., Cui, L., and Dong, Q. [2020]. Reliability modeling for a two-phase degradation system with a change point based on a Wiener process. *Reliability Engineering & Systemn Safety*, **193**: 106601.

Guida, M., Postiglione, F., and Pulcini, G. [2015]. A random-effects model for long-term degradationnanalysis of solid oxide fuel cells, *Reliability Engineering & System Safety*, **140**: 88 – 98.

Hamada, M. [2005]. Using degradation data to assess reliability, *Quality Engineering* **17**: 615–620.

Hong, Y., Duan, Y., Meeker, W. Q., Stanley, D. L. and Gu, X. [2015]. Statistical methods for degradation data with dynamic covariates information and an application to outdoor weathering data, *Technometrics* **57**(2): 180–193.

Kim, Seong-Joon and Bae, Suk Joo [2017]. Degradation Test Plan for a Nonlinear Random-Coefficients Model, *Statistical Modeling for Degradation Data*, Springer, pp.127-147.

Lim, P., Goh, C., Tan, K. and Dutta, P. [2017]. Multimodal degradation prognostics based on switching Kalman filter ensembler", *IEEE Transactions on Neuronal Networks and Learning Systems* **28**(1): 136–148.

Liu, B., Zhao, X., Liu, G., andLiu, Y. [2020]. Life cycle cost analysis considering multiple dependent degradation processes and environmental influence. *Reliability Engineering & System Safety*, **197**: 106784.

Lu, C. J. and Meeker, W. O. [1993a]. Using degradation measures to estimate a time-to-failure distribution, *Technometrics* **35**(2): 161–174.

Lu, C., Meeker, W. and Escobar, L. [1996]. Using degradation measurements to estimate a time-to-failure distribution, *Statistica Sinica* **6**: 531–546.

Lu, J., Park, J. and Yang, Q. [1997]. Statistical inference of a time-to-failure distribution derived from linear degradation data, *Technometrics* **39**(4): 391–400.

Meeker, W. Q. and Escobar, L. A. [1998]. *Statistical Methods for Reliability Data*, Wiley Series in Probability and Statistics, First Edition.

Oliveira, R. P. B., Loschi, R. H. and Freitas, M. A. [2018]. Skew-heavy-tailed degradation models: An application to train wheel degradation, *IEEE Transactions on Reliability* **67**(1): 129–141.

Park, C. and Padgett, W. J. [2005]. New cumulative damage models for failure using stochastic processes as initial damage, *IEEE Transactions on Reliability* **54**(3): 530–540.

Park, C. [2017]. Stochastic accelerated degradation models based on a generalized cumulative damage approach, *Statistical Modeling for Degradation Data,* Springer, pp. 3-20.

Peng, C.-Y. and Tseng, S.-T. [2013]. Statistical lifetime inference with skew-Wiener linear degradation models, *IEEE Transactions on Reliability* **62**(2): 338–350.

Peng, C.-Y. and Cheng, Y.-S. [2019]. Student-t Processes for Degradation Analysis, *Technometrics* **62** (2): 223-235.

Peng, W., Huang, H.-Z., Xie, M., Yang, Y. and Liu, Y. [2013]. A Bayesian approach for system reliability analysis with multilevel pass-fail, lifetime and degradation data sets, *IEEE Transactions on Reliability* **62**(3): 689–699.

Petris, G., Petrone, S. and Campagnoli, P. [2009]. *Dynamic Linear Models with R*, Use R! Series, Springer, New York.

R Development Core Team [2018]. *R: A Language and Environment for Statistical Computing*, R Foundation for Statistical Computing, Vienna, Austria.

Robinson, M. and Crowder, M. [2000a]. Bayesian methods for a growth-curve degradation model with repeated measures., *Lifetime Data Anaysis* **6**: 357–374.

Saha, B., Goebel, K. and Christophersen, J. [2009]. Comparison of prognostic algorithms for estimating remaining useful life of batteries, *Transactions of the Institute of Measurement and Control* **31**(3-4): 293–308.

Santos, C.C. and Loschi, R.H. [2020]. Semi-parametric Bayesian models for heterogeneous degradation data: An application to Laser data, *Reliability Engineering and System Safety* **202**, 107038.

Shephard, N. [1994]. Partial non-gaussian state space, *Biometrika* **81**(1): 115–131.

Si, X.-S., Wang, W., Hu, C.-H., Chen, M.-Y. and Zhou, D.-H. [2013]. A Wiener-process-based degradation model with a recursive filter, *Mechanical Systems and Signal Processing* **35**(1-2): 219-237.

Sotiris, V. A., Peter, W. T. and Pecht, M. G. [2010]. Anomaly detection through a Bayesian support vector machine, *IEEE Transactions on Reliability* **59**(2): 277–286.

Wang, W. [2012]. An overview of the recent advances in delay-time-based maintenance modelling, *Reliability Engineering & System Safety* **106**: 165–178.

Wang, Z., Cao, J., Ma, X., Qiu, H., Zhang, Y., Fu, H. and Krishnaswamy, S. [2017]. An improved independent increment process degradation model with bilinear properties, *Arabian Journal for Science and Engineering* **42**: 2927?2936.

West, M. and Harrison, J. [1997]. *Bayesian forecasting and dynamic models*, Springer series in statistics, Springer, Segunda Edição.

West, M., Harrison, P. J. and Migon, H. S. [1985]. Dynamic generalized linear models and Bayesian forecasting, *Journal of the American Statistical Association* **80**(389): 73–83.

Xiang, Y., Coit, D. W. and Feng, Q. [2013]. n subpopulations experiencing stochastic degradation: Reliability modeling, burn-in, and preventive replacement optimization, *IIE Transactions* **45**(4): 391–408.

Yang, G. [2007]. *Life cycle reliability engineering*, John Wiley & Sons.

Ye, Z. S., Tang, L. C. and Xie, M. [2011]. A burn-in scheme based on percentiles of the residual life, *Journal of Quality Technology* **43**(4): 334–345.

Ye, Z.-S. and Xie, M. [2015]. Stochastic modelling and analysis of degradation for highly reliable products, *Applied Stochastic Models in Business and Industry* **31**(1): 16–32.

Yuan, T. and Ji, Y. [2015]. A hierarchical Bayesian degradation model for heterogeneous data, *IEEE Transactions on Reliability* **64**(1): 63–70.

Appendix

A1 Case Study 3: Train Wheels Degradation Data

In this appendix, the linear Weibull degradation model and dynamic degradation model without the random intercept will be used to analyze the train wheel dataset on MA11 position presented in Freitas et al. [2009] (Figure A1). In the study, 3 wheels failed and, after reaching the critical degradation threshold, the measurements were no longer collected in these units. Thus, at the end of 600000 km, 3 degradation paths contain missing data. However, as mentioned in the paper, dynamic linear models are able to accommodate this data due to their structure.

Note the degradation trajectory of three trains (A, B and C). The first train (A) is the one that degrades the most in the study, and is no longer followed up after this event. Train B has a change in the inclination of its trajectory and Train C was the one that degraded the least during the study. The degradation increments of these three trains are high at the beginning of the study, as shown in the Figure A1. It is of interest to verify whether the dynamic linear degradation model can adapt to this oscillation and provide better estimates for the failure times of the units under test, if compared to the usual linear Weibull degradation model.

For the fit of both models, the time was transformed so that the unit of measure is 10^4 Km. Initially, the performance of the linear Weibull and dynamic degradation models are compared considering their predictive capacity by omitting observations from the database. In this context, the last m observations of each degradation path were removed, with $m = 1, 2, \ldots, 6$, representing the omission of approximately 46% of the data. Table A1 presents the prediction accuracy measures MSE, MAPE and MAD calculated for the withdrawn observations. In all scenarios, the dynamic linear degradation model presented lower values of the predictive accuracy measures, indicating a better capacity to accommodate the omitted observations.

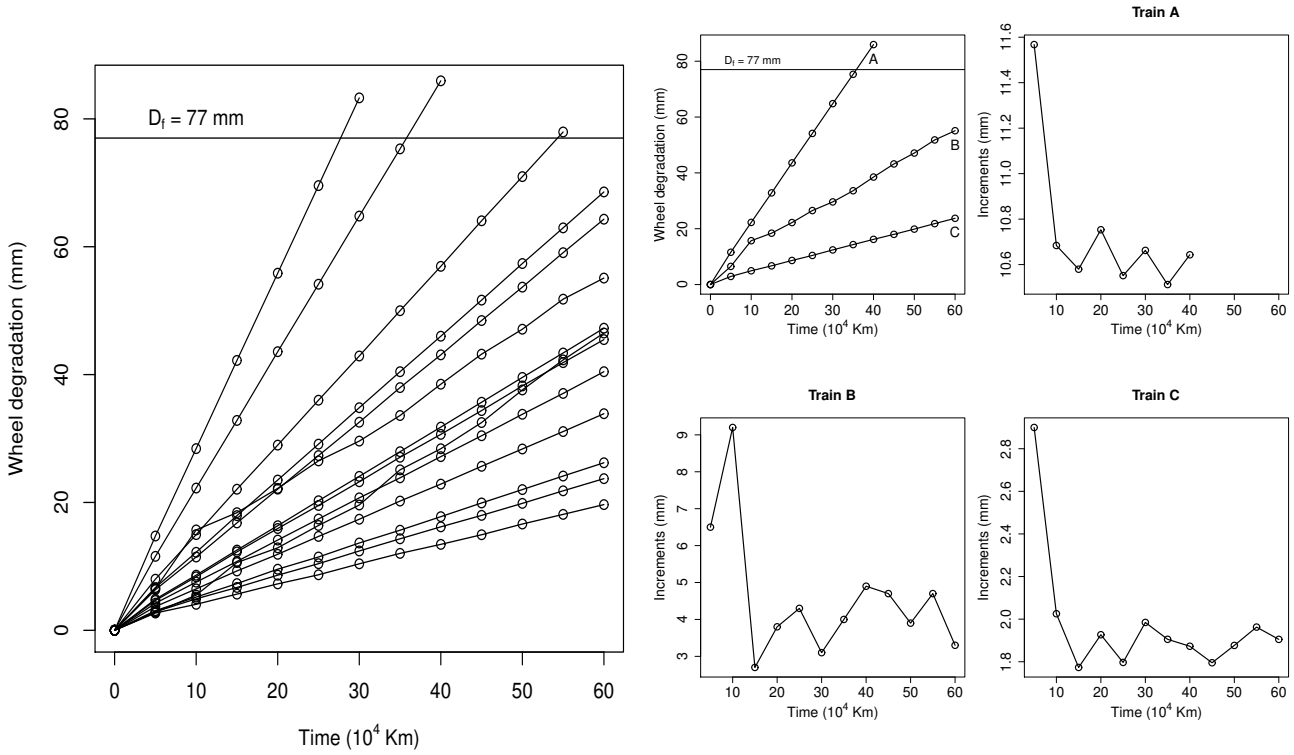

Figure A1: Degradation paths of train wheels degradation data of position MA11 and increments for some units under test

Table A1: Predictive accuracy measures for the linear Weibull (W) and dynamic (D) degradation models (train wheels degradation data)

m	1		2		3		4		5		6	
Model	W	D	W	D	W	D	W	D	W	D	W	D
MSE	2.10	0.21										
MAPE	2.45	0.56										
MAD	1.03	0.25										
MSE	1.57	0.11	3.17	0.45								
MAPE	2.39	0.49	3.06	1.04								
MAD	0.93	0.19	1.28	0.45								
MSE	1.59	0.28	2.59	0.70	4.78	1.59						
MAPE	2.63	0.74	3.06	1.16	3.78	1.74						
MAD	0.93	0.29	1.19	0.47	1.58	0.76						
MSE	1.02	0.04	2.47	0.50	3.78	1.09	6.61	2.20				
MAPE	2.72	0.58	3.40	1.26	3.84	1.70	4.61	2.33				
MAD	0.83	0.15	1.19	0.44	1.48	0.65	1.90	0.97				
MSE	1.21	0.04	1.98	0.12	4.00	0.60	5.79	1.24	9.62	2.41		
MAPE	3.03	0.72	3.74	1.23	4.42	1.91	4.86	2.35	5.70	3.02		
MAD	0.89	0.19	1.16	0.33	1.55	0.64	1.87	0.87	2.35	1.21		
MSE	2.08	0.52	2.79	0.64	4.28	1.23	7.48	2.95	10.25	4.64	16.11	7.54
MAPE	3.77	1.56	4.35	2.13	5.15	2.78	5.83	3.44	6.26	3.87	7.21	4.66
MAD	1.00	0.41	1.28	0.60	1.62	0.83	2.06	1.19	2.44	1.48	2.99	1.92

Figure A2 shows the prediction for $m = 5$ withdrawn observations. The dashed lines represent the posterior means and the HPD intervals with 95% credibility for the fit associated to the Weibull linear degradation model. The solid lines represent the posterior estimates associated to the dynamic linear degradation model, together with the 95% credibility HPD intervals. Predictions for train A are identical for both models. This result is expected, as only one observation was omitted in this case, as the train failed and the wheel was no longer observed. In trains B and C, the prediction provided by the linear dynamic degradation model was superior to that obtained by the linear Weibull degradation model.

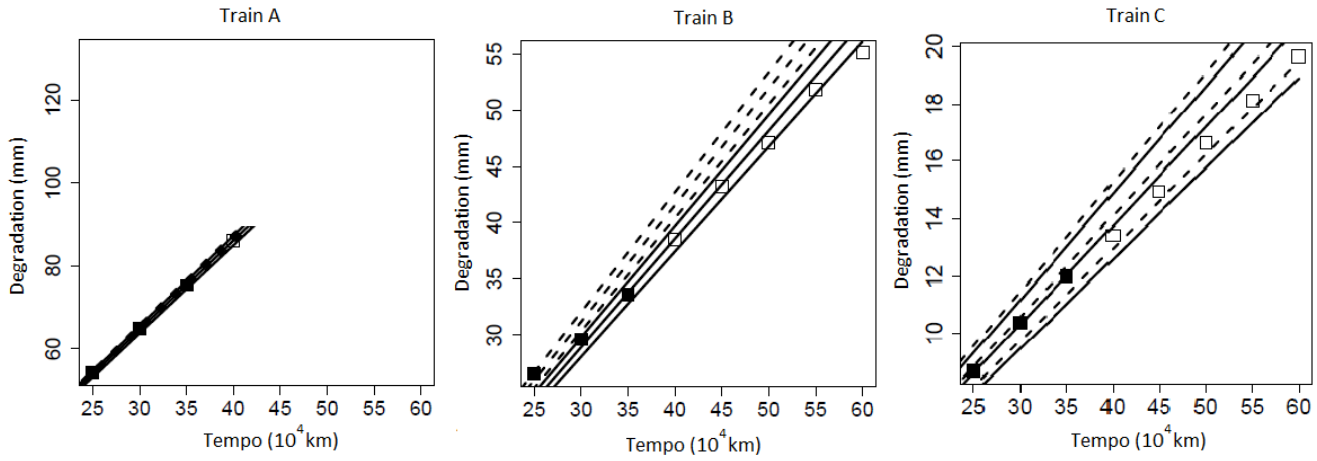

Figure A2: Forecast for $l = 5$ omitted observations (white squares) considering linear Weibull (dashed line) and dynamic (continuous line) degradation models for trains A, B and C.

When fitting the dynamic linear degradation model, the variability associated with the measurement error has a drop of 56.8 %, on average, from 0.944 to 0.408, as shown in Table A2.

Table A2: Posterior estimates of the variance components for the linear Weibull (W) and dynamic (D) degradation models (train wheels degradation data)

Model	Parameter	Mean	Mode	Std. Dev.	HPD 95%	
W	σ_v	0.944	0.941	0.053	0.983	1.048
D	σ_v	0.408	0.406	0.045	0.325	0.498
	σ_w	0.028	0.028	0.002	0.023	0.033

The degradation rates estimated by the two models are shown in Figure A3. The dashed and continuous lines show the posterior mean estimates and 95% credibility intervals, considering the linear Weibull and dynamic degradation models, respectively. All the train wheels have a decay pattern of estimates, which at the end of the test are smaller than those recorded by the linear Weibull degradation model. Due to the presence of missing data in the units under test that failed (Train A), the degradation rates are not of interest after the failure.

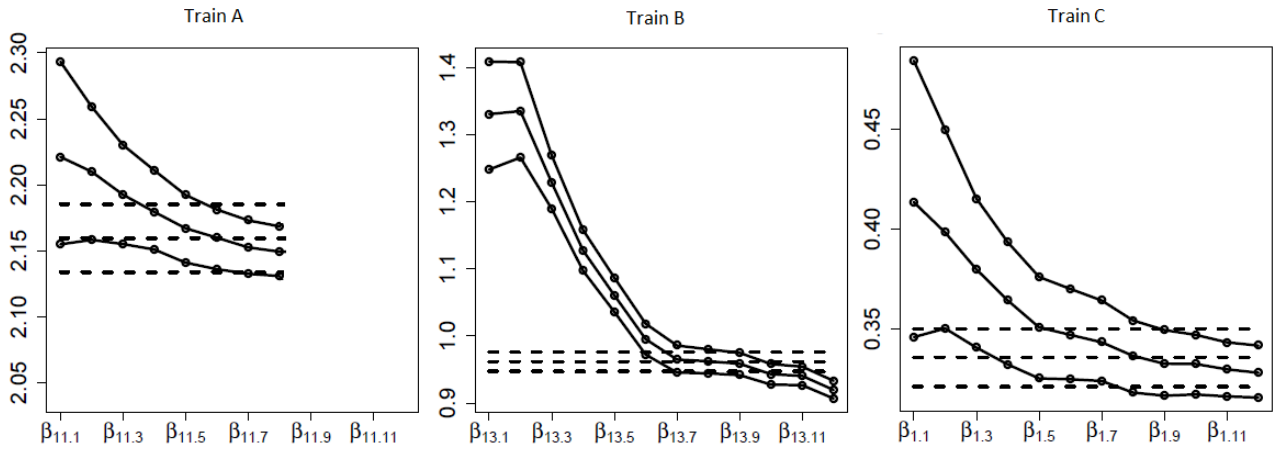

Figure A3: Posterior means and 95% credibility HPD intervals for the degradation rates adjusted by WLD (dashed line) and DLD (continuous line) models for trains A to C

Considering the inferential methods presented in the paper, Table A3 presents a summary of the predictive posterior distribution of the failure times for trains A, B, C and a future unit considering the linear Weibull and dynamic degradation, respectively.

Table A3: Reliability (R), mean time to failure (MTTF), $\overline{RUL}$ and percentiles ($t_{p|\boldsymbol{Y}}(\alpha|\boldsymbol{y})$) of order α for the failure time (in 10^4 km) posterior predictive distribution for trains A, B and C and a new unit assuming WLD and DLD models.

Laser	Model	$R_{T\|\boldsymbol{Y}}(300000\|\boldsymbol{y})$	$\overline{RUL}\|\boldsymbol{y}$	$MTTF\|\boldsymbol{y}$	$t_{p\|\boldsymbol{Y}}(0.025\|\boldsymbol{y})$	$t_{p\|\boldsymbol{Y}}(0.1\|\boldsymbol{y})$	$t_{p\|\boldsymbol{Y}}(0.5\|\boldsymbol{y})$	$t_{p\|\boldsymbol{Y}}(0.975\|\boldsymbol{y})$
A	W	——	——	35.656	35.237	35.384	35.653	36.087
	D	——	——	35.774	35.440	35.556	35.772	36.111
B	W	——	20.064	80.064	78.884	79.279	80.057	81.293
	D	——	23.736	83.736	82.544	82.966	83.732	84.918
C	W	——	160.513	229.513	219.935	223.230	229.371	239.857
	D	——	174.951	234.951	226.007	229.027	234.852	244.748
New	W	0.929	——	105.716	27.537	35.599	98.661	231.299
	D	0.857	——	106.851	27.604	35.730	98.562	236.615

The MTTF estimated by the linear Weibull degradation model for trains A, B , C and a future unit are lower than the observed in the dynamic linear degradation model. The estimated reliability for a future unit at the distance of 300000 km has a drop from 0.929 in the Weibull linear degradation model to 0.857 in the dynamic linear degradation model.

Chapter 3

Dynamic Multivariate Gamma Model: a General Path Approach for Positive Degradation Measurements

Abstract

The reliability of highly reliable systems is assessed through degradation mechanisms. Generally, degradation measures are positive and the degradation rate is related to the conditions of use and the quality of materials used in the devices' production. We introduce a general path Gamma model for degradation measures, which are related to different functions of the inspection times, obtaining flexible forms of degradation paths. The degradation rate evolves through time and depends of two components. One quantifying the specific features of each device and a dynamic one, common to all devices, measuring the impact of the environment. The model is identifiable under mild constraints. Besides producing gains regarding the interpretability of the parameters, this decomposition generates a parsimonious model, reducing computational time. The relation between degradation and failure time is obtained, allowing a computational approximation for the failure time distribution. The model performance is evaluated through simulation helping to guide the prior specifications to model identification. The proposed model is applied to analyze fatigue crack-size and stress relaxation data. Results show that the proposed methodology is competitive to predict failure times and to estimate the remaining useful life.

Keywords: Failure Time, Degradation rate decomposition, Model identifiability, Reliability

---

3.1 Introduction

When studying highly reliable devices, a great challenge is to find summaries of the lifetime distribution, such as the quantiles or the remaining useful life (RUL). For such devices, the number of failures is small or null, making lifetime models inapplicable to infer about the system reliability. To access lifetime information, it is necessary to know the underlying mechanism that produces the failure. Once find this mechanism, an experiment based on a repeated measure of the degradation is performed to evaluate the evolution of the system degradation through time, and a failure is detected if the cumulative degradation reaches a pre-defined threshold. The system reliability is, thus, measured indirectly through data related to a degradation mechanism.

Among the main approaches for analyzing degradation data are the class of stochastic process models [Bagdonavicius *et al.*, 2010; Doksum and Hoyland , 1993; Law and Crowder, 2004; Sun *et al.*, 2021; Wang *et al.*, 2017], and the general degradation path models [Hamada, 2005; Lu and Meeker , 1993; Meeker and Escobar, 1998; Oliveira *et al.*, 2018; Robinson and Crowder, 2000]. An overview about these classes of models can be found in Ye and Xie [2015].

The Wiener process has become a popular approach in the class of degradation models based on stochastic process because it has excellent mathematical properties and physical interpretations. However, it is not appropriate for modeling monotonic degradation. More recently, Wang *et al.* [2018] introduced a generalized Gaussian degradation process with a linear mean and a quadratic variance which accounts for both increasing and decreasing variance. Despite their flexibilities, Gaussian and Wiener processes are inappropriate to account for degradation measures assuming values in the 0-1 interval. A strategy to handle data with this feature is discussed by Ling *et al.* [2014] which fitted a Gamma process to the log-transformation of the degradation measurements.

The delay time models, for example, consider that the degradation process is divided into two phases: the detection of the defect and the deterioration until the occurrence of the failure [Wang , 2012]. As mentioned by Wang *et al.* [2019] the system degradation may experience different phases degrading slowly in some stages and faster in others. In these cases, degradation models assuming a single functional form to the whole deterioration process are inappropriate. A popular approach to handle this type of degradation data is change points degradation models [Chen *et al* , 2021; Wang *et al.*, 2019]. Wang *et al.* [2019] focused on two-stage degradation processes and assumed a normal model where the correlation among the degradation measurements after the change point presents a quadratic regularity. Chen *et al* [2021] developed a two-phase Gaussian process with a time transformation where the variance structure represents linear or nonlinear paths in both monotonic and non-monotonic dispersity situations. Another approach to this problem is given by Wang *et al.* [2020] that proposed a mixed-effect model based on the Wiener process to two-phases degradation model that simultaneously considers phases correlation and unit heterogeneity. Kumar and Gardoni [2014] proposed a renewal theory-based model for life-cycle analysis in deterioration systems providing the equations of the instantaneous probability of the system being in service and age of the system in finite time

horizon. Peng *et al.* [2016] addressed the problem where several different and dependent degradation indicators may influence the system reliability. They also assume that these degradation indicators are affected by non-constant external factors. The multivariate model proposed by these authors correlates the degradation of the different indicators at the same time, and the random unit-to-unit effect correlates the measurement at the same unit. Environmental conditions (temperature, humidity, etc.) that may change during the study are included in the model throughout covariates allowing for changes in the rate of the Wiener process and the mean Inverse-Gaussian process. This approach allows obtaining important life-cycle variables such as the system reliability and time lost in repair. The shock model is another way to model damages produced by random shocks [Esary *et al.* , 1973; Li and Luo , 2005]. Kumar *et al.* [2015] proposed a model that combines an independent shock and gradual deterioration processes to address the problem of system failures that originate from both demand exceeding capacity and accumulated damage exceeding a threshold. In this model structure, it is assumed that the state variables (material, structural properties, etc.) at the time of the shock are independent of the shock deterioration and the sequence of shocks are independent and identically distributed. Jia and Gardoni [2018A,B, 2019] proposed different approaches for modeling deterioration processes that allow identifying multiple deterioration processes and their interactions by modeling the changes in the system state variables due to different deterioration processes. This approach is based on a renewal theory life-cycle analysis with state-dependent stochastic models. It produces more flexible models removing some strong assumptions under which Kumar *et al.* [2015] model is built. Under this new structure, the change of the system state variable (material, structural properties, etc.) is time-variant due to different deterioration processes. Chang *et al* [2021] approaches dependent degradation-shock failure processes proposing a model where the degradation rates increase with the degradation levels. In contrast, hard failure thresholds decrease if the system degradation reaches certain critical levels.

General degradation path models is an approach for repeated-measures designs that assume a random effect to correlate the degradation measures performed in the same unit. The general path models, that is the approach adopted in this paper, assumes that the relationship between time and degradation is given by a function $D(\cdot;\boldsymbol{\beta})$ where the random effects $\boldsymbol{\beta}$ account for the correlation among the degradation measures and is related to the rate in which the devices degrade. Different data features may be accommodated assuming different structures $D(\cdot;\boldsymbol{\beta})$ or different distributions for the random effects $\boldsymbol{\beta}$. Linear models have been discussed by Lu and Meeker [1993], Lu *et al.* [1996], Hamada [2005], Kim and Bae [2017], Oliveira *et al.* [2018] and many others. Non-linear degradation models are presented in Robinson and Crowder [2000] and Guida *et al.* [2015], for instance. Recent developments in this field include degradation models for devices coming from different populations. **?** assumed a finite mixture of normal distributions to model the behavior of the degradation rate in the linear degradation model. Santos and Loschi [2020] introduced semi-parametric degradation models based on the Dirichlet process mixture of both, normal and skew-normal distributions, for the random effects. Another approach for heterogeneous population is considered by Wang *et al.* [2021] which introduced a random-

effects Wiener process model to account for the unit-to-unit heterogeneity in the degradation. A generalized inverse Gaussian (GIG) distribution models the unit-specific degradation rate behavior.

We will focus on the general degradation path model that experiences non-linear or polynomial structures for the trajectories like those shown in Figure 3.1. The fatigue crack size dataset given in Figure 3.1a was analyzed by Meeker and Escobar [1998] considering a general degradation path model adapted to convex trajectories. This figure exhibits the accumulated size of fatigue cracks, in inches, as a function of the number of cycles for 10 test specimens. Figure 3.1b displays the degradation paths of the stress relaxation of 6 units tested at 100^{o}C. Yang [2007] and Wang *et al.* [2016] fitted inverse Gaussian processes to model these degradation paths. More details and physical characteristics of the degradation data shown in Figure 3.1 can be found in the cited references.

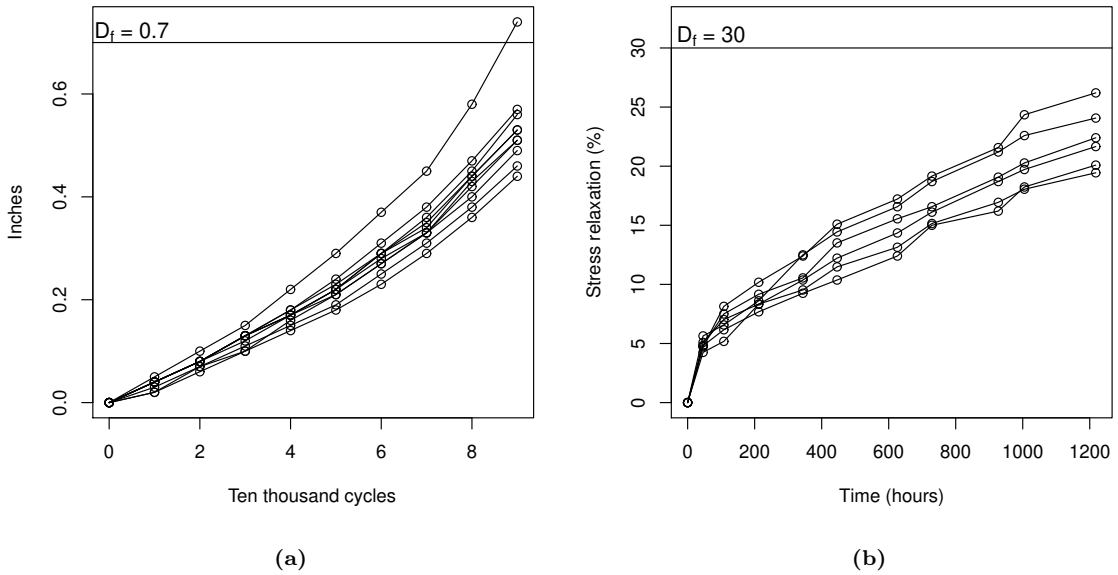

(a) **(b)**

Figure 3.1: Fatigue crack size data (a) and Stress relaxation data (b)

General path models usually assume the same functional form for all trajectories and that the degradation rate only depends on the individual features of the devices, such as variations in the properties of the raw materials in the production process. It is also assumed that the units degradation rates do not vary along time. These assumptions can be a substantial simplification of reality. The rate at which the units degrade may evolve through time and is not only affected by the quality of the materials. The impact of the environment, under which all units are subjected, may affect the rate at which the devices degrade through time, producing changes in the degradation paths. To handle time-variant degradation rates, a common approach is to include into the model covariates evolving through time such as temperature, pressure, humidity and others. However, in some degradation trials, such covariates are not available.

Dynamic models can be used to circumvent the imposition of a regular functional form that controls the behavior of degradation trajectories. Such models provide a piecewise approxima-

tion for the true degradation path, better accommodating the oscillations during the study. In the reliability literature, dynamic approaches of general path models are not commonly used to analyze degradation data. Jiang and Yongcang [2002] model each degradation path as a Markovian process. The dynamic general degradation path model introduced by Hong *et al.* [2015] considers individual random effects to describe degradation paths and assumes a time series model to describe the dynamic covariate behavior influencing the degradation process. Veloso and Loschi [2021] proposed a dynamic linear degradation path model with degradation baselines and rates varying over time. As this dynamic structure provides a local linear approximation for the true degradation path, this model may accommodate different shapes for the degradation paths providing a way to handle data on heterogeneous populations. All these models consider a normal distribution for the observed degradation measures.

Considering the different factors that influence the intensity in which the process degrades and assuming that the degradation measures are necessarily positive, we develop (Section 2) a dynamic multivariate gamma model (DMGM) under the general path models approach. To circumvent the absence of time-variant covariates explaining the degradation rate, we assume that the degradation rate associated with the DMGM depends on two random effect components: a unit-specific component measuring the effect of particular features of the devices, such as the materials' quality they are made of, and a dynamic component measuring the effect of the typical environment to which all units under test are subject. The proposed model also accommodates different forms of the degradation trajectories, including that shown in Figure 3.1, as it assumes that the degradation measures are related to different functions of the inspection times. Thus, the model developed by Aktekin *et al.* [2021] for positive time series is a particular case of our approach. It also introduces a time-variant discount factor which is essential when the degradation data have not equidistant inspection times as noted in the data given in Figure 3.1b. This assumption produces a more flexible model, as it allows controlling the amount of information passed from one inspection time to the next, accommodating different degrees of uncertainty about the effect of time on the degradation rate over time.

Besides the traditional time to failure analysis, the proposed approach allows for a deeper understanding of the degradation mechanism. As in other general path degradation models, we infer the unit-specific effect on the degradation rate. Additionally, this approach allows us to evaluate the time influence in the devices' degradation capturing smooth changes on the degradation rate along the time. To the best of our knowledge, this type of decomposition has not being previously considered in degradation studies using general path models. Another advantage of assuming the decomposition related to the proposed degradation rate is to obtain a parsimonious dynamic model and, consequently, more computational efficiency. However, by doing so, the model becomes non-identifiable. Non-identifiability issues usually bring some challenges for modeling since to estimate the model, constraints should be imposed on the parametric space, or additional information about the parameters is required [Rothenberg, 1971]. For the proposed model, however, this is not a cumbersome problem as identifiability is obtained by specifying an informative prior distribution for the effect on the degradation rate

of the time of use of the devices before starting the degradation test. If all devices are new, this prior distribution should reveal a null expected time effect. We discuss the model identifiability in Section 3.2.1 formally presenting the constraints for its identification.

The unknown parameters of the DMGM are estimated considering a MCMC approach discussed in Sections 3.2.2.1 and 3.2.2.2. In Section 3.3, the relation between the failure time and the parameters of the model is established, and the inference for the failure time distribution is conducted for future and under test units. These results are essential to access, for instance, the RUL and the system reliability. To that end, we need to discuss forecasting procedures for future degradation measures under the gamma model, providing another extension of Aktekin *et al.* [2021]. We run simulation studies (Section 3.4) to evaluate the performance of the proposed model in different scenarios. This study also provides some guidelines to specify the prior distributions for parameters involved in the model identification constraints. We apply the proposed model (Section 3.5) to analyse the fatigue crack-size [Meeker and Escobar, 1998] and the stress relaxation [Yang, 2007] datasets. Section 3.6 closes the paper with some discussion and main conclusions.

3.2 Dynamic Multivariate Gamma Model

Let Y_{ij} be a positive degradation measurement for the ith experimental unit accumulated until the jth inspection time, $i = 1, 2, \ldots, n$, $j = 1, 2, \ldots, m_i$, where m_i is the number of degradation measures collected for unit i. Suppose that, at each inspection time interval, all units under test are subject to the same random influence of the environment and that such environmental effect varies over time. Denote by ψ_{ij} the random component that represents the joint effect of the i-th unit feature at the j-th measurement instant in the degradation paths. Let $\mathbf{\Psi} = (\psi_{11}, \ldots, \psi_{nm_n})$ and $\mathbf{t} = (t_{11}, \ldots, t_{nm_n})$ where t_{ij} is the jth inspection time for unit i. Assume also that, given $\mathbf{\Psi}$ and $\mathbf{t}$, the positive degradation measures for all units under test, $(y_{11}, \ldots, y_{nm_n})$, are independent and subject to the same degradation structure such that

$$Y_{ij}|\mathbf{\Psi}, \mathbf{t} \overset{ind}{\sim} Gamma\left(g(t_{ij}), \psi_{ij}\right), \quad i = 1, 2, \ldots, n,\ j = 1, 2, \ldots, m_i. \tag{3.1}$$

where $g(t_{ij})$ is a positive increasing function of t_{ij} characterizing the form of the true degradation path $D(t_{ij}, \mathbf{\Psi})$. Under this assumption, the true degradation path is given by the expected of expression (3.1), that is, $D(t_{ij}, \mathbf{\Psi}) = E(Y_{ij}|\mathbf{\Psi}, \mathbf{t}) = \frac{g(t_{ij})}{\psi_{ij}}$. If the degradation path is linear g should be a identity function. For degradation paths behaving as that in Figures 3.1 (a) and 3.1 (b), the function $g(t_{ij})$ should be equal to t_{ij}^2 and $\sqrt{(}t_{ij})$, respectively.

The model in (3.1) is over-parameterized which can lead to a high computational time to estimate the parameters. Besides this parametrization does not allow us to separately distinguish the effect of time and of the specific feature associated to each unit in its degradation. The identification of these effects is an important tool to understand the mechanisms underlying the degradation process.

To obtain a parsimonious and more conveniently interpretable model, we assume that the intensity with which devices degrade is determined by two factors: the specific features of each unit, that does not change during the trials, such as variations in the raw materials from which they are produced, and the environmental conditions they are exposed to, such as temperature and pressure. To take these two features into account, we decompose ψ_{ij} in a product of two components letting $\psi_{ij} = \lambda_i\theta_j$ where $\lambda_i > 0$ is the static and specific component of unit i and $\theta_j > 0$ represents the random effects that capture the common influence of environment at the jth inspection time. Considering this new parametrization, the vector of parameters becomes $\boldsymbol{\Psi} = (\boldsymbol{\lambda}, \boldsymbol{\theta})$, where $\boldsymbol{\lambda} = (\lambda_1, \ldots, \lambda_n)$, $\boldsymbol{\theta} = (\theta_1, \ldots, \theta_J)$ and $J = \max\{m_i, i = 1, 2, \cdots, n\}$. If $m_i < J$, for some unit i, or if some degradation measures are not observed, data imputation procedures can be considered to impute the missing observations. In dynamic models, data imputation is easily implemented in the state components inferential process using procedures discussed in Petris *et al.* [2009].

The observational equation can be rewritten as

$$Y_{ij}|\boldsymbol{\Psi}, \mathbf{t} \overset{ind}{\sim} Gamma\left(g(t_{ij}), \lambda_i\theta_j\right), \quad i = 1, 2, \ldots, n, \; j = 1, 2, \ldots, m_i. \tag{3.2}$$

Independence is a strong assumption whenever we deal with longitudinal data. However, the model in (3.2) is based on a weaker assumption as independence only follows conditionally on the parameter. Under this model structure, we consider that the degradation measures for the ith unit under test, $Y_{i1}, Y_{i2}, \ldots, Y_{im_i}$, are independent given $\boldsymbol{\theta}$, $\boldsymbol{\lambda}$ and $\mathbf{t}$. Similar hypothesis is assumed for the degradation measures at the jth inspection time by considering that $Y_{1j}, Y_{2j}, \ldots, Y_{nj}$ are independent conditionally on $\boldsymbol{\theta}$, $\boldsymbol{\lambda}$ and $\mathbf{t}$.

By eliciting a prior distribution for the random effect λ_i quantifying our prior knowledge about the specific characteristics of the unit i. A prior distribution for the dynamic component θ_j measuring the environment effect plays an important role in the model as it correlates the degradation measurements of all units at the j-th inspection time.

Under the model in (3.2), the instantaneous degradation rate is a function of the static component λ_i and the time-dependent component θ_j. As the true degradation path is $E\left(Y_{ij}|\lambda_i, \theta_j, t_{ij}\right) = D(t_{ij}; \lambda_i, \theta_j) = (\lambda_i\theta_j)^{-1}g(t_{ij})\ (\lambda_i\theta_j)^{-1}g(t_{ij})$, for any differentiable function g, the instantaneous degradation rate at any time $t \in [j, j+1)$ is $(\lambda_i\theta_j)^{-1}\frac{d}{dt}g(t)$. If g is the identity function, the degradation rate at any time t into the inspection time interval $[j, j+1)$ is constant and equal to $(\lambda_i\theta_j)^{-1}$. Thus, the units under test tend to fail less frequently when the values of θ_j and λ_i are high. If $g(t) = t^2$, the degradation rate assumes different values for any $t \in [j, j+1)$. For instance, if both, $t = 1$ and $t = 2$, belong to the inspection time interval $[j, j+1)$, the instantaneous degradation rate at time $t = 2$ is two times $2(\lambda_i\theta_j)^{-1}$ that is the degradation rate at time $t = 1$. Fixing λ_i and θ_j, both the expectation and the variance of the conditional distribution for the degradation measurements given in (3.2) increase over time. In fact, we expect that the units under test are more prone to fail and the variability on the degradation measures to be higher as the time of operation of the devices increases.

Besides the gain in interpretability, as it allows to separately infer the environment and unity-specific effects on the degradation, the decomposition strategy proposed in (3.2) greatly facilitates the computational implementation of the model. Since θ_j is a scalar, there is a reduction in the dimension of the state components requiring less computational effort if compared to usual dynamic model approach defined in (3.1).

To complete our model specification, we need to specify the prior distributions for all λ_i and θ_j. We assume *a priori* that the unit-specific effects λ_i, $i = 1, \ldots, n$, are independent with the gamma distributions

$$\lambda_i \overset{ind.}{\sim} Gamma(a_i, b_i) \quad \text{for } i = 1, 2, \ldots, n, \tag{3.3}$$

where $a_i > 0$ and $b_i > 0$ are hyperparameters and should be specified to represent the prior knowledge about how the specific features of unit i affects the degradation rate. This distribution should reveal our a priori knowledge on how, for example, the raw material the device is made of affects how quickly the device degrades.

To model the prior uncertainty about the dynamic components θ_j, we will assume that they evolve over time, allowing for changes in the degradation rates. This evolution imposes that the dynamic component at inspection time t_{ij} is related to that observed in inspection time $t_{i(j-1)}$. It is reasonable to assume that the effect of the environment is similar when measured in close inspection times. To model the time-dependence between the parameters $\theta_j \in \boldsymbol{\theta}$, following Smith and Miller [1986] and Santos *et al.* [2017], we consider the Markovian evolution equation given by

$$\theta_j = \frac{\theta_{j-1}}{\gamma_j}\epsilon_j, \text{ for } j = 1, 2, ..., J, \tag{3.4}$$

where γ_j is the discount factor at each inspection time j and the error term ϵ_j has the following beta distribution

$$\epsilon_j | \mathbf{D}^{j-1}, \boldsymbol{\lambda}, \mathbf{t} \sim Beta\left[\gamma_j \alpha_{j-1}, (1-\gamma_j)\alpha_{j-1}\right], \tag{3.5}$$

where $\alpha_{j-1} > 0$ and $\mathbf{D}^{j-1} = \{\mathbf{D}^{j-2}, Y_{1,j-1}, \ldots, Y_{n,j-1}, t_{1,j-1}, \ldots, t_{n,j-1}\}$ represents the sequential arrival of degradation measurements and inspection times. If $t_{ij} = t_j$ for all units i, following Santos *et al.* [2017], we can consider a simpler structure by assuming $\gamma_j = \gamma^{z_j}$, with $0 < \gamma < 1$ and, $z_j = [J(t_j - t_{(j-1)})][\sum_{j=1}^{J}(t_j - t_{(j-1)})]^{-1}\mathbf{1}\{j \leq m_i\}$, where $\mathbf{1}\{A\}$ is the indicator function assuming 1 if event A ocurrs.

At the initial measurement instant $j = 0$, we assume the prior distribution $\theta_0 | \mathbf{D}^0 \sim Gamma(\alpha_0, \beta_0)$, where $\alpha_0 > 0$ and $\beta_0 > 0$ are specified to represent our prior knowledge about the effect of the environment on the units degradation. We also assume that θ_0 and each of the parameters in $\boldsymbol{\lambda}$ are independent. For a discussion on how to specify the prior distribution for θ_0 see Sections 3.2.1 and 3.4.

Although the evolution equation given in (3.4) is multiplicative, if considered in the log scale [Smith and Miller, 1986], it is a random walk. Furthermore, if the inspection times in (3.4) are equally spaced, it follows that $z_j = 1$ and $\gamma_j = \gamma$, recovering the discount factor specification

of the Aktekin *et al.* [2021]'s model.

Differently from the approach considered by Aktekin *et al.* [2018] and Aktekin *et al.* [2021] that assumes a common discrete discount factor, we suppose that the discount factor γ_j at each inspection time j is a function of an unknown parameter γ and varies over time according to the range of each time interval. This modification in the discount factor makes the model more flexible controlling the amount of information passed from one inspection time to the next. If the length of the interval between two subsequent inspection times is large (small), we have a high (low) uncertainty imposing that the discount factor is small (large). This structure may be more appropriate to analyze degradation data with non-equidistant inspection times, such as the stress relaxation data (Figure 3.1b). In our model, we only consider that the discount factor varies with the range of the interval. Other structures can be assumed for z_j as discussed in Santos *et al.* [2017].

3.2.1 The Model Identifiability

Although the structure for ψ_{ij} assumed in equation (3.2) generates a parsimonious dynamic model that allows for a deeper understanding of the mechanism underlying the degradation process, the model in (3.2) is non-identifiable. For a non-identifiable model, the likelihood function associated with the observed sample assumes the same value for a subset A composed by several different values of the parameters $\boldsymbol{\Psi} = (\boldsymbol{\lambda}, \boldsymbol{\theta})$, which prevents us to estimate the parameters exclusively from the observed data. The model is fully identified if the subset A of such parameters values is empty [Gustafson , 2005].

To learn if the model is identifiable, we should evaluate the likelihood function to assess whether the data provide enough information to estimate all model parameters $\boldsymbol{\Psi}$. Regardless of the paradigm underlying the adopted inferential process, the usual ways to detect an unidentifiable model are to identify whether the Fisher information matrix is singular or whether the number of independent sufficient statistics is equal to the number of parameters to be estimated (see Rothenberg [1971] and Gustafson [2005] for more details).

Different approaches are considered to identify the model, thus allowing for its estimation. We can impose some constraints on the parametric space so that the subset A is empty, for instance, we can fix part of the parameters in some known values. Another approach is to get extra information from other sources, such as validation datasets [Rothenberg, 1971]. From the Bayesian point-of-view, model identifiability is obtained by considering information from experts to build a prior distribution for the parameters that puts zero probability mass to the subset A [Gustafson , 2005; Oliveira *et al.*, 2021].

As it will be shown in the following, for the proposed model, lack of identifiability is not a cumbersome problem. As will be proven, if we assume an informative prior distribution for the effect on the degradation rate of the devices usage time before starting the degradation test, then we can estimate all the parameters of the model. These theoretical aspects are not discussed by Aktekin *et al.* [2021] which time series model is a particular case of our model.

Without losing generality, in this section, we consider common inspection times for all units doing $t_{ij} = t_j$, for all i. This is a usual assumption in most degradation experiments. It is noteworthy that the hyperparameter γ does not play a role in the model identifiability as the full likelihood of DMGM is free of γ. This parameter is part of the evolution equation and is accessed indirectly from the information about $\boldsymbol{\theta}$.

Proposition 3.2.1. *The Fisher information matrix associated with the proposed DMGM given in expression (3.2) is singular.*

Proof. Considering the assumptions of model in (3.2), the log-likelihood function related to the DMGM is

$$l(\boldsymbol{Y}|\boldsymbol{\Psi}, \boldsymbol{t}) = \sum_{i=1}^{n}\sum_{j=1}^{J} \left[g(t_j)\log(\lambda_i\theta_j) - \log(\Gamma(g(t_j))) + g(t_j)\log(y_{ij}) - \lambda_i\theta_j y_{ij}\right], \tag{3.6}$$

where $\boldsymbol{Y} = [\boldsymbol{Y}_1, \boldsymbol{Y}_2, \cdots, \boldsymbol{Y}_J]$ with $\mathbf{Y}_j = (Y_{1j}, \ldots, Y_{nj})$, the degradation measurements collected at the j-th inspection time, for $j = 1, 2, \ldots, J$. Thus, the Fisher information matrix $\mathcal{I}(\boldsymbol{\Psi})$ for the DMGM is

$$\mathcal{I}(\boldsymbol{\Psi}) = \begin{bmatrix} \sum_{j=1}^{J}\frac{g(t_j)}{\lambda_1^2} & 0 & \cdots & 0 & \frac{g(t_1)}{\lambda_1\theta_1} & \frac{g(t_2)}{\lambda_1\theta_2} & \cdots & \frac{g(t_J)}{\lambda_1\theta_J} \\ 0 & \sum_{j=1}^{J}\frac{g(t_j)}{\lambda_2^2} & \cdots & 0 & \frac{g(t_1)}{\lambda_2\theta_1} & \frac{g(t_2)}{\lambda_2\theta_2} & \cdots & \frac{g(t_J)}{\lambda_2\theta_J} \\ \vdots & \vdots & \ddots & \vdots & \vdots & \vdots & \ddots & \vdots \\ 0 & 0 & \cdots & \sum_{j=1}^{J}\frac{g(t_j)}{\lambda_n^2} & \frac{g(t_1)}{\lambda_n\theta_1} & \frac{g(t_2)}{\lambda_n\theta_2} & \cdots & \frac{g(t_J)}{\lambda_n\theta_J} \\ \frac{g(t_1)}{\lambda_1\theta_1} & \frac{g(t_1)}{\lambda_2\theta_1} & \cdots & \frac{g(t_1)}{\lambda_n\theta_1} & \frac{ng(t_1)}{\theta_1^2} & 0 & \cdots & 0 \\ \frac{g(t_2)}{\lambda_1\theta_2} & \frac{g(t_2)}{\lambda_2\theta_2} & \cdots & \frac{g(t_2)}{\lambda_n\theta_2} & 0 & \frac{ng(t_2)}{\theta_2^2} & \cdots & 0 \\ \vdots & \vdots & \ddots & \vdots & \vdots & \vdots & \ddots & \vdots \\ \frac{g(t_J)}{\lambda_1\theta_J} & \frac{g(t_J)}{\lambda_2\theta_J} & \cdots & \frac{g(t_J)}{\lambda_n\theta_J} & 0 & 0 & \cdots & \frac{ng(t_J)}{\theta_J^2} \end{bmatrix}. \tag{3.7}$$

Let C_k be the k-th column of $\mathcal{I}(\boldsymbol{\Psi})$, $k = 1, 2, \ldots, n + J$. Considering the following transformation $-\lambda_k \times C_k$ if $k = 1, \ldots, n$ and $\theta_{k-n} \times C_k$ if $k = n + 1, \ldots, n + J$ it follows that $-\lambda_1 C_1 - \lambda_2 C_2 - \cdots - \lambda_n C_n + \theta_1 C_{n+1} + \theta_2 C_{n+2} + \cdots + \theta_J C_{n+J} = \mathbf{0}$. Thus, the columns in (3.7) are linearly dependent and, consequently, $\mathcal{I}(\boldsymbol{\Psi})$ is a singular matrix. □

According to the results obtained in Rothenberg [1971], it is impossible to ensure local identifiability for regular points in the parametric space $\boldsymbol{\Psi}$. As local identifiability is a necessary condition for global identifiability, it follows from Proposition 3.2.1 that the DMGM is globally non-identifiable.

Proposition 3.2.2. *The DMGM defined in equation (3.2) is identifiable if at least one of the parameters in $\boldsymbol{\Psi}$ is known.*

Proof. Without losing generality, assume that θ_1 is known. Under this assumption, the Fisher information matrix associated with the DMGM is obtained removing the row and column

related to θ_1 from the matrix in (3.7). In the resulting Fisher information matrix $I(\boldsymbol{\Psi}^{[-\theta_1]})$, the rows and columns associated with λ_i are multiplied by $\frac{1}{\lambda_i}$, for $i = 1, 2, \cdots, n$ and the rows and columns with respect to θ_j are multiplied by $\frac{g(t_j)}{\theta_j}$ and $\frac{1}{\theta_j}$, respectively, for $j = 1, 2, \cdots, J$. Thus, it follows from some properties of matrix algebra that the determinant of $I(\boldsymbol{\Psi}^{[-\theta_1]})$ is

$$|I(\boldsymbol{\Psi}^{[-\theta_1]})| = \frac{\prod_{j=2}^{J} g(t_j)}{\prod_{i=1}^{n}\lambda_i^2 \prod_{j\neq 1}\theta_j^2} \begin{vmatrix} \sum_{j=1}^{J} g(t_j) & 0 & \cdots & 0 & g(t_2) & \cdots & g(t_J) \\ 0 & \sum_{j=1}^{J} g(t_j) & \cdots & 0 & g(t_2) & \cdots & g(t_J) \\ \vdots & \vdots & \ddots & \vdots & \vdots & \ddots & \vdots \\ 0 & 0 & \cdots & \sum_{j=1}^{J} g(t_j) & g(t_2) & \cdots & g(t_J) \\ 1 & 1 & \cdots & 1 & n & \cdots & 0 \\ 1 & 1 & \cdots & 1 & 0 & \cdots & 0 \\ \vdots & \vdots & \ddots & \vdots & \vdots & \ddots & \vdots \\ 1 & 1 & \cdots & 1 & 0 & \cdots & n \end{vmatrix}. \quad (3.8)$$

The determinant of the matrix in (3.8) can be calculated by reducing it to a triangular matrix. For this, we swapped the first with the last row, changing the sign of the determinant. he resulting triangular matrix is given by

$$\begin{pmatrix} 1 & 1 & \cdots & 1 & 0 & 0 & \cdots & 0 & n \\ 0 & \sum_{j=1}^{J} g(t_j) & \cdots & 0 & g(t_2) & g(t_3) & \cdots & g(t_{J-1}) & g(t_J) \\ \vdots & \vdots & \ddots & \vdots & \vdots & \vdots & \ddots & \vdots & \vdots \\ 0 & 0 & \cdots & \sum_{j=1}^{J} g(t_j) & g(t_2) & g(t_3) & \cdots & g(t_{J-1}) & g(t_J) \\ 0 & 0 & \cdots & 0 & n & 0 & \cdots & 0 & -n \\ 0 & 0 & \cdots & 0 & 0 & n & \cdots & 0 & -n \\ \vdots & \vdots & \ddots & \vdots & \vdots & \vdots & \ddots & \vdots & \vdots \\ 0 & 0 & \cdots & 0 & 0 & 0 & \vdots & n & -n \\ 0 & 0 & \cdots & 0 & 0 & 0 & \cdots & 0 & -ng(t_1) \end{pmatrix},$$

whose determinant is $-(\sum_{j=1}^{J} g(t_j))^{n-1} n^{J-1} g(t_1)$. Consequently, the determinant of $I(\boldsymbol{\Psi}^{[-\theta_1]})$ is

$$|I(\boldsymbol{\Psi}^{[-\theta_1]})| = \frac{n^{J-1}\left[\prod_{j=1}^{J} g(t_j)\right](\sum_{j=1}^{J} g(t_j))^{n-1}}{\prod_{i=1}^{n}\lambda_i^2 \prod_{j\neq 1}\theta_j^2}. \quad (3.9)$$

As all parameters and functions are positive, the determinant in expression (3.9) will always be positive. More generally, the same reasoning can be used by fixing any of the other parameters. Therefore, the resulting Fisher information matrices are non-singular. Since this model belongs to the exponential family, from Theorem 3 in Rothenberg [1971], the DMGM with at least one known parameter is globally identifiable. □

Another way to verify the model identifiability is to examine if the number of independently sufficient statistics is equal to the number of parameters to be estimated. The proof and technical details about this discussion are formally presented in Section S1 of the Supplementary

Materials.

In degradation trials, it is expected that the effect of time in the device degradation at the beginning of the experiment is small or null as the devices are usually new. Thus, the initial degradation rates depend basically on the static component of each unit, and a better learning of these static components is initially obtained. The random effects of the common environment will appear during the study if it exists. In practice, it is challenging to establish a prior knowledge about the effect of the static parameters λ_i, for $i = 1, 2, \ldots, n$, in the degradation since these components measure the impact of the devices individual features. It is common to assume that the units under test are similar and are selected in the same population. Thus, to identify the model, it is more feasible to place prior knowledge on the initial dynamic component θ_0. If all devices under test are new, we expect a null effect of environment on the degradation rate at this initial instant. This null effect may be described by a prior distribution for θ_0 centered around 1 as such an assumption imposes that $E(\psi_{i1}) = E(\lambda_i)E(\theta_0) = E(\lambda_i)$. In this case we may identify the model assuming that, *a priori*, $\theta_0|\mathbf{D}^0 \sim Gamma(\alpha_0, \beta_0)$ such that $E(\theta_0|\mathbf{D}^0) = 1$. If the environmental effect is expected to be positively high at the beginning of the experiment, this reveals that prior distribution for θ_0 should concentrate its probability mass in values close to zero.

On the other hand, for example, if the model is fitted to volatility data obtained in several countries at the same time as discussed in Aktekin *et al.* [2021], usually, there is available some prior information about the influence of the more stable economy in the volatility of other markets. Thus, it could be more natural to identify the model through the prior distribution of this country's static component in the evolution of the volatility.

Result in Proposition 3.2.2 provides some mathematical constraints needed to guarantee that all parameters may be estimated from the observed data. However, even considering such restrictions, there is no guarantee that all parameters will be well estimated. Theoretical identifiability may not guarantee practical identifiability. Even for an identifiable model, large sample sizes might be required to obtain reasonable parameter estimates in some situations. However, some parameters might not be estimated for a nonidentifiable model, even if a large sample size is available.

3.2.2 Posterior inference

3.2.2.1 The Filtering Distribution

One feature of the DMGM is that it allows analytically treatable sequential filtering, conditioned on static parameters. To obtain the filtering distributions, assume the prior specifications given in the introduction of Section 3.2. By assuming the distribution for ϵ_j given in (3.5), it follows from the state evolution defined in (3.4) that the conditional distribution of the environment effect θ_j at the jth inspection time, given such effect in the previous inspection time

θ_{j-1}, $\boldsymbol{\lambda}$, the data information $\mathbf{D}^{j-1}$ and γ is the scaled beta distribution with density

$$\begin{aligned} p(\theta_j|\theta_{j-1},\mathbf{D}^{j-1},\boldsymbol{\lambda},\gamma) &= \frac{\Gamma(\alpha_{j-1})}{\Gamma(\gamma_j\alpha_{j-1})\Gamma((1-\gamma_j)\alpha_{j-1})}\left(\frac{\gamma_j}{\theta_{j-1}}\right)^{\gamma_j\alpha_{j-1}}\theta_j^{\gamma_j\alpha_{j-1}-1} \\ &\times \left(1-\frac{\gamma_j}{\theta_{j-1}}\theta_j\right)^{(1-\gamma_j)\alpha_{j-1}-1}, \quad 0<\theta_j<\frac{\theta_{j-1}}{\gamma_j}, \end{aligned} \tag{3.10}$$

where $\alpha_{j-1}>0$ and $\gamma_j\in(0,1)$, for $j=1,\ldots,J$. This distribution plays an important role in updating the dynamic parameters, besides being useful to find the marginal conditional distribution associated with the degradation measurements.

Another important distribution in the updating of the dynamic components is the posterior distribution of θ_{j-1}, given $\mathbf{D}^{j-1}$, $\boldsymbol{\lambda}$ and γ. By assuming, *a priori*, that $\theta_0|\mathbf{D}^0\sim Gamma(\alpha_0,\beta_0)$ and sequentially using the Bayes theorem, it follows by that the posterior distribution of θ_{j-1}, given $\mathbf{D}^{j-1}$, $\boldsymbol{\lambda}$ and γ, for all $j=1,\ldots,J$,

$$\theta_{j-1}|\mathbf{D}^{j-1},\boldsymbol{\lambda},\gamma\sim Gamma(\alpha_{j-1},\beta_{j-1}), \tag{3.11}$$

where $\alpha_{j-1}=\sum_{i=1}^n g(t_{ij-1})+\gamma_{j-1}\alpha_{j-2}$ and $\beta_{j-1}=\sum_{i=1}^n\lambda_i y_{ij-1}+\gamma_{j-1}\beta_{j-2}$. The prior distribution for θ_j is given by $p(\theta_j|\mathbf{D}^{j-1},\boldsymbol{\lambda},\gamma)=\int p(\theta_j|\theta_{j-1},\mathbf{D}^{j-1},\boldsymbol{\lambda},\gamma)p(\theta_{j-1}|\mathbf{D}^{j-1},\boldsymbol{\lambda},\gamma)d\theta_{j-1}$. Considering the results in (3.10) and (3.11), this *a priori* distribution is

$$\theta_j|\mathbf{D}^{j-1},\boldsymbol{\lambda},\gamma\sim Gamma(\gamma_j\alpha_{j-1},\gamma_j\beta_{j-1}). \tag{3.12}$$

Considering $\boldsymbol{t}_j=(t_{ij},t_{2j},\ldots,t_{nj})$, the filtering density can be obtained mixing the likelihood in (3.1) and the prior specification in (3.12) doing $p(\theta_j|\mathbf{D}^j,\boldsymbol{\lambda},\gamma)\propto p(Y_{1j},\ldots,Y_{nj}|\theta_j,\boldsymbol{\lambda},\boldsymbol{t}_j)$ $p(\theta_j|\mathbf{D}^{j-1},\boldsymbol{\lambda},\gamma)$. Thus, the filtering distribution for θ_j is

$$\theta_j|\mathbf{D}^j,\boldsymbol{\lambda},\gamma\sim Gamma(\alpha_j,\beta_j) \tag{3.13}$$

where $\alpha_j=\sum_{i=1}^n g(t_{ij})+\gamma_j\alpha_{j-1}$ and $\beta_j=\sum_{i=1}^n\lambda_i y_{ij}+\gamma_j\beta_{j-1}$. Note that the error term associated to the markovian evolution given in expression (3.4) basically depends on t_{ij}. This means that the inspection times play an important role also in the evolution of the random effects associated to the common environment.

3.2.2.2 Inference on Unknown Parameters

We use MCMC techniques for sequentially estimate the static parameters λ_i, $i=1,\ldots,n$, the dynamic components θ_j, $j=1,\ldots,J$ and γ. Samples from the posterior distribution of the parameters $(\boldsymbol{\theta},\boldsymbol{\lambda},\gamma)$ are generated using the following scheme:

i. Generate $\boldsymbol{\theta}$ via $p\left(\boldsymbol{\theta}|\boldsymbol{\lambda},\gamma,\mathbf{D}^J\right)$;

ii. Generate $\boldsymbol{\lambda}$ via $p\left(\boldsymbol{\lambda}|\boldsymbol{\theta},\gamma,\mathbf{D}^J\right)$;

iii. Generate γ via $p\left(\gamma|\boldsymbol{\lambda},\boldsymbol{\theta},\mathbf{D}^J\right)$.

For the first step, we use the non-Gaussian version of the forward filtering and backward sampling (FFBS). Details on this procedure can be found in Gamerman *et al.* [2013], Carter and Kohn [1994], Fruhwirth-Schnatter [1994] and Shepard [1994]. For this step we must notice that the joint conditional density $p(\boldsymbol{\theta}|\boldsymbol{\lambda},\gamma,\mathbf{D}^J) = p(\theta_J|\boldsymbol{\lambda},\gamma,\mathbf{D}^J)p(\theta_{J-1}|\theta_J,\boldsymbol{\lambda},\gamma,\mathbf{D}^{J-1})\ldots p(\theta_1|\theta_2,\boldsymbol{\lambda},\gamma,\mathbf{D}^1)$, in which the first term is the filtering distribution given in (3.13) associated with the J-th inspection time. Using the FFBS, we first generate samples of the last state component θ_J using its filtering distribution and, samples of all other component θ_{j-1}, $j = J, J-1,\ldots,2$, are generated, retrospectively, from the following distribution

$$\begin{aligned} p(\theta_{j-1}|\theta_j,\mathbf{D}^{j-1},\boldsymbol{\lambda},\gamma) &= \frac{p(\theta_j|\theta_{j-1},\mathbf{D}^{j-1},\boldsymbol{\lambda},\gamma)p(\theta_{j-1}|\mathbf{D}^{j-1},\boldsymbol{\lambda},\gamma)}{p(\theta_j|\mathbf{D}^{j-1},\boldsymbol{\lambda},\gamma)} \\ &= \frac{(\theta_{j-1}-\gamma_j\theta_j)^{(1-\gamma_j)\alpha_{j-1}-1}\beta_{j-1}^{(1-\alpha_{j-1})\alpha_{j-1}}e^{-\beta_{j-1}(\theta_{j-1}-\gamma_j\theta_j)}}{\Gamma((1-\alpha_{j-1})\alpha_{j-1})}, \end{aligned} \tag{3.14}$$

if $\theta_{j-1} > \gamma_j\theta_j$. The expression in (3.14) is a particular case of the Pearson Type III distribution [Abramowitz *et al.*, 1988] which is the generalized gamma distribution widely used in hydrologic frequency analysis.

In the second step, as we assume that the components of vector $\boldsymbol{\lambda}$ are conditionally independent, given the dynamic parameters $\boldsymbol{\theta}$ and $\mathbf{D}^J$, the posterior full conditional posterior distribution (fcd) of λ_i is obtained using the standard procedure and is

$$\lambda_i|\boldsymbol{\theta}_j,\mathbf{D}^J,\gamma \sim Gamma\left(\sum_{j=1}^{J} g(t_{ij}) + a_i, \sum_{j=1}^{J}\theta_j y_{ij} + b_i\right). \tag{3.15}$$

To generate from the posterior distribution of γ (Step (iii)), we partially collapse the Gibbs Sampler integrating $\boldsymbol{\theta}$ out. To obtain the posterior fcd of γ free of the $\boldsymbol{\theta}$, considering equations (3.1) and (3.12), we firstly obtain the distribution of Y_{ij} given $\boldsymbol{\lambda}$ and γ as

$$\begin{aligned} p(y_{ij}|\mathbf{D}^{j-1},\boldsymbol{\lambda},\gamma,t_{ij}) &= \int p(y_{ij}|\theta_j,\lambda_i,t_{ij})p(\theta_j|\mathbf{D}^{j-1},\boldsymbol{\lambda},\gamma)d\theta_j \\ &= \frac{\Gamma(g(t_{ij})+\gamma_j\alpha_{j-1})}{\Gamma(g(t_{ij}))\Gamma(\gamma_j\alpha_{j-1})}\frac{(\frac{\gamma_j\beta_{j-1}}{\lambda_i})^{\gamma_j\alpha_{j-1}}y_{ij}^{g(t_{ij})-1}}{\left(y_{ij}+\frac{\gamma_j\beta_{j-1}}{\lambda_i}\right)^{g(t_{ij})+\gamma_j\alpha_{j-1}}}. \end{aligned} \tag{3.16}$$

This distribution is a particular case of the gamma-gamma distribution [Bernardo and Smith, 2009]. It is essential when inferring about the failure time of the units under test and future ones as it allows to find the relationship between the failure time and the model parameters as we discuss in Section 3.3.

The joint distribution of the measures at the j-th inspection time given $\boldsymbol{\lambda}$ and γ for all units

is obtained considering (3.16) and the conditional independence assumptions as

$$\begin{aligned} p(\boldsymbol{Y}_j|\boldsymbol{\lambda}, \mathbf{D}^{j-1}, \gamma, \boldsymbol{t}_j) &= \int p(\boldsymbol{y}_j|\theta_j, \boldsymbol{\lambda}, \boldsymbol{t}_j) p(\theta_j|\mathbf{D}^{j-1}, \boldsymbol{\lambda}, \gamma) d\theta_j \\ &= \frac{\Gamma(\sum_{i=1}^{n} g(t_{ij}) + \gamma_j \alpha_{j-1})}{\prod_i \Gamma(g(t_{ij}))\Gamma(\gamma_j \alpha_{j-1})} \left[\prod_i \lambda_i^{g(t_{ij})} y_{ij}^{g(t_{ij})-1}\right] (\gamma_j \beta_{j-1})^{\gamma_j \alpha_{j-1}} \\ &\times \left(\sum_{i=1}^{n} \frac{y_{ij}\lambda_i}{\beta_{j-1}} + \gamma_j\right)^{-\left(\sum_{i=1}^{n} g(t_{ij}) + \gamma_j \alpha_{j-1}\right)}. \end{aligned} \tag{3.17}$$

Assuming, *a priori*, that $p(\gamma) \sim Beta(p, q)$, $q > 0$, $p > 0$, and considering the equation (3.17), the posterior fcd of γ is

$$p\left(\gamma|\lambda_1, \ldots, \lambda_n, \theta_1, \ldots, \theta_J, \mathbf{D}^J\right) \propto \gamma^{p-1}(1-\gamma)^{q-1} \prod_{j=1}^{J} p(\boldsymbol{Y}_j|\boldsymbol{\lambda}, \mathbf{D}^{j-1}, \gamma, \boldsymbol{t}_j). \tag{3.18}$$

This distribution is unknown, and a Metropolis-Hastings step is required to sample from the posterior of γ. In this step, the candidates are generated from the uniform distribution (0,1).

3.2.2.3 The K-step ahead forecast distributions

In general path models, the forecasting of future degradation measurements plays a vital role in the development of methods to infer about the failure time.

Considering the proposed model defined in equations (3.1) and (3.4), the K-step ahead forecast is obtained in two steps: we should first obtain the distribution of θ_{J+K}, given $\boldsymbol{D}^{J+K-1}$, $\boldsymbol{\lambda}$ and γ and, after that, we should calculate the distribution of $y_{i(J+K)}$ given $\boldsymbol{D}^J$, $\boldsymbol{\lambda}$, γ and $t_{i(J+K)}$. For $K = 1$, such distributions are analytically obtained. The distribution for the one-step ahead dynamic component is given by

$$p(\theta_{J+1}|\boldsymbol{D}^J, \boldsymbol{\lambda}, \gamma) \sim Gamma(\gamma_J \alpha_J, \gamma_J \beta_J), \tag{3.19}$$

where α_J, β_J and γ_J are as in Equation (3.13). The one-step ahead forecast distribution for $Y_{i(J+1)}$ is obtained considering the distribution in (3.19) as the mixing distribution and, for $y_{i(J+1)} > 0$, is given by

$$\begin{aligned} p(y_{i(J+1)}|\mathbf{D}^J, \boldsymbol{\lambda}, \gamma, t_{i(J+1)}) &= \int p(y_{i(J+1)}|\theta_{J+1}, \lambda_i, t_{i(J+1)}) p(\theta_{J+1}|\mathbf{D}^J, \boldsymbol{\lambda}, \gamma) d\theta_{J+1} \\ &= \frac{\Gamma(g(t_{i(J+1)}) + \gamma_J \alpha_J)}{\Gamma(g(t_{i(J+1)}))\Gamma(\gamma_J \alpha_J)} \frac{(\frac{\gamma_J \beta_J}{\lambda_i})^{\gamma_J \alpha_J} y_{i(J+1)}^{g(t_{i(J+1)})-1}}{\left(y_{i(J+1)} + \frac{\gamma_J \beta_J}{\lambda_i}\right)^{g(t_{i(J+1)}) + \gamma_J \alpha_J}}, \end{aligned} \tag{3.20}$$

which is a particular case of the gamma-gamma distribution [Bernardo and Smith, 2009]. For each unit under test, the future degradation measure one-step ahead is obtained considering

the posterior mean of the distribution in (3.20) given by

$$E(Y_{i(J+1)}|\mathbf{D}^J, \boldsymbol{\lambda}, \gamma_J, t_{i(J+1)}) = \frac{g(t_{i(J+1)})\gamma_J\beta_J}{\lambda_i(\gamma_J\alpha_J - 1)}. \tag{3.21}$$

In some practical situations, it is of interest to obtain predictions for the degradation measures K-steps ahead, $K > 1$ [Peng *et al.*, 2016]. However, the prediction process is challenging for $K > 1$ as it is not simple to obtain the distribution for the K-step ahead dynamic component. An approximation for such a distribution can be found in Gamerman *et al.* [2013]. Although promising, in our analysis, this strategy did not provide reasonable forecasts for the failure time (results not show), generating more biased predictions. Thus, we decided to follow the forecasting method recommended by Gamerman *et al.* [2013].

To forecast degradation measures K-step ahead, $K > 1$, we propose to consider a sequential analysis incorporating the forecast obtained at step $J+1$ to forecast the degradation measurement at step $J+2$ and so on, repeatedly using expressions (3.19) and (3.20). Considering K future inspection times, the algorithm for forecasting $Y_{i(J+K)}$ is the following:

1. Fit the model to the observed data and calculate the predictions considering $\hat{y}_{i(J+1)} = [g(t_{i(J+1)})\hat{\gamma}_J\hat{\beta}_J][\hat{\lambda}_i(\hat{\gamma}_J\hat{\alpha}_J - 1)]^{-1}$, where $\hat{\psi}$ denotes the posterior mean of parameter ψ.

2. For $k = 2, \ldots, K$, fit the model incorporating the previous forecast $\hat{y}_{i(J+k-1)}$. Then, calculate

$$\begin{aligned} \hat{y}_{i(J+k)} &= \hat{E}(Y_{i(J+k)}|\mathbf{D}^{J+k-1}, \boldsymbol{\lambda}, \gamma_{J+k-1}, t_{i(J+k)}) \\ &= [g(t_{i(J+k)})\hat{\gamma}_{J+k-1}\hat{\beta}_{J+k-1}][\hat{\lambda}_i(\hat{\gamma}_{J+k-1}\hat{\alpha}_{J+k-1} - 1)]^{-1}. \end{aligned} \tag{3.22}$$

his algorithm is based on the forecast function, which is a conditional expectation of the following K-step ahead predicted distribution for the i-th unit:

$$p(y_{i(J+K)}|D_{J+K-1}, \boldsymbol{\lambda}, \gamma, t_{i(J+K-1)}) \approx$$

$$\begin{aligned} &= \int p(y_{i(J+1)}, \ldots, y_{i(J+K)}|D_{J+K-1}, \boldsymbol{\lambda}, \gamma, t_{i(J+k-1)})dy_{i(J+1):(J+K-1)} \\ &= \int \prod_{k=1}^{K} p(y_{i(J+k)}|D_{J+k-1}, \boldsymbol{\lambda}, \gamma, t_{i(J+k-1)})dy_{i(J+1):(J+K-1)}, \end{aligned}$$

where the set D is augmented adding the previous forecasts, then $D_{J+K-1} = \{D^J, \hat{y}_{i(J+1)}, \ldots, \hat{y}_{i(J+K-1)}\}$, for $i = 1, \ldots, n$. To draw a sample of joint future values $y_{i(J+1)}, \ldots, y_{i(J+K)}$ for the i-th unit, we can sample the conditional distributions given the previous forecasts, using Monte Carlo integration.

3.3 Inference for Failure Time

In degradation trials, the system reliability is indirectly accessed through the degradation mechanism, assuming that a failure occurs if the degradation path exceeds a threshold D_f that is pre-defined based on the prior knowledge of experts. In this section, we will develop some methods to infer about the failure time for units under test and future units.

3.3.1 Inference for Units Under Test

Consider a unit i under test that did not fail during the experimental study; that is, it fails after the maximum measurement instant J. Let T_i be the failure time associated with a unit i under test. The distribution of T_i is thus obtained from the relationship imposed by the model between degradation and time. Following the methodology usually considered in linear general path models [Freitas *et al*, 2010, 2009], if we assume the model in (3.2) such a relationship is given by

$$D(t_{ij}, \boldsymbol{\Psi}) = E(Y_{iJ} \mid \boldsymbol{\lambda}, \boldsymbol{\theta}, \mathbf{t}) = D_f \Rightarrow T_i = g^{-1}(D_f \lambda_i \theta_J). \tag{3.23}$$

To predict when the true degradation paths reach D_f is a vital step for establishing the system reliability and the remaining useful life (RUL). In dynamic linear degradation models, the method introduced by Veloso and Loschi [2021] is appealing as it replaces the posterior estimation for θ_J in (3.23) to forecast future degradation measurements and, from that, to estimate the failure time. The failure time forecast K-steps ahead is based on the local linear approximation related to the last observed time interval.

If equation (3.23) is non-linear, this strategy may introduce more bias in our predictions. To improve the time-to-failure prediction, we propose a sequential approach where the one-step ahead forecast for the degradation measure at time $J+1$ is incorporated into the analysis to predict the degradation measure at time $J+2$ and so on until the threshold D_f has been reached. Consequently, such a sequential feature is also taken into account when we infer the failure time of the units. This proposed procedure requires the estimation of θ_{J+k} for all $k \geq 1$ until D_f has been reached, which can be computationally expensive.

To reduce the computational cost, we adopt the strategy proposed by Gamerman *et al.* [2013] integrating the $\boldsymbol{\theta}$ out and obtaining an exact distribution to forecast degradation measurements one-step ahead given in equation (3.20). Considering the results obtained in Section 3.2.2.3, to estimate T_i, we propose to consider

$$\begin{aligned} D_f &= E_{\theta_{J+1}|\boldsymbol{D}^J,\boldsymbol{\lambda},\gamma}\left\{E(Y_{i(J+1)}|\boldsymbol{\lambda},\boldsymbol{\theta},\mathbf{t})\right\} \\ &= \frac{g(T_{i(J+1)})}{\lambda_i} E(\theta_{J+1}^{-1} \mid \boldsymbol{D}^J, \boldsymbol{\lambda}, \gamma) = \frac{g(t_{i(J+1)})\gamma_J \beta_J}{\lambda_i(\gamma_J \alpha_J - 1)}. \end{aligned}$$

If the function $g(t_{ij})$ is invertible, we can write T_i as

$$T_i = g^{-1}\left(\lambda_i D_f [E(\theta_J^{-1})]^{-1}\right) = g^{-1}\left(\lambda_i D_f \frac{(\gamma_J \alpha_J - 1)}{\gamma_J \beta_J}\right), \tag{3.24}$$

where $\alpha_J = \sum_{i=1}^{n} g(t_{iJ}) + \gamma_J \alpha_{J-1}$ and $\beta_J = \sum_{i=1}^{n} \lambda_i y_{iJ} + \gamma_J \beta_{J-1}$. If $g(t_{ij})$ is not invertible, then numerical methods can be used to approximate T_i. Expression (3.24) highlights the important relationship between the failure time T_i and the model parameters.

The influence of the unit-specific effect λ_i in the failure time is evident, but the degradation measurements of all units, the inspection times, and other static parameters are indirectly incorporated in the calculation of the failure time of unit i through the estimates of α_J and β_J.

Under these assumptions, the posterior predictive failure time distribution $F_{T_i|\boldsymbol{D^J}}(t|\boldsymbol{D^J})$ associated to a unit i under test evaluated at a time t is given by

$$\begin{aligned} F_{T_i|\boldsymbol{D^J}}(t|\boldsymbol{D^J}) &= P\left(g^{-1}\left(\lambda_i D_f \frac{(\gamma_J \alpha_J - 1)}{\gamma_J \beta_J}\right) \leq t|\boldsymbol{D^J}\right) \\ &= \int_0^1 \int_{\mathcal{C}} f_{\boldsymbol{\lambda},\gamma_J|\boldsymbol{D^J}}(\boldsymbol{\lambda}, \gamma_J|\boldsymbol{D^J}) d\boldsymbol{\lambda} d\gamma_J. \end{aligned}$$

where $\mathcal{C} = \{(\lambda_1, \ldots, \lambda_n) \in \mathbb{R}^n : \lambda_i(\gamma_J \alpha_J - 1)[\gamma_J \beta_J]^{-1} \leq g(t)[D_f]^{-1}\}$.

We obtain a posterior sampling for the failure time distribution of unit i as follows. Having available the posterior sample $\boldsymbol{\lambda}^{(l)}$ and $\gamma^{(l)}$ of the model parameters $\boldsymbol{\lambda}$ and γ, we calculate

$$T_i^{(l)} = g^{-1}\left(\frac{\lambda_i^{(l)} D_f (\gamma_J^{(l)} \alpha_J^{(l)} - 1)}{\gamma_J^{(l)} \beta_J^{(l)}}\right), \quad \text{for } l = 1, 2, \cdots, L,$$

where L is the posterior sample size. The posterior predictive cdf of T_i evaluated at time t is approximated by

$$\hat{F}_{T_i|\boldsymbol{D^J}}(t|\boldsymbol{D^J}) = \frac{\sum_{l=1}^{L} \mathbb{1}\{T_i^{(l)} \leq t\}}{L}.$$

In many practical situations, the remaining useful life (RUL) for units under test is of most interest. The RUL for a unit i under test that has been monitored until inspection time t_{im_i} is given by $RUL_i = E(T_i - t_{im_i}|T_i > t_{im_i})$ and can then be used to compare different models in specific scenarios of the inspection times, as in Wang *et al.* [2020]. Under the Bayesian paradigm, as in Veloso and Loschi [2021], the estimate for the RUL of a unit under i test, that has not failed, is given by $\overline{RUL_i} = [\sum_{l=1}^{L}(T_i^{(l)} - t_{im_i})]L^{-1}$.

3.3.2 Future Unit

Suppose that a new unit is included in the study. Assume that this unit is subject to the same interference of the environment as the units under test. To calculate the posterior predictive cdf for the failure time T_{n+1} of this new unit $F_{T_{n+1}|\boldsymbol{D^J}}(t|\boldsymbol{D^J})$, we assume that T_{n+1} has the same distribution as the failure times T_i of the units under test. Following Robinson and Crowder

[2000], we consider that the posterior sample of $\lambda_{(n+1)}$ is obtained sampling from the posterior distributions of the parameters λ_i, $i = 1, \ldots, n$. Thus, the estimation of $F_{T_{n+1}|\boldsymbol{D^J}}(t|\boldsymbol{D^J})$ at time t is given by

$$T_{n+1}^{(l)} = g^{-1}\left(\frac{\lambda_i^{(l)} D_f(\gamma_J^{(l)}\alpha_J^{(l)} - 1)}{\gamma_J^{(l)}\beta_J^{(l)}}\right), \quad i = 1, 2, \cdots, n, l = 1, 2, \cdots, L.$$

The posterior estimate for the predictive cdf of T_{n+1} evaluated at time t is given by

$$\hat{F}_{T_{n+1}|\boldsymbol{D^J}}(t|\boldsymbol{D^J}) = \frac{\sum_{l=1}^{L}\sum_{i=1}^{n} \mathbb{1}\left\{T_i^{(l)} \leq t\right\}}{nL}.$$

3.4 Simulation Studies: The effect of the prior distributions for θ_0 and γ

Despite dynamic models being widely used in multivariate time series, degradation data cannot be seen as just a cutout of such data types. Degradation data have certain specific features, usually not experienced by time series. For instance, at the beginning of the test, the units are often new and share the same degradation measure. This kind of standard brings information about the environmental effect at the first inspection time. This information allows identifying the model by fixing θ_1 in a known value (see discussion in Section 3.2.1). Instead of adopting a known value for θ_1, we assume a weaker constraint by specifying informative prior distributions for θ_0. In this section, we evaluate the effect of such prior specification in the posterior inference providing a sensitivity analysis to the proposed model.

We generate the degradation data from equations (3.1) and (3.4), considering $g(t_{ij}) = t_{ij}^2$. A sample of $n = 10$ units under test is considered and we assume that degradation is measured at $m_i = 10$ equidistant inspection times varing from 0 to 9. The unit-specific parameters λ_i, $i = 1, \cdots, 10$, are fixed in the following values $\lambda_1 = \lambda_2 = \lambda_3 = \lambda_4 = 1$, $\lambda_5 = \lambda_6 = \lambda_7 = \lambda_8 = 1.5$ and $\lambda_9 = \lambda_{10} = 2$. The parameter γ is defined to be $\gamma = 0.25$ and the initial state component is generated from $\theta_0 \sim$ Gamma $(\alpha_0 = 100, \beta_0 = 100)$. A failure occurs if the degradation path reaches the critical degradation threshold $D_f = 150$. We consider $R = 100$ replications of the data and Figure 3.2 represents one of these simulated datasets.

To assess the influence of the prior choice in the posterior inference, we consider the following prior distributions for θ_0: (1) $\theta_0 \sim$ Gamma$(0.01, 0.01)$, (2) $\theta_0 \sim$ Gamma$(1, 1)$, (3) $\theta_0 \sim$ Gamma$(10, 10)$, (4) $\theta_0 \sim$ Gamma$(100, 100)$ and (5) $\theta_0 \sim$ Gamma$(400, 200)$. Priors (1) to (4) have different variances revealing different degrees of uncertainty about the parameter but are all centered around 1, which is the expected value of the distribution of θ_0 used in the data generation. Aiming to assess the impact of placing an informative shifted prior distribution for θ_0, the distribution in (5) is centered in 2. We also assume different priors for γ: $\gamma \sim$ Beta(1,1) and $\gamma \sim$ Beta(2.08,4.26). These distributions are centered in the means 0.5 and

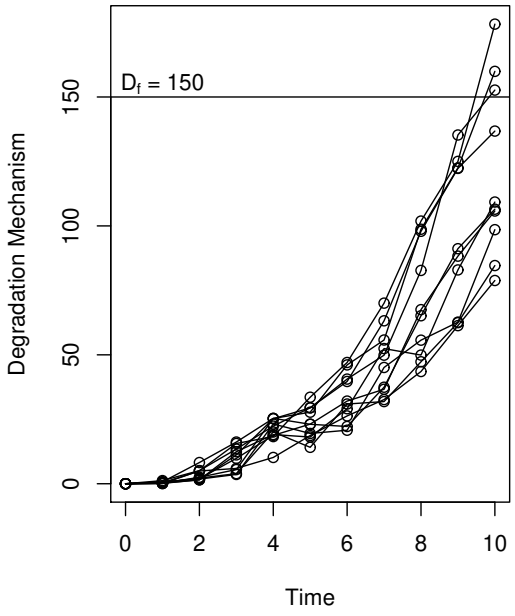

Figure 3.2: A simulated degradation dataset.

0.25 (the true value) and have variances 0.083 and 0.035, respectively. We also assume that $\lambda_i \sim \text{Gamma}(0.001, 0.001)$, for all $i = 1, \ldots, 10$.

For the MCMC algorithm, in each dataset, we collect $1,000$ iterations after discarding the first $50,000$ as burn-in. The chain autocorrelation is weaker if we assume a more informative prior distribution for θ_0. Thus, chains of different sizes are generated in each scenario. The algorithm was implemented using RStudio [Allaire, 2012].

Tables 3.1 and 3.2 shows the relative bias (RB) given by the average of the relative differences between the posterior means and true parameter; the average of the posterior variances (MV); the relative variance (RVM) calculated as the variance of the posterior means divided by the true value of the parameters; and the coverage percentage (CP) of the highest posterior density intervals with probability 0.95 for the DMGM parameters and failure times of the units under test assuming priors (1) to (5) for θ_0 and if, respectively, $\gamma \sim$ Beta(1,1) and $\gamma \sim$ Beta(2.08,4.26).

Assuming a uniform prior distribution for γ and considering a flat prior distribution for θ_0 by setting $\theta_0 \sim Gamma(0.01, 0.01)$, Table 3.1 shows that we obtain poor estimates for the model parameters. In this case, the relative biases of the posterior means and the posterior variances for parameters λ_i, $i = 1, \ldots, n$, and γ are very high. As expected, the best estimates for the environmental effects $\boldsymbol{\theta}$ are obtained if the model is fitted assuming priors for θ_0 that are concentrated around the true value of $\theta_0 = 1$. Assuming $\theta_0 \sim Gamma(10, 10)$ and $\theta_0 \sim Gamma(100, 100)$ we obtain similar estimates for these parameters; however, under the first assumption, the estimates are less biased and with small variances. Under these two priors, we also obtained the best estimates for the unit effects $\boldsymbol{\lambda}$ and the prior with lower variance obtained less biased estimates.

Table 3.1: Summary of relative bias (RB), variances of the posterior samples (MV), relative variance of the posterior mean estimates(RMV) and coverage percentage of the 95% credibility interval (CP) for the DMGM paramenters and failure times of the units under test considering the five prior distributions for θ_0 and $\gamma \sim$ Beta(p=1,q=1).

	$\theta_0 \sim$ Gamma$(0.01, 0.01)$				$\theta_0 \sim$ Gamma$(1, 1)$				$\theta_0 \sim$ Gamma$(10, 10)$				$\theta_0 \sim$ Gamma$(100, 100)$				$\theta_0 \sim$ Gamma$(400, 200)$			
	RB	MV	RVM	CP	RB	MV	RVM	CP	RB	MV	RVM	CP	RB	MV	RVM	CP	RB	MV	RVM	CP
θ_1	32.66	11794.75	207.64	100	0.447	4.511	0.093	100	0.099	0.353	0.044	100	0.092	0.039	0.040	94	-0.455	0.005	0.010	2
θ_2	32.12	13764.07	294.33	100	0.428	5.091	0.197	100	0.098	0.449	0.117	100	0.131	0.070	0.113	88	-0.425	0.012	0.030	24
θ_3	31.86	16393.15	287.09	100	0.414	5.730	0.204	100	0.087	0.445	0.120	100	0.130	0.072	0.135	89	-0.422	0.012	0.038	21
θ_4	32.70	24072.39	317.31	100	0.455	7.697	0.218	100	0.116	0.554	0.114	100	0.161	0.084	0.133	86	-0.405	0.014	0.038	23
θ_5	31.97	15651.70	279.80	100	0.429	5.601	0.201	100	0.100	0.441	0.118	100	0.143	0.068	0.134	86	-0.415	0.011	0.037	18
θ_6	31.83	18911.49	249.92	100	0.427	6.464	0.186	100	0.099	0.488	0.116	100	0.143	0.073	0.135	83	-0.415	0.012	0.038	19
θ_7	31.81	17708.61	248.57	100	0.427	6.158	0.185	100	0.097	0.466	0.111	100	0.141	0.070	0.130	85	-0.416	0.011	0.037	20
θ_8	31.76	16384.65	243.12	100	0.424	5.864	0.180	100	0.095	0.446	0.109	100	0.139	0.067	0.128	82	-0.417	0.011	0.036	19
θ_9	31.80	14889.49	246.64	100	0.426	5.339	0.183	100	0.097	0.422	0.111	100	0.142	0.064	0.131	86	-0.416	0.010	0.037	19
θ_{10}	31.98	15314.17	255.61	100	0.433	5.459	0.192	100	0.103	0.431	0.117	100	0.147	0.065	0.136	86	-0.413	0.010	0.038	22
λ_1	7.639	550.65	2.026	100	6.029	299.24	3.328	100	0.697	8.847	0.550	100	0.043	0.104	0.103	82	0.995	0.229	0.385	30
λ_2	7.490	533.16	1.807	100	5.931	291.12	3.349	100	0.676	8.866	0.563	100	0.028	0.103	0.104	84	0.967	0.227	0.387	29
λ_3	7.569	542.19	1.978	100	5.995	296.11	3.556	100	0.688	8.605	0.555	100	0.037	0.104	0.107	82	0.986	0.229	0.402	27
λ_4	7.564	541.22	1.984	100	5.960	292.51	3.293	100	0.675	8.357	0.523	100	0.031	0.102	0.096	85	0.974	0.225	0.362	33
λ_5	7.547	1210.78	1.811	100	5.974	667.21	3.518	100	0.685	20.28	0.583	100	0.033	0.233	0.102	84	0.977	0.516	0.382	31
λ_6	7.498	1201.32	1.589	100	5.945	660.32	3.438	100	0.676	19.74	0.556	100	0.028	0.231	0.101	82	0.967	0.507	0.376	32
λ_7	7.597	1227.09	1.832	100	6.022	674.35	3.581	100	0.695	19.84	0.567	100	0.039	0.237	0.104	81	0.989	0.522	0.388	31
λ_8	7.526	1205.77	1.747	100	5.965	660.69	3.453	100	0.680	19.49	0.546	100	0.032	0.230	0.103	84	0.976	0.512	0.388	36
λ_9	7.507	2128.71	1.849	100	5.950	1175.49	3.482	100	0.674	33.33	0.529	100	0.029	0.407	0.100	84	0.969	0.911	0.373	31
λ_{10}	7.541	2144.38	1.864	100	5.959	1174.94	3.238	100	0.682	35.68	0.555	100	0.032	0.406	0.101	84	0.976	0.897	0.382	30
γ	0.865	0.039	0.343	83	0.723	0.037	0.324	87	0.634	0.037	0.317	91	0.605	0.038	0.321	94	0.592	0.038	0.309	94
T_1	0.0062	0.1022	0.0008	94	0.0056	0.1014	0.0007	94	0.0056	0.1020	0.0007	93	0.0055	0.1017	0.0007	94	0.0056	0.1016	0.0007	95
T_2	-0.0014	0.1011	0.0005	98	-0.0017	0.1003	0.0005	98	-0.0018	0.0996	0.0005	100	-0.0021	0.0999	0.0005	98	-0.0019	0.1008	0.0005	99
T_3	0.0027	0.1023	0.0005	100	0.0024	0.1015	0.0005	99	0.0021	0.1006	0.0005	99	0.0020	0.1009	0.0005	99	0.0021	0.1008	0.0005	100
T_4	0.0021	0.1016	0.0008	93	0.0017	0.1003	0.0008	92	0.0013	0.1000	0.0008	94	0.0013	0.1002	0.0008	94	0.0015	0.1003	0.0008	94
T_5	0.0017	0.1529	0.0006	97	0.0012	0.1500	0.0005	98	0.0013	0.1512	0.0005	96	0.0010	0.1512	0.0005	96	0.0011	0.1511	0.0005	97
T_6	-0.0004	0.1518	0.0007	98	-0.0009	0.1492	0.0007	97	-0.0010	0.1499	0.0007	97	-0.0013	0.1482	0.0007	97	-0.0010	0.1490	0.0007	98
T_7	0.0048	0.1531	0.0006	99	0.0042	0.1519	0.0006	98	0.0042	0.1515	0.0006	98	0.0040	0.1515	0.0006	98	0.0040	0.1523	0.0006	98
T_8	0.0010	0.1524	0.0005	99	0.0006	0.1510	0.0005	100	0.0004	0.1515	0.0005	100	0.0003	0.1516	0.0005	99	0.0004	0.1517	0.0005	100
T_9	0.0001	0.2018	0.0007	98	-0.0004	0.1997	0.0007	98	-0.0004	0.1980	0.0007	98	-0.0006	0.1983	0.0007	98	-0.0006	0.1988	0.0007	98
T_{10}	0.0016	0.2040	0.0005	99	0.0012	0.2016	0.0005	99	0.0010	0.2023	0.0005	98	0.0009	0.2019	0.0005	99	0.0010	0.2004	0.0005	99

Table 3.2: Summary of relative bias (RB), variances of the posterior samples (MV), relative variance of the posterior mean estimates(RMV) and coverage percentage of the 95% credibility interval (CP) for the DMGM paramenters and failure times of the units under test considering the five prior distributions for θ_0 and $\gamma \sim$ Beta(p=2.08,q=4.26).

	$\theta_0 \sim$ Gamma(0.01, 0.01)				$\theta_0 \sim$ Gamma(1, 1)				$\theta_0 \sim$ Gamma(10, 10)				$\theta_0 \sim$ Gamma(100, 100)				$\theta_0 \sim$ Gamma(400, 200)			
	RB	MV	RVM	CP	RB	MV	RVM	CP	RB	MV	RVM	CP	RB	MV	RVM	CP	RB	MV	RVM	CP
θ_1	37.08	12722.36	143.19	100	0.496	4.848	0.077	100	0.099	0.382	0.045	100	0.087	0.041	0.040	97	-0.457	0.005	0.010	2
θ_2	36.31	14307.09	217.48	100	0.470	5.427	0.186	100	0.090	0.483	0.114	100	0.108	0.079	0.101	94	-0.436	0.013	0.027	22
θ_3	35.95	16010.14	215.24	100	0.452	5.960	0.186	100	0.076	0.487	0.117	100	0.099	0.083	0.111	92	-0.438	0.014	0.030	21
θ_4	36.69	20916.99	221.51	100	0.489	7.536	0.184	100	0.101	0.565	0.109	100	0.125	0.094	0.107	95	-0.425	0.016	0.030	21
θ_5	36.04	15682.57	206.96	100	0.463	5.901	0.173	100	0.085	0.472	0.113	100	0.106	0.079	0.108	95	-0.435	0.013	0.029	22
θ_6	35.96	18160.99	187.71	100	0.462	6.664	0.165	100	0.085	0.510	0.112	100	0.107	0.084	0.109	94	-0.434	0.014	0.030	23
θ_7	35.88	16909.73	185.45	100	0.459	6.437	0.161	100	0.082	0.495	0.108	100	0.105	0.082	0.105	94	-0.435	0.013	0.029	21
θ_8	35.89	16387.11	185.33	100	0.456	6.100	0.157	100	0.080	0.478	0.106	100	0.102	0.079	0.103	95	-0.437	0.013	0.028	21
θ_9	35.94	14985.22	184.67	100	0.458	5.761	0.157	100	0.082	0.461	0.106	100	0.104	0.077	0.104	94	-0.436	0.013	0.028	19
θ_{10}	36.08	15190.41	193.66	100	0.465	5.860	0.167	100	0.087	0.466	0.112	100	0.109	0.077	0.108	94	-0.433	0.013	0.030	21
λ_1	7.403	535.58	1.505	100	6.726	351.51	2.439	100	0.788	8.637	0.539	100	0.080	0.126	0.098	92	1.058	0.287	0.358	33
λ_2	7.266	519.98	1.308	100	6.610	342.36	2.370	100	0.761	8.506	0.536	100	0.064	0.124	0.097	92	1.027	0.282	0.353	34
λ_3	7.326	524.87	1.331	100	6.674	347.15	2.479	100	0.775	8.272	0.531	100	0.074	0.126	0.101	92	1.047	0.288	0.370	32
λ_4	7.315	524.16	1.342	100	6.638	344.46	2.304	100	0.767	8.345	0.523	100	0.068	0.123	0.091	94	1.035	0.281	0.332	36
λ_5	7.314	1180.15	1.348	100	6.662	780.35	2.602	100	0.774	19.39	0.560	100	0.069	0.281	0.095	92	1.037	0.642	0.345	31
λ_6	7.275	1172.79	1.394	100	6.630	772.63	2.542	100	0.767	19.49	0.547	100	0.065	0.278	0.096	93	1.028	0.636	0.347	38
λ_7	7.369	1199.23	1.474	100	6.704	784.30	2.589	100	0.784	19.10	0.546	100	0.076	0.285	0.099	94	1.051	0.652	0.358	31
λ_8	7.296	1176.95	1.315	100	6.658	781.09	2.538	100	0.768	18.66	0.531	100	0.069	0.280	0.096	94	1.037	0.635	0.351	34
λ_9	7.294	2094.56	1.547	100	6.633	1372.89	2.504	100	0.764	32.20	0.517	100	0.066	0.497	0.095	93	1.031	1.133	0.344	31
λ_{10}	7.306	2092.07	1.309	100	6.651	1383.55	2.406	100	0.773	35.33	0.542	100	0.068	0.492	0.095	95	1.037	1.126	0.350	35
γ	0.466	0.0187	0.118	98	0.373	0.018	0.106	99	0.311	0.017	0.108	99	0.280	0.017	0.106	99	0.269	0.018	0.106	99
T_1	0.0058	0.0974	0.0007	94	0.0054	0.0979	0.0007	96	0.0051	0.0980	0.0007	94	0.0052	0.0977	0.0007	96	0.0050	0.0970	0.0007	96
T_2	-0.0019	0.0967	0.0005	96	-0.0024	0.0967	0.0005	97	-0.0027	0.0966	0.0005	97	-0.0024	0.0973	0.0005	98	-0.0027	0.0972	0.0005	96
T_3	0.0021	0.0988	0.0005	100	0.0018	0.0971	0.0005	99	0.0017	0.0969	0.0005	98	0.0017	0.0973	0.0005	100	0.0016	0.0972	0.0005	99
T_4	0.0015	0.0973	0.0008	94	0.0010	0.0969	0.0007	96	0.0008	0.0960	0.0007	95	0.0010	0.0967	0.0007	94	0.0009	0.0971	0.0007	93
T_5	0.0010	0.1465	0.0005	96	0.0008	0.1467	0.0005	97	0.0008	0.1446	0.0005	97	0.0004	0.1456	0.0005	97	0.0004	0.1453	0.0005	97
T_6	-0.0013	0.1447	0.0006	97	-0.0013	0.1457	0.0006	98	-0.0015	0.1454	0.0006	98	-0.0014	0.1444	0.0006	97	-0.0018	0.1464	0.0006	99
T_7	0.0040	0.1473	0.0005	98	0.0036	0.1465	0.0005	98	0.0037	0.1455	0.0005	98	0.0035	0.1473	0.0005	99	0.0034	0.1440	0.0005	98
T_8	0.0005	0.1472	0.0005	100	0.0001	0.1456	0.0005	100	0.0001	0.1462	0.0005	99	-0.0002	0.1448	0.0005	99	-0.0002	0.1457	0.0005	100
T_9	-0.0006	0.1911	0.0007	98	-0.0008	0.1912	0.0007	98	-0.0009	0.1921	0.0007	98	-0.0009	0.1918	0.0007	98	-0.0010	0.1900	0.0007	98
T_{10}	0.0010	0.1937	0.0005	99	0.0006	0.1943	0.0005	99	0.0006	0.1928	0.0005	99	0.0003	0.1916	0.0005	99	0.0003	0.1944	0.0005	99

The posterior variances of all parameters tend to be small if the prior uncertainty about θ_0 is small. However, the coverage percentage of the credible intervals is below 36% for the parameters in $\boldsymbol{\lambda}$ and $\boldsymbol{\theta}$ if *a priori* $\theta_0 \sim Gamma(400, 200)$, that is, if the environmental effect at the first inspection time is *a priori* poorly estimated. Under this prior specification, the environmental effects are underestimated, but, in absolute value, the relative biases are very close to the ones obtained assuming a non-precise prior distribution $\theta_0 \sim Gamma(1, 1)$. By eliciting the prior distribution $\gamma \sim$ Beta(2.08,4.26) that precisely estimates the discount factor γ, there is non substantial improvement in the posterior estimates for the parameters in $\boldsymbol{\lambda}$ and $\boldsymbol{\theta}$ (Table 3.2). In this case, there is a smoothed reduction in the relative biases of the failure time estimates, and we greatly improve the estimates for γ.

When making inferences for the failure times of the units under test, the prior distribution for θ_0 did not influence the estimates. As the estimates for the failure time strongly depend on the parameters involved in the last inspection times, the prior distribution for θ_0 is no longer so influential as shown in Tables 3.1 and 3.2.

We also assess the impact of using informative prior distributions for γ and $\boldsymbol{\lambda}$, showing that it does not substantially influence the inference for the failure time. These results can be found in Section S2 in the Supplementary Materials.

In summary, the simulation study provides some guidelines to obtain model identifiability and shows, for instance, that flat prior distributions for θ_0 should be avoided. Although the prior distribution $\theta_0 \sim Gamma(0.01, 0.01)$ is centered around the true value of θ_0, this prior is very flat and tends to be dominated by the (non-identifiable) likelihood producing poor posterior estimates for the model parameters. Having theoretical identifiability, however, may not guarantee the practical identifiability as such constraints do not guarantee that all parameters will be well estimated. When we elicited $\theta_0 \sim Gamma(400, 200)$, a prior distribution very concentrated around 2 and is a wrong value for θ_0. Although, this prior identifies the model it also leads to poor estimates for the model parameters.

It is important notice that, as pointed by Oliveira *et al.* [2021], large sample sizes might be required to obtain good parameter estimates even for an identifiable model. However, if the model is a non-identifiable, some parameters might not be estimated even with large datasets if the identifiability constraints are not considered.

If our interest is only to predict the failure time, this simulation study also shows that the prior for θ_0 does not play an important role. However, it is also of interest to infer the model parameters, we learn from the simulation that we should take the expert opinion into account and build an informative prior θ_0. If the expert reveals that the environment has no effect on the degradation trajectories at the initial time, such prior should be centered in 1. This assumption is reasonable if, for instance, all units under test are new and, therefore, there is no previous influence of the environment on their degradation paths. If in the expert's opinion the environment has a positive effect on the degradation trajectories at the initial time, the prior for θ_0 should be concentrated in some positive value θ_0^* smaller than 1. In this case, a possible way to define the prior for θ_0 is to find α_0 and β_0 such that $E(\theta_0) = \theta_0^*$.

An additional simulation study is provided in the Supplementary Materials, Section S2.3, illustrating the performance of the DMGM to degradation forecasting K-steps ahead when K is large.

3.5 Case Studies

The fatigue crack size [Meeker and Escobar, 1998] and the stress relaxation [Yang, 2007] datasets shown in Figure 3.1 are analyzed considering the proposed DMGM, the Weibull linear (WLDM) degradation model [Hamada, 2005] and the dynamic linear (DLDM) degradation model [Veloso and Loschi , 2021]. The DMGM is fitted assuming $g(t_{ij}) = t_{ij}^2$ and $g(t_{ij}) = \sqrt{t_{ij}}$ for fatigue crack size and stress relaxation data, respectively.

For both datasets, the DMGM is fitted considering the prior specifications $\theta_0 \sim \text{Gamma}(100, 100)$, $\gamma \sim \text{Beta}(1, 1)$ and $\lambda_i \sim \text{Gamma}(0.001, 0.001)$, for $i = 1, 2, \ldots, n$. For WLDM and DLDM, we established flat priors for all parameters. These models are fitted collecting 2000 MCMC iterates after discarding the first 50000 as the burn-in period and thinning by 100. To evaluate the computational times, both applications were fitted on an Intel (R) Core (TM) i7-8550U 1.80GHz CPU with 8GB RAM. Further details on these case studies can be found in the Supplementary Materials, Section S3.

3.5.1 Case Study 1: Fatigue Crack Size Data

Figure 3.1a shows the size of fatigue cracks as a function of the number of cycles of applied stress to 10 test units. The data were collected to obtain information on crack growth rates for the alloy as reported in Meeker and Escobar [1998]. A crack with a cumulative size of 0.7 inches is considered a failure.

To evaluate the model's performance in predicting the omitted measures for all units under test, we remove from one to three degradation measures in the final of all degradation paths. Table 3.3 shows the mean squared error (MSE), the mean absolute percentage error (MAPE), and the mean absolute deviance (MAD) for the forecasts of the omitted fatigue crack sizes, given by the posterior means.

If one or two observations are omitted, the proposed model outperforms the other models. When the last three observations are removed, WLDM and DLDM models showed better performance. This result may be explained by approximated linear behavior that the true degradation paths experience at the beginning of the experiment.

Table 3.3: Accuracy measurements(AcM) for k-step ahead forecasting, $k = 1, 2, 3$, under DMGM, WLDM and DLDM for fatigue crack size data removing the last (L), the two-last ($2L$) and, the three-last ($3L$) observations in each degradation path.

Removed Obs.	AcM	Fitted Model								
		WLDM	DLDM	DMGM	WLDM	DLDM	DMGM	WLDM	DLDM	DMGM
		$k=1$			$k=2$			$k=3$		
3L	MSE	0.0013	0.0002	0.0049	0.0067	0.0031	0.0134	0.0187	0.0113	0.0296
	MAPE	10.2641	3.9998	19.6575	18.4754	12.3971	26.3550	24.7480	18.9055	32.3775
	MAD	0.0355	0.0138	0.0683	0.0810	0.0546	0.1148	0.1333	0.1024	0.1710
2L	MSE	0.0046	0.0017	0.0018	0.0146	0.0080	0.0067			
	MAPE	15.1608	8.8530	9.8624	21.7265	15.6362	15.4993			
	MAD	0.0666	0.0393	0.0427	0.1173	0.0852	0.0810			
L	MSE	0.0095	0.0021	0.0016						
	MAPE	17.3832	7.7614	7.4293						
	MAD	0.0940	0.0425	0.0382						

Graphics of the posterior estimates associated with the DMGM parameters are shown in Figure 3. Figure 3.3a shows the boxplot of the posterior distributions effects λ_i of the units' individual features on the degradation rate. This effect is an indicator of the quality of the ith unit and may be different form unit-to-unit. A low value for λ_i indicates the poor quality of device i. Comparing units 1 and 10, for instance, Figure 3.3a shows that the quality of unit 1 is worse than that for unit 10. This indicates that these units had been produced using different materials, came from different populations, etc. Figure 3.3a also shows that the unit-specific effects are similar for almost all devices, indicating that the units under test originate from populations with similar characteristics. The most significant differences are observed for unit 1 that fails during the experiment for which the unit effect is the smallest and, for Units 9 and 10, which effects are smoothly higher.

The effect of environment on degradation (Figure 3.3b) increases with time and strongly influence the product $\lambda_i\theta_j$ (Figure 3.3d) and, consequently, the degradation rate. The environmental effect is around one in the first inspection time, which means that the environmental effect at the beginning of the experiment is insignificant. Their increase is expected, as the devices are more prone to degrade as they are more exposed to the environment and time of use. The observed environment effects reinforce the need for dynamic models to analyze degradation data. The degradation rates depend on the function $\lambda_i\theta_j$ given in figure 3.3d. This function has the same behavior as the dynamic parameters weighted by the specific components of the unit. The curve below all others shows the behavior for the only unit that failed. The type of analysis would not be possible if we do not assume the proposed decomposition of the degradation rate as considered in other degradation path models in the literature.

The posterior distribution of the discount factor in 3.3c concentrates most of its probability mass in the lower values of the domain, meaning that there exists a weaker dependence among the environmental effects than it was assumed *a priori*. The computational time spent fitting the DMGM to the fatigue crack size data is 59.53 seconds.

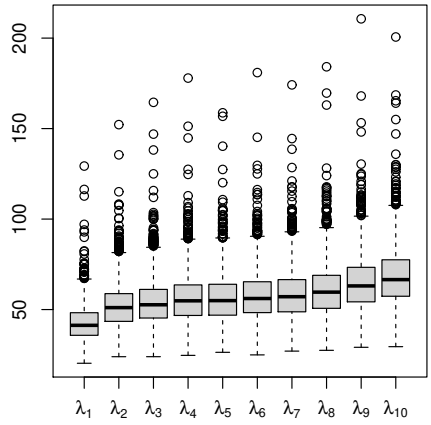

(a) Unit effect

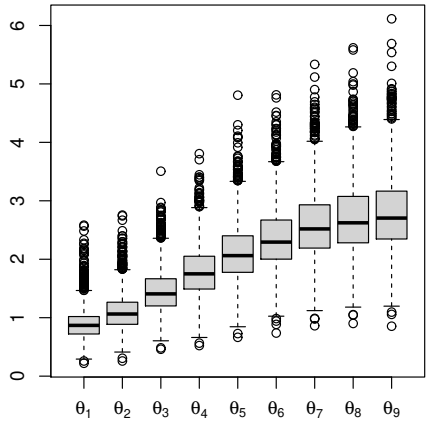

(b) Environmental effect

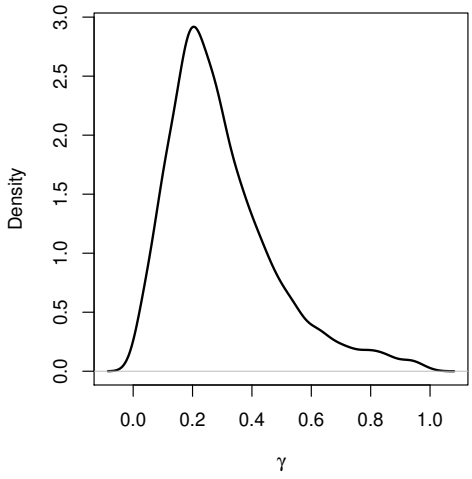

(c) discount factor

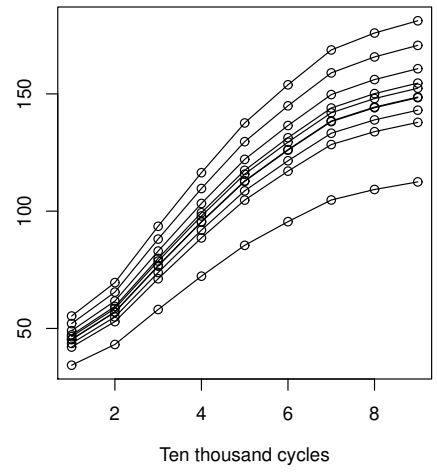

(d) $\lambda_i\theta_j$

Figure 3.3: Boxplots of the posterior samples of the static parameters λ_i (a) and of the dynamic components θ_j (b), the posterior distribution for discount factor γ (c), and the evolution of the product $\lambda_i\theta_j$ (d), for fatigue crack size data. In (a) and (b) the ∘ represents the outliers.

Table 3.4 presents the $\overline{RUL}$ (except for unit 1 that fails during the test), the MTTF, and some percentiles of the posterior predictive distribution associated with failure times, in ten thousand cycles, for the units under test and a new one. All these measures follow the same standard as the posterior estimates for $\lambda_i\theta_j$, assuming higher values for units 9 and 10 and the smallest value for unit 1. The RUL and MTTF for units 2 to 7 are close, which is these units are from similar populations. This result corroborates our findings in Figure 3.3 where the λ_is for these units were also close. In all cases, the MTTF is close to the median failure times, possibly indicating symmetrical posterior distributions for all the failure times of the units under test. For a new unit, we conclude that, for example, 10% of the devices operating on the same conditions as those in the study will reach a crack of size 0.7 before 9.27×10^4

cycles.

Table 3.4: MTTF, $\overline{RUL}$ and α-percentiles ($t_{p|\boldsymbol{Y}}(\alpha)$) of the posterior predictive distribution of the failure times (10^4 cycles) for new and under test units, fatigue crack size data.

Failure Time	$MTTF$	$\overline{RUL}$	$t_{p\|\boldsymbol{Y}}(0.025)$	$t_{p\|\boldsymbol{Y}}(0.1)$	$t_{p\|\boldsymbol{Y}}(0.5)$	$t_{p\|\boldsymbol{Y}}(0.975)$
T_1	8.86	——-	8.28	8.50	8.86	9.41
T_2	9.83	0.83	9.22	9.41	9.82	10.47
T_3	10.01	1.01	9.34	9.58	10.01	10.66
T_4	10.16	1.16	9.46	9.74	10.15	10.81
T_5	10.19	1.19	9.50	9.76	10.20	10.86
T_6	10.30	1.30	9.60	9.87	10.32	10.97
T_7	10.39	1.39	9.68	9.95	10.40	11.04
T_8	10.59	1.59	9.92	10.13	10.59	11.27
T_9	10.92	1.92	10.26	10.48	10.92	11.63
T_{10}	11.25	2.25	10.49	10.77	11.25	12.00
T_{n+1}	10.25	——-	8.66	9.27	10.28	11.55

The posterior means of the filtering distributions and the 95% credibility intervals in each inspection time show that these estimates precisely recovered the true degradation measurements (Figure 3.4). Using the sequential forecasting method, these posterior distributions also provide precise forecasts for future degradation and reasonable estimates of the failure times. Figure 3.4 shows that the predicted measurements in which the trajectories cross the degradation threshold coincides with the MTTF and the filtering estimates and the forecasting for three selected units under test.

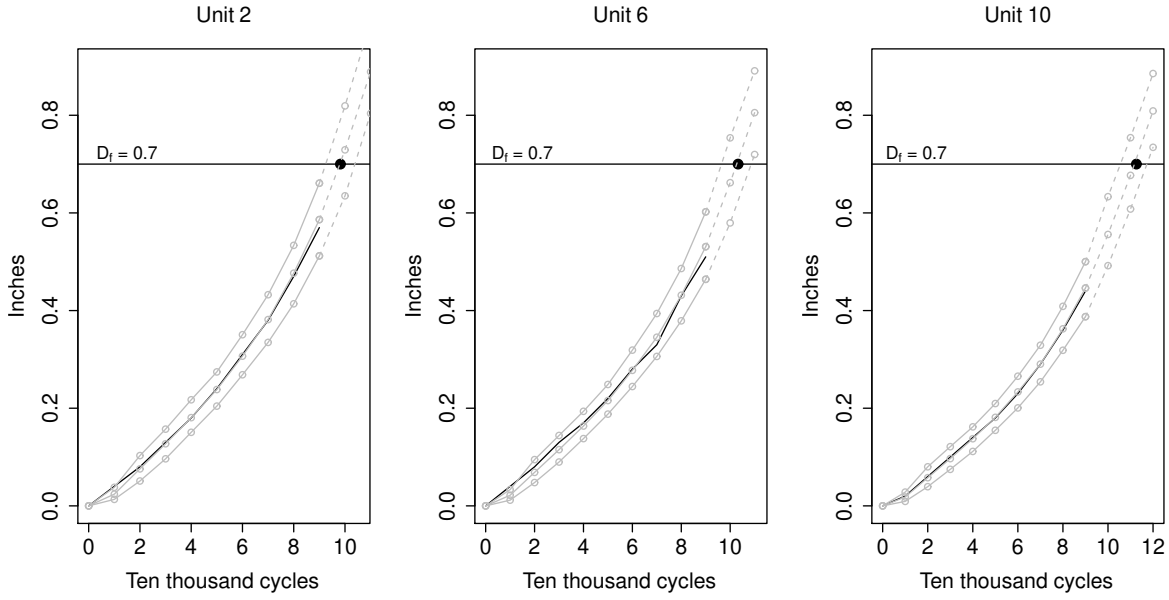

Figure 3.4: Degradation measure (black solid line), MTTF (black point), posterior means for the filtering distribution (grey solid line), the sequential forecasting (grey dashed line) and the 95% credibility intervals for three units under test, fatigue crack size data.

Table 3.5 shows the $\overline{RUL}$ by fitting DMGM, WLDM, and DLDM to analyze the fatigue crack size data in different scenarios. The $\overline{RUL}$ was calculated considering different last inspection

times t_J, given in ten thousand cycles, by omitting the k last observations, $k = 0, 1, 2, 3$. If $k = 0$, then we consider all observed data and $t_J = 9$. If $k = 3$, then $t_J = 6$. As noticed from Figure 3.1a, Unit 1 failed during the study between 8 and 9 ten thousand cycles. Table 3.5 shows that when considering as last inspection time $t_J = 6$, thus omitting $k = 3$ observations, the proposed DMGM provides that the RUL for unit 1 is $\overline{RUL} = 2.06$ and, consequently, the predict failure time for this unit is 8.06 ten thousand cycles which belongs to the time interval in which the failure occurred. A similar conclusion was drawn for the other values of k. Even considering all observed degradation measurements, WLDM and DLDM overestimate the failure time for this unit predicting it as higher than 9 ten thousand cycles.

Results in Table 3.5 also shows that under the DMGM the fewer the observed degradation measurements, the lower is the forecast for the failure times of all units under test. An opposed behavior is obtained by fitting the DLDM and WLDM, which provided the highest estimates for failure times in all analyzed scenarios.

Table 3.5: $\overline{RUL}$ in ten thousand cycles obtained considering DMGM, WLDM and DLDM for fatigue crack size data with different values of the last inspection times t_J.

Model	t_J	Unit									
		1	2	3	4	5	6	7	8	9	10
DMGM	9	—-	0.83	1.01	1.16	1.19	1.30	1.39	1.59	1.92	2.25
	8	0.73	1.61	1.80	1.92	1.97	2.06	2.18	2.36	2.66	3.03
	7	1.53	2.30	2.51	2.63	2.68	2.78	2.89	3.04	3.36	3.74
	6	2.06	2.81	2.99	3.06	3.06	3.15	3.29	3.50	3.81	4.17
WLDM	9	1.14	3.57	4.00	4.44	4.53	4.87	5.12	5.59	6.49	7.45
	8	2.97	5.24	5.86	6.20	6.29	6.57	6.91	7.42	8.37	9.49
	7	4.68	6.96	7.62	7.95	8.13	8.42	8.81	9.13	10.20	11.47
	6	6.15	8.60	9.20	9.54	9.55	9.77	10.33	10.87	12.03	13.49
DLDM	9	—-	2.03	2.22	2.84	2.86	3.32	3.33	3.74	4.52	5.07
	8	1.67	3.84	4.40	4.68	4.71	5.01	5.30	5.77	6.32	7.19
	7	3.80	5.77	6.45	6.89	7.20	7.70	7.74	7.59	8.18	9.29
	6	5.30	7.26	8.26	8.33	8.38	8.85	9.47	9.09	9.93	11.20

3.5.2 Case Study 2: Stress Relaxation Data

Stress relaxation is the loss of stress in a component subjected to a constant strain over time. The contacts of electrical connectors often fail due to excessive stress relaxation [Yang, 2007]. An electrical connector fails if the stress relaxation exceeds 30%. Data in Figure 3.1b correspond to the stress relaxation of 6 connectors, tested at 100^oC. The unit degradation is measured at the same non-equidistant inspection times, and no unit failed during the study.

To analyze the data, DMGM, WLDM and DLDM are fitted. DMGM is fitted letting $g(t_{ij}) = \sqrt{t_{ij}}$. We also consider a modification of Hammada's Weibull model (WRDM) by assuming the following relationship between time and degradation:$Y_{it} = \beta\sqrt{t_{ij}} + \epsilon_{ij}$. Analogously to the previous case study, from one to three degradation measures in the final of all degradation paths were removed and predicted using the models. Table 3.6 shows that the DMGM has the

best performance providing the smallest accuracy measures in almost all cases. The exception occurs when forecasting the first degradation measure in scenes where two observations are removed from data. In this case, the DLDM provided a better result. As expected, the WLDM presented the worse performance. However, an improvement is observed if we assume a non-linear relationship between inspection time and degradation (WRDM).

Table 3.6: Accuracy measurements(AcM) for k-step ahead forecasting, $k = 1, 2, 3$, under DMGM, WLDM and DLDM for stress relaxation data removing the last (L), the two-last ($2L$) and, the three-last ($3L$) observations in each degradation path.

Removed Obs.	AcM	Fitted Models											
		WLDM	WRDM	DLDM	DMGM	WLDM	WRDM	DLDM	DMGM	WLDM	WRDM	DLDM	DMGM
		$k=1$				$k=2$				$k=3$			
3L	MSE	25.01	0.25	2.09	0.09	29.83	1.82	1.45	0.80	85.53	1.45	10.75	0.51
	MAPE	26.14	2.26	7.35	1.43	26.38	6.04	5.85	3.57	41.03	4.87	14.42	2.36
	MAD	4.96	0.43	1.38	0.27	5.41	1.25	1.18	0.75	9.16	1.08	3.22	0.53
2L	MSE	10.74	1.56	0.43	0.75	43.13	1.21	2.51	0.51				
	MAPE	15.71	5.46	2.08	3.32	29.03	4.28	6.39	2.21				
	MAD	3.22	1.13	0.44	0.70	6.48	0.95	1.43	0.50				
L	MSE	27.93	0.65	3.49	0.23								
	MAPE	23.37	3.00	7.90	1.69								
	MAD	5.22	0.67	1.79	0.38								

After fitting the DMGM to the stress relaxation data, the unit-specific effects λ_i for the devices under test (Figure 3.5a) are different showing that the units 1 and 2 are similar, and the others may originate from different populations. Differently from what was observed for the fatigue crack size data (Figure 3.3b), the environmental effects distribution smoothly change over time as shown in Figure 3.5b. Their posterior medians are close to one at all inspection times indicating that the environment has few influences on the degradation rate of stress relaxation data. Such medians present a subtle parabolic shape which increases until the inspection time $t_{ij} \leq 4$ and decreases after that until reaching an almost constant behavior in the last three inspection times. Although all medians are close to one at all inspection times, this subtle fluctuation produced variations over time in the degradation rates as it is a function of $\lambda_i\theta_j$. The function of $\lambda_i\theta_j$ also has a parabolic shape and reaches its maximum at the 4th inspection time (Figure 3.5d) for all units. It is noticed, however, that the unit-specific effect has a greater influence on degradation than the time of use.

The discount factors considered in the evolution equation given by (3.4) vary according to the amplitudes of the inspection times intervals (Figure 3.5c). The greater the interval sizes, the lower the discount factor is. Thus, it is possible a better to control the uncertainty and the information that is passed from one inspection time to the next when the are unbalanced. In other words, the model assumes great (small) uncertainty for the degradation measures belonging to time intervals with large (small) lengths. The computational time spent fitting the DMGM to this data is 60.07 seconds.

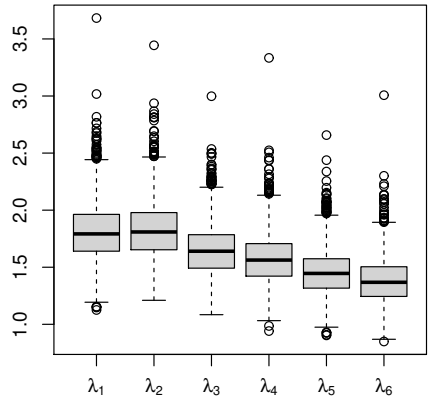

(a) Unit effect

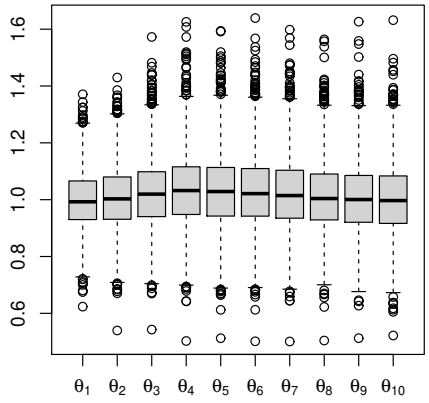

(b) Environment effect

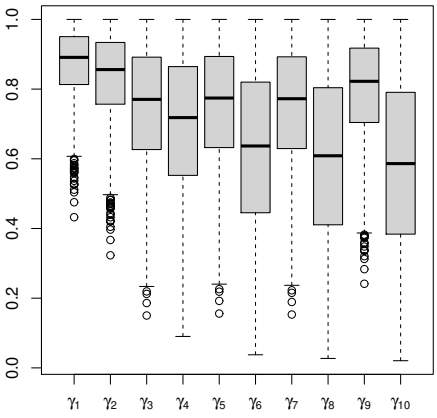

(c) Discount factors

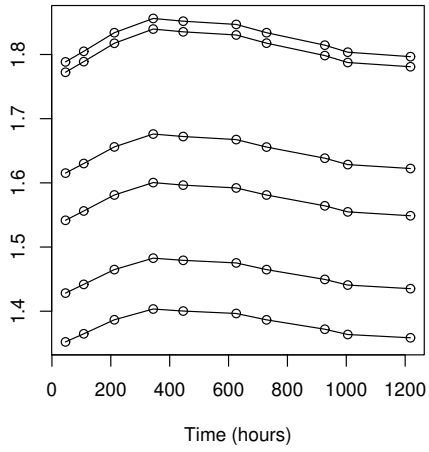

(d) $\lambda_i\theta_j$

Figure 3.5: Boxplots of the posterior samples of the static parameters λ_i (a), the dynamic components θ_j (b) and the discount factors γ_j (c) and the evolution of the product $\lambda_i\theta_j$ (d), for stress relaxation data. In (a), (b) and (c) the ∘ represents the outliers.

Table 3.7 presents the MTTF, $\overline{RUL}$, and some percentiles of the posterior predictive distribution for the failure times, in hours, for a future unit and the units under test. Units 6 and 5 show fewer resistents and present an MTTF below 2.000 hours. The RUL for the majority of the units is below 1200 hours, the study time. Figure 3.6 shows the posterior means and the HPD with probability 0.95 of the filtering distributions for three selected units.

As in the previous case study, this posterior distribution provides a precise forecast for future degradation measures and a reasonable estimate for the failure time of the units under test. In addition, the instants of the predicted degradation paths cross the degradation threshold and coincide with the MTTF. The figure that contains the fit and forecasting for all units under test can be found in Section S3.2 of the Supplementary Materials. Section S3.2 also presents a comparison of the $\overline{RUL}$ by fitting DMGM, WLDM, WRDM, and DLDM in different scenarios,

Table 3.7: MTTF, $\overline{RUL}$ and α-percentiles ($t_{p|\boldsymbol{Y}}(\alpha)$) of the posterior predictive distribution of the failure times (hours) for new and under-test units, stress relaxation data.

Failure Time	$MTTF$	$\overline{RUL}$	$t_{p\|\boldsymbol{Y}}(0.025)$	$t_{p\|\boldsymbol{Y}}(0.1)$	$t_{p\|\boldsymbol{Y}}(0.5)$	$t_{p\|\boldsymbol{Y}}(0.975)$
T_1	2877.63	1677.63	2101.24	2343.72	2866.23	3763.81
T_2	2956.28	1756.28	2188.90	2418.24	2927.74	3870.24
T_3	2399.49	1199.49	1756.72	1967.61	2380.43	3111.41
T_4	2205.06	1005.06	1622.13	1819.39	2187.18	2876.17
T_5	1866.39	666.39	1385.57	1527.68	1848.42	2476.75
T_6	1685.25	485.25	1220.29	1364.75	1671.23	2248.49
T_{n+1}	2331.68	——-	1392.44	1611.16	2272.19	3571.07

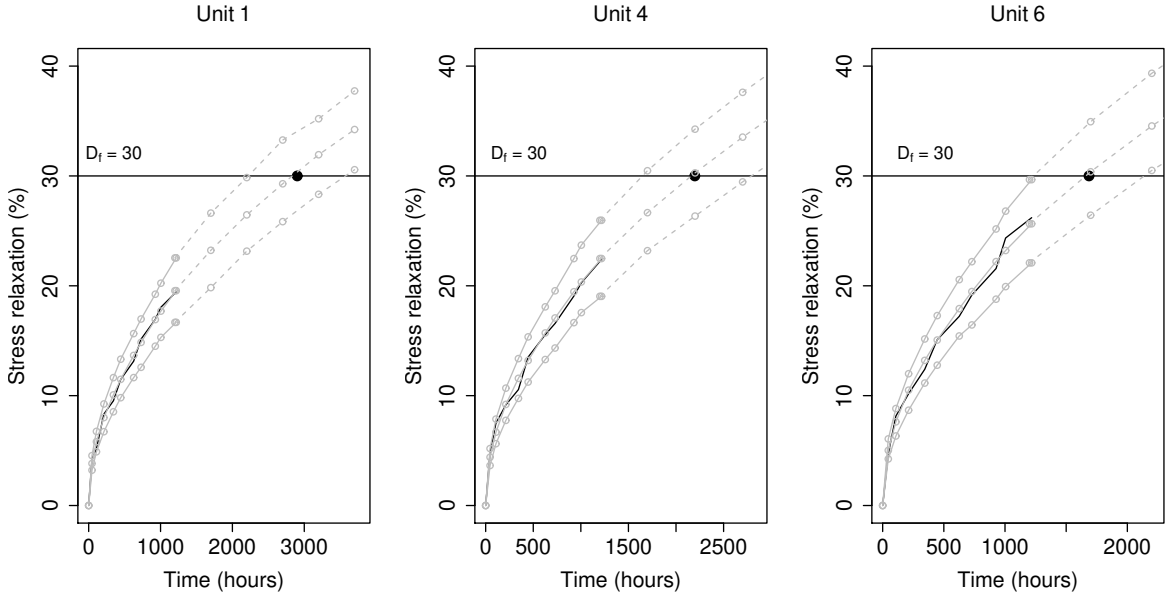

Figure 3.6: Degradation measure (black solid line), MTTF (black point), posterior means for the filtering distribution (grey solid line), the sequential forecasting (grey dashed line) and the 95% credibility intervals for three units under test, stress relaxation data.

similar to that shown for Case Study 1.

3.6 Concluding Remarks

We introduced a new class of general gamma degradation path models that have a dynamic functional form. To obtain a parsimonious model, for each unit, the degradation rate is a function of two components: a static and unit-specific effect and another that measures the environmental impact. The dynamic structure is introduced into the model through the prior distribution for the environmental effects, which assumes a Markovian dependence among them. Although the Gamma dynamic model has been introduced by Aktekin *et al.* [2021], the proposed approach extends this previous model in several directions. Firstly, a more general structure (not only linear) relates the inspection time and the degradation measurements allowing to accommodate different shapes for the degradation paths. Constraints to identify the model are theoretically derived, and a useful discussion is presented about how to these constraints may be

specified in the contexts of time series and degradation tests. The forecast of future degradation measurements is discussed. The crucial relationship between failure time and model parameters is obtained, and the inference for the remaining useful life is discussed for units under test and a future one.

The usefulness and versatility of the proposed model are illustrated by analyzing two datasets (fatigue crack size and stress relaxation data) whose degradation paths have different shapes. In both cases, the proposed model outperforms some well-known models. The simulation studies provided some valuable guidelines to establishes the prior distributions of the environmental effect needed to attain the model identification. These studies showed that if the goal is to infer the failure time behavior, the prior specifications for the parameter θ_0 and γ do not play an important role. However, if the goal is to get information about the environmental or unit-specific effects, we should obtain trustful information about θ_0 allowing us to build an informative prior for it.

Our results show that the proposed degradation model is competitive and can be a valuable approach to model positive degradation data coming from populations with different shapes for the degradation path. Furthermore, the individual and environmental effects' analysis can be separately done for degradation data.

The proposed methodology is defined only for positive degradation measures and assumes that covariates explaining the degradation mechanism are not available. Future extensions of the proposed approach include considering similar decomposition for the degradation rate and developing new dynamic degradations models assuming other distributions for the degradation measures as well as other distributions with positive support for the units effects as log-normal, Weibull, and log-skew-elliptical distributions. These prior choices will bring some new theoretical and computational challenges as these families are not conjugate with the Gamma family. Models assuming covariates to explain the degradation rate are other interesting topic for future research.

Supplementary Materials

Section S1 contains an alternative proof about the validation of the DMGM identifiability considering sufficient statistics. Additional simulation studies are presented in Section S2 to verify the impact in the estimation of the failure times and forecasting. Section S3 presents the details associated to the DMGM fit and forecasting for all the units under test for the fatigue crack size and stress relaxation datasets.

References

Abramowitz, M., Irene A. S. & Robert H. R. (1988). *Handbook of mathematical functions with formulas, graphs, and mathematical tables*. American Association of Physics Teach-

ers.

Aktekin, T., Polson, N., & Soyer, R. (2018). Sequential Bayesian analysis of multivariate count data. *Bayesian Analysis*, 13(2), 385-409.

Aktekin, T., Polson, N., & Soyer, R. (2021). *A family of multivariate non-gaussian time series models. Journal of Time Series Analysis*, 41(5), 691-721.

Allaire, J. (2012). *RStudio: Integrated development environment for R.*

Bagdonavicius, V., Masiulaityte, I & Nikulin, MS. (2010). *Advances in Degradation Modeling*, Springer, 275-291.

Bernardo, J. M. & Smith, A.F.M. (2009). *Bayesian Theory* Springer, John Wiley & Sons.

Carter, C. K. & Kohn, R. (1994). On Gibbs sampling for state space models. *Biometrika*, 81(3), 541-553.

Chang, M., Huang, X., Coolen, F.P.A., Coolen-Maturi, T. (2021). Reliability analysis for systems based on degradation rates and hard failure thresholds changing with degradation levels. *Reliability Engineering & System Safety*, 216, 108007.

Chen, Z., Li, Y., Zhou, D., Xia, T., & Pan, E. (2021). Two-phase degradation data analysis with change-point detection based on Gaussian process degradation model. *Reliability Engineering & System Safety*, 216, 107916.

Doksum, KA. & Hoyland, A.(1993). Models for variable-stress accelerated life testing experiments based on wiener processes and the inverse gaussian distribution. *Theory of Probability & Its Applications*, 37(1), 137-139.

Esary, J. D., & Marshall, A. W. (1973). Shock models and wear processes. *The Annals of Probability*, 627-649.

Freitas, M. A., Colosimo, E. A., Santos, T. R. & Pires, M. C. (2010). Reliability assessment using degradation models: Bayesian and classical approaches. *Pesquisa Operacional*, 30(1), 194-219.

Freitas, M. A., Toledo, M. L. G., Colosimo, E. A., & Pires, M. C. (2009). Using degradation data to assess reliability: a case study on train wheel degradation. *Quality and Reliability Engineering International*, v. 25, p. 607-629, 2009.

Fruhwirth-Schnatter, S. (1994). Data augmentation and dynamic linear models. *Journal of Time Series Analysis*, 15(2), 183-202.

Gamerman, D., dos Santos, T. R. and Franco, G. C. (2013). A non-Gaussian family of state-space models with exact marginal likelihood. *Journal of Time Series Analysis*, 34(6), 625-645.

Guida, M., Postiglione, F. and Pulcini, G. (2015). A random-effects model for long-term degradation analysis of solid oxide fuel cells, *Reliability Engineering & System Safety*, 140, 88-98.

Gustafson, P. (2005). On Model Expansion, Model Contraction, Identifiability and Prior Information: Two Illustrative Scenarios Involving Mismeasured Variables, *Statistical Science*, 20(2), 111-140.

Hamada, M. (2005). Using degradation data to assess reliability. *Quality Engineering*, 17(4), 615-620.

Hong, Y., Duan, Y., Meeker, W. Q., Stanley, D. L., & Gu, X. (2015). Statistical methods for degradation data with dynamic covariates information and an application to outdoor weathering data. *Technometrics* 57(2), 180-193.

Jia, G., & Gardoni, P. (2018a). State-dependent stochastic models: A general stochastic framework for modeling deteriorating engineering systems considering multiple deterioration processes and their interactions. *Structural Safety* 72, 99-110.

Jia, G., & Gardoni, P. (2018b). Simulation-based approach for estimation of stochastic performances of deteriorating engineering systems. *Probabilistic Engineering Mechanics* 52, 28-39.

Jia, G., & Gardoni, P. (2019). Stochastic life-cycle analysis: Renewal-theory life-cycle analysis with state-dependent deterioration stochastic models. *Structure and Infrastructure Engineering* 15(8), 1001-1014.

Jiang, M. & Yongcang, Z (2002). Dynamic modeling of degradation data. *Annual Reliability and Maintainability Symposium. 2002 Proceedings* (Cat. No. 02CH37318). IEEE

Kim, S.J. and Bae, Suk J. (2017). *Degradation Test Plan for a Nonlinear Random-Coefficients Model* Statistical Modeling for Degradation Data, Editors Ding-Geng (Din) Chen, Yuhlong Lio, Hon Keung Tony Ng, Tzong-Ru Tsai (Eds.) Springer, 127-147.

Kumar, R., & Gardoni, P. (2014). Renewal theory-based life-cycle analysis of deteriorating engineering systems. *Structural Safety*, 50, 94-102.

Kumar, R., Cline, D. B., & Gardoni, P. (2015). A stochastic framework to model deterioration in engineering systems. *Structural Safety*, 53, 36-43.

Lawless, J. & Crowder, M. (2004). Covariates and random effects in a gamma process model with application to degradation and failure. *Technometrics*, 10(3), 213-227.

Li, G., & Luo, J. (2005). Shock model in Markovian environment. *Naval Research Logistics (NRL)*, 2(3), 253-260.

Ling, M. H., Tsui, K. L. & Balakrishnan, n. (2014). Accelerated degradation analysis for the quality of a system based on the gamma process. *IEEE Transactions on Reliability*, 64(1), 463-472.

Lu, C. J. & Meeker, W. O. (1993). Using degradation measures to estimate a time-to-failure distribution. *Technometrics*, 35(2), 161-174.

Lu, C., Meeker, W. and Escobar, L. (1996). Using degradation measurements to estimate a time-to-failure distribution, *Statistica Sinica* 6, 531–546.

Meeker, W. Q. & Escobar, L. A. (1998). *Statistical Methods for Reliability Data*. Wiley Series in Probability and Statistics, First Edition.

Oliveira, R. P. B., Loschi, R. H. & Freitas, M. A. (2018). Skew-heavy-tailed degradation models: An application to train wheel degradation. *IEEE Transactions on Reliability*, 67(1), 129-141.

Oliveira, G.L. and Argiento, R. and Loschi, R.H. and Assunção, R. M. and Rugeri, F. and Branco, M. D. (2021). Bias Correction in Clustered Underreported Data. *Bayesian Analysis*, Advance Publication- https://doi.org/10.1214/20-BA1244, 1-32.

Peng, W., Li, Y. F., Mi, J., Yu, L., & Huang, H. Z. (2016). Reliability of complex systems under dynamic conditions: A Bayesian multivariate degradation perspective. *Reliability Engineering & System Safety*, 153, 75-87.

Petris, G., Petrone, S. & Campagnoli, P. (2009). *Dynamic linear models with R* Springer, John Wiley & Sons.

Robinson, M. & Crowder, M. (2000). Bayesian methods for a growth-curve degradation model with repeated measures. *Lifetime Data Anaysis*, 6(4), 357-374.

Rothenberg, T. J. (1971). Identification in parametric models, *Econometrica: Journal of the Econometric Society*, 577-591.

Santos, T. R., Gamerman, D. & Conceição, F. G. (2017). Reliability analysis via non-Gaussian state-space models. *IEEE Transactions on Reliability*, 66(2), 309-318.

Santos, C.C. and Loschi, R.H. (2020). Semi-parametric Bayesian models for heterogeneous degradation data: An application to Laser data, *Reliability Engineering & System Safety,* 202, 107038.

Shephard, N. (1994). Partial non-Gaussian state space. *Biometrika*, 81(1), 115-131.

Smith, R. L., & Miller, J. E. (1986). A non-Gaussian state space model and application to prediction of records. *Journal of the Royal Statistical Society: Series B (Methodological)*, 48(1), 79-88.

Sun, F., Li, H., Cheng, Y., & Liao, H. (2021). Reliability analysis for a system experiencing dependent degradation processes and random shocks based on a nonlinear Wiener process model *Reliability Engineering & System Safety*, 215, 107906.

Veloso, G. & Loschi, R. (2021). Dynamic linear degradation model: Dealing with heterogeneity in degradation paths. *Reliability Engineering & System Safety*, DOI: 10.1016/j.ress.2021.107446.

Wang, W. (2012). An overview of the recent advances in delay-time-based maintenance modelling. *Reliability Engineering & System Safety*, 106, 165-178.

Wang, H., Ma, X., & Zhao, Y. (2020). A mixed-effects model of two-phase degradation process for reliability assessment and RUL prediction. *Microelectronics Reliability*, 107, 113622.

Wang, Z., Zhai, Q., Chen, P. (2021). Degradation modeling considering unit-to-unit heterogeneity-A general model and comparative study. *Reliability Engineering & System Safety*, 216, 107897.

Wang, Z., Cao, J., Ma, X., Qiu, H., Zhang, Y., Fu, H. & Krishnaswamy, S. (2017). An improved independent increment process degradation model with bilinear properties. *Arabian Journal for Science and Engineering*, 42(7), 2927-2936.

Wang, Z., Wei, Y., Wu, Q., & Liu, C. (2019). A two-stage degradation model considering the stage-varying of dispersity regulation. *Quality and Reliability Engineering International*, 35(7), 2115-2129.

Wang, H., Wang, G. J., & Duan, F. J. (2016). Planning of step-stress accelerated degradation test based on the inverse Gaussian process. *Reliability Engineering & System Safety*, 154, 97-105.

Wang, Z., Wu, Q., Zhang, X., Wen, X., Zhang, Y., Liu, C., & Fu, H. (2018). A generalized degradation model based on Gaussian process. *Microelectronics Reliability*, 85, 207-214.

Yang, G. (2007). *Life cycle reliability engineering.* John Wiley & Sons.

Ye, Zhi-Sheng & Xie, M. (2015). Stochastic modelling and analysis of degradation for highly reliable products. *Applied Stochastic Models in Business and Industry*, 31(1), 16-32.

Yuan, T. and Ji, Y. (2015). A hierarchical Bayesian degradation model for heterogeneous data, *IEEE Transactions on Reliability* 64(1), 63–70.

Supplementary Materials

S1 Proofs and Technical Details

Another way to verify the model identifiability is through sufficient statistic theory. A model is identifiable if the number of independent sufficient statistics is equal to the number of parameters to be estimated. We explore this approach for the proposed model in the following proposition.

Proposition S1.1. *Assume the DMGM given in* (3.2) *and the evolution equation defined in (3.4). Under these assumptions it follows that*

(a) The number of unknown parameters in the DMGM exceeds by one the number of linearly independent sufficient statistics.

(b) If one of the coordinates of vector $\boldsymbol{\Psi} = (\boldsymbol{\lambda}, \boldsymbol{\theta})$ *is fixed at a known value, then the number of linearly independent sufficient statistics is equal to the number of unknown model parameters.*

Proof. (a) The distribution associated with the observational equation given in (3.2) belongs to the exponential family. Consequently, the likelihood function associated to the proposed model can be written as

$$f(\boldsymbol{Y}|\boldsymbol{t}, \boldsymbol{\lambda}, \boldsymbol{\theta}) = \exp\left\{\sum_{i=1}^{n}\sum_{j=1}^{J} g(t_j)\log(\lambda_i\theta_j) - \sum_{i=1}^{n}\sum_{j=1}^{J}\log(\Gamma(g(t_j))) + \sum_{i=1}^{n}\sum_{j=1}^{J} g(t_j)\log(y_{ij}) - \sum_{i=1}^{n}\sum_{j=1}^{J}\lambda_i\theta_j y_{ij}\right\}. \tag{S1}$$

According to the factorization theorem, the sufficient statistics for the model para-meters can be obtained from expression $\sum_{i=1}^{n}\sum_{j=1}^{J}\lambda_i\theta_j y_{ij}$ in (S1). Expanding this equation, we have that

$$\sum_{i=1}^{n}\sum_{j=1}^{J}\lambda_i\theta_j y_{ij} = \begin{cases} & \lambda_1\theta_1 y_{11} & + & \lambda_1\theta_2 y_{12} & + & \ldots & + & \lambda_1\theta_J y_{1J} \\ + & \lambda_2\theta_1 y_{21} & + & \lambda_2\theta_2 y_{22} & + & \ldots & + & \lambda_2\theta_J y_{2J} \\ + & \lambda_3\theta_1 y_{31} & + & \lambda_3\theta_2 y_{32} & + & \ldots & + & \lambda_3\theta_J y_{3J} \\ + & \vdots & + & \vdots & + & \ddots & + & \vdots \\ + & \lambda_n\theta_1 y_{n1} & + & \lambda_n\theta_2 y_{n2} & + & \ldots & + & \lambda_n\theta_J y_{nJ}. \end{cases} \tag{S2}$$

Thus, the degradation measure y_{ij} for unit i at time j is a sufficient statistic for the pair $\lambda_i\theta_j$, proving that the model is not identifiable. Considering the evolution equation (3.4), we obtain a more parsimonious model as it follows that

$$\theta_j = \theta_1\prod_{k=2}^{j}\frac{\epsilon_k}{\gamma_k},\ j > 1. \tag{S3}$$

Replacing the result in equation (S3) in equation (S2), it follows that each line i in expression $(S2)$ can be rewritten as

$$\lambda_i\sum_{j=1}^{J}\theta_j y_{1j} = \lambda_i\theta_1\left(y_{i1} + \sum_{j=2}^{J} y_{ij}\prod_{k=2}^{j}\frac{\epsilon_k}{\gamma_k}\right).$$

Consequently, the sufficient statistic for the parameters $(\lambda_1, \ldots, \lambda_n, \theta_1)$ is the vector

$$\left(y_{11} + \sum_{j=2}^{J} y_{1j} \prod_{k=2}^{j} \frac{\epsilon_k}{\gamma_k}, \ldots, y_{n1} + \sum_{j=2}^{J} y_{nj} \prod_{k=2}^{j} \frac{\epsilon_k}{\gamma_k} \right),$$

which is n-dimensional proving that even assuming the relationship given by the evolution equation (3.4), the model remains non-identifiable.

(b) Without losing generality, assume that θ_1 is known thus the model parameters are $\psi = (\lambda_1, \ldots, \lambda_n)$. As proved in item (a), the sufficient statistic is the vector

$$\left(y_{11} + \sum_{j=2}^{J} y_{1j} \prod_{k=2}^{j} \frac{\epsilon_k}{\gamma_k}, \ldots, y_{n1} + \sum_{j=2}^{J} y_{nj} \prod_{k=2}^{j} \frac{\epsilon_k}{\gamma_k} \right),$$

which have the same dimension as ψ. □

S2 Additional Simulation Studies

This section presents some additional simulation scenarios. In the first two studies, (Section S2.1 and Section S2.2), new simulations are performed to assess the impact of the prior distribution for γ and $\boldsymbol{\lambda}$, respectively, on the posterior estimates for the quantities of interest in the DMGM. In Section S2.3, we generate a degradation data with a large number of measurements and perform predictions considering big steps to show the efficiency of our sequential prediction procedure.

S2.1 The effect of the prior distributions for γ

In the following, two new scenarios are considered where it is assumed that $\gamma \sim$ Beta(p=9.13,q=27.35) and $\gamma \sim$ Beta(p=24.5,q=24.5). In both distributions, $V(\gamma) = 0.005$ but the prior means are, respectively, 0.25 (true value) and 0.5. Our goal is to verify if these specifications produce a higher impact on the estimates of the DMGM parameters and in the failure times of the units under test than that more flat prior assumed in the paper. Tables S1 and S2 show the relative bias (RB); the average of the posterior variances (MV) of the parameters; the relative variance (RVM); and the coverage percentage (CP) with probability 0.95 for the DMGM paramaters and failure times of the units under test assuming different prior distributions for θ_0 and if, respectively, $\gamma \sim$ Beta(9.13,27.35) and $\gamma \sim$ Beta(24.5,24.5).

Table S1: Summary of relative bias, variances of the posterior samples, relative variance of the posterior mean estimates and coverage percentage of the 95% credibility interval for the DMGM paramenters and failure times of the units under test considering the five prior distributions for θ_0 and $\gamma \sim$ Beta(p=9.13,q=27.35).

	$\theta_0 \sim$ Gamma$(0.01, 0.01)$				$\theta_0 \sim$ Gamma$(1, 1)$				$\theta_0 \sim$ Gamma$(10, 10)$				$\theta_0 \sim$ Gamma$(100, 100)$				$\theta_0 \sim$ Gamma$(400, 200)$			
	RB	MV	RVM	CP	RB	MV	RVM	CP	RB	MV	RVM	CP	RB	MV	RVM	CP	RB	MV	RVM	CP
θ_1	42.97	15174.03	104.60	100	0.556	5.425	0.074	100	0.093	0.415	0.047	100	0.082	0.043	0.040	99	-0.459	0.005	0.010	2
θ_2	42.12	17108.09	186.40	100	0.532	6.139	0.203	100	0.086	0.524	0.127	100	0.086	0.091	0.094	95	-0.447	0.014	0.024	22
θ_3	41.31	17149.72	171.85	100	0.508	6.286	0.197	100	0.070	0.531	0.129	100	0.073	0.097	0.101	99	-0.452	0.017	0.026	23
θ_4	42.27	19536.73	171.81	100	0.541	6.983	0.186	100	0.091	0.569	0.117	100	0.096	0.102	0.097	99	-0.440	0.017	0.026	23
θ_5	41.38	16492.18	162.56	100	0.515	6.081	0.184	100	0.075	0.513	0.121	100	0.078	0.092	0.097	100	-0.450	0.016	0.025	23
θ_6	41.39	17639.81	151.87	100	0.514	6.417	0.178	100	0.076	0.532	0.122	100	0.080	0.095	0.099	99	-0.449	0.016	0.026	24
θ_7	41.33	17315.82	148.71	100	0.510	6.273	0.172	100	0.073	0.524	0.117	100	0.077	0.094	0.096	99	-0.450	0.016	0.025	22
θ_8	41.24	16804.63	148.55	100	0.508	6.079	0.171	100	0.071	0.514	0.119	100	0.075	0.091	0.095	98	-0.451	0.015	0.025	24
θ_9	41.36	16636.57	149.43	100	0.511	5.989	0.170	100	0.074	0.511	0.117	100	0.077	0.091	0.094	99	-0.450	0.015	0.024	23
θ_{10}	41.51	16601.51	158.45	100	0.515	6.011	0.177	100	0.077	0.510	0.120	100	0.081	0.090	0.098	99	-0.448	0.015	0.025	23
λ_1	7.206	530.51	1.511	100	7.623	414.07	1.918	100	0.871	7.141	0.429	100	0.120	0.152	0.099	95	1.123	0.357	0.345	34
λ_2	7.076	513.96	1.323	100	7.486	400.21	1.803	100	0.842	7.122	0.415	100	0.103	0.148	0.097	97	1.090	0.346	0.337	37
λ_3	7.153	527.14	1.439	100	7.569	408.78	2.009	100	0.857	6.903	0.419	100	0.114	0.151	0.102	95	1.111	0.352	0.357	33
λ_4	7.140	524.36	1.460	100	7.561	410.70	2.026	100	0.849	7.190	0.412	100	0.107	0.148	0.092	98	1.099	0.347	0.321	40
λ_5	7.125	1171.72	1.324	100	7.545	919.06	1.936	100	0.853	15.99	0.432	100	0.108	0.334	0.095	96	1.099	0.785	0.328	36
λ_6	7.090	1163.85	1.303	100	7.512	910.00	2.019	100	0.849	16.27	0.438	100	0.105	0.335	0.098	97	1.092	0.780	0.334	39
λ_7	7.168	1187.34	1.347	100	7.602	928.15	2.079	100	0.865	15.75	0.431	100	0.116	0.342	0.099	98	1.115	0.799	0.344	33
λ_8	7.115	1172.17	1.317	100	7.546	920.04	2.007	100	0.851	15.82	0.422	100	0.109	0.337	0.098	96	1.100	0.787	0.337	36
λ_9	7.110	2079.99	1.498	100	7.516	1615.22	1.952	100	0.846	27.18	0.414	100	0.105	0.594	0.096	96	1.094	1.388	0.330	36
λ_{10}	7.115	2072.98	1.330	100	7.550	1634.04	1.969	100	0.851	29.11	0.426	100	0.108	0.593	0.095	97	1.101	1.389	0.335	39
γ	0.082	0.004	0.011	100	0.053	0.004	0.011	100	0.027	0.004	0.011	100	0.010	0.004	0.011	100	0.006	0.004	0.012	100
T_1	0.0052	0.0966	0.0007	95	0.0050	0.0955	0.0007	95	0.0048	0.0959	0.0007	94	0.0047	0.0957	0.0007	96	0.0048	0.0957	0.0007	96
T_2	-0.0025	0.0952	0.0005	96	-0.0025	0.0954	0.0005	97	-0.0028	0.0945	0.0005	95	-0.0028	0.0946	0.0005	95	-0.0028	0.0951	0.0005	97
T_3	0.0016	0.0955	0.0005	99	0.0015	0.0963	0.0005	98	0.0015	0.0960	0.0005	98	0.0014	0.0952	0.0005	99	0.0014	0.0955	0.0005	98
T_4	0.0009	0.0951	0.0007	94	0.0008	0.0952	0.0007	94	0.0007	0.0954	0.0007	95	0.0005	0.0949	0.0007	95	0.0006	0.0952	0.0007	93
T_5	0.0004	0.1446	0.0005	97	0.0005	0.1436	0.0005	98	0.0003	0.1422	0.0005	98	0.0002	0.1425	0.0005	96	0.0001	0.1434	0.0005	97
T_6	-0.0016	0.1408	0.0006	98	-0.0018	0.1418	0.0006	99	-0.0018	0.1417	0.0006	99	-0.0019	0.1418	0.0006	97	-0.0020	0.1421	0.0006	99
T_7	0.0035	0.1443	0.0005	98	0.0034	0.1438	0.0005	98	0.0033	0.1433	0.0005	98	0.0032	0.1439	0.0005	98	0.0032	0.1430	0.0005	98
T_8	0.0001	0.1428	0.0005	100	-0.0001	0.1433	0.0005	99	-0.0002	0.1442	0.0005	100	-0.0002	0.1437	0.0005	100	-0.0004	0.1424	0.0005	99
T_9	-0.0010	0.1890	0.0007	98	-0.0012	0.1878	0.0006	98	-0.0013	0.1881	0.0007	98	-0.0014	0.1872	0.0007	98	-0.0013	0.1896	0.0007	98
T_{10}	0.0004	0.1909	0.0005	99	0.0004	0.1913	0.0005	100	0.0001	0.1912	0.0005	99	0.0002	0.1912	0.0005	99	0.0001	0.1912	0.0005	99

Table S2: Summary of relative bias, variances of the posterior samples, relative variance of the posterior mean estimates and coverage percentage of the 95% credibility interval for the DMGM paramenters and failure times of the units under test considering the five prior distributions for θ_0 and $\gamma \sim$ Beta(p=24.5,q=24.5).

	$\theta_0 \sim$ Gamma$(0.01, 0.01)$				$\theta_0 \sim$ Gamma$(1, 1)$				$\theta_0 \sim$ Gamma$(10, 10)$				$\theta_0 \sim$ Gamma$(100, 100)$				$\theta_0 \sim$ Gamma$(400, 200)$			
	RB	MV	RVM	CP	RB	MV	RVM	CP	RB	MV	RVM	CP	RB	MV	RVM	CP	RB	MV	RVM	CP
θ_1	25.18	4611.42	33.02	100	0.276	2.371	0.050	100	0.087	0.215	0.042	100	0.083	0.022	0.040	86	-0.459	0.003	0.010	0
θ_2	24.81	4627.02	58.42	100	0.264	2.423	0.117	100	0.092	0.251	0.103	100	0.138	0.039	0.112	80	-0.423	0.005	0.031	17
θ_3	24.52	4699.06	59.65	100	0.257	2.424	0.131	100	0.088	0.252	0.116	100	0.145	0.045	0.139	80	-0.415	0.007	0.040	19
θ_4	25.02	4855.25	53.28	100	0.283	2.498	0.119	100	0.109	0.257	0.104	100	0.169	0.046	0.133	82	-0.402	0.007	0.039	19
θ_5	24.80	4599.84	55.35	100	0.273	2.384	0.124	100	0.099	0.245	0.108	100	0.155	0.044	0.127	83	-0.410	0.007	0.036	18
θ_6	24.75	4756.69	55.46	100	0.269	2.423	0.123	100	0.097	0.247	0.109	100	0.154	0.045	0.131	78	-0.410	0.007	0.037	19
θ_7	24.68	4704.60	51.34	100	0.268	2.405	0.118	100	0.096	0.246	0.104	100	0.153	0.044	0.128	80	-0.411	0.007	0.037	20
θ_8	24.66	4661.03	50.67	100	0.266	2.378	0.116	100	0.094	0.243	0.102	100	0.151	0.044	0.124	81	-0.412	0.007	0.036	19
θ_9	24.70	4618.76	51.41	100	0.267	2.369	0.117	100	0.095	0.242	0.103	100	0.152	0.044	0.127	80	-0.411	0.007	0.037	18
θ_{10}	24.86	4609.33	54.79	100	0.275	2.368	0.120	100	0.102	0.242	0.106	100	0.159	0.043	0.129	81	-0.408	0.007	0.037	21
λ_1	7.598	548.64	2.113	100	5.454	250.85	1.604	100	0.339	0.910	0.151	100	0.007	0.058	0.091	81	0.953	0.136	0.390	26
λ_2	7.449	527.78	1.715	100	5.348	241.87	1.486	100	0.319	0.878	0.147	100	-0.008	0.057	0.092	81	0.924	0.131	0.391	28
λ_3	7.523	534.80	1.802	100	5.413	246.84	1.686	100	0.331	0.899	0.155	100	0.002	0.058	0.097	78	0.944	0.135	0.412	24
λ_4	7.500	532.79	1.674	100	5.387	244.77	1.471	100	0.324	0.890	0.142	100	-0.005	0.057	0.086	83	0.931	0.132	0.366	26
λ_5	7.495	1198.98	1.610	100	5.387	550.91	1.549	100	0.326	2.003	0.148	100	-0.003	0.128	0.090	79	0.934	0.299	0.389	25
λ_6	7.469	1195.76	1.731	100	5.373	548.42	1.600	100	0.321	1.997	0.151	100	-0.008	0.127	0.089	84	0.925	0.297	0.381	27
λ_7	7.552	1212.97	1.741	100	5.420	556.41	1.493	100	0.335	2.028	0.155	100	0.003	0.130	0.092	82	0.946	0.303	0.391	25
λ_8	7.492	1195.43	1.698	100	5.379	547.19	1.517	100	0.325	1.998	0.152	100	-0.003	0.128	0.092	83	0.935	0.299	0.396	26
λ_9	7.488	2141.46	1.998	100	5.375	979.43	1.608	100	0.321	3.496	0.148	100	-0.007	0.226	0.087	81	0.925	0.523	0.368	21
λ_{10}	7.505	2136.32	1.898	100	5.393	984.89	1.600	100	0.326	3.545	0.148	100	-0.003	0.228	0.092	81	0.936	0.534	0.396	23
γ	0.925	0.005	0.013	0	0.900	0.005	0.013	1	0.888	0.005	0.013	1	0.881	0.005	0.013	1	0.878	0.005	0.013	1
T_1	0.0068	0.0965	0.0008	92	0.0067	0.0970	0.0007	93	0.0069	0.0967	0.0007	94	0.0067	0.0967	0.0007	93	0.0068	0.0960	0.0007	92
T_2	-0.0008	0.0949	0.0005	98	-0.0009	0.0962	0.0005	98	-0.0008	0.0951	0.0005	99	-0.0009	0.0961	0.0005	97	-0.0009	0.0958	0.0005	100
T_3	0.0034	0.0966	0.0005	98	0.0034	0.0974	0.0005	100	0.0031	0.0964	0.0005	98	0.0032	0.0963	0.0005	98	0.0033	0.0966	0.0005	100
T_4	0.0026	0.0953	0.0008	93	0.0027	0.0953	0.0008	92	0.0025	0.0948	0.0008	93	0.0025	0.0960	0.0008	92	0.0026	0.0952	0.0008	93
T_5	0.0022	0.1436	0.0005	96	0.0022	0.1441	0.0006	97	0.0023	0.1444	0.0005	97	0.0021	0.1433	0.0005	97	0.0022	0.1437	0.0005	96
T_6	0.0000	0.1411	0.0007	96	0.0003	0.1427	0.0007	96	0.0001	0.1422	0.0007	97	0.0001	0.1432	0.0007	96	0.0003	0.1432	0.0007	97
T_7	0.0052	0.1431	0.0006	99	0.0053	0.1448	0.0005	98	0.0052	0.1450	0.0005	98	0.0051	0.1433	0.0005	99	0.0053	0.1448	0.0006	99
T_8	0.0017	0.1441	0.0006	99	0.0018	0.1445	0.0006	97	0.0015	0.1438	0.0005	99	0.0014	0.1448	0.0005	99	0.0016	0.1436	0.0005	99
T_9	0.0007	0.1900	0.0007	98	0.0007	0.1897	0.0007	98	0.0005	0.1903	0.0007	97	0.0007	0.1895	0.0007	98	0.0007	0.1896	0.0007	98
T_{10}	0.0022	0.1930	0.0005	99	0.0022	0.1910	0.0005	99	0.0023	0.1924	0.0005	99	0.0021	0.1930	0.0005	99	0.0022	0.1910	0.0005	99

If the prior distribution for γ is centered on the true value, the estimates for the static and dynamic parameters are improved if compared to the ones obtained by assuming a flatter prior shown in the paper. Also, taking that $\theta_0 \sim$ Gamma(100,100), we got a better performance of the HPD intervals as coverage percentages increased if compared to the scenarios analyzed previously in the paper. By shifting the prior distribution of γ to 0.5, it strongly affects the posterior estimates of γ, but the estimates for the static and dynamic parameters are similar to those obtained in our previous analysis (Section 4 in the paper). Concerning the estimated failure times of the units under test, both prior distributions provide very similar estimates. Thus, our prior specifications for γ and θ_0 only smoothly influenced the posterior estimates of the failure times associated with the units.

S2.2 The effect of the prior distributions for $\lambda_i,\ i = 1, 2, \ldots, n$

To evaluate the effect of the prior distribution of λ_i, $i = 1, 2, \ldots, 10$, on the posterior inference of the DMGM parameters, we consider the following two scenarios: $\lambda_i \overset{ind.}{\sim} Gamma(0.49, 0.35)$ (Scenario 1) and $\lambda_i \overset{ind.}{\sim} Gamma(12.88, 9.20)$ (Scenario 2). These prior distributions are both centered in 1.4, the mean of the generated λ_i, and have variances 0.2 and 4, respectively. We also assume $\theta_0 \sim Gamma(0.01, 0.01)$ and $\gamma \sim Beta(1, 1)$. All other specifications are as for the other simulation studies. The results of the two new scenarios of simulation are presented in Table S3.

The posterior estimates for $\boldsymbol{\lambda}$ and the failure time forecasts are few biased and not greatly influenced by the prior specifications for $\boldsymbol{\lambda}$. We noticed a significant improvement in the posterior estimates for the dynamic parameters compared to that shown in Table 1. For these parameters, to consider more informative prior distributions for $\boldsymbol{\lambda}$ led to less biased estimates. On the other hand, the posterior estimates for γ lost quality and experienced a higher biased than in all different scenarios analyzed in our studies.

S2.3 Degradation forecasts K-steps ahead, K large

To evaluate the performance of DMGM in long-term forecasting of the degradation measurements, we consider a simulated data set from which the last 10 measures are removed from all units for being predicted.

Data are generated as in Section 4 but now considering $m_i = 31$ equally spaced inspection times starting in $t = 0$. The following prior distributions are assumed: $\theta_0 \sim$ Gamma($\alpha_0 = 100, \beta_0 = 100$), $\gamma \sim$ Beta(1,1) and $\lambda_i \sim$ Gamma(0.001, 0.001), for all $i = 1, \ldots, 10$. The 10 removed degradation measures are predicted using the sequential procedure described in Section 2. We collected 2000 MCMC iterates after discarding the first 50000 as the burn-in period and thinning by 100. Figure S1 shows that the DMGM forecasting procedure well recovered the removed measurements.

Table S3: Summary of relative bias, variances of the posterior samples, relative variance of the posterior mean estimates and coverage percentage of the 95% credibility interval for the DMGM paramenters and failure times of the units under test considering different priors for λ_i, $i = 1, 2, \ldots, 10$.

	$\lambda_i \overset{ind.}{\sim} Gamma(0.49, 0.35)$				$\lambda_i \overset{ind.}{\sim} Gamma(12.88, 9.20)$			
	RB	MV	RVM	CP	RB	MV	RVM	CP
θ_1	0.301	0.785	0.078	100	0.049	0.098	0.053	97
θ_2	0.241	0.650	0.036	100	-0.003	0.030	0.021	95
θ_3	0.250	0.650	0.019	100	0.005	0.018	0.009	99
θ_4	0.273	0.660	0.013	100	0.023	0.015	0.006	100
θ_5	0.272	0.676	0.010	100	0.022	0.014	0.004	100
θ_6	0.260	0.682	0.009	100	0.012	0.013	0.002	100
θ_7	0.244	0.688	0.008	100	-0.001	0.012	0.002	100
θ_8	0.242	0.709	0.007	100	-0.002	0.012	0.001	100
θ_9	0.246	0.722	0.007	100	0.001	0.013	0.001	100
θ_{10}	0.248	0.723	0.007	100	0.003	0.013	0.001	100
λ_1	-0.003	0.205	0.005	100	0.006	0.010	0.002	100
λ_2	0.015	0.213	0.005	100	0.024	0.011	0.003	100
λ_3	-0.005	0.204	0.005	100	0.004	0.010	0.002	100
λ_4	0.011	0.211	0.005	100	0.020	0.011	0.002	100
λ_5	-0.001	0.463	0.004	100	-0.003	0.023	0.003	100
λ_6	0.001	0.464	0.005	100	-0.001	0.023	0.003	100
λ_7	0.011	0.473	0.004	100	0.009	0.023	0.002	100
λ_8	0.004	0.468	0.005	100	0.002	0.023	0.002	100
λ_9	-0.004	0.816	0.004	100	-0.016	0.038	0.002	100
λ_{10}	-0.002	0.818	0.004	100	-0.015	0.039	0.002	100
γ	0.919	0.041	0.268	84	0.928	0.041	0.272	85
T_1	0.003	0.123	0.001	93	-0.002	0.120	0.001	96
T_2	-0.007	0.125	0.001	94	-0.011	0.122	0.001	92
T_3	0.003	0.122	0.000	98	-0.001	0.119	0.000	99
T_4	-0.005	0.124	0.001	97	-0.009	0.121	0.001	96
T_5	0.001	0.186	0.001	93	0.002	0.178	0.001	95
T_6	0.000	0.184	0.001	95	0.002	0.177	0.001	94
T_7	-0.005	0.185	0.001	97	-0.003	0.180	0.001	97
T_8	-0.001	0.184	0.001	96	0.000	0.178	0.001	99
T_9	0.002	0.243	0.001	97	0.009	0.234	0.001	93
T_{10}	0.002	0.244	0.001	96	0.009	0.236	0.001	94

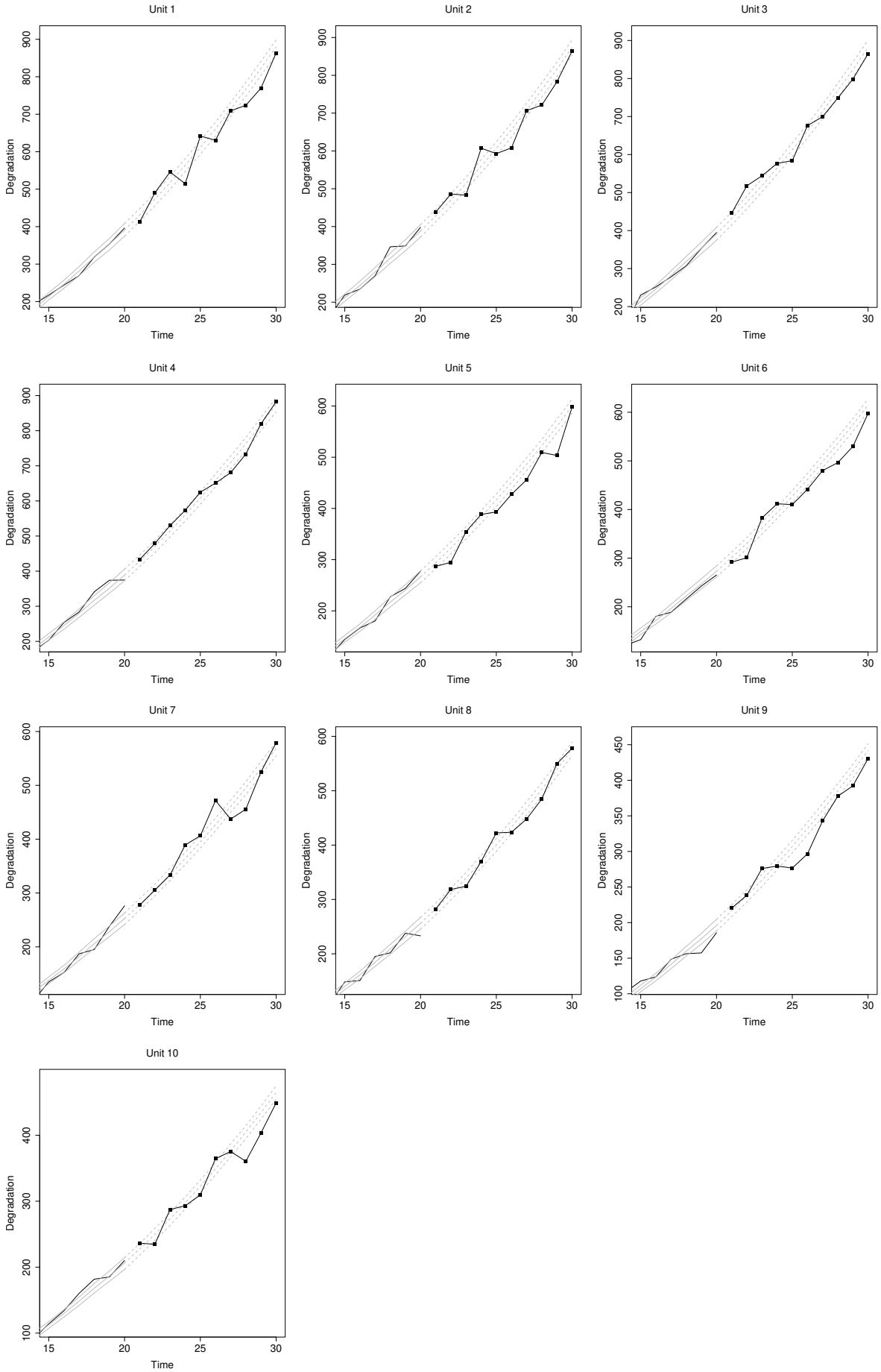

Figure S1: True degradation measure (black solid line), posterior means for the filtering distribution (grey solid line) the sequential forecasting (grey dashed line) the removed observations (black solid line with squares) and the 95% credibility intervals for the units under test, simulated degradation data.

S3 A Closer Look at our Case Studies

This section presents some complementary material related to the analysis of the fatigue crack size and stress relaxation datasets (Section S3.1 and Section S3.2, respectively). It includes the point and interval posterior estimates of the DMGM parameters, additional graphics with the fit and sequential forecasting of the degradation measures for all units and a RUL comparison between different models.

S3.1 Fatigue Crack Size Data

For the fatigue crack size data presented in Meeker and Escobar [1998], the table S4 gives a numerical detail for the point and interval estimates of the DMGM parameters.

Table S4: Posterior point estimates and 95% credibility interval bounds of the DMGM parameters, fatigue crack size data.

Parameter	Mean	Median	Mode	HPD	
θ_1	0.89	0.87	0.87	0.41	1.44
θ_2	1.1	1.06	1.07	0.5	1.7
θ_3	1.45	1.41	1.32	0.77	2.18
θ_4	1.8	1.75	1.69	1.06	2.7
θ_5	2.12	2.06	2.03	1.2	3.14
θ_6	2.37	2.29	2.24	1.29	3.41
θ_7	2.59	2.52	2.47	1.51	3.8
θ_8	2.71	2.62	2.63	1.6	3.99
θ_9	2.79	2.7	2.52	1.64	4.09
λ_1	42.71	41.28	36.36	23.77	62.19
λ_2	52.31	51.07	50.15	30.34	77.61
λ_3	54.31	52.65	51.59	30.67	79.93
λ_4	56.37	54.83	51.79	31.82	82.77
λ_5	56.4	54.94	56.01	33.77	84.07
λ_6	57.86	56.11	55.95	32.73	84.08
λ_7	58.68	57.1	55.35	31.43	84.19
λ_8	61.03	59.62	61.98	35.93	91.54
λ_9	64.78	63.06	56.26	35.81	93.19
λ_{10}	68.77	66.55	66.84	37.66	99.06
γ	0.3	0.26	0.21	0.02	0.67

Aiming a broad look at the ten units under test, Figure S2 presents the sequential forecasting together with the 95% credibility intervals until reaching the critical degradation threshold.

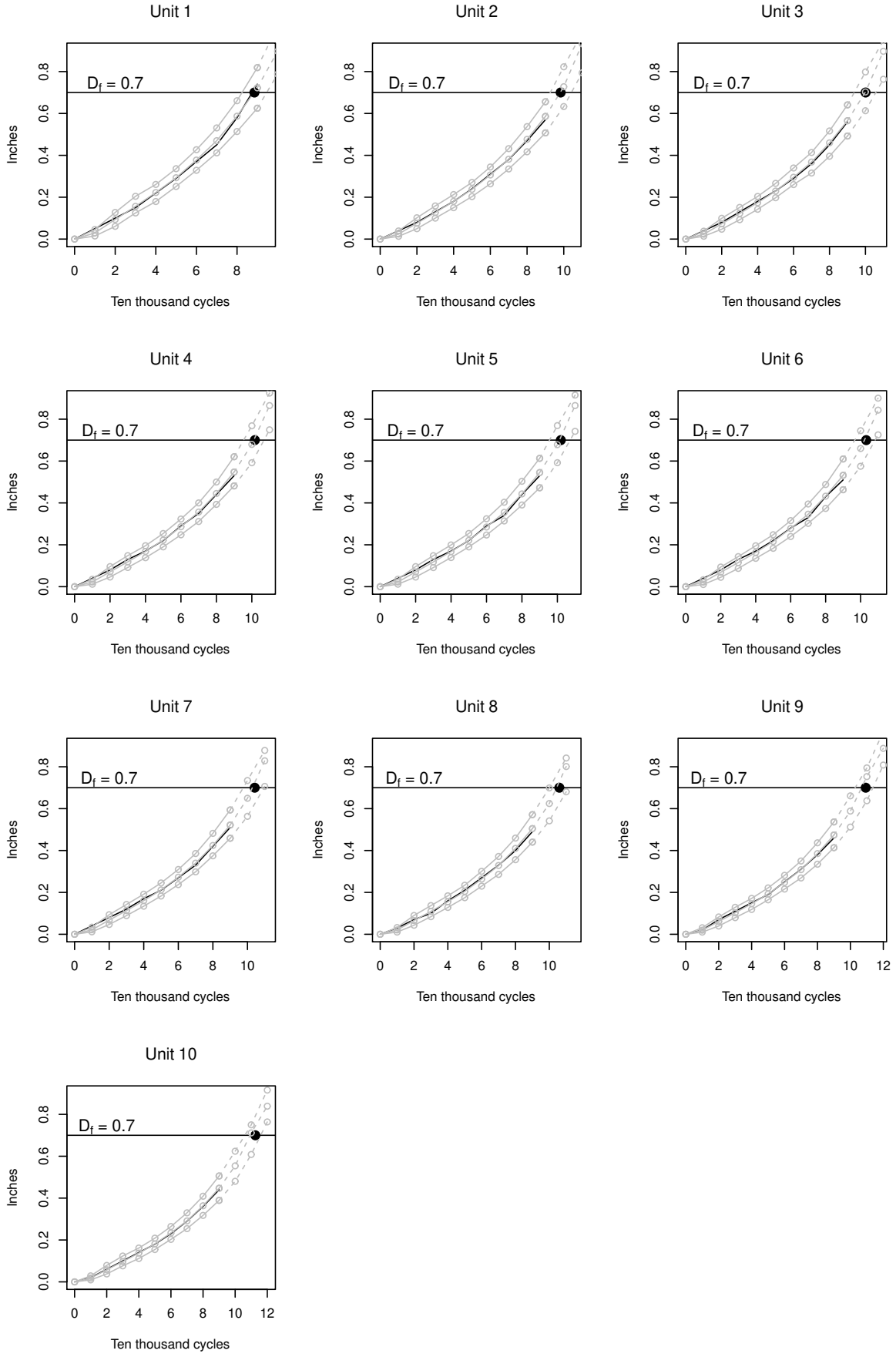

Figure S2: Degradation measure (black solid line), MTTF (black point), posterior means for the filtering distribution (grey solid line), the sequential forecasting (grey dashed line) and the 95% credibility intervals for the units under test, fatigue crack size data.

S3.2 Stress Relaxation Data

Some posterior estimates of the DMGM static and dynamic parameters applied to the data are detailed in Table S5 and Figure S3 presents the sequential forecasting together with the 95% credibility intervals until reaching the critical degradation threshold.

Table S5: Posterior point estimates and 95% credibility interval bounds of the DMGM parameters, stress relaxation data.

Parameter	Mean	Median	Mode	HPD
θ_1	1.00	0.99	1.00	0.78 1.19
θ_2	1.00	1.00	0.99	0.78 1.21
θ_3	1.02	1.02	1.01	0.78 1.24
θ_4	1.03	1.03	1.03	0.78 1.27
θ_5	1.03	1.03	0.97	0.78 1.27
θ_6	1.03	1.02	0.96	0.78 1.28
θ_7	1.02	1.01	0.99	0.79 1.28
θ_8	1.01	1.00	1.00	0.78 1.26
θ_9	1.00	1.00	0.95	0.75 1.24
θ_{10}	1.00	1.00	0.97	0.75 1.25
λ_1	1.81	1.79	1.77	1.32 2.29
λ_2	1.83	1.82	1.80	1.39 2.35
λ_3	1.65	1.64	1.77	1.25 2.10
λ_4	1.58	1.57	1.55	1.20 2.02
λ_5	1.46	1.44	1.39	1.07 1.85
λ_6	1.39	1.37	1.23	1.00 1.76
γ	0.71	0.74	0.92	0.36 1.00

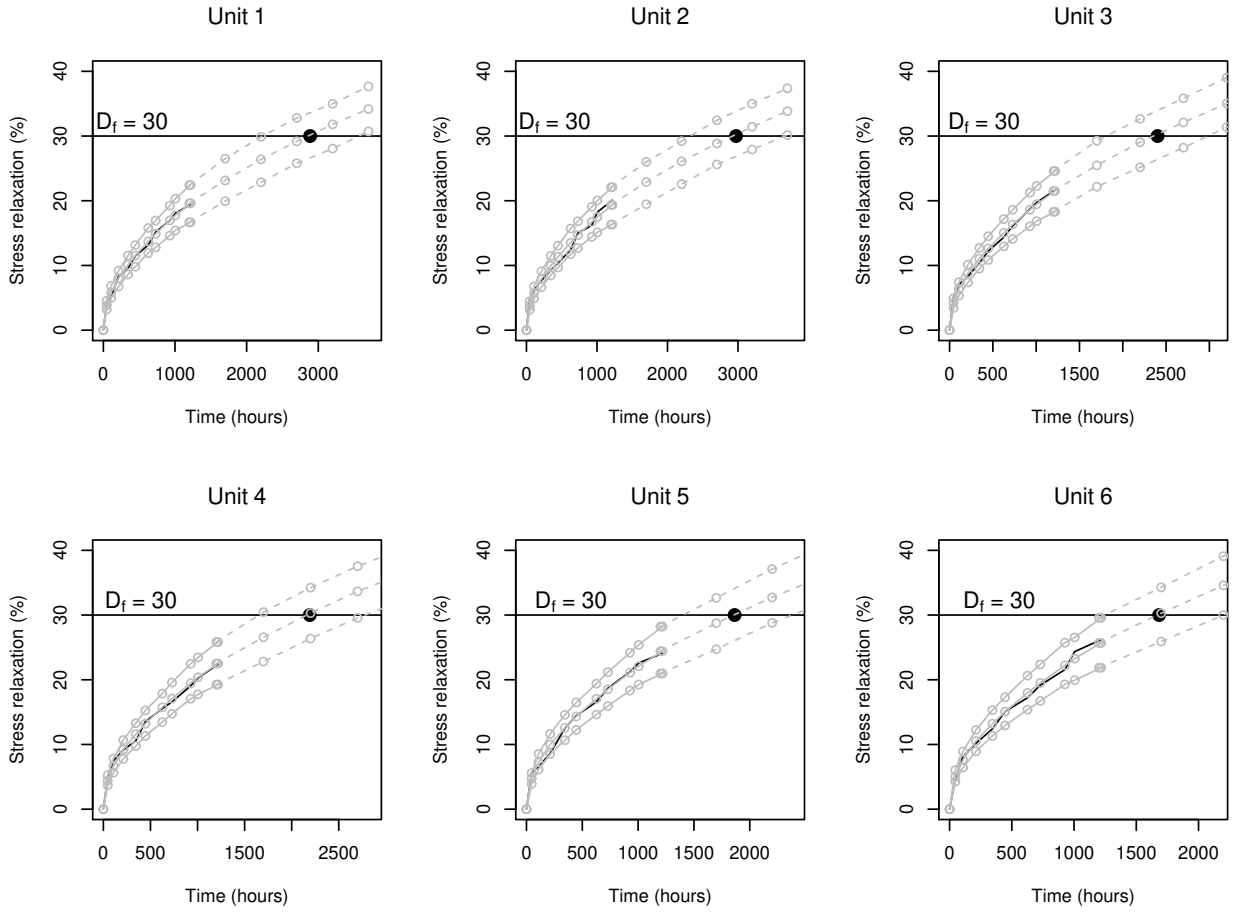

Figure S3: Degradation measure (black solid line), MTTF (black point), posterior means for the filtering distribution (grey solid line), the sequential forecasting (grey dashed line) and the 95% credibility intervals for the units under test, stress relaxation data.

Table S6 shows the $\overline{RUL}$ by fitting DMGM, WLDM, WRDM and DLDM to analyze the stress relaxation data in different scenarios. The $\overline{RUL}$ was calculated considering different last inspection times t_J, given in hours. Specifically, for all units under test, we evaluate the $\overline{RUL}$ from complete data in which $t_J = 1218$ and removing from 1 to 3 degradation measurements. Removing the last 3 degradation measurements from the data, the final inspection time is $t_J = 729$.

The RUL values for the WRDM are only slightly higher than those obtained by fitting the DMGM, showing that these two models are comparable in predicting the remaining useful life of the units under test. However, compared to WRDM, the DMGM provides better predictive accuracy measures (See Table 5). The lowest RUL estimates are obtained by fitting WLDM for all units under test. Considering the WLDM and letting $t_J = 1218$, the estimated RUL for unit 6 is negative indicating erroneously that unit 6 failured before $t_J = 1218$ hours.

Table S6: $\overline{RUL}$ in hours obtained considering DMGM, WLDM, WRDM and DLDM for stress relaxation data with different values of t_J.

Model	t_J	Unit					
		1	2	3	4	5	6
DMGM	1218	1659.63	1738.28	1181.49	987.06	648.39	467.25
	1005	1914.23	2022.26	1412.73	1193.18	873.15	705.77
	927	2075.17	2214.12	1561.36	1322.86	1013.82	868.85
	729	2330.22	2451.12	1821.71	1557.72	1262.48	1075.80
WLDM	1218	383.09	394.01	242.89	191.14	61.73	—-
	1005	490.05	528.42	364.89	315.09	189.74	135.77
	927	498.04	560.51	382.21	323.39	212.91	177.03
	729	576.56	631.39	484.82	411.82	317.09	277.73
WRDM	1218	1728.63	1805.78	1241.32	1051.00	687.43	495.93
	1005	1959.57	2111.80	1486.50	1285.68	905.82	738.95
	927	2088.65	2327.58	1623.65	1388.81	1025.29	889.81
	729	2329.58	2550.36	1885.39	1596.92	1265.01	1100.04
DLDM	1218	803.12	749.73	574.13	485.68	375.27	199.11
	1005	821.87	829.23	657.16	578.21	418.34	264.71
	927	890.88	1044.9	712.46	647.92	498.91	418.69
	729	921.68	1095.08	834.91	739.87	593.37	487.09

Chapter 4

General Path Dynamic Model for Degradation Data with Fixed Covariates

Abstract

Degradation data provide a useful resource for obtaining reliability information for some highly reliable products and systems. In addition to the degradation measurements, it is common to record the system usage as a function of observed covariates that can distinctly influence the failure times of the units under test. In this context, we propose a general path dynamic model for degradation data with fixed covariates. This proposed methodology is able to allow the degradation rate to be writen as a function of two components. The first component represents the particularities of each unit and has a regression structure that accommodates the fixed covariates. The other component represents the random effects of the common environment and evolve over time. In addition, the inspection times are included in the model from generic functions, allowing for different practical representations to be accommodated. After defining the proposed model, its identifiability is investigated along with the MCMC procedure used to make the inferential process. The relation of the model parameters and the failure time is found and methods for estimating the remaining useful life for units under test and a future one are discussed. We conduct a simulation study to verify the effectiveness of the proposed algorithm and applied the methodology to the scar width degradation data.

Keywords: Covariates, Failure Time, Degradation rate decomposition, Model identifiability, Reliability

---

4.1 Introduction

The increasing demand for highly reliable products has been posing big challenges on reliability assessment. A major challenge for life tests of these products is how to quickly and efficiently extract failure information to assess the remaining useful life of the devices. A degradation model which measures the physical degradation path as a function of time can provide a direct connection between the product failure time and the inherent degradation mechanism, and hence improves accuracy and credibility of the predicted reliability. Most existing work in the literature focuses on modeling and analysis of degradation data with a single characteristic. In some degradation tests, multiple characteristics of a degradation process are measured to understand different aspects of the reliability performance [Lu *et al*, 2021].

As a motivating practical situation, Figure 4.1 brings an experiment conducted to test the wear resistance of a particular metal alloy [Meeker and Escobar, 1998]. The sliding test was conducted over a range of different applied weights in order to study the effect of weight and to gain a better understanding of the wear mechanism. Thus, 12 units were tested and divided according to different applied weights of 0.10kg, 0.05kg and 0.01kg. These units were monitored over 9 non-equidistant inspection times and it was established that the critical threshold of the scar width is D_f =50 microns. Note that the applied weights contribute to different degradation trajectories and strongly influence the failure time of the units under test.

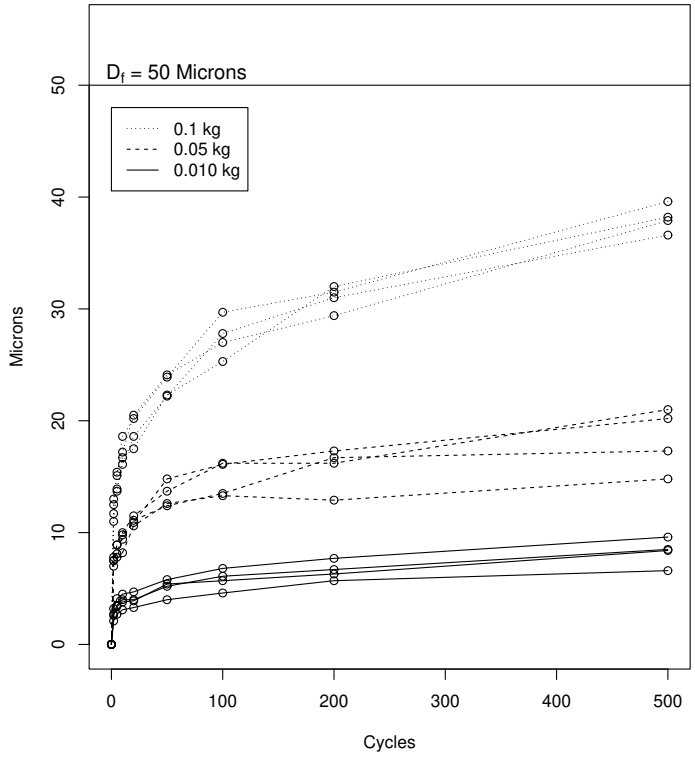

Figure 4.1: Scar width resulting from a metal-to-metal sliding test for different applied weights

The literature on modeling degradation data with multiple characteristics is scarce. To capture the influences of both accelerated conditions and material characteristics as well as the influence of unobserved factors, Sun *et al* [2021] propose a degradation modeling framework with mixed type covariates and latent heterogeneity. In Wang *et al* [2021], a multivariate Wiener process is constructed as a baseline model, on top of which two types of models are developed to meaningfully characterize the time-variant covariates and imperfect maintenance effects. Hong *et al* [2015] use a general path model with individual random effects to describe degradation paths and a vector time series model to describe the covariate process. Bagdonavicius and Nikulin [2001] model degradation by a gamma process and include possibly time-dependent covariates. The same process is used in Lawless and Crowder [2004], where the authors incorporate random effects and covariates in their proposed methodology. Motivated by the photodegradation process of polymeric material, Lu *et al* [2021] propose a multivariate general path model for analyzing degradation data with multiple degradation characteristics incorporating covariates for modeling the nonlinear degradation path.

We propose a methodology capable of helping to fill this gap in the literature of degradation models for data with covariates. The novelty is in the use of dynamic models together with a regression structure to model the data with fixed covariates. In section 4.2, the dynamic degradation model with fixed covariates is defined, together with the proof that it is identifiable. This section also details the inferential procedure to estimate the parameters of interest in the proposed model. Section 4.3 discusses the relation between the model parameters and the failure time and presents the process of estimating the remaining useful life of the units under test and a future one. A brief simulation study is conducted in Section 4.4 to verify the efficiency of the proposed estimation algorithm. Section 4.5 presents the application of the model to the scar width degradation data (Figure 4.1). Finally, Section 4.6 closes this chapter with interesting topics for future research.

4.2 Dynamic Degradation Model with Fixed Covariates

Suppose that a sample of n independent units are under test. Let Y_{ij} be the degradation at unit i, $i = 1, 2, \ldots, n$, accumulated until the measurement instant j, $j = 1, 2, \ldots, m_i$ and m_i is the number of time intervals in which degradation is measured on unit i. Assume that all units under test are subject to the same dynamic structure which, in a general context, is given by

$$\begin{cases} Y_{ij} = \alpha_{ij} + (\lambda_i + \mu_j) g(t_{ij}) + \epsilon_{ij} \\ \alpha_{ij} = \alpha_{i(j-1)} + \nu_{ij} \\ \mu_j = \mu_{j-1} + \omega_j \end{cases}, \tag{4.1}$$

where α_{ij} is the baseline degradation, λ_i is a specific component associated to each unit i, μ_j is the effect of the common environment at the measurement instant j, $g(t_{ij})$ is a positive increasing function of the inspection times t_{ij}, ϵ_{ij} is the observational error and ν_{ij} and ω_j are

the evolution errors. To incorporate the fixed covariates into the proposed model, λ_i is defined as

$$\lambda_i = \exp\{\boldsymbol{\beta X_i}\} = \exp\{\beta_0 + \beta_1 X_{i1} + \beta_2 X_{i2} + \ldots + \beta_p X_{ip}\}, \tag{4.2}$$

where $\boldsymbol{\beta} = [\beta_0, \beta_1, \ldots, \beta_p]^t$ is the $(p+1)$-vector of regression parameters and $\boldsymbol{X_i} = [X_{1i}, X_{2i}, \ldots, X_{pi}]^t$ is the vector of p fixed covariates. The definition of the model is added by the fact that $\epsilon_{ij} \overset{ind}{\sim} N(0, \sigma^2_{\epsilon i})$, $\nu_{ij} \overset{ind}{\sim} N(0, \sigma^2_{\nu i})$, for $i = 1, 2, \ldots n$, and $\omega_j \overset{ind}{\sim} N(0, \sigma^2_{\omega})$, where $\sigma^2_{\epsilon i}$, $\sigma^2_{\nu i}$ and σ^2_{ω} are invariant and unknown.

Note that the structure of the model given in (4.1) implies that the degradation rate of the units under test is a function of $(\lambda_i + \mu_j)$. This decomposition is done by adding two effects, one static and particular for each unit and the other dynamic representing the random effects of the common environment. Furthermore, the proposed methodology can also be used in degradation data that do not have fixed covariates. In this case, $\lambda_i = \exp\{\beta_{0i}\}$, for $i = 1, 2, \ldots, n$.

As in Chapter 3, before starting the inferential process of the proposed model, it is necessary to investigate the model's identifiability. One of the ways to verify this property is to examine if the number of independently sufficient statistics is equal to the number of parameters to be estimated.

The model given by equation (4.1) imposes the following likelihood function
$\prod_{i=1}^{n}\prod_{j=1}^{J} f(y_{ij}|t_{ij}, \alpha_{ij}, \boldsymbol{\beta}, \mu_j, \sigma^2_{\epsilon i}) =$

$$\begin{aligned}
&= \prod_{i=1}^{n}\prod_{j=1}^{J}\left(\frac{1}{2\pi\sigma^2_{\epsilon i}}\right)^{\frac{1}{2}} \exp\left\{-\frac{[y_{ij} - (\alpha_{ij} + (\lambda_i + \mu_j)g(t_{ij}))]^2}{2\sigma^2_{\epsilon i}}\right\} \\
&= \prod_{i=1}^{n}\left(\frac{1}{2\pi\sigma^2_{\epsilon i}}\right)^{\frac{J}{2}} \exp\left\{-\sum_{i=1}^{n}\sum_{j=1}^{J}\frac{[y_{ij} - (\alpha_{ij} + (\lambda_i + \mu_j)g(t_{ij}))]^2}{2\sigma^2_{\epsilon i}}\right\} \\
&= \prod_{i=1}^{n}\left(\frac{1}{2\pi\sigma^2_{\epsilon i}}\right)^{\frac{J}{2}} \exp\left\{-\sum_{i=1}^{n}\sum_{j=1}^{J}\frac{(\alpha_{ij} + (\lambda_i + \mu_j)g(t_{ij}))^2}{2\sigma^2_{\epsilon i}} - \sum_{i=1}^{n}\sum_{j=1}^{J}\frac{y^2_{ij}}{2\sigma^2_{\epsilon i}}\right\} \\
&\times \exp\left\{\sum_{i=1}^{n}\sum_{j=1}^{J}\frac{[\alpha_{ij}y_{ij} + \lambda_i g(t_{ij})y_{ij} + \mu_j g(t_{ij})y_{ij}]}{\sigma^2_{\epsilon i}}\right\}
\end{aligned} \tag{4.3}$$

Thus, by the factorization criterion, $\sum_{j=1}^{J} y^2_{ij}$ is a sufficient statistic for each $\sigma^2_{\epsilon i}$, y_{ij} is a sufficient statistic for α_{ij}, $\sum_{j=1}^{J} g(t_{ij})y_{ij}$ is a sufficient statistic for λ_i and $\sum_{i=1}^{n} g(t_{ij})y_{ij}$ is a sufficient statistic for μ_j.

4.2.1 Posterior Inference

Analogously to the inferential process conducted in Section 2.2.1, following West & Harrison [1997], we consider the matrix representation of the proposed model in (4.1). Note that the

expression $\lambda_i g(t_{ij})$ for $i = 1, 2, \ldots, n$ and $j = 1, 2, ..., m_i$ do not depend on dynamic components. In this way, for all $j \geq 1$, assume that

$$\begin{cases} \boldsymbol{Y_j^*} = \boldsymbol{F_j}\boldsymbol{\theta_j} + \boldsymbol{\epsilon_j} & \boldsymbol{\epsilon_j} \sim N_n(0, \boldsymbol{\sigma_\epsilon^2}\mathbb{I}_{n\times n}) \\ \boldsymbol{\theta_j} = \boldsymbol{\theta_{j-1}} + \boldsymbol{\gamma_j} & \boldsymbol{\gamma_j} \sim N_{n+1}(0, \boldsymbol{\Gamma_j}), \end{cases} \tag{4.4}$$

where $\boldsymbol{Y_j^*} = \{[(Y_{1j} - \lambda_1 g(t_{1j})], \ldots, [Y_{nj} - \lambda_n g(t_{nj})]\}^T \in R^n$, $\boldsymbol{\theta_j} = (\alpha_{1j}, \ldots, \alpha_{nj}, \mu_j)^T$, $\boldsymbol{\epsilon_j} = (\epsilon_{1j}, \ldots, \epsilon_{nj})^T$, $\boldsymbol{\gamma_j} = (\nu_{1j}, \ldots, \nu_{nj}, \omega_j)^T$, $\boldsymbol{\sigma_\epsilon^2} = (\sigma_{\epsilon 1}^2, \ldots, \sigma_{\epsilon n}^2)^T$, $\boldsymbol{\Gamma_j} = (\boldsymbol{\sigma_\nu^2}, \sigma_\omega^2)^T \mathbb{I}_{(n+1)\times(n+1)}$ is the $(n+1) \times (n+1)$ covariance matrix, $\mathbb{I}_{p\times p}$ is the identity matrix of order p, $\boldsymbol{\sigma_\nu^2} = (\sigma_{\nu 1}^2, \ldots, \sigma_{\nu n}^2)^T$ and the $n \times (n+1)$ regression matrix is

$$\boldsymbol{F_j} = \begin{pmatrix} 1 & 0 & \cdots & 0 & g(t_{1j}) \\ 0 & 1 & \cdots & 0 & g(t_{2j}) \\ \vdots & \vdots & \ddots & \vdots & \\ 0 & 0 & \cdots & 1 & g(t_{nj}) \end{pmatrix}.$$

To complete the model specification, for the state vector of parameters $\boldsymbol{\theta}_j$ at the initial time $j = 0$, we consider $\boldsymbol{\theta}_0 \sim N_{n+1}(\boldsymbol{m}_0, \boldsymbol{C}_0)$, where $\boldsymbol{m}_0 \in \mathbb{R}^{n+1}$ and $\boldsymbol{C}_0 \in \mathbb{R}^{n+1} \times \mathbb{R}^{n+1}$ are, respectively, the mean vector and the covariance matrix specified based on the available prior information. For the variances, we assume $\psi_{\epsilon i} = \sigma_{\epsilon i}^{-2} \sim \text{Gamma}(a_{1i}, b_{1i})$, $\psi_{\nu i} = \sigma_{\nu i}^{-2} \sim \text{Gamma}(a_{2i}, b_{2i})$, for $i = 1, 2, \ldots, n$ and $\psi_\omega = \sigma_\omega^{-2} \sim \text{Gamma}(a_3, b_3)$, where all the hyperparameters are bigger than 0. The vector $\boldsymbol{\beta}$ of regression parameters have a prior distribution given by $\boldsymbol{\beta} \sim N(\boldsymbol{m}, \boldsymbol{V})$, where $\boldsymbol{m}$ is a vector of dimension $p+1$ of means and $\boldsymbol{V}$ is a $(p+1) \times (p+1)$ covariance matrix.

The posterior distributions of $\boldsymbol{\beta}$, $\boldsymbol{\theta_{0:J}}$, $\boldsymbol{\psi_\epsilon}$, $\boldsymbol{\psi_\nu}$ and ψ_ν, where $J = max(m_i)$, for $i = 1, 2, \ldots, n$, $\boldsymbol{\psi_\epsilon} = (\psi_{\epsilon 1}, \ldots, \psi_{\epsilon n})^T$ and $\boldsymbol{\psi_\nu} = (\psi_{\nu 1}, \ldots, \psi_{\nu n})^T$, are obtained mixing the likelihood function given in equation (4.3) with the prior distributions previously mentioned. Considering $\mathbf{D}^{j-1} = \{\mathbf{D}^{j-2}, Y_{1,j-1}, \ldots, Y_{n,j-1}, t_{1,j-1}, \ldots, t_{n,j-1}\}$, we have the following Markov chain Monte Carlo (MCMC) scheme:

i Generate $\boldsymbol{\beta}$ via $\pi(\boldsymbol{\beta}|\boldsymbol{\theta_{0:J}}, \boldsymbol{\psi_\epsilon}, \boldsymbol{\psi_\nu}, \psi_\omega, \boldsymbol{D}^J)$

ii Generate $\boldsymbol{\theta_{0:J}}$ via $\pi(\boldsymbol{\theta_{0:J}}|\boldsymbol{\beta}, \boldsymbol{\psi_\epsilon}, \boldsymbol{\psi_\nu}, \psi_\omega, \boldsymbol{D}^J)$

iii Generate $\boldsymbol{\psi_\epsilon}$ via $\pi(\boldsymbol{\psi_\epsilon}|\boldsymbol{\beta}, \boldsymbol{\theta_{0:J}}, \boldsymbol{\psi_\nu}, \psi_\omega, \boldsymbol{D}^J)$

iv Generate $\boldsymbol{\psi_\nu}$ via $\pi(\boldsymbol{\psi_\nu}|\boldsymbol{\beta}, \boldsymbol{\theta_{0:J}}, \boldsymbol{\psi_\epsilon}, \psi_\omega, \boldsymbol{D}^J)$

v Generate ψ_ω via $\pi(\psi_\omega|\boldsymbol{\beta}, \boldsymbol{\theta_{0:J}}, \boldsymbol{\psi_\epsilon}, \boldsymbol{\psi_\nu}, \boldsymbol{D}^J)$

In step (i), considering $\boldsymbol{Y_j} = (Y_{1j}, Y_{2j}, \ldots, Y_{nj})$ and the expression given in (4.2), the poste-

rior conditional distribution of $\boldsymbol{\beta}$ is

$$\begin{aligned}\pi(\boldsymbol{\beta}|\boldsymbol{\theta},\boldsymbol{\psi_\epsilon},\boldsymbol{\psi_\nu},\psi_\omega,\boldsymbol{D}^J) &\propto \pi(\boldsymbol{Y_{1:J}}|\boldsymbol{\beta},\boldsymbol{\theta_{0:J}},\boldsymbol{\psi_\epsilon})\pi(\boldsymbol{\beta})\\ &\propto \exp\left\{-\sum_{i=1}^{n}\sum_{j=1}^{J}\frac{(\alpha_{ij}+(\exp\{\boldsymbol{\beta X_i}\}+\mu_j)g(t_{ij}))^2}{2\sigma^2_{\epsilon i}}\right\}\\ &\times \exp\left\{-\sum_{i=1}^{n}\sum_{j=1}^{J}\frac{\exp\{\boldsymbol{\beta X_i}\}g(t_{ij})y_{ij}}{\sigma^2_{\epsilon i}}-\frac{1}{2}(\boldsymbol{\beta}-\boldsymbol{m})^T V^{-1}(\boldsymbol{\beta}-\boldsymbol{m})\right\}.\end{aligned}$$

This distribution does not have a closed form. Thus, we use a Metropolis Hastings step, generating the candidates of $\boldsymbol{\beta}$ from a multivariate normal distribution with mean given by the vector obtained in the immediately previous step and the variance is calibrated aiming at a satisfactory acceptance percentage of the algorithm.

To generate the posterior estimates for the dynamic components $\boldsymbol{\theta_{0:J}}$ in step (ii) we consider the forward filtering backward sampling (FFBS) discussed in Section 2.2.1. applied in the model rewritten in expression (4.4).

In steps (iii) and (iv), the posterior conditional distribution of $\boldsymbol{\psi_\epsilon}$ and $\boldsymbol{\psi_\nu}$ can be broken into the marginal conditional distribution of each component of both vectors. Therefore, for $i = 1, 2, \ldots, n$, we have that

$$\begin{aligned}\pi(\psi_{\epsilon i}|\boldsymbol{\beta},\boldsymbol{\theta_{0:J}},\boldsymbol{\psi_\nu},\psi_\omega,\boldsymbol{D}^J) &\propto \pi(\boldsymbol{y_{1:J}}|\boldsymbol{\beta},\boldsymbol{\theta_{0:J}},\psi_{\epsilon i},\boldsymbol{\psi_\nu},\psi_\omega)\pi(\psi_{\epsilon i})\\ &\propto \psi_{\epsilon i}^{\frac{J}{2}}\exp\left\{-\frac{\psi_{\epsilon i}}{2}\sum_{j=1}^{J}[y_{ij}-\alpha_{ij}-(\lambda_i+\mu_j)g(t_{ij})]^2\right\}\psi_{\epsilon i}^{a_{1i}-1}exp\left\{-b_{1i}\psi_{\epsilon i}\right\}\end{aligned}$$

and

$$\begin{aligned}\pi(\psi_{\nu i}|\boldsymbol{\beta},\boldsymbol{\theta_{0:J}},\boldsymbol{\psi_\epsilon},\psi_\omega,\boldsymbol{D}^J) &\propto \pi(\boldsymbol{y_{1:J}}|\boldsymbol{\beta},\boldsymbol{\theta_{0:J}},\psi_{\epsilon i},\boldsymbol{\psi_\nu},\psi_\omega)\pi(\psi_{\nu i})\\ &\propto \psi_{\nu}^{\frac{J}{2}}\exp\left\{-\frac{\psi_{\nu i}}{2}\sum_{j=1}^{J}(\alpha_{ij}-\alpha_{i(j-1)})^2\right\}\psi_{\nu i}^{a_{2i}-1}exp\left\{-b_{2i}\psi_{\nu i}\right\}.\end{aligned}$$

Consequently, $\psi_{\epsilon i}|\boldsymbol{\beta},\boldsymbol{\theta_{0:J}},\boldsymbol{\psi_\nu},\psi_\omega,\boldsymbol{D}^J \sim \text{Gamma}\left(a_{1i}+J/2, b_{1i}+1/2\sum_{j=1}^{J}[y_{ij}-(\lambda_i+\mu_j)g(t_{ij})]^2\right)$ and $\psi_{\nu i}|\boldsymbol{\beta},\boldsymbol{\theta_{0:J}},\boldsymbol{\psi_\epsilon},\psi_\omega,\boldsymbol{D}^J \sim \text{Gamma}\left(a_{2i}+J/2, b_{2i}+1/2\sum_{j=1}^{J}(\alpha_{ij}-\alpha_{i(j-1)})^2\right)$.

In step (v), the posterior conditional distribution of ψ_ω is given by

$$\begin{aligned}\pi(\psi_\omega|\boldsymbol{\beta},\boldsymbol{\theta_{0:J}},\boldsymbol{\psi_\epsilon},\boldsymbol{\psi_\nu},\boldsymbol{D}^J) &\propto \pi(\boldsymbol{y_{1:J}}|\boldsymbol{\beta},\boldsymbol{\theta_{0:J}},\psi_{\epsilon i},\boldsymbol{\psi_\nu},\psi_\omega)\pi(\psi_{\nu i})\\ &\propto \psi_{\omega}^{\frac{J}{2}}\exp\left\{-\frac{\psi_{\omega i}}{2}\sum_{j=1}^{J}(\mu_j-\mu_{(j-1)})^2\right\}\psi_{\omega}^{a_3-1}exp\left\{-b_3\psi_\omega\right\}\end{aligned}$$

so that $\psi_\omega|\boldsymbol{\beta},\boldsymbol{\theta_{0:J}},\boldsymbol{\psi_\epsilon},\boldsymbol{\psi_\nu},\boldsymbol{D}^J \sim \text{Gamma}\left(a_3+J/2, b_3+1/2\sum_{j=1}^{J}(\mu_j-\mu_{j-1})^2\right)$.

4.3 Failure Time Distribution

Analogously to what was done in the Section 2.3, we suppose that some units under test fail during the experiment and others fail after the maximum measurement instant J. Assume that a unit i fails at the time interval which lower bound is γ_i. If unit i does not fail during the experiment the bound $\gamma_i = J$; otherwise, $\gamma_i < J$. From the relationship between time and degradation given by the model in expression (4.1) and assuming that the function $g(\cdot)$ is invertible, the failure time for the ith unit is given by

$$T_i = g^{-1}\left(\frac{D_f - \alpha_{i\gamma_i}}{\lambda_i + \mu_{\gamma_i}}\right), \tag{4.5}$$

where $\alpha_{i\gamma_i}$ and μ_{γ_i} are the state components prior to failure for unit i. If the function $g(\cdot)$ is not invertible, then computational numerical methods can be used to approximate the relationship obtained in (4.5). For units that do not fail during the experiment, inference for the failure time will consider the state vector related to the last time interval we measured the degradation [Petris *et al.* , 2009].

We obtain a posterior sampling for the failure time of unit i as follows. Having available the posterior sample of $\boldsymbol{\theta}_{i\gamma_i}^{(l)} = (\alpha_{i\gamma_i}^{(l)}, \mu_{\gamma_i}^{(l)})^T$ and $\lambda_i^{(l)}$ associated to the degradation model parameters $\boldsymbol{\theta}_{i\gamma_i} = (\alpha_{i\gamma_i}, \beta_{i\gamma_i})^T$ and λ_i, we calculate $T_i = g^{-1}\left(\frac{D_f - \alpha_{i\gamma_i}^{(l)}}{\lambda_i^{(l)} + \mu_{\gamma_i}^{(l)}}\right)$, for $l = 1, \dots L$, where L is the posterior sample size. This is made by considering the following scheme

$$\begin{pmatrix} \alpha_{i\gamma_i}^{(1)}, & \alpha_{i\gamma_i}^{(2)}, & \dots, & \alpha_{i\gamma_i}^{(L)} \\ \mu_{\gamma_i}^{(1)}, & \mu_{\gamma_i}^{(2)}, & \dots, & \mu_{\gamma_i}^{(L)} \\ \lambda_i^{(1)}, & \lambda_i^{(2)}, & \dots, & \lambda_i^{(L)} \end{pmatrix} \Rightarrow \text{ evaluate } \boldsymbol{\theta}_{i\gamma_i}, \lambda_i | \boldsymbol{D}^J \text{ in } T_i = g^{-1}\left(\frac{D_f - \alpha_{i\gamma_i}}{\lambda_i + \mu_{\gamma_i}}\right)$$

$$\Rightarrow \left(T_i^{(1)} | \boldsymbol{\theta}_{i\gamma_i}^{(1)} \lambda_i^{(1)}, T_i^{(2)} | \boldsymbol{\theta}_{i\gamma_i}^{(2)} \lambda_i^{(2)}, \ \dots \ , T_i^{(L)} | \boldsymbol{\theta}_{i\gamma_i}^{(L)} \lambda_i^{(L)}\right)$$

The posterior predictive cdf of T_i evaluated at time t is approximated by

$$\hat{F}_{T_i|\boldsymbol{D}^J}(t|\boldsymbol{D}^J) = \sum_{l=1}^{L} \frac{\mathbb{1}\{T_i^{(l)} | \boldsymbol{\theta}_{i\gamma_i}^{(l)} \lambda_i^{(l)} \leq t\}}{L}.$$

To calculate the posterior predictive cdf for the failure time T_{n+1} of a new device, we assume that T_{n+1} has the same distribution as the failure times T_i of the units under test. Following Robinson and Crowder [2000], we assume that a posterior sample of $\boldsymbol{\theta}_{(n+1)\gamma_{n+1}}$ and λ_{n+1} is obtained sampling from the posterior distributions of the parameters $\boldsymbol{\theta}_{i\gamma_i}$ and λ_i, for $i = 1, \dots, n$, associated with the time intervals when unit i experienced the failure. Thus, to estimate $F_{T_{n+1}|\boldsymbol{D}^J}(t|\boldsymbol{D}^J)$ at time t we consider the total posterior sample of $\boldsymbol{\theta}_{\boldsymbol{0:J}}$ and $\boldsymbol{\lambda} = (\lambda_1, \lambda_2, \dots, \lambda_n)^T$. For each sample $\boldsymbol{\theta}_{ij}^{(l)} = (\alpha_{i\gamma_i}^{(l)}, \mu_{\gamma_i}^{(l)})^T$ and $\lambda_i^{(l)}$, we calculate

$T_{n+1} = g^{-1}\left(\frac{D_f - \alpha_{i\gamma_i}^{(l)}}{\lambda_i^{(l)} + \mu_{\gamma_i}^{(l)}}\right)$,, $i = 1, \ldots, n$, $l = 1, \ldots, L$, as follows

$$\begin{pmatrix} \alpha_{1\gamma_1}^{(1)} & \alpha_{1\gamma_1}^{(2)} & \ldots & \alpha_{1\gamma_1}^{(L)} \\ \mu_{\gamma_1}^{(1)} & \mu_{\gamma_1}^{(2)} & \ldots & \mu_{\gamma_1}^{(L)} \\ \lambda_1^{(1)} & \lambda_1^{(2)} & \ldots & \lambda_1^{(L)} \\ \vdots & \vdots & \ddots & \vdots \\ \alpha_{n\gamma_n}^{(1)} & \alpha_{n\gamma_n}^{(2)} & \ldots & \alpha_{n\gamma_n}^{(L)} \\ \mu_{\gamma_n}^{(1)} & \mu_{\gamma_n}^{(2)} & \ldots & \mu_{\gamma_n}^{(L)} \\ \lambda_n^{(1)} & \lambda_n^{(2)} & \ldots & \lambda_n^{(L)} \end{pmatrix} \Rightarrow \text{ evaluate } \boldsymbol{\theta}_{i\gamma_i}, \lambda_i | \boldsymbol{D}^J \text{ in } T_{n+1} = g^{-1}\left(\frac{D_f - \alpha_{i\gamma_i}}{\lambda_i + \mu_{\gamma_i}}\right)$$

$$\Rightarrow \begin{pmatrix} T_{n+1}^{(1)}|\boldsymbol{\theta}_{1\gamma_1}^{(1)}\lambda_1^{(1)}, & T_{n+1}^{(2)}|\boldsymbol{\theta}_{1\gamma_1}^{(2)}\lambda_1^{(2)}, & \ldots, & T_{n+1}^{(L)}|\boldsymbol{\theta}_{1\gamma_1}^{(L)}\lambda_1^{(L)} \\ T_{n+1}^{(1)}|\boldsymbol{\theta}_{2\gamma_2}^{(1)}\lambda_2^{(1)}, & T_{n+1}^{(2)}|\boldsymbol{\theta}_{2\gamma_2}^{(2)}\lambda_2^{(2)}, & \ldots, & T_{n+1}^{(L)}|\boldsymbol{\theta}_{2\gamma_2}^{(L)}\lambda_2^{(L)} \\ \vdots & \vdots & \ddots & \vdots \\ T_{n+1}^{(1)}|\boldsymbol{\theta}_{n\gamma_n}^{(1)}\lambda_n^{(1)}, & T_{n+1}^{(2)}|\boldsymbol{\theta}_{n\gamma_n}^{(2)}\lambda_n^{(2)}, & \ldots, & T_{n+1}^{(L)}|\boldsymbol{\theta}_{n\gamma_n}^{(L)}\lambda_n^{(L)} \end{pmatrix}$$

The posterior estimate for the predictive cdf of T_{n+1} evaluated at time t is given by

$$\hat{F}_{T_{n+1}|\boldsymbol{D}^J}(t|\boldsymbol{D}^J) = \sum_{l=1}^{L}\sum_{i=1}^{n} \frac{\mathbb{1}\left\{T_{n+1}^{(l)}|\boldsymbol{\theta}_{i\gamma_i}^{(l)}\lambda_i^{(l)} \leq t\right\}}{nL}.$$

4.4 Simulation Study

In this section, we investigate the model's performance in a simulated degradation test similar to the data from scar width degradation data (Figure 4.1). The simulated data, therefore, has 12 units under test monitored at the non equidistant inspection times 2, 5, 10, 20, 50, 100, 200 and 500 cycles. A continuous variable X, divides the units in three groups of same size: $X = 0.1$kg, X=0.05kg or X=0.01kg. The regression structure adopted is $\lambda_i = \exp \beta_1 X_i$, for $i = 1, 2, \ldots, 12$ and $\beta_1 = 15$. Consequently, $\lambda_1 = \lambda_2 = \lambda_3 = \lambda_4 = 1.16$, $\lambda_5 = \lambda_6 = \lambda_7 = \lambda_8 = 2.12$ and $\lambda_9 = \lambda_{10} = \lambda_{11} = \lambda_{12} = 4.48$. For simplification, we will denote $\lambda_{0.01} = 1.16$, $\lambda_{0.05} = 2.12$ and $\lambda_{0.1} = 4.48$. The standard deviations associated to the observational error of each unit under test are given by $\sigma_{\epsilon 1} = \sigma_{\epsilon 2} = 0.15, \sigma_{\epsilon 3} = \sigma_{\epsilon 4} = 0.25, \sigma_{\epsilon 5} = \sigma_{\epsilon 6} = 0.5, \sigma_{\epsilon 7} = \sigma_{\epsilon 8} = 0.7, \sigma_{\epsilon 9} = \sigma_{\epsilon 10} = 0.9$ and $\sigma_{\epsilon 11} = \sigma_{\epsilon 12} = 0.8$. The standard deviations associated to the evolution errors of the baseline degradation are established as $\sigma_{\nu 1} = \sigma_{\nu 2} = 0.2, \sigma_{\nu 3} = \sigma_{\nu 4} = 0.3, \sigma_{\nu 5} = \sigma_{\nu 6} = 0.5, \sigma_{\nu 7} = \sigma_{\nu 8} = 0.6, \sigma_{\nu 9} = \sigma_{\nu 10} = 0.7$ and $\sigma_{\nu 11} = \sigma_{\nu 12} = 0.8$. The real values of the standard deviations of the model errors is finalized considering that $\sigma_\omega = 0.15$. Each dynamic component present in $\boldsymbol{\theta_0}$ is generated from the distribution $N(1.2, 0.45^2)$. The function of the inspection times adopted here is $g(t_{ij}) = log(t_{ij})$, for $i = 1, 2, \ldots, 12$ and $j = 1, 2, \ldots, 8$. Figure shows one degradation

data generated considering the specifications cited before and the model (4.1):

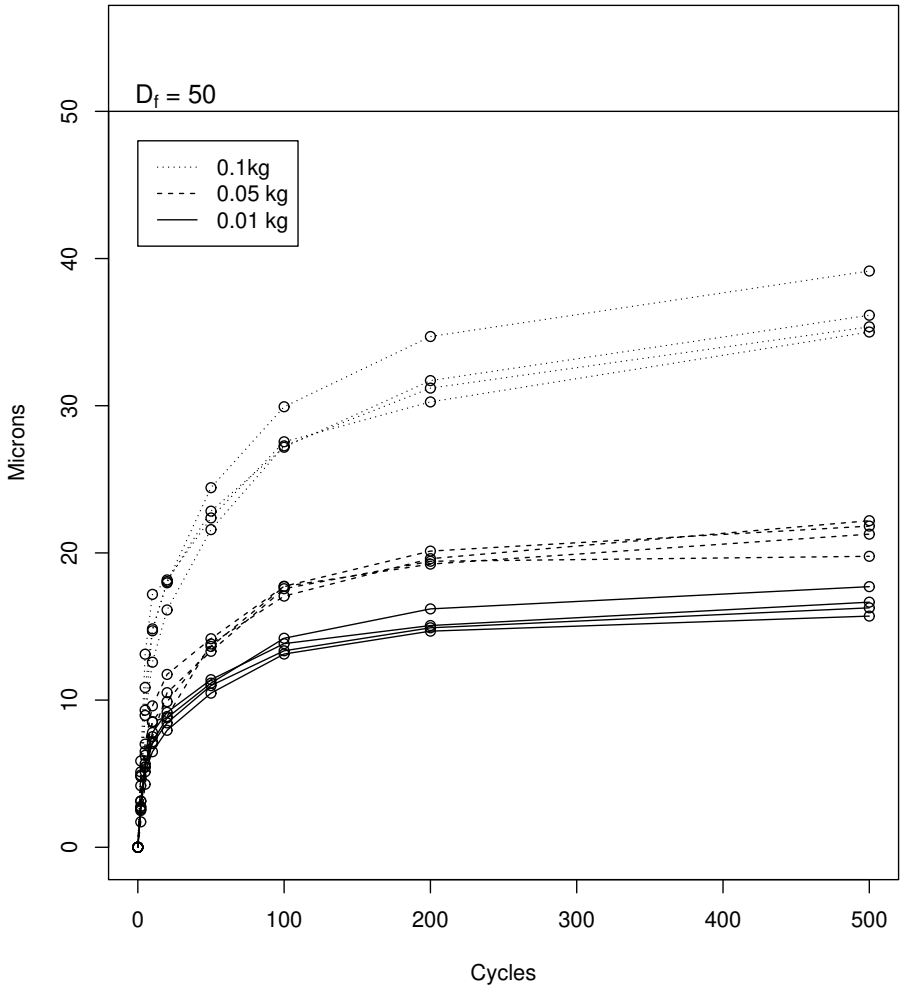

Figure 4.2: A simulated degradation data with covariates

To estimate the model parameters and compare to the real values, we used the following prior distributions: $\beta_1 \sim \mathrm{N}(0, 10^2)$, $\boldsymbol{\theta_0} \sim \mathrm{N}_{13}(\mathbf{0}, 1000\, \mathbb{I}_{13\times 13})$, $\psi_\omega \sim$ Gamma$(0.01, 0.01)$, $\psi_{\epsilon i} \overset{iid}{\sim}$ Gamma$(0.01, 0.01)$ and $\psi_{\nu i} \overset{iid}{\sim}$ Gamma$(0.01, 0.01)$, for $i = 1, 2, \ldots, 12$. The proposed methodology is fitted collecting 1000 MCMC iterates after discarding the first 50000 as the burn-in period and thinning by 200. Table 4.1 provides a summary of the posterior estimates, along with the 95% HPD credibility interval for some model parameters, considering the data from Figure 4.2.

The posterior mean obtained for the regression parameter β_1 is practically equal to the simulated real value and, consequently, the estimates for $\lambda_{0.01}$, $\lambda_{0.05}$ and $\lambda_{0.10}$ also show the same behavior, with respect to the real values of these parameters. The posterior point estimates for the dynamic parameters μ_j, for $j = 1, 2, \ldots, 8$, underestimated most of the real values, but the 95% HPD credibility covered the simulated values of these parameters. All the parameters mentioned before have the posterior means very close to the posterior medians, being a strong

Table 4.1: Posterior point estimates and 95% credibility interval bounds of some model parameters, simulated degradation test (Figure 4.2)

Parameter	True	Mean	Median	St. Dev	95% HPD	
β_1	15.000	14.986	15.016	0.522	13.983	16.065
$\lambda_{0.01}$	1.162	1.162	1.162	0.006	1.150	1.174
$\lambda_{0.05}$	2.117	2.116	2.119	0.055	2.012	2.233
$\lambda_{0.10}$	4.482	4.481	4.489	0.233	4.006	4.941
μ_1	1.619	1.516	1.518	0.345	0.876	2.237
μ_2	1.601	1.548	1.543	0.200	1.147	1.932
μ_3	1.611	1.463	1.460	0.151	1.181	1.743
μ_4	1.363	1.314	1.314	0.121	1.074	1.540
μ_5	1.390	1.351	1.350	0.096	1.173	1.539
μ_6	1.539	1.553	1.552	0.081	1.409	1.721
μ_7	1.514	1.497	1.495	0.074	1.357	1.648
μ_8	1.292	1.305	1.306	0.067	1.170	1.430
$\sigma_{\epsilon 1}$	0.150	0.247	0.224	0.136	0.051	0.499
$\sigma_{\epsilon 2}$	0.150	0.169	0.148	0.086	0.051	0.335
$\sigma_{\epsilon 3}$	0.250	0.174	0.156	0.086	0.046	0.349
$\sigma_{\epsilon 4}$	0.250	0.193	0.164	0.117	0.056	0.412
$\sigma_{\epsilon 5}$	0.500	0.676	0.635	0.436	0.058	1.489
$\sigma_{\epsilon 6}$	0.500	0.299	0.266	0.177	0.064	0.589
$\sigma_{\epsilon 7}$	0.700	0.635	0.619	0.384	0.062	1.281
$\sigma_{\epsilon 8}$	0.700	0.356	0.334	0.174	0.061	0.679
$\sigma_{\epsilon 9}$	0.900	0.422	0.342	0.303	0.057	1.014
$\sigma_{\epsilon 10}$	0.900	0.491	0.400	0.368	0.053	1.230
$\sigma_{\epsilon 11}$	0.800	0.616	0.424	0.554	0.058	1.749
$\sigma_{\epsilon 12}$	0.800	0.309	0.242	0.221	0.057	0.741
$\sigma_{\nu 1}$	0.150	0.317	0.292	0.172	0.062	0.643
$\sigma_{\nu 2}$	0.200	0.175	0.155	0.090	0.053	0.353
$\sigma_{\nu 3}$	0.200	0.187	0.165	0.102	0.044	0.375
$\sigma_{\nu 4}$	0.300	0.307	0.286	0.138	0.095	0.596
$\sigma_{\nu 5}$	0.300	0.839	0.797	0.508	0.052	1.732
$\sigma_{\nu 6}$	0.500	0.323	0.288	0.182	0.055	0.676
$\sigma_{\nu 7}$	0.500	0.676	0.601	0.463	0.060	1.502
$\sigma_{\nu 8}$	0.600	0.328	0.270	0.225	0.060	0.780
$\sigma_{\nu 9}$	0.600	0.674	0.646	0.371	0.081	1.406
$\sigma_{\nu 10}$	0.700	0.732	0.694	0.419	0.060	1.473
$\sigma_{\nu 11}$	0.700	1.355	1.322	0.556	0.298	2.459
$\sigma_{\nu 12}$	0.800	0.665	0.609	0.328	0.130	1.267
σ_ω	0.800	0.179	0.162	0.074	0.089	0.324

indication of symmetric posterior distributions. With respect to the standard deviations associated with the model errors, the posterior point estimates were satisfactory, compared to the real values. There are two standard deviations ($\sigma_{\epsilon 8}$ and $\sigma_{\epsilon 12}$) whose 95% HPD intervals did not recover the simulated values. In all cases, the posterior means obtained were greater than the posterior median values, indicating asymmetry of the posterior distributions associated to standard deviations of the model errors.

The behavior of the mean posterior estimates for the 96 baseline degradations with respect to the simulated values is represented in Figure 4.3. The points in this figure are randomly arranged around the line, indicating that the posterior samples of the baseline degradations were able to recover regions close to the simulated real values of these parameters.

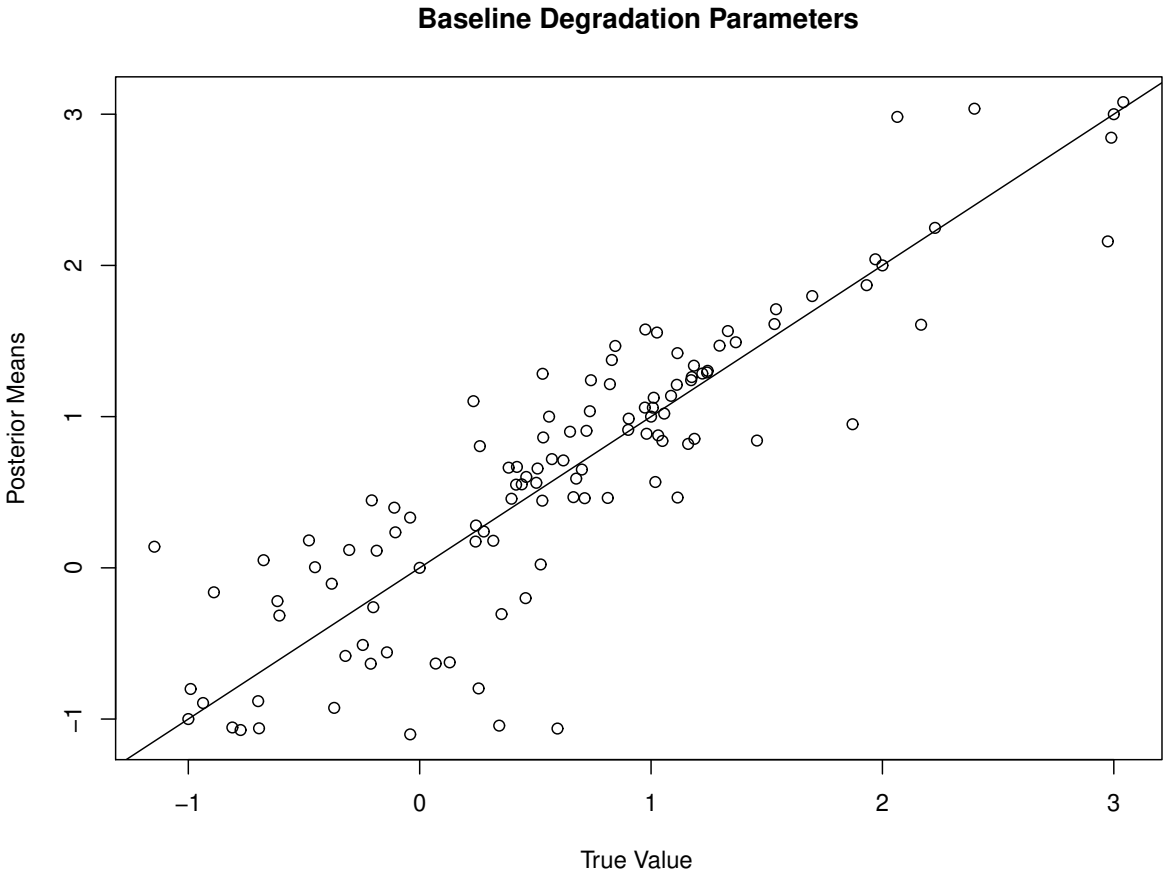

Figure 4.3: Real values of all the 96 baseline degradations versus the posterior means obtained for these parameters, simulated degradation test (Figure 4.2)

For a better visualization, Figures 4.4, 4.5 and 4.6 show the boxplots of the posterior samples of all the model parameters together with the simulated real values (in red). With an algorithm acceptance rate of 25%, the posterior samples for β_1, $\lambda_{0.01}$, $\lambda_{0.05}$ e $\lambda_{0.10}$ have little variability and are centered on the simulated real values, as shown in the Figures 4.4a e 4.4b. The simulated values for μ_j, for $j = 1, 2, \ldots, 8$, did not show a specific pattern and oscillated during the study until reaching its lowest value in the last inspection time (Figure 4.4c). The variability of the posterior sample associated to these parameters decreased over time, while the precision of the estimates increased. Furthermore, it is important to emphasize that the simulated values, as well as the posterior samples, are positive and far from 0. Thus, considering the model given in equation (4.1) and knowing that $\lambda_i > 0$, for all i, the random effects of the common environment in this simulated data contributed to a increase in the degradation rates.

With respect to the standard deviations associated with the observational errors (Figure 4.5a), the estimates obtained for the first group ($X = 0.01$) were more accurate. However, for the other groups, the posterior means were more distant from the simulated real values. This may be a particular issue found in this dataset. To verify whether there is a global problem in the estimates obtained for these standard deviations, it would be necessary to conduct a Monte Carlo study generating more replicas of the data in Figure 4.2. For the standard deviations associated with the evolution errors (Figure 4.5b), the posterior samples are more close to the real values. The highlight in this figure is the posterior sample of σ_ϵ, which captured the simulated real value of this parameter, allowing a correct understanding of the evolution of random effects in the common environment.

The behavior of the posterior samples for the 96 baseline degradations are in Figure 4.6. Note that the simulated real values of these parameters were well recovered and there is no pattern observed for these parameters on all units under test. There are posterior samples with a tendency to grow (units 4 and 12), decrease (unit 11) and stability (units 1,2,3,8,9 and 10). Differently from the evolution parameters associated with the random effects of the common environment (Figure 4.4c), the posterior samples of the baseline degradations did not show smaller variability over time. In most units under test this variability remained stable or increased slightly.

The fit of the proposed model in this simulated data is shown in Figure 4.7, containing the posterior means for the filtering distribution with the 95% credibility intervals for the units under test. As the data does not show much oscillation, the entire trajectory observed was captured by the posterior means of the filtering distribution, together with the interval amplitudes of the 95% credibility intervals. Also, note that the 95% credibility amplitudes are smaller for the group where $X = 0.01$ and larger for the group where $X = 0.10$. This can be easily explained by noting the difference in the scale of the degradation observed in each group. Such difference in scale is common in degradation data with fixed covariates and motivated us to bring standard deviations associated with model errors varying according to each unit i.

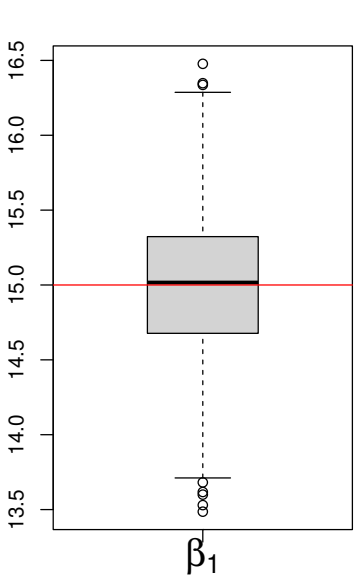

(a) Regression parameter

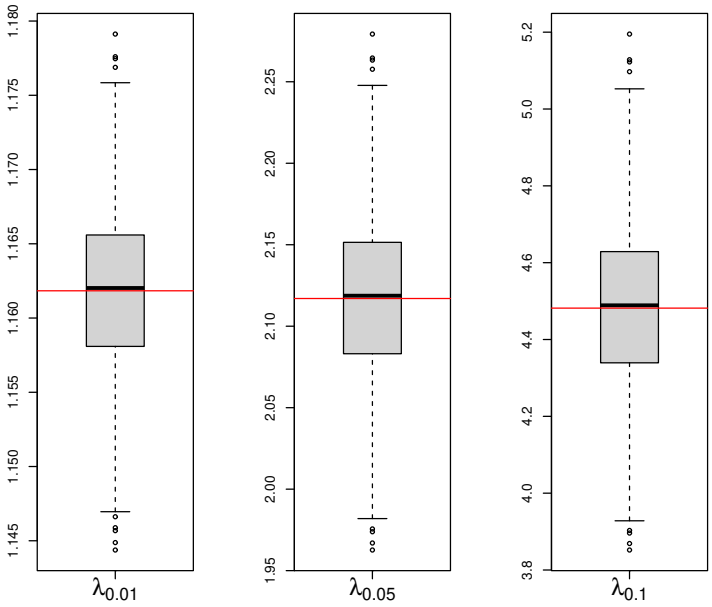

(b) Specific component of each group

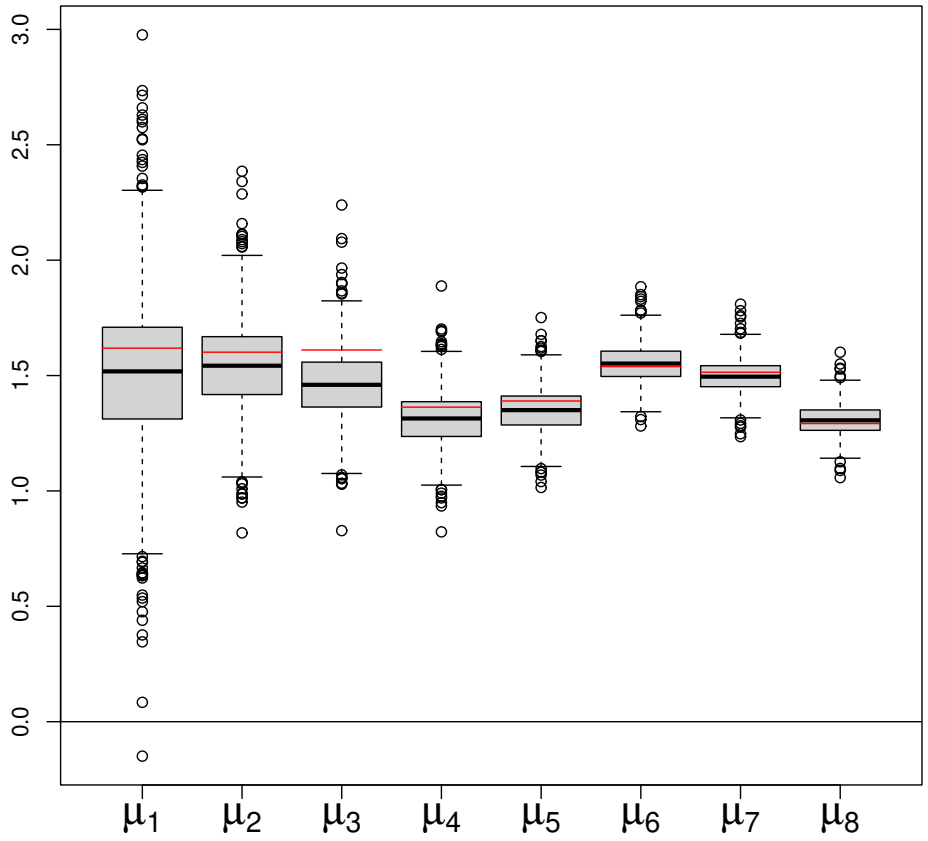

(c) Evolution of the dynamic components

Figure 4.4: Boxplot of the posterior samples associated to β_1, $\lambda_{0.01}$, $\lambda_{0.05}$, $\lambda_{0.10}$ and μ_j, for $j = 1, 2, \ldots, 8$, together with the real values (in red), simulated degradation test (Figure 4.2)

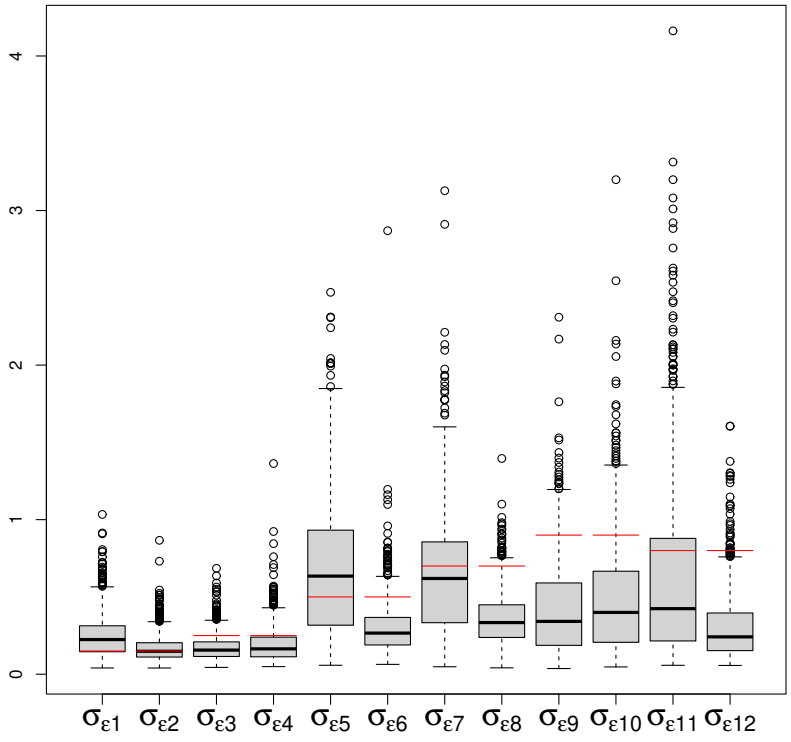

(a) Standard deviations associated with the observational errors

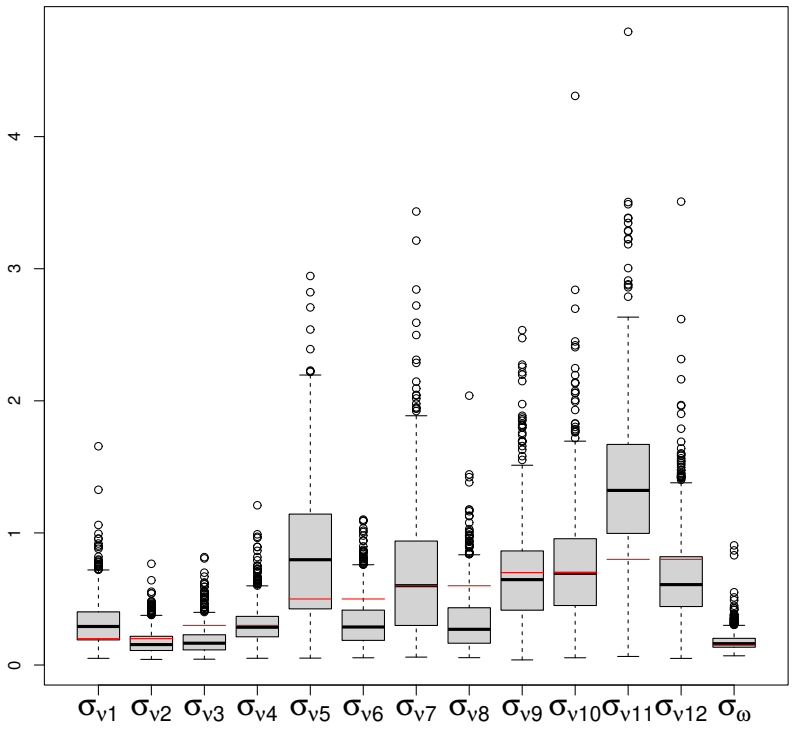

(b) Standard deviations associated with the evolution errors

Figure 4.5: Boxplot of the posterior samples associated to the model errors, together with the real values (in red), simulated degradation test (Figure 4.2)

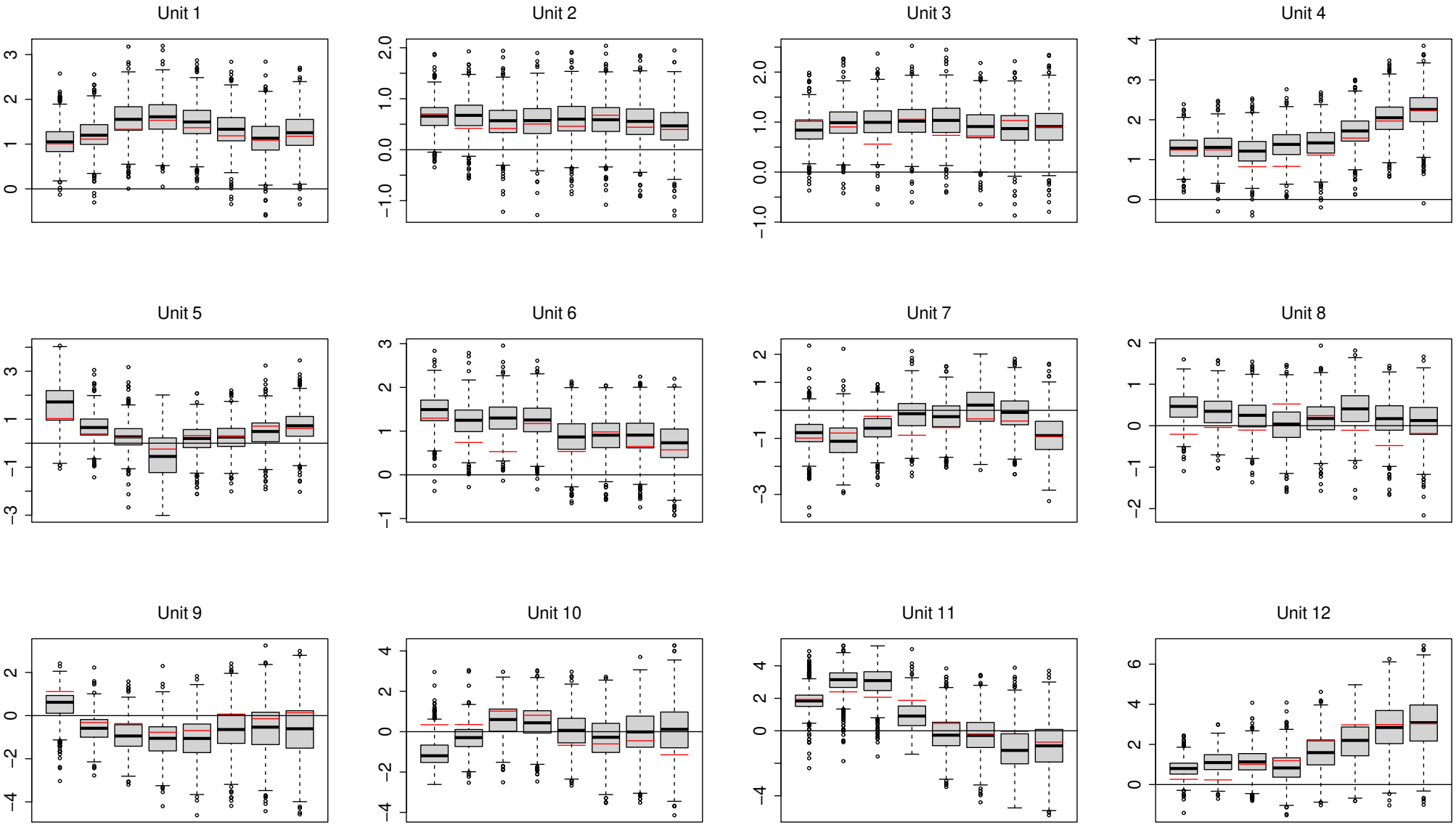

Figure 4.6: Boxplot of the posterior samples associated to the baseline degradation parameters, together with the real values (in red), simulated degradation test (Figure 4.2)

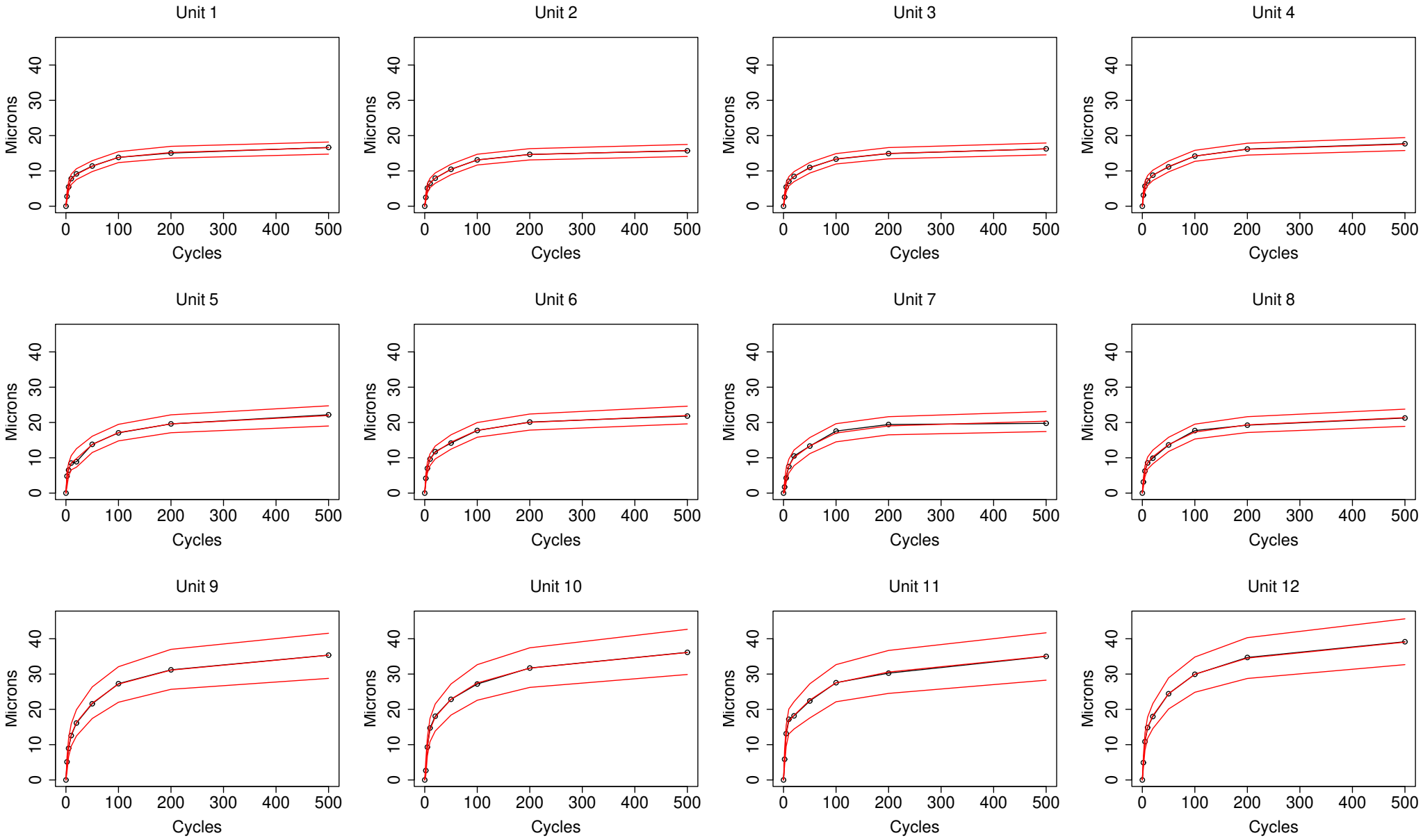

Figure 4.7: Degradation measure (black solid line), posterior means for the filtering distribution (red solid line) with the 95% credibility intervals for the units under test, simulated degradation data (Figure 4.2)

4.5 Case Study: Scar Width Degradation Data

In this section, the proposed methodology is applied to the scar width degradation data presented in Figure 4.1 [Meeker and Escobar, 1998]. The specifications of the prior distributions for the parameters are the same as in the simulation study depicted in the previous section. Only in the algorithm specifications, the lag went from 200 to 125. To evaluate the computational time, the application was fitted on an Intel (R) Core (TM) i7-8550U 1.80GHz CPU with 8GB RAM.

The posterior inference for the model parameters is detailed in Table 4.2 and Figures 4.8, 4.9 and 4.10. With an acceptance rate of 29%, the posterior mean estimate for the regression parameter β_1 is 15.58. This estimate makes the posterior mean of the specific rate associated to the third group $\lambda_{0.10}$ to be almost 4 times greater than the estimated rate for the first group $\lambda_{0.01}$ (Table 4.2). Also in this table, The posterior point estimates for μ_j, with $i = 1, 2, \ldots, 8$, are all negative, indicating that, for the scar width degradation data, the random effects of the common environment are unfavorable to the degradation of the units. Furthermore, the only 95% credibility interval of these parameters that include 0 is the one associated with μ_1, whose posterior sample has the greatest variability.

As in the simulated study discussed in the last section, the variability of the posterior samples for μ_j, with $j = 1, 2, \ldots, 8$, decreases over time (Figure 4.8c). The estimates for these parameters decrease until the measurement instant $j = 4$, where the most unfavorable scenario of the common environment occurs, and grow again until reaching its highest value at the end of the study.

The posterior estimates for the standard deviations associated with the observational errors and evolution errors from baseline degradations are smaller for the group in which $X = 0.01$kg (Figures 4.9a and 4.9b). The last group $X = 0.10$ kg, on the other hand, presents the greatest posterior variability. These results reinforce the need to consider different standard deviations for each unit. The posterior median obtained for σ_ϵ is 0.13. This result explains the little oscillation obtained in the evolution of the μ_j, for $j = 1, 2, \ldots, 8$.

The posterior estimates for the baseline degradations are all positive, with the exception of unit 3 (Figure 4.10). As they vary according to being far from 0, the estimates reinforce the need to include a random intercept in the model. The more the unit degraded in the study, the higher the estimates obtained for the baseline degradations.

The fit of the proposed model in the scar width degradation data is shown in Figure 4.11, containing the posterior means for the filtering distribution with the 95% credibility intervals for the 12 units under test. As in the simulation study discussed before, these data do not have much oscillation and the amplitude of the 95% HPD credibility interval is strongly influenced by the numerical scale observed in each category of the covariate. The time taken to fit the proposed methodology to the scard width degradation data was 10.33 minutes.

Table 4.2: Posterior point estimates and 95% credibility interval bounds of some model parameters, scar widh degradation data

Parameter	Mean	Median	St. Dev	95% HPD	
β_1	15.579	15.586	0.502	14.601	16.530
$\lambda_{0.01}$	1.169	1.169	0.006	1.157	1.180
$\lambda_{0.05}$	2.180	2.180	0.055	2.075	2.285
$\lambda_{0.10}$	4.755	4.752	0.239	4.307	5.222
μ_1	-0.349	-0.354	0.292	-0.892	0.263
μ_2	-0.366	-0.362	0.179	-0.756	-0.047
μ_3	-0.418	-0.413	0.132	-0.664	-0.154
μ_4	-0.522	-0.520	0.104	-0.709	-0.317
μ_5	-0.385	-0.380	0.084	-0.545	-0.215
μ_6	-0.324	-0.324	0.077	-0.475	-0.181
μ_7	-0.293	-0.289	0.070	-0.427	-0.155
μ_8	-0.130	-0.127	0.064	-0.273	-0.017
$\sigma_{\epsilon 1}$	0.145	0.125	0.074	0.048	0.287
$\sigma_{\epsilon 2}$	0.212	0.190	0.103	0.063	0.415
$\sigma_{\epsilon 3}$	0.267	0.230	0.156	0.060	0.559
$\sigma_{\epsilon 4}$	0.143	0.126	0.074	0.052	0.281
$\sigma_{\epsilon 5}$	0.551	0.379	0.494	0.060	1.622
$\sigma_{\epsilon 6}$	0.478	0.397	0.352	0.063	1.174
$\sigma_{\epsilon 7}$	0.726	0.680	0.304	0.079	1.323
$\sigma_{\epsilon 8}$	0.671	0.650	0.324	0.074	1.268
$\sigma_{\epsilon 9}$	0.931	0.869	0.606	0.062	2.046
$\sigma_{\epsilon 10}$	0.597	0.490	0.415	0.055	1.399
$\sigma_{\epsilon 11}$	1.168	1.149	0.667	0.090	2.385
$\sigma_{\epsilon 12}$	0.891	0.626	0.775	0.062	2.469
$\sigma_{\nu 1}$	0.182	0.160	0.096	0.062	0.371
$\sigma_{\nu 2}$	0.219	0.186	0.128	0.046	0.458
$\sigma_{\nu 3}$	0.346	0.310	0.174	0.079	0.681
$\sigma_{\nu 4}$	0.156	0.139	0.081	0.042	0.305
$\sigma_{\nu 5}$	1.118	1.084	0.524	0.074	1.966
$\sigma_{\nu 6}$	0.742	0.696	0.364	0.075	1.385
$\sigma_{\nu 7}$	0.420	0.293	0.361	0.053	1.157
$\sigma_{\nu 8}$	0.602	0.482	0.448	0.066	1.394
$\sigma_{\nu 9}$	1.009	0.923	0.690	0.075	2.309
$\sigma_{\nu 10}$	0.898	0.851	0.502	0.100	1.853
$\sigma_{\nu 11}$	0.910	0.681	0.749	0.056	2.302
$\sigma_{\nu 12}$	1.535	1.516	0.800	0.065	2.801
σ_ω	0.142	0.131	0.052	0.065	0.245

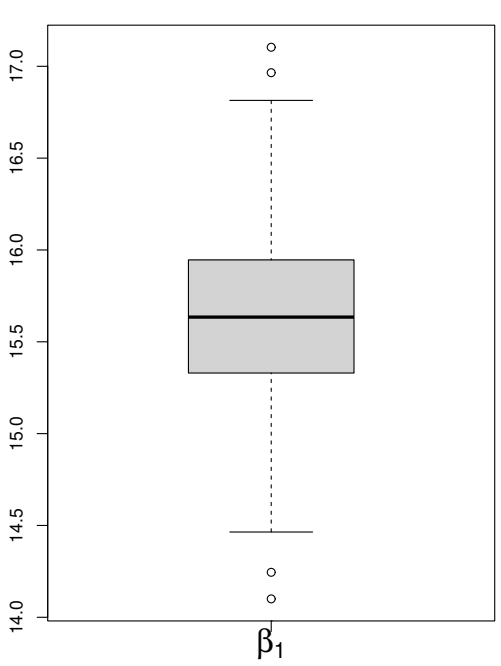

(a) Regression parameter

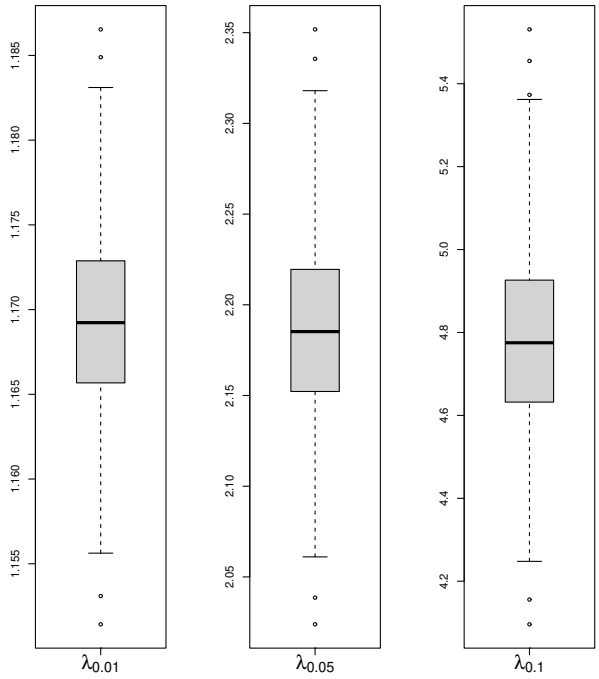

(b) Specific component of each group

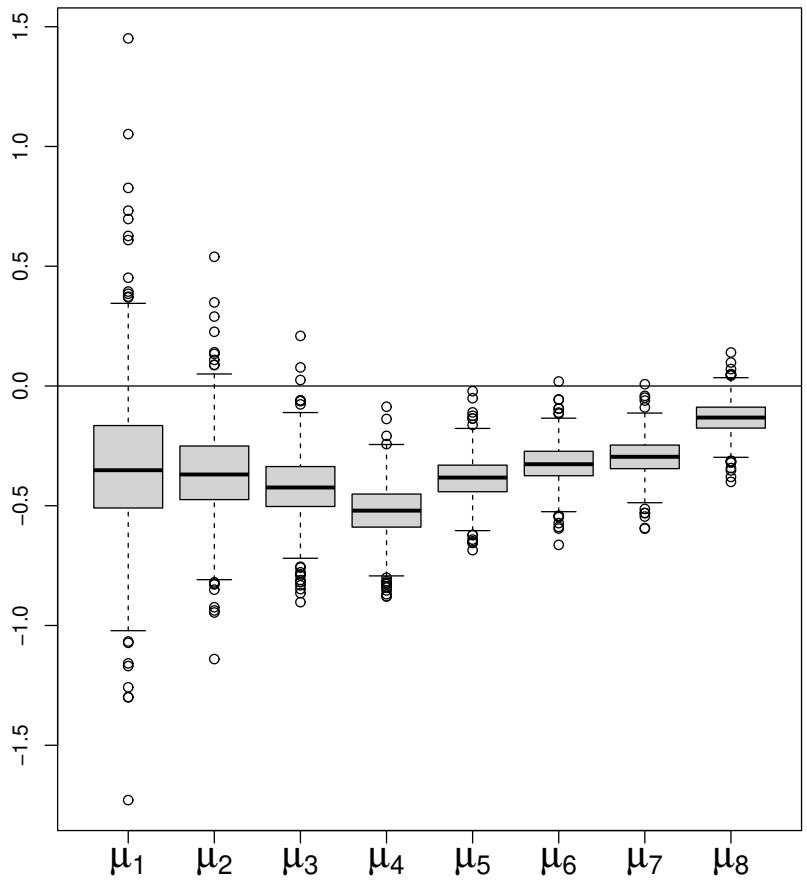

(c) Evolution of the dynamic components

Figure 4.8: Boxplot of the posterior samples associated to β_1, $\lambda_{0.01}$, $\lambda_{0.05}$, $\lambda_{0.10}$ and μ_j, for $j = 1, 2, \ldots, 8$, scar width degradation data

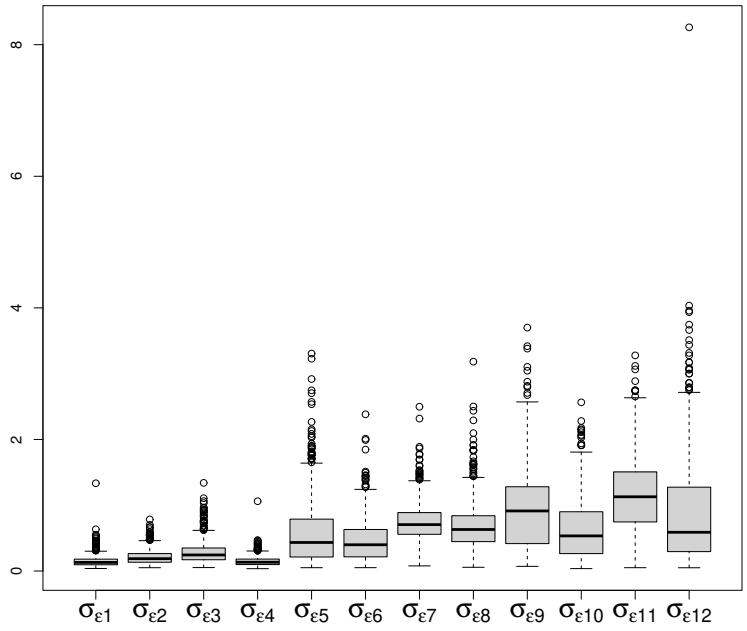

(a) Standard deviations associated with the observational errors

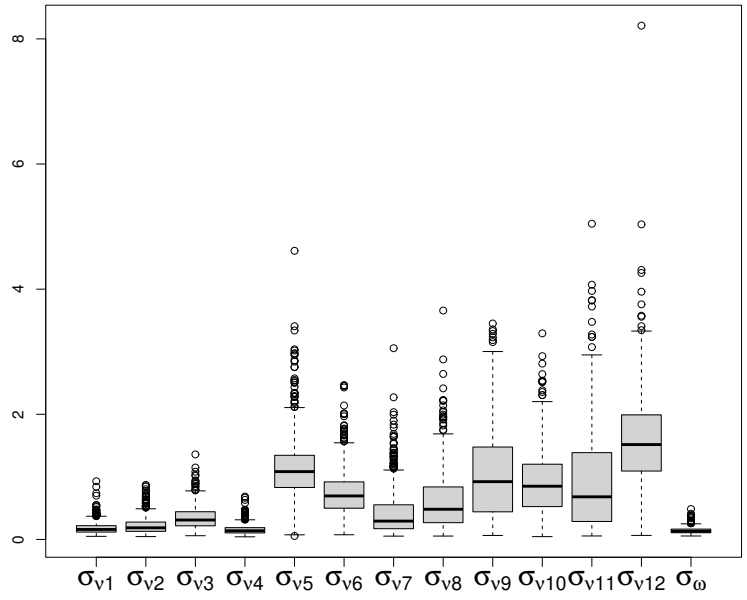

(b) Standard deviations associated with the evolution errors

Figure 4.9: Boxplot of the posterior samples associated to the model errors, scar width degradation data

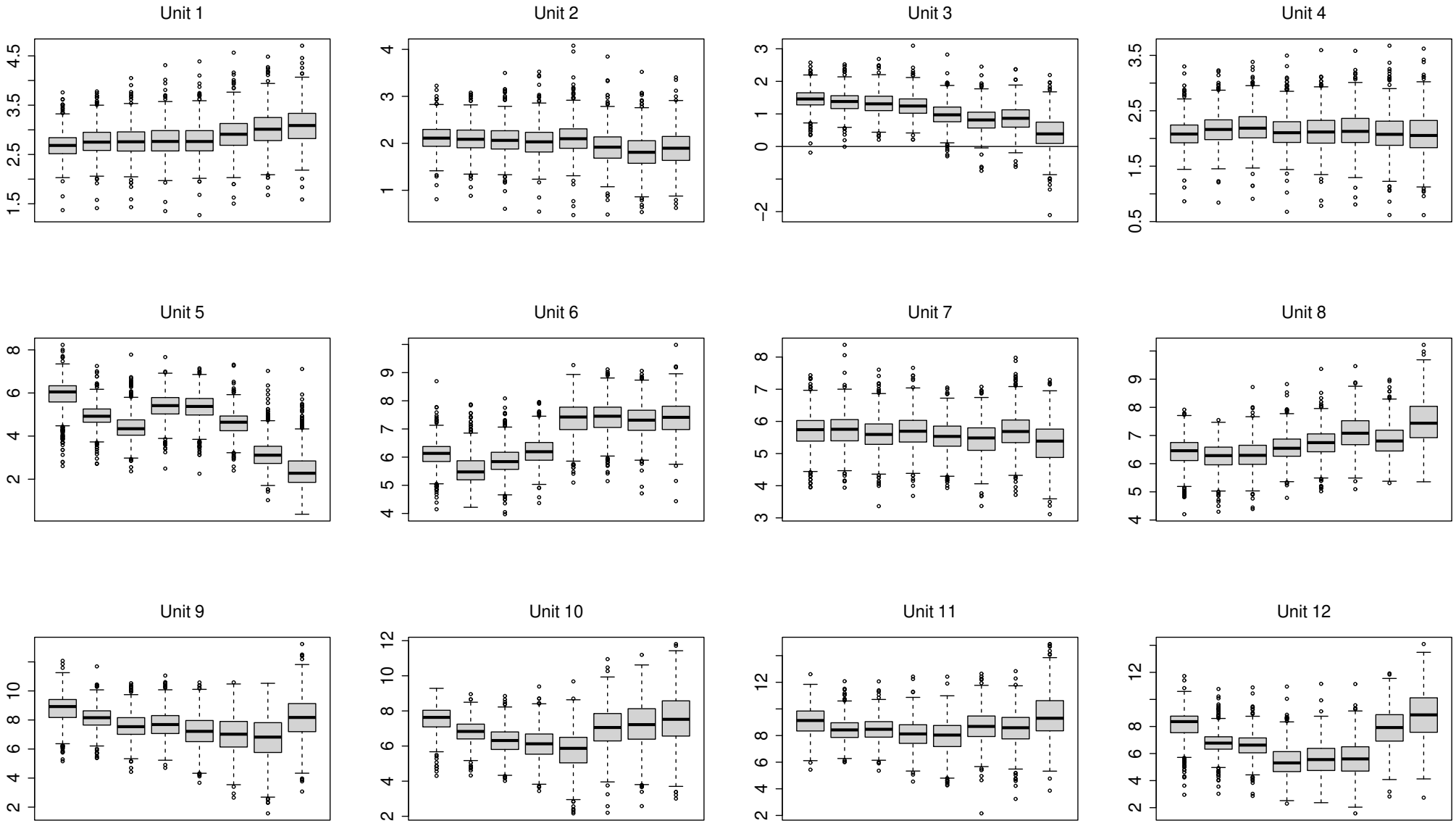

Figure 4.10: Boxplot of the posterior samples associated to the baseline degradation parameters, scar width degradation data

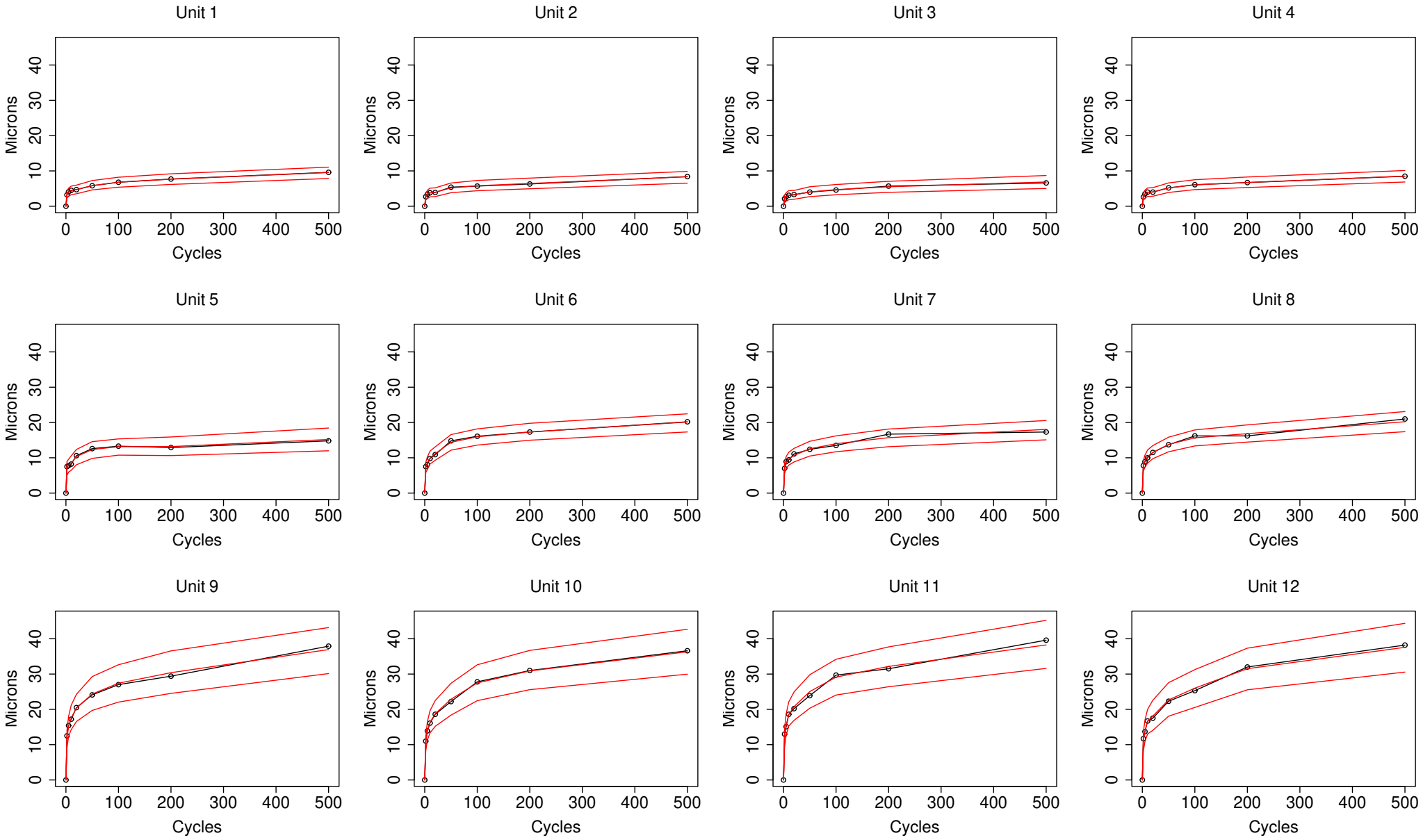

Figure 4.11: Degradation measure (black solid line), posterior means for the filtering distribution (red solid line) with the 95% credibility intervals for the units under test, scar width degradation data

As in the work of Meeker and Escobar [1998], the failure times of the units under test and a future one for the scar width degradation data will also be handled on the log scale. That is, we did not use the inverse function $g^{-1}(t_{ij}) = \exp\{t_{ij}\}$ for $i = 1, 2, \ldots, 12$ and $j = 1, 2, \ldots, 8$ in expression (4.5). Considering the degradation trajectories in the Figure 4.1, many cycles will be required for the units under test to reach the critical degradation threshold, especially those that are subject to a weight of 0.001 kg.

After conduction the inferential procedure described in Section 4.3, Table 4.3 brings the mean time to failure (MTTF) and α-percentiles ($t_{p|\boldsymbol{Y}}(\alpha)$) of the posterior predictive distribution of the failure times (log scale) for the 12 units under test considering the scar width degradation data. As expected, the estimates obtained for failure times of the units under test belonging to the same group are similar. Furthermore, both MTTF and $t_{p|\boldsymbol{D}^J}(0.5)$ were very close in all estimates, indicating possibly symmetric posterior distributions for these parameters.

Table 4.3: MTTF and α-percentiles ($t_{p|\boldsymbol{Y}}(\alpha)$) of the posterior predictive distribution of the failure times (log scale) for the units under test, scar width degradation data.

Failure time	$MTTF\|\boldsymbol{D}^J$	$t_{p\|\boldsymbol{D}^J}(0.025)$	$t_{p\|\boldsymbol{D}^J}(0.1)$	$t_{p\|\boldsymbol{D}^J}(0.5)$	$t_{p\|\boldsymbol{D}^J}(0.975)$
T_1	45.53	41.24	42.74	45.35	50.78
T_2	46.70	42.25	43.76	46.44	52.28
T_3	48.11	43.44	45.05	47.94	53.78
T_4	46.51	42.07	43.64	46.25	52.16
T_5	23.21	21.78	22.29	23.21	24.57
T_6	20.80	19.73	20.09	20.79	21.95
T_7	21.80	20.55	21.01	21.80	23.15
T_8	20.75	19.65	20.01	20.72	22.11
T_9	9.03	8.55	8.68	8.99	9.70
T_{10}	9.15	8.75	8.89	9.14	9.65
T_{11}	8.72	8.21	8.38	8.70	9.30
T_{12}	8.90	8.44	8.56	8.85	9.66

The procedure to obtain estimates for the time to failure of a future unit was performed for each category of the covariate weight. Table 4.4 brings the result containing the MTTF and α-percentiles ($t_{p|\boldsymbol{Y}}(\alpha)$) of the posterior predictive distribution of the failure times (log scale) for a future unit according to the applied weight, considering the scar width degradation data. According to the scale used, note that MTTF when the applied weight is 0.001 kg is approximately 5 times bigger than the MTTF observed in the applied weight of 0.10 kg.

Table 4.4: MTTF and α-percentiles ($t_{p|\boldsymbol{Y}}(\alpha)$) of the posterior predictive distribution of the failure times (log scale) for a future unit according to the applied weight, scar width degradation data.

Weight	$MTTF\|\boldsymbol{D}^J$	$t_{p\|\boldsymbol{D}^J}(0.025)$	$t_{p\|\boldsymbol{D}^J}(0.1)$	$t_{p\|\boldsymbol{D}^J}(0.5)$	$t_{p\|\boldsymbol{D}^J}(0.975)$
0.01 kg	46.71	41.93	43.49	46.49	52.75
0.05 kg	21.64	19.84	20.28	21.38	24.19
0.10 kg	8.95	8.36	8.54	8.94	9.63

4.6 Future Research

The results obtained by fitting the dynamic degradation model with covariates in the simulated data (Figure 4.2) and in the scar width degradation data (Figure 4.1) are promising, but as we said in the introduction of this doctoral dissertation, the model is still under construction. For future research, we want to discuss the model identifiability, develop a Monte Carlo simulation study to better understand the properties of the model, in addition to verifying if there is any pattern in the estimates obtained for the parameters. This study may also include simulations involving failure times of the units under test, focusing on the predictive capacity of the model. Another object of future research is to verify the performance of the proposed model in a context without fixed covariates and compare it with usual models in the literature. Furthermore, there are two new applications of interest that we want to apply the proposed methodology. This step is important to make the model as generic as possible, being adaptable to the greatest possible number of practical representations found in the literature. The two new datasets are detailed in the next subsection.

4.6.1 New Motivating Practical Situations

Here, we present two new datasets with fixed covariates that will be studied for future research. The first one corresponds to the light emitting diodes degradation data, presented in Chaluvadi [2008]. The complete train wheels degradation data is presented in sequence. The Figure 1.1 shows only the degradation obtained in a position among 8 existing in the original dataset.

4.6.1.1 Light Emitting Diodes Degradation Data

As a solid-state lighting source, the light emitting diodes (LEDs) have been increasingly used in display backlighting, communications, medical services, signage, and general illumination. The light intensity of a LED decreases over time, leading to a soft failure when its light intensity drops below a critical threshold level. We use the dataset presented in Chaluvadi [2008] for an illustrative purpose. A sample of 24 units are put into test under constant accelerated levels of electric current, which are 35 mA and 40 mA. The degradation level of each unit was measured every 50 hours until 250 hours, totalizing 6 measures. The degradation data are depicted in Figure 4.12. More details of the degradation data can be found in Chaluvadi [2008]. Following the engineering routine, the failure threshold level is set as 50%. The effect of the electric current variable on the degradation paths is evident. In the work of Tang *et al* [2014], the data in Figure 4.12 is analyzed considering a nonlinear Wiener process with random effects.

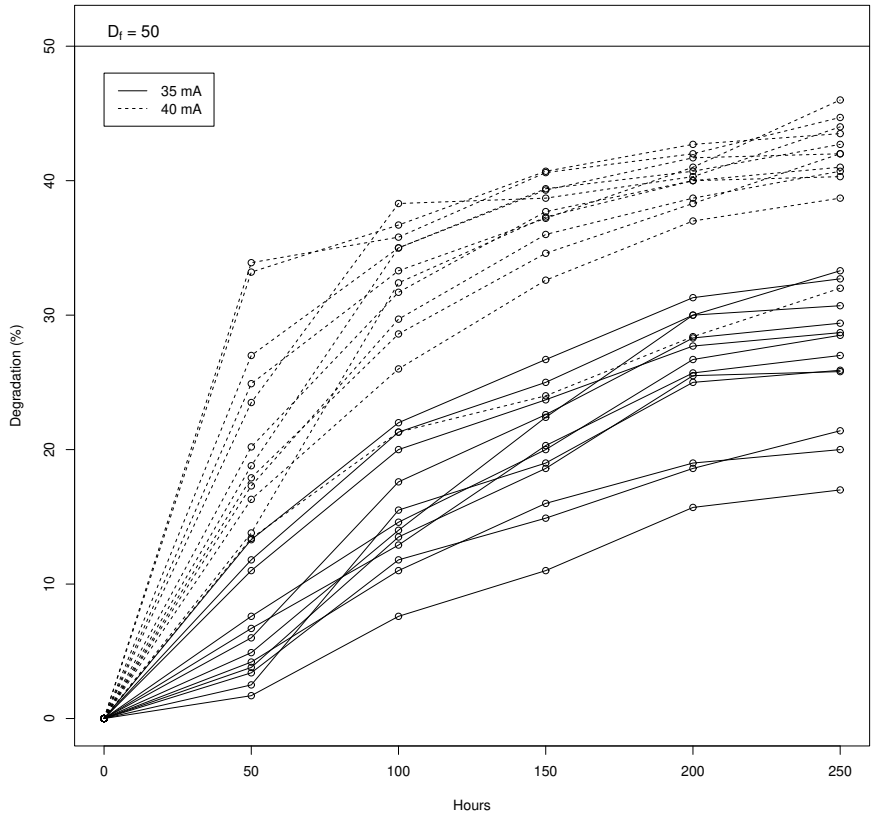

Figure 4.12: Degradation paths of LED monitored at 35mA and 40mA

4.6.1.2 The Complete Train Wheels Degradation Data

For a better understanding the complete train wheel degradation data, remember that 14 trains were monitored at 13 equally spaced inspection times: t_0 = 0km; t_1 = 50000km; t_2 = 100000km,. . ., t_{13} = 600000km. At each inspection time, was collected the diameter measurements of the wheels, given in mm. Physically, a train consists of a locomotive (to provide power) and 3 (three) unpowered vehicles (cars) attached to it. Each car (either a locomotive or an unpowered car) has two trucks; each truck has two axles with two wheels each (Figure 4.13). The wheels are labeled according to their working positions in a given car using a three-dimension indicator vector, representing in this order position (side) within an axle (left = 0; right = 1), truck position (front = 0; back = 1) and axle position within a truck (outer = 0; inner = 1). The data used here refer to the diameter measurements of the wheels of the locomotive cars only (8 wheels for each of the 14 locomotives). More details can be found in Ferreira *et al* [2012].

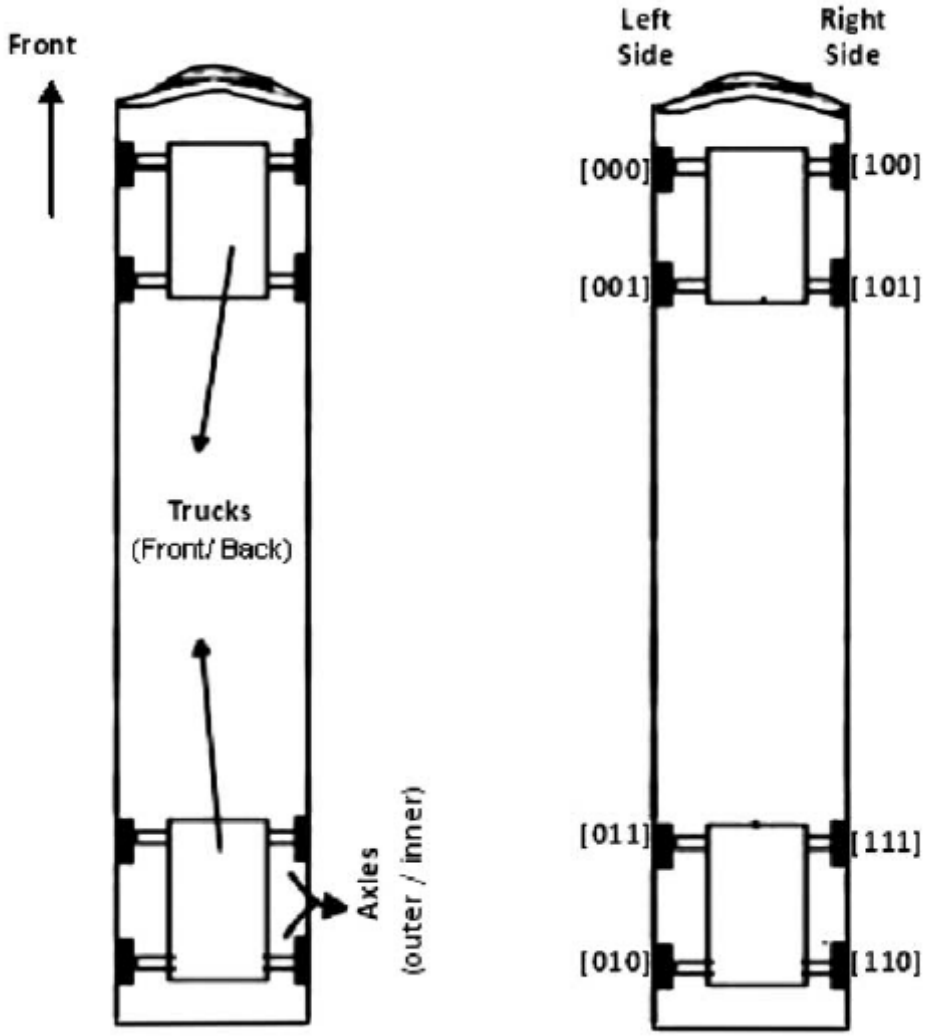

Figure 4.13: The location of the wheels: side, axles and trucks within a car and their corresponding labels.

The nominal diameter of a new wheel is 966mm. When the diameter reaches 889mm, the wheel is replaced by a new one. Figure 4.14 presents the degradation paths of the 112 wheels under study. The points on each plot are the amount of wear (in mm), at each inspection time (distance in km). The event "failure" occurs when the degradation (wear) reaches the threshold level Df = 77mm = (966mm - 889mm).

The goal of this work is to try to answer some specific engineering questions such as (1) Do the different working positions have (statistically) significant effect on the wheel wear? (2) If this is the case, what is the time-to-failure distribution of wheels in different working positions? In addition, it is important to get estimates of key reliability summary figures, such as the MTTF (mean time to failure or, more specifically, mean distance to failure) and some quantiles of the time-to-failure distribution (e.g. 0.01, 0.10 and the median, 0.50).

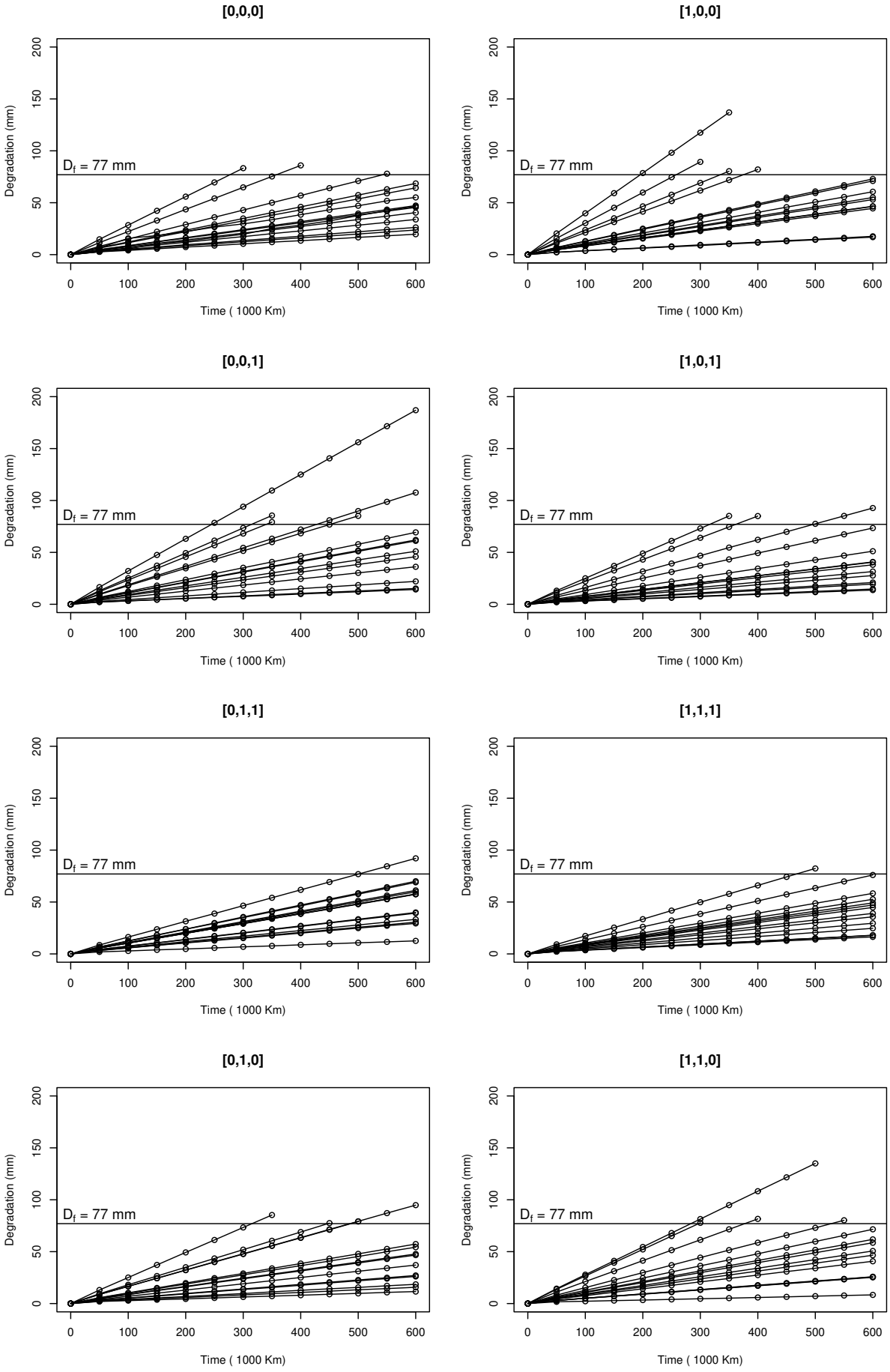

Figure 4.14: Wheel degradation paths by working position.

References

Bagdonavicius, V., & Nikulin, M. S. 2001 *Estimation in degradation models with explanatory variables*. ifetime Data Analysis, 7(1), 85-103.

Chaluvadi, V. 2008 *Accelerated life testing of electronic revenue meters*. M.S. Thesis.

Ferreira, J. C., Freitas, M. A., & Colosimo, E. A. 2012 *Degradation data analysis for samples under unequal operating conditions: a case study on train wheels*. Journal of Applied Statistics, 39(12), 2721-2739.

Hong, Y., Duan, Y., Meeker, W. Q., Stanley, D. L., & Gu, X. 2015 *Statistical methods for degradation data with dynamic covariates information and an application to outdoor weathering data*. Technometrics, 57(2), 180-193.

Lawless, J., & Crowder, M. 2004 *Covariates and random effects in a gamma process model with application to degradation and failure.* . Lifetime data analysis, 10(3), 213-227.

Lu, L., Wang, B., Hong, Y., & Ye, Z. 2021 *General path models for degradation data with multiple characteristics and covariates*. Technometrics, 63(3), 354-369.

Meeker, W. Q. & Escobar, L. A. 1998 *Statistical Methods for Reliability Data*. Wiley Series in Probability and Statistics, First Edition.

Petris, G., Petrone, S. & Campagnoli, P. (2009). *Dynamic linear models with R* Springer, John Wiley & Sons.

Robinson, M. & Crowder, M. (2000). Bayesian methods for a growth-curve degradation model with repeated measures. *Lifetime Data Anaysis*, 6(4), 357-374.

Sun, X., Cai, W., & Li, M. 2021 *A hierarchical modeling approach for degradation data with mixed-type covariates and latent heterogeneity.*. Reliability Engineering & System Safety, 216, 107928.

Tang, S., Guo, X., Yu, C., Xue, H. & Zhou, Z. 2014 *Accelerated degradation tests modeling based on the nonlinear Wiener process with random effects*. Mathematical Problems in Engineering, 2014, Hindawi.

Wang, X., Gaudoin, O., Doyen, L., Bérenguer, C., & Xie, M. 2021 *Modeling multivariate degradation processes with time-variant covariates and imperfect maintenance effects.*.Applied Stochastic Models in Business and Industry, 37(3), 592-611.

West, M. and Harrison, J. 1997 *Bayesian forecasting and dynamic models*. Springer series in statistics, Springer, Second Edition.

Chapter 5

Final Discussion and Future Work Directions

Over the years, components and systems have become more and more reliable, mainly because of the increased demand for this type of product. One of the challenges in reliability that arises in this context lies in the development of models that can be useful in decision-making and in predicting failures that often generate a high cost and can be catastrophic for both the customer and the supplier.

Methodologies that use degradation data have been widely used to make inferences about highly reliable systems. All degradation models developed in this doctoral dissertation belong to the approach of general degradation path models. Therefore, all three models built have in common two steps that this approach needs. In the first stage, a mixed linear or non linear model for a continuous response variable is fitted. The adopted functional form for the degradation paths is assumed to be the same for all population. For each specific unit, the true degradation path is a function of time conditional on the random-effects parameters representing the units feature. Finishing the first step, the unknown parameters of the model are estimated. The second step of this approach is to estimate the failure time distribution. This estimation depends on the model structure and can be obtained analytically, through Monte Carlo simulations or some other computational procedure. Another similarity between all the models developed here is the incorporation of a dynamic structure in the modeling. This structure allows a local approximation to the true degradation path and is able to adapt to the oscillations of the trajectories observed throughout the inspection times.

In Chapter 2, we introduced a dynamic general path model to handle data which degradation rate and the baseline degradation are time-variant. The dynamic structure of this model allows accommodating different behaviors of the degradation paths including linear and non-linear ones. Therefore, the model provides a solution for the "disadvantage" of the general path

models, proposing a functional form that is not regular along the time also allowing for structural breaks. The model was compared to the Weibull linear degradation model, a model that is frequently used to analyze degradation data. We conclude, from the simulations, that the dynamic linear degradation model has better performance than the Weibull model to analyze data which degradation rate dynamically changes over time. It also shows to be a competitive model to analyze data coming from a population where the degradation rate for each unit does not change along the time. The train wheel and laser emitters degradation data are commonly analyzed by the Weibul linear degradation model. By assuming a dynamic structure in fitting these data, the forecasts for the degradation measurements are less biased than the observed in the linear degradation model. If we consider forecasts are done many steps ahead, the proposed model performed much better than the linear degradation model. Despite its good performance, in our analysis, we only explore a dynamic model with a normal degradation rate. Possible extensions of this model may consider different distributions for this rate making the model even more flexible. Another limitation of the proposed model is the lack of parsimony. Although in the situations approached in the paper we did not experienced problems regarding the computational cost, the lack of parsimony may lead to a high computational cost if data to be analyzed are captured in a massive way and with high temporal resolution. To be effectively used in practical situations like these, we must look for strategies to reduce computational time without losing the quality in the inferences.

The limitations observed in the model built in Chapter 2 motivated the development of the model discussed in the following chapter. We introduced a new class of general gamma degradation path models that have a dynamic functional form. To obtain a parsimonious model, for each unit, the degradation rate is a function of two components: a static and unit-specific effect and another that measures the environmental impact. The dynamic structure is introduced into the model through the prior distribution for the environmental effects, which assumes a Markovian dependence among them. A more general structure (not only linear) relates the inspection time and the degradation measurements allowing to accommodate different shapes for the degradation paths. Constraints to identify the model were theoretically derived, and a useful discussion is presented about how to these constraints may be specified in the contexts of time series and degradation tests. The forecast of future degradation measurements is discussed. The crucial relationship between failure time and model parameters is obtained, and the inference for the remaining useful life is discussed for units under test and a future one. The simulation studies provided some valuable guidelines to establishes the prior distributions of the environmental effect needed to attain the model identification. These studies showed that if the goal is to infer the failure time behavior, the prior specifications for the parameter θ_0 and γ do not play an important role. However, if the goal is to get information about the environmental or unit-specific effects, we should obtain trustful information about θ_0 allowing us to build an informative prior for it. The usefulness and versatility of the this model are illustrated by analyzing two datasets (fatigue crack size and stress relaxation data) whose degradation paths have different shapes. In both cases, the proposed model outperforms some well-known models.

The proposed methodology is defined only for positive degradation measures and assumes that covariates explaining the degradation mechanism are not available.

This last limitation motivates the model constructed in Chapter 4. The model developed in this chapter is also a normal dynamic degradation model as assumed in the first model. Extending this first approach, we now assume that the degradation rate is decomposed in the same two components considered in the DMGM but now with an addictive structure. We also assume that the effect that quantifies the specific physical features of the devices is a function of fixed covariates. This approach introduces more flexibility to the analysis since, in some degradation tests, multiple characteristics are observed to understand different aspects of system reliability. Therefore, this chapter detailed the entire inferential procedure for the model parameters and failure times developed so far. The methodology is still under construction, but we obtained promising results in a brief simulation study and in the application of the scar width degradation data.

Future extensions of the proposed models include considering similar decompositions for the degradation rate and developing new dynamic degradations models assuming other distributions for the degradation measures as well as other distributions with positive support for the units effects as log-normal, Weibull, and log-skew-elliptical distributions. These prior choices will bring some new theoretical and computational challenges as these families are not conjugate with the Gamma family. Another interesting future work is the construction of a model that incorporates time-dependent covariates.